INDEPENDENT POWER FLOW CONTROL OF MULTIPLE ENERGY SOURCES USING A SINGLE ELECTRIC MACHINE

AHMAD ANAD ABDUALLAH

A thesis submitted in partial fulfilment of the requirements of Liverpool John Moores University for the degree of Doctor of Philosophy

April 2019

ABSTRACT

In this thesis, an independent power flow control of different energy sources connected to a single electric machine with a multitude of three-phase winding sets has been investigated. These machines are highly suitable for high power and critical applications. Additionally, these machines utilise the well-established three-phase power electronics technologies. The interest towards electrification of the transportation systems makes having multiple energy source a viable solution in the near future. Independent power flow control will enable the integration of hybrid energy storage systems on electrical vehicles such that the regenerative power can be directed to a super-capacitor while the cruising power is consumed from a battery bank. Nevertheless, this technique can be envisaged for different applications, from wind turbines to microgrids. In order to make all of this possible, the current amplitude of each winding set needs to be controlled first. Therefore, the control of the individual winding set's currents' amplitude and direction for multiple three-phase machines is the main subject of this thesis. The developed control schemes are based on vector space decomposition (VSD) rather than multi-stator (MS) approach. The former approach has a unique harmonic mapping and a single flux and torque producing subspace. Primarily in the thesis, current sharing strategy has been developed for both symmetrical and asymmetrical multiple three-phase machines with a common mode of operation for all the winding sets (motoring or generation). The strategy is based on the correlation of the x_i-y_i currents of the VSD and the α_i-β_i currents of the MS approach. These links enable the control of the current amplitude of the winding sets separately while maintaining the same torque and speed. The correlations between these modelling approaches combine good features of both modelling methods, the ability of the MS approach to control each winding set individually, and the VSD feature to perform the control in a completely decoupled subspace. Afterwards, the same strategy is employed to change the power flow direction as well as the amplitude of the multiple three-phase winding sets currents such that concurrent motoring and generation mode of operation is established. Two novel power sharing schemes have been proposed and analysed in this thesis. Both are based on VSD. The first scheme is sharing the flux and torque producing currents equally, while the second one is controlling the power by the torque producing current while preserving the same flux producing current. The transferred power efficiency has been improved significantly using the second approach. The same power sharing technique has been applied to an unorthodox type of machine – a twelve-phase machine implemented as a six-phase machine with double winding (hence, consisting of two six-phase sub-machines). The proposed power sharing scheme here is using a hybrid control approach combining two vector control schemes, based on MS and VSD. The control based on MS is controlling the power transfer from one six-phase sub-machine to the other one, while the control based on VSD, and with auxiliary current control, is sharing and directing power to a specific three-phase winding set within each sub-machine. Last but not least, two novel regenerative test methods have been proposed for multiple three-phase machines. The first approach is based on utilising a modified power sharing control strategy to operate the machine with

rated current while maintaining the speed and circulating the power among the winding sets. The approach can be implemented differently based on the number of winding sets. With an even number of neutral points, half of the winding sets will be in motoring while the other half are in generation mode. However, when there is an odd number of winding sets, one of the winding sets will be in no-load mode of operation. The second approach is implementing the motoring and generation of the winding sets using a unique *y*-current component of the VSD. This method is only applicable to multiple three-phase machines with an even number of neutral points. The regenerative test can be applied to induction and synchronous machines equally but with a completely different outcome. For synchronous machines, the test can be used for efficiency evaluation and temperature rise test while for the induction machines the test can provide a straightforward experimental approach to segregate constant losses (core and mechanical losses) from load dependent losses (copper losses). All the proposed control methods have been validated by simulation and experimentally, except for the double winding machine where experiments were not done.

ACKNOWLEDGMENT

After thanks to God, I would like to express my deepest gratitude to a few people who helped me to achieve this thesis.

Initially, I would like to express my sincere appreciation to my supervisors, Dr Obrad Dordevic and Dr Martin Jones for their exceptional guidance and support during my studies. Without your patience and vast knowledge this thesis would not be possible. I would like to express my genuine gratitude to Prof Emil Levi for his support and for giving me the chance to complete my PhD at Liverpool John Moores University, thank you Professor.

Next, I would like to thank my childhood friends Mr Naif Yousif, Mr Nasser Aish and Mr Emad Yousif. Also, I would like to thank my friends, Dr Ivan Zoric, Dr Engku Ahmed Rafiqi and Mr Marko Slunjski, sharing the office with you was a delight.

Finally, I would like to thank my Mother and my father for their many sacrifices in order for me to complete my education. Words cannot express my gratitude to them, hopefully my action will do. To all my siblings, thank you for your support, we have been through a lot in this life together and I pray to god that we will remain united and on one heart forever. To my fiancée, without you nothing is possible, thanks. Moreover, I would like to dedicate this thesis to my Mother and Father, this is your accomplishment.

TABLE OF CONTENTS

Abstract ..... **iii**

Acknowledgment ..... **v**

Table of Contents ..... **vi**

List of Principal Symbols ..... **ix**

List of Used Abbreviations ..... **x**

Chapter 1: Introduction **1**

1.1 Preliminary Remarks 1

1.2 An Overview of the Multiple Three-Phase Machines 3

1.3 Research Objectives and Novelty 6

1.4 Organisation of the Thesis 7

Chapter 2: Literature Review **10**

2.1 Introduction 10

2.2 Multiphase Machines and Power Electronic Converters 10

2.3 Multiphase Machine Modelling 14

2.4 Multiphase Machine Control Methods 15

2.5 Current Control Schemes for Multiphase Machines 15

2.6 Power Sharing among Winding Sets 17

2.7 Fault Tolerance 18

2.8 Synthetic Loading 19

2.9 Summary 21

Chapter 3: Current Sharing for Symmetrical Multiple Three-Phase Induction Machines **22**

3.1 Introduction 22

3.2 Modelling of Multiphase Induction Machines 22

3.3 Clarke's Decoupling Transformation 28

3.4 Rotational Transformation 31

3.5 Modelling of Multiple Three-Phase Induction Machines 34

3.6 Field-Oriented Control (FOC) 36

3.7 Current Sharing for Multiple Three-Phase Machines 42
3.8 Simulation Results 49
3.9 Experimental Results 54
3.10 Summary 57
Chapter 4: Current Sharing for Asymmetrical Multiple Three-Phase Induction Machines 59
4.1 Introduction 59
4.2 Modelling of Asymmetrical Multiphase Induction Machines 59
4.3 Vector Space Decomposition Transformation 62
4.4 VSD Transformation with Multiple Neutral Points 65
4.5 Current Sharing for Asymmetrical Multiple Three-Phase Machines 68
4.6 Simulation Results 71
4.7 Experimental Results 75
4.8 Summary 79
Chapter 5: Power Sharing for Multiple Three-Phase Induction Machines 80
5.1 Introduction 80
5.2 Multiple Energy Sources Supplying a Single Machine 81
5.3 Power Sharing Utilising Current Sharing Strategy 83
5.4 Efficient Power Sharing Strategy 84
5.5 Simulation Results 87
5.6 Experimental Results 91
5.7 Summary 95
Chapter 6: Power Flow Control among Double-Winding Multiple Three-Phase Machines' Winding Sets 96
6.1 Introduction 96
6.2 Double-Winding Multiple Three-Phase Machines 97
6.3 Mathematical Model of Double-Winding Multiple Three-Phase Machines 97
6.4 Control Strategy 100
6.5 Simulation Results 105
6.6 Summary 111

Chapter 7: Regenerative Test for Multiple Three-Phase Machines 112

7.1 Introduction 112

7.2 Full-Load and Temperature Rise Test 113

7.3 Regenerative Test using MS Approach 114

7.4 Regenerative Test using Current Sharing Approach (VSD) 117

7.5 Regenerative Test using a Unique Y-Current Component 119

7.6 Simulation Results 121

7.7 Experimental Results 128

7.8 Summary 133

Chapter 8: Conclusion and Future Work 134

8.1 Summary and Conclusions 134

8.2 Future Work 136

Chapter 9: References 138

Appendix A: Derivation and Matlab Codes 149

A.1 Asymmetrical Fifteen-Phase MS and VSD Correlations 149

A.2 Symmetrical and Asymmetrical Twelve-Phase Machine MS and VSD Correlations 154

A.3 Symmetrical and Asymmetrical Eighteen-Phase Machine MS and VSD Correlations 154

A.4 Matlab and Simulink Code 155

Appendix B: Description of Experimental Setup 159

B.1 Hardware Description 159

B.2 Software Description 161

Appendix C: Publication Resulting from the Thesis 162

C.1 Journal Publications 162

C.2 Conference Publications 162

LIST OF PRINCIPAL SYMBOLS

$\bar{F}$	Line above the variable denotes a complex value
$\hat{\bar{F}}$	Denotes a variable complex conjugate
$[F]$	Square brackets denote matrix or vector value
a	Number of phases in a single winding set
$a, b, c, \ldots$	Machine phases in phase variable reference frame
$[C]$	Clarke's decoupling transformation matrix
$[D]$	Rotational transformation matrix
d-q	Indices denoting values in rotational reference frame
e_d, e_q	Cross-coupling decoupling terms
F^*	Asterisk donates reference value
G_i	Power sharing coefficients
i	Current in general (determined by index)
J	Inertia in general
k	Number of winding sets
K_{di} , K_{qi}	Flux and torque producing currents sharing coefficients
K_i	Current sharing coefficients
L, M	Inductance in general (determined by index)
n	Number of phases
P	Number of pole pairs
P_{cu}	Copper losses
P_{Fe}	Core losses
P_{fw}	Friction and windage losses
P_{Si}	Average input power
R	Resistance in general (determined by index)
r	In sub-script denotes rotor variable
s	In sub-script denotes stator variable
T	Torque in general (determined by index)
v	Voltage in general (determined by index)
α-β, x-y, 0_i	Indices denoting values in stationary reference frame
ψ	Flux-linkage in general (determined by index)
ω	Angular speed

LIST OF USED ABBREVIATIONS

APOD-PWM	Alternating phase opposition disposition PWM
BERR	Business enterprise and regulatory reform
BPM	Brushless permanent magnet
CHB	Cascaded H-bridge
DFT	Discreate Fourier transform
DTC	Direct torque control
EMF	Electromotive force
EVs	Electric vehicles
FCHEV	Fuel-cell hybrid electric vehicle
FSCW	Fractional-slot concentrated winding
HESS	Hybrid energy storage systems
ICE	Internal combustion engine
IPM	Interior permanent magnet
IRFOC	Indirect rotor-field oriented control
LS-PWM	Level shifted PWM
MC	Matrix converter
MMF	Magneto-motive force
MPC	Model predictive control
MS	Multi-stator
NPC	Neutral point clamped
OeW	Open-end winding
PD-PWM	In-phase disposition
PI	Proportional-integral
PM	Permanent magnet
POD-PWM	Phase opposition disposition
PR	Proportional-resonant
PS-PWM	Phase-shifted PWM
PTC	Predictive torque control
PWM	Pulse width modulation
SPM	Surface permanent magnet
SRM	Synchronous reluctance machine
SVM	Space vector modulation
THD	Total harmonics distortion
V2G	Vehicle-to-grid
VSD	Vector space decomposition
VSI	Voltage source inverter

CHAPTER 1

INTRODUCTION

1.1 PRELIMINARY REMARKS

Achieving the U.K. target of reducing CO_2 emissions by 80% before 2050 will require an increase in renewable electric energy generation and substantial new developments in the areas of electric transportation. It will also require new forms of electric energy distribution and utilisation. In the case of electric vehicles, a gradual shift towards vehicles with multiple energy sources can be anticipated (in contrast to the current state-of-the-art where at most two energy sources are combined). Additionally, a substantial contribution to the target will be achieved via further developments in remote offshore wind energy generation and dc microgrids.

Currently, fully electric vehicles (EVs) are typically either battery or hydrogen (fuel cell) powered. A combination of the two energy sources (hybrid hydrogen fuel-cell plug-in electric vehicles, FCHEV) is an obvious alternative that has been extensively considered and developed [Offer et al. (2010)]. In [Offer et al. (2010)] it is predicted that the capital cost and life cycle cost of FCHEV will be the lowest, among the other EVs and the internal combustion engine (ICE) vehicles, by 2030. This prediction is based on a report published by BERR and the DFT in the UK. The capital cost of EVs and the lack of charging infrastructure are the main difficulties facing the wider adoption of EVs. The growth in demand for EVs in recent years will make the charging infrastructure more economically viable. It is not beyond imagination that at some point in the future, new materials will be discovered that will enable the use of the surface of a vehicle for solar electric energy generation. The possibility of producing an EV with multiple energy sources (subject to finding another convenient prime energy source) which are utilised simultaneously or individually is becoming more likely. An obvious question that arises is: what is the best way of controlling such a multitude of electric energy sources, with a view to optimising the driving range through optimal power flows from one energy source to another while maximising the efficiency of the energy conversion?

Remote high-power offshore wind farms are employing electrical generators of ever-increasing powers and the positioning of the plant requires the existence of fault tolerance as a built-in feature of the generation system. Due to the limitations of the current semiconductor technology, increase in the power rating of the generator requires paralleling of power electronic converters in the standard back-to-back converter topology. Hence, use of a standard three-phase generator system, which typically has low fault tolerance, becomes undesirable. The wind generation systems are moving toward a fully-rated

converter system due to the increase in the power level (>10 MW) and the laws of the voltage transmission forced by the grid codes. The low voltage generator (high power wind turbine) requires high-current power electronics (>2000 A), which needs several three-phase converters connected in parallel to achieve the high-power conversion [Duran and Barrero (2016)]. Therefore, it seems to be reasonable to use a multiple of three-phase multiphase generators to avoid zero-sequence current flow between the set of converters and the wind turbine and to increase the reliability of the system. Moreover, the MMF harmonics and torque ripples are reduced in the multiple three-phase machine if the winding sets are spatially shifted and the zero-sequence circulating current is eliminated by isolating the neutral points of the stator winding sets [Duran and Barrero (2016)]. For the purposes of better power flow control and for an improved fault tolerance it becomes mandatory to use multiphase solutions, such as for example [Che et al. (2014c), Ditmanson et al. (2014)].

The described application scenarios are quite different in nature, but both have in common a need for efficient power flow control between different subsystems, which could be achieved by using an electric machine with a multiphase stator winding structure. The premise of this research originates from the realisation that such a multiphase stator winding topology can be obtained by using a multitude k of winding sets with a lower phase number a, such that the total number of phases of the machine n equals $n = ka$. By configuring each winding with an isolated neutral point, one then has n individual electric ports of the machine for connection to different electric energy sources in an electric vehicle or for providing the desired generated power sharing between different wind generator output sub-systems. The desirable feature, pertinent to EV applications, is that the power flow through a winding set can be both positive and negative (i.e. motoring and generation, with some of the sub-systems operating with positive and some with negative powers simultaneously). In the case of the remote offshore wind generator the desirable feature is that the power generated at different sub-systems can be controlled independently (but the power flow direction does not need to change). If such an operation can be realised, then an EV would become capable of working in the propulsion mode while simultaneously re-charging the battery (i.e. a sub-system operating in generating mode), while in the case of microgrid interconnection one could transfer energy freely through the machine so that a microgrid with a surplus of electric energy supplies other microgrids that are at a given point in time deficient in terms of the available energy. In the remote offshore wind energy generator case, only one power flow direction is required; however, it should be possible to independently control power at the outputs of different sub-systems.

Realisation of such an operating scenario requires the development of sophisticated algorithms for the converter/electric machine control and electric energy/power management, which do not exist at present. Thus the specific challenge, to be addressed in this thesis, can be summarised as follows: Development of a strategy for independent energy management and power sharing between different energy sources, through appropriate power electronic converters and multiple three-phase machine's

winding sets, taking into account their differing natures (e.g. different voltage levels, unidirectional or bidirectional power flow nature), so that the requirements of the exemplar applications, discussed above, can be met as illustrated in Fig. 1.1.

A short overview of the multiple three-phase machines with emphasis placed on the relevant current control scheme, is given in the following section.

1.2 AN OVERVIEW OF THE MULTIPLE THREE-PHASE MACHINES

Utilisation of multiple three-phase machines in critical high-power applications is nowadays of a great interest due to the advantages of the multiphase machines and the well-established three-phase power electronics technologies, leading to a better high-performance drive, compared to the existing solutions. Therefore, the utilisation of such machines, synchronous or asynchronous, will combine both advantages of the multiphase machines and mature three-phase power electronics technologies in addition to the three-phase modulation schemes and control strategies.

The first published paper to investigate a multiphase induction machine was by [Ward and Härer (1969)] where a five-phase machine was developed to reduce the torque ripple produced by the three-phase machines supplied using a VSI operating in six-step mode. The benefits of using multiphase machines compared to three-phase machines can be summarised in the following two points:

- The ability to split up the power among *n* phases instead of three, compared to the three-phase machines and the ability to provide post-fault operation compared to the three-phase machines from the power electronics point of view in the case of multiple three-phase machines.

However, multiple three-phase machines possess more advantages compared to the multiphase machines. These features are as follows:

- The ability to utilise the well-established three-phase power electronics technologies and
- More fault-tolerance capability compared to the multiphase machines from the power electronics converter point of view [Duran and Barrero (2016)].

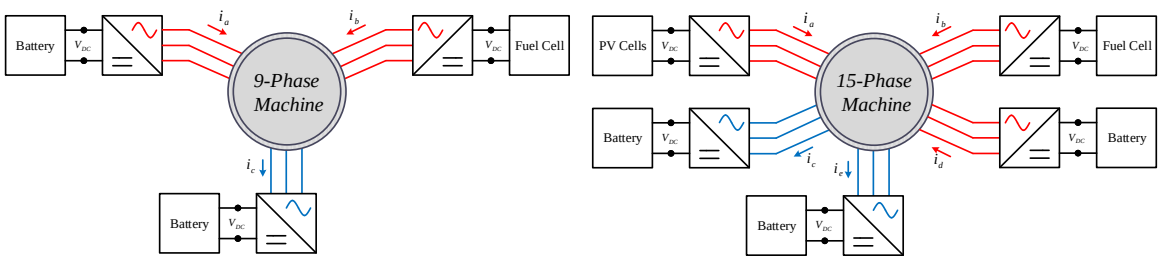

a) b)

Fig. 1.1: Exemplar application of a) nine-phase machine and b) fifteen-phase machine supplied by multiple sources working in generation and motoring mode simultaneously.

The aim of this research is to explore the use of multiple three-phase machines while supplying them with multiple energy sources. Although the research is applicable to synchronous machines, this thesis deals mainly with multiple three-phase induction machines. This is because of the simple construction and wide utilisation of induction machines in industry. It is also worth mentioning that the production cost of high power multiple three-phase drives is less than the same power rated three-phase drives as demonstrated by [Tessarolo (2010)]. This is due to the ability of splitting the power among the *n* number of phases of the multiple three-phase machines. Furthermore, the availability of medium power three-phase power converters is higher compared to high power three-phase converters. On the contrary, control schemes for three-phase machines are well understood compared to multiphase machines. With all the attractive features of the multiphase machines, the adoption rate of them into industry is still small compared to the three-phase machines.

High performance control of multiple three-phase machines' speed or torque is compulsory for a full utilisation of the machine. The most used high-performance control scheme for multiple three-phase machines is the Indirect Rotor-Field Oriented Control (IRFOC). IRFOC, also known as vector control, can be implemented using an MS approach (Multi-Stator) or a VSD (Vector Space Decomposition) approach. Vector control can be implemented using three different fields i.e. stator, air-gap or the rotor field. Rotor-field oriented control is the simplest among the three especially for synchronous machines. The control implementation is easier utilising the flux and torque producing currents using the synchronous rotating reference frame *d*-*q*, in other words by eliminating the time-dependent terms (α-β). Multiple vector control (MS approach) is the most widely utilised and it has been investigated for a six-phase induction machine in [Singh et al. (2005)]. On the other hand, vector control utilising the VSD has been investigated for six-phase induction machines with auxiliary current control [Che et al. (2014c)] and for nine-phase machines [Subotic et al. (2015)]. High-performance control of multiple three-phase machines is not limited to vector control, there are other control schemes such as Model Predictive Control (MPC) [Rubino et al. (2018b)], Direct Torque Control (DTC) [Bojoi et al. (2005a)] and many others [Riveros et al. (2013)], however, it is the most common among them.

Auxiliary current control of multiple three-phase machines has been reported for six-phase induction machines in [Che et al. (2014c)] and for twelve-phase machines in [Tani et al. (2013)]. Both works utilise the auxiliary currents to achieve different objectives. The former being to eliminate the dead-time effect and the asymmetry introduced by the machine's windings while the latter utilised them to achieve post-fault operation of the twelve-phase machine. Furthermore, current control can be employed to achieve power sharing among the winding sets of the machine as proposed in [Zoric et al. (2018)] where the sharing among the winding sets takes place while all the winding sets are in motoring mode or generation mode. Since the auxiliary currents (*x*-*y*) have low impedance compared to the flux and torque producing currents, a significant current can flow if asymmetry in the winding set exists. Therefore, it is always necessary to control all the currents of multiphase machines in the synchronous

reference frame (*d-q* and *x-y*) [Jones et al. (2009)]. Another technique for controlling the individual winding sets' currents is to use an MS approach (multiple vector control), where each winding set *d-q* currents are controlled using two PI regulators as in [Bojoi et al. (2003), Hua et al. (2006)]. However, by using this approach it is necessary to decouple the coupling between the winding sets [Zabaleta et al. (2017), Zabaleta et al. (2018)]. As mentioned earlier, the MS modelling approach along with the multiple vector control is the most commonly found method in industrial applications.

Interest in the multiple three-phase machines has increased in recent years especially in the high-power applications. The development of new machines is always accompanied by numerous tests. The most common is the full-load test, in which the machine is loaded from zero up to the full load. From this test various characteristics of the machine (e.g. efficiency, temperature rise curve – provided that thermal sensors are built into the machine, etc.) can be obtained before the machine is placed into production. A common method for performing the full-load test is by coupling the tested machine mechanically with another one, which behaves as a load. During this test, back-to-back configuration of the machines and the converters (used to supply tested and loading machine) is commonly used [Trout (1935), McSharry et al. (1998), Tada et al. (2017)]. Testing the high-power machines in this way is time-consuming and costly, meaning that alternative methods to perform full-load test have been developed. Several options to perform the test, without the need to couple the tested machine with another one, are available for three-phase machines, including: the two-frequency method [Meyer and Lorenzen (1979)], phantom loading [Fong (1972)] and the inverter driven method [Sheng and Grantham (1994), Soltani et al. (2002)]. From the perspective of the temperature rise, these methods are equivalent to the back-to-back method and the effective voltage and the stator current are equal to the rated values of the machine [Ho and Fu (2001)]. The difference is that the back-to-back configuration can recirculate the power while these methods cannot (and hence are accompanied by high power losses). In the back-to-back configuration, if the dc-links of the used converters are connected, the only power taken from the supply will be for the losses of the machines and the power electronics converters. However, this way of testing is still very expensive for the electrical machines with high power rating (a few MW wind turbine).

A somewhat different approach for regenerative testing of concentrated winding permanent magnet synchronous machine under the full-load condition, without the need for mechanical coupling, has been introduced in [Luise et al. (2012a), Luise et al. (2012b)]. In this method the power is circulated between the different sections of the machine. The machine had four three-phase sections; hence, two opposite sections were connected in parallel and supplied by two three-phase converters with common dc-link. One converter operated in generation and the other in motoring mode. This system can be also observed as a multiphase system. As the control was done independently for each converter, one can say that it corresponds to multiple *d-q* (or MS) control approach of a multiphase machine [Levi et al. (2007)].

1.3 RESEARCH OBJECTIVES AND NOVELTY

The aim of this research is to explore the possibility of connecting multiple energy sources to a single multiple three-phase machine and to independently control the power flow of each source passing through the multiple three-phase machine. This thesis is based on current sharing strategy among multiple three-phase machines which is established in [Zoric (2018)]. This thesis adds to the work of [Zoric (2018)] in terms of considering simultaneous motoring and generation of the winding sets which was not tackled there. The aforementioned will be achieved by completing the following objectives:

1) To develop a mathematical model of the multiple three-phase induction machine using the phase variable reference frame and the VSD transformation for symmetrical and asymmetrical configurations of the machine. Additionally, the VSD transformation matrices are generalised for symmetrical and asymmetrical configurations with a single neutral point or multiple neutral points.

2) To develop a high-performance control scheme for multiple three-phase machines utilising field-oriented control. Furthermore, in addition to controlling the flux and torque producing currents, the non-producing flux and torque currents are also controlled to eliminate any asymmetry between the windings of the multiphase machines.

3) To understand the correlations between the MS and VSD modelling approaches. By understanding the mapping of the individual winding sets' currents into the auxiliary currents of the VSD, the ability to control the winding set currents individually utilising the VSD instead of the MS approach is conceivable.

4) To develop a current sharing strategy among the winding sets of multiple three-phase machines. The developed current sharing strategy is based on the VSD and general for induction and synchronous machines in symmetrical and asymmetrical configurations.

5) To develop a power sharing strategy among the winding sets of the multiple three-phase machines. The power sharing strategy is based on the current sharing strategy. The energy can be transferred from one energy source to another using the machine instead of using additional DC-DC converters.

6) To develop an efficient power sharing strategy among the energy sources connected to a single multiple three-phase machine. The efficient power sharing strategy is based on sharing the torque producing currents only rather than sharing the flux and torque producing currents as in the power sharing strategy developed in 5).

7) To validate the developed current sharing, power sharing and efficient power sharing schemes for symmetrical and asymmetrical induction machines by simulation and experimental results using Matlab/Simulink and dSPACE rapid prototyping platform, respectively.

8) To develop a control strategy based on FOC for double-winding multiple three-phase machines (multiphase machines where each winding has its corresponding (double) winding set spatially shifted by zero electrical degrees) utilising combination of both VSD and MS approaches. The developed control scheme is further improved by controlling the auxiliary currents to achieve current, torque and efficient power sharing among the all windings sets.

9) To develop a synthetic loading scheme for multiple three-phase machines utilising VSD and FOC. The scheme is based on loading the multiple three-phase machines utilising their own winding sets.

10) To evaluate the developed regenerative test schemes for induction machines by simulation and experimental approach.

The novelty of the conducted research comes from the completion of objectives 4 to 10 which are mentioned above. Furthermore, the development of multidirectional power flow control among double-winding machines with multiple three-phase winding sets [Abduallah et al. (2017)], the ability to direct the power from one sub-machine to another and from one winding set to another using a hybrid control scheme between the vector control and double vector control is the main novelty of this work. The developed control scheme is applicable for both symmetrical and asymmetrical machines. Furthermore, a synthetic loading scheme has been developed for symmetrical and asymmetrical six-phase machines utilising a unique *y*-current component, as reported in [Abduallah et al. (2018a)]. The six-phase machine is tested at nominal stator currents while circulating the power between the two winding sets. Furthermore, a regenerative test for nine-phase machines with triple three-phase winding sets has been developed utilising a modified power sharing strategy and presented in [Abduallah et al. (2018b)]. Finally, the regenerative test utilising a single and unique *y*-current component for multiple three-phase machines with an even number of neutral points has been investigated. The main contribution of this work is in reducing the complexity and the number of current controllers required to implement the test. The proposed regenerative test is equivalently applicable to synchronous and induction machines; however, the outcome of the test is different for each type. The proposed regenerative test can be utilised to test the synchronous machine's efficiency and thermal design. It can also be applied to an induction machine in-order to segregate the machine's losses experimentally.

1.4 ORGANISATION OF THE THESIS

This thesis is divided into 9 chapters as follows:

Chapter 1 introduces the multiple three-phase machines in general. A brief discussion of the advantages that multiphase machines possess over three-phase ones and the advantages of multiple three-phase machines over multiphase machines is given. In addition, the recent advancements with regards to modelling approaches, control strategy, current and power sharing plus synthetic loading

techniques are outlined. This chapter is completed with a list of research objectives and a discussion about the novelty and the organisation of the thesis.

Chapter 2 provides a literature survey of the current state-of-the-art in multiphase machines' drives and their applications. The survey covers multiphase machines in general, modelling, current control, current and power sharing, fault-tolerance, synthetic loading and regenerative tests for multiple three-phase machines.

Chapter 3 considers the current sharing strategy of symmetrical multiple three-phase machine. The current sharing control strategy starts with the derivation of the generalised mathematical model of multiple three-phase induction machines in phase variables, the stationary and rotating reference frames. Then, a generalised IRFOC scheme for symmetrical multiple three-phase machines with auxiliary currents control is derived.

Chapter 4 introduces the current sharing strategy for asymmetrical multiple three-phase machine winding sets. Initially, a generalised model of the asymmetrical multiple three-phase machine is derived in phase variable form before moving on to the stationary and rotating reference frame models. Next, the current sharing strategy for asymmetrical multiple three-phase machines is developed.

Chapter 5 considers two power sharing schemes, the first is based on sharing the flux and torque producing currents while the second approach shares the torque producing current only. Therefore, a more efficient power sharing scheme is obtained.

Chapter 6 provides a novel power sharing control scheme for multiple three-phase machines with double winding. This machine can be considered as consisting of two multiphase sub-machines sharing the same stator slots. The scheme is a hybrid scheme between the vector and multiple vector control. Two novel approaches are introduced in this chapter. The first approach is based on sharing the flux and torque producing currents while the more efficient scheme is based on sharing the torque producing current of the sub-machines and of the winding sets.

Chapter 7 develops two novel regenerative testing schemes for multiple three-phase machines. The first one utilises a modified version of the power sharing scheme while the second one uses a unique *y*-current component of the VSD for six-, twelve- and eighteen-phase machines. The approach is applicable to both synchronous and asynchronous machines. However, different outcomes can be obtained depending on the type of the machine under test. The efficiency and temperature rise of the synchronous machines can be determined, while for induction machines, separation of the constant losses from the load-dependent losses is the expected outcome.

Chapter 8 summarises the work done in the thesis and provides conclusions and suggestions for future work.

Chapter 9 provides a list of references used in the thesis.

The last part of the thesis consists of appendices, where in appendix A the current sharing derivation and mathematical model of 15 phase machine is presented. Next, a description of the experimental setup, including hardware and software, is detailed in (Appendix B). Finally, publications resulting from the thesis are listed (Appendix C).

CHAPTER 2

LITERATURE REVIEW

2.1 INTRODUCTION

The literature review in this chapter focuses on the modelling and current control schemes of multiphase machines and their sub-category, multiple three-phase machines. At first, multiphase machines, are surveyed. Further background information, related to modulation schemes, supply options and control methods, is provided next. Special attention is paid to the vector space decomposition (VSD) method, as one of the main and most powerful ways for multiphase machines modelling and control and for MS approach. Then, the existing current control schemes for multiphase machines are revisited. Also, power sharing among multiple three-phase machines is surveyed. Then, a literature review on synthetic loading testing for three-phase machines is presented. Finally, the regenerative test for multiple three-phase machines is revisited at the end of this literature survey.

Prior to the survey of the areas closely related to this research, a short review of multiphase machines is due. Comprehensive surveys of multiphase machines which include the basic properties of multiphase machines, modelling, modulations schemes, control schemes, supplying techniques are available in [Levi et al. (2007), Levi (2008), Barrero and Duran (2016), Duran and Barrero (2016), Levi (2016)]. Other older survey papers [Singh (2002), Parsa (2005)] considered the advantages of multiphase machines such as smaller per-phase currents, lower torque pulsations and other benefits. There are other advantages when compared to high-power three-phase machines concerning the winding and construction of multiphase machines as discussed in [Tessarolo (2010)].

2.2 MULTIPHASE MACHINES AND POWER ELECTRONIC CONVERTERS

Multiphase machine-based variable-speed motor drives and generation systems have gained significant importance over the last two decades, due to several application-related advantages that they possess, when compared to the three-phase counterparts [Levi (2008)]. In addition to the obvious advantages of splitting the power rating over more than three phases and thus reducing the required semiconductor power ratings, there are other advantages possessed by the multiphase machines related to the existence of additional degrees of freedom, as will be discussed shortly.

The most recent advancements and developments of the multiphase technology have been addressed in several survey papers [Barrero and Duran (2016), Duran and Barrero (2016), Levi (2016)]. These papers discuss and explain various aspects of multiphase machines, such as their design,

modelling, control and power supply options. Multiphase machines can be summarised into the following categories [Barrero and Duran (2016)];

1- multiphase induction machines [Abdel-Khalik and Ahmed (2012)],

2- multiphase permanent magnet (PM) machines [Cavagnino et al. (2013)],

3- multiphase synchronous reluctance machines [Labak and Kar (2013)], and

4- multiphase switched reluctance machines.

The first category, multiphase induction machines, represents the most commonly utilised multiphase machines in industrial applications. Multiphase induction machines can be designed to achieve higher torque compared to the three-phase machines and to optimise the magnetic field of the air-gap by the injection of odd harmonics to the stator currents [Abdelkhalik et al. (2010), Pereira et al. (2012), Barrero and Duran (2016)]. There are multiple variants of the second category of the multiphase PM machines [Barrero and Duran (2016)]. Fractional-slot concentrated winding (FSCW) PM multiphase machine is one of these variants which offers numerous advantages such as low cogging torque, high power density, high slot fill factor and high efficiency. These benefits make them very attractive to the automotive industry and for some high-frequency applications [Zheng et al. (2013), Sui et al. (2014)]. On the other hand, their excessive rotor losses are the main downside in high-speed applications because they have large spatial harmonic components [Boglietti et al. (2014)]. The torque density and efficiency can be enhanced by increasing the number of rotor poles. Multiphase PM machines can be categorised from the rotor's construction point of view as surface and interior PM (SPM and IPM) machines [Scuiller et al. (2009), K. Wang et al. (2014)]. The IPM corresponds to the salient-pole rotor machines (since permeability of permanent magnets is very close to the permeability of the air, thus causing considerably higher magnetic reluctance in the rotor area where the magnets are embedded, compared to the rotor area where there is only ferromagnetic material). On the other hand, the SPMs behave like the machines with a cylindrical rotor structure [Levi et al. (2007)]. The brushless PM machine (BPM) is another variant of the PM multiphase machines, which generates the highest torque density [Ede et al. (2007)]. However, the BPM is typically not used in high-performance applications, where precise motion control is required. The synchronous reluctance machine (SRM) falls into the category of the PM-less machines [Labak and Kar (2013)]. The low cost of these machines is the main attraction [Barrero and Duran (2016)]. A modified version of the SRM, which belongs to the category of PM assisted SRMs, is claimed to offer the combined advantages of the BPM and the SRM which is called a flux-switching PM FSPM [Zhu et al. (2009), Xue et al. (2013)]. The last category from the design standpoint for the multiphase machines is the superconducting machines [Wang et al. (2013), J. Wang et al. (2014)]. These machines are still in the early stages of research and development. The structure and design of these machines can avoid the PM availability problems. Also, they have lower

weight and smaller size compared to PM and induction type multiphase machines [Barrero and Duran (2016)].

Carrier-based pulse width modulation (PWM) and space vector modulation (SVM) are the main modulation schemes for the two-level multiphase voltage source inverters (VSIs) [Levi et al. (2007), Levi (2008)]. With appropriate zero-sequence harmonic injection applied to sinusoidal carrier-based PWM, an improvement of the dc-link voltage utilisation can be obtained [Levi et al. (2008)]. However, this improvement in the dc-link utilisation decreases as the number of phases increase. To eliminate the low order harmonics generated in the SVM scheme, a total of n-1 space vectors should be applied in each sector [Iqbal and Levi (2005)]. Thus, to generate a sinusoidal output with a higher phase number machine, a huge number of switching states should be considered and applied. Multi-frequency space vector generation is where the concept of space partitioning is applied [Lega et al. (2009)]. A general approach of PWM generation of multiphase VSIs has been developed in [Lopez et al. (2008), Lopez et al. (2009)].

Another important configuration is the multilevel converter supplied multiphase machine where the high-power are the main user for this configuration. Using multilevel VSIs enables the increase of the drive voltage rating whereas increasing the number of phases enables an increase of the drive current rating. The multilevel VSIs such as neutral point clamped (NPC) [López et al. (2016)], cascaded H-bridge (CHB) [Choi et al. (2014)] and flying capacitor [Cheng and He (2016)], are the most commonly used multilevel topologies. However, NPC and CHB topologies are dominant in the field of single-sided supplied multilevel multiphase machines. There are various modulation schemes for the multiphase VSIs, which are extensions from the multilevel three-phase VSIs modulation schemes. For instance, the level shifted PWM (LS-PWM) [Kim et al. (2016)] and the phase-shifted PWM (PS-PWM) [Capella et al. (2015)] are the most common carrier-based modulation techniques for multilevel multiphase VSIs. In-phase disposition (PD-PWM), phase opposition disposition (POD-PWM) and alternating phase opposition disposition PWM (APOD-PWM) techniques are some examples of LS-PWM. The least distorted voltage waveforms can be obtained from the PD-PWM technique. On the other hand, the development of the SVM technique for multi-level multiphase VSIs can be difficult due to the huge number of switching states. The switching states increase as the number of phases and number of levels increase [Dordevic (2013), Levi (2016)].

The dual-sided supplied multiphase drive topology relies on the use of open-end winding (OeW) machines [Levi et al. (2012), Chowdhury et al. (2016)]. The OeW topology possesses several advantages over the single-sided supply topology, such as use of the inverters with lower dc-link voltages, increased fault tolerance and absence of the need for the dc-link voltage balancing hardware. Modulation methods, used for single-sided supply topologies, can be easily modified and equally applied to the OeW case. The PD-PWM technique offers the best voltage THD profile for the three-phase and five-phase dual-

inverter supplied machines. Alternatively, by considering the current THD profile, APOD-PWM and PS-PWM offer the best performance. However, APOD-PWM offers lower CMV instantaneous values compared to PS-PWM [Levi (2016)].

Multiphase ac-ac converters such as matrix converters (MC) have attracted researchers in the last few years [Ahmed et al. (2015), Levi (2016)]. The main advantage of this topology is absence of the dc-link and bulky dc-link capacitor. However, the biggest disadvantage of the MC is the limited output to input voltage ratio in the linear modulation region. By utilising the SVM technique, an increase of this ratio for a three-to-five phase MC can be noticed (from 76.2% to 78.86%), compared to the adapted carrier-based PWM method. The ratio of the output to input voltage of the MC depends on the number of input and output phases. For instance, the output to input voltage ratio is as high as 112% for a nine-to-three phase MC while it is reduced to 76.2% when the MC operates as a three-to-nine phase converter. Nevertheless, the MC can be used in a dual-sided supply for the OeW multiphase machines and its output voltage is significantly increased in the linear modulation region when compared to the case when the MC is used as a single-sided supply.

Multiphase machines, when compared to their three-phase counterparts, offer some other advantages due to the existence of additional degrees of freedom. The non-traditional use of these degrees of freedom is described in [Levi et al. (2007), Levi (2008), Levi (2016), Subotic et al. (2016d)]. Some of the most interesting applications of these additional degrees of freedom are the single multiphase VSI supplying multi-motor drives and the integrated on-board battery chargers for EVs. The multi-motor drive application can be realised by connecting the motors in series or in parallel connection. Utilising multi-motor drives in series connection is a viable solution when they are supplied by a single inverter and controlled using field-oriented control (FOC), however, the multi-motor system connected in parallel has no prospect for applications in the real world [Levi (2016)]. Another possible application utilises the degrees of freedom for integrated on-board battery chargers for EVs. These chargers consist of a multiphase machine and converter only. The concept of this charger is to utilise the stator winding of the multiphase machines as a filter [Subotic et al. (2014), Subotic et al. (2015), Subotic et al. (2016a), Subotic et al. (2016b), Subotic et al. (2016c), Subotic et al. (2016d)]. For example, if a nine-phase machine is used, fast charging of the EV's batteries is possible by connecting the three-phase mains to the three neutral points of the multiphase machine (each winding set with three phases has an isolated neutral point). This will provide fast charging of the batteries while avoiding generation of a rotating field (torque). The converter will have dual functionality such that it will be used as a rectifier during the charging mode and as an inverter during vehicle-to-grid (V2G) mode. This charger topology is equally applicable for symmetrical and asymmetrical induction or PM multiphase machines [Levi (2016)].

2.3 MULTIPHASE MACHINE MODELLING

High performance control of the multiphase machines requires an accurate and appropriate mathematical model of the multiphase machine. The mathematical model in phase variable domain is the most obvious choice while modelling multiphase machines [Dordevic et al. (2010)]. Using phase variables, the multiphase induction machine is represented by a mathematical model consisting of $2n+1$ differential equation. However, the model complexity is the main obstacle against implementing the control in this domain and so to design and implement accurate control methods different transformations are used.

For multiple three-phase machines, a decoupling transformation is usually employed. For instance, the MS modelling approach introduced in [Nelson and Krause (1974)] is based on [Park (1929)] where a three-phase synchronous machine is represented in a synchronous reference frame (*d*-*q*-0). To apply the decoupling transformation for multiple three-phase machines, each three-phase winding set can be modelled as a separate three-phase machine as in [Nelson and Krause (1974), Lipo (1980)]. This Multi-stator approach decouples each winding set into separate torque and flux producing currents. Therefore, six-phase machines can be easily controlled using this modelling approach, as shown in [Singh et al. (2005)] where a six-phase induction machine is considered. By aligning the *d*-axis with the rotor flux of the machine, an indirect RFOC is obtained in this paper. The MS approach is applied to a nine-phase machine with triple three-phase winding sets for an ultra-high speed elevator application in [Jung et al. (2012)]. In [Rubino et al. (2016)], the author utilised the MS modelling approach to control a twelve-phase stator/generator for an electric aircraft application where high fault tolerance machines are necessary. Controlling multiple three-phase machines utilising the MS modelling approach is combined with the necessity for decoupling the cross coupling between the winding sets [Camillis et al. (2001), Kallio et al. (2013)]. In addition, low order harmonics introduced by the non-ideal design of the machine and dead-time effect of the converter, cannot be easily eliminated when this modelling approach is utilised. Finally, this approach is applicable only to multiple three-phase machines.

Developing a decoupled machine model is possible using Clarke's decoupling transformation. Clarke's decoupling transformation can be considered as a special case of the symmetrical components theory originally developed by [Fortescue (1918)]. This theory has been used in [Zhao and Lipo (1995)] to develop the VSD modelling approach for an asymmetrical six-phase induction machine. by utilising the decoupling transformation, multiphase machines with an odd number of phases, *n*, can be resolved into $(n–1)/2$ independent planes and one zero-sequence axis, while the ones with an even number of phases produce $(n–2)/2$ independent subspace plus two zero-sequence axes. The decomposition approach of the three-phase machine can be extended to multiphase machines using the VSD approach [Zhao and Lipo (1995)]. In these papers, a dual three-phase machine is decomposed, starting with a six-dimensional vector space, into three two-dimensional orthogonal subspaces (the third subspace 0_1-0_2

was formed by two orthogonal zero-sequence axes). Therefore, a six-phase machine model can be represented with three groups of decoupled equations. The authors have proven that these subspaces are orthogonal to each other. The first subspace is denoted as *d-q*, while the others are denoted as x_1-y_1, x_2-y_2 and so on. The fundamental components of the machine variables map into the *d-q* subspace and these variables are responsible for the electromechanical energy conversion. The remaining (x_i-y_i) subspaces are responsible for non-electromechanical energy conversion, where the non-zero-sequence harmonics map. The zero-sequence harmonics map into the 0_1-0_2 subspace. The VSD modelling approach is not as straightforward as the MS modelling approach. Several alternatives have been proposed by researchers [Abbas et al. (1984), Tessarolo (2009b), Tessarolo (2009a), Rockhill and Lipo (2010), Rockhill and Lipo (2015)]. The proposed transformation matrices are comparable to each other and so they uniquely map odd harmonics into the decoupled subspaces.

2.4 MULTIPHASE MACHINE CONTROL METHODS

There are different techniques for controlling the multiphase machines, such as FOC [Bojoi et al. (2005b), Bojoi et al. (2006), Jones et al. (2009), Abdel-Khalik et al. (2012), Hu et al. (2014), Karttunen et al. (2014), Yepes et al. (2015)], direct torque control (DTC) [Bojoi et al. (2005a), Gao et al. (2011), Zheng et al. (2011), Taheri et al. (2012), Karampuri et al. (2014)], predictive torque control (PTC) [Riveros et al. (2013)]. The most frequently utilised control strategy is the FOC, which basically consists of current control loops with an outer speed control loop. Typically, the so-called, indirect rotor FOC (IRFOC) is utilised. Alternatively, the model predictive control (MPC) method [Lim et al. (2011), Guzman et al. (2014), Lim et al. (2014), Rubino et al. (2018a), Tenconi et al. (2018)], has the same structure as FOC but MPC-based controllers are used instead of the inner PI current loop controllers. The DTC approach is difficult to implement for the multiphase machines due to the high number of degrees of freedom, since DTC is typically a two-variable control scheme and hence well-suited to the three-phase machine control (which has only two degrees of freedom). The hysteresis-based DTC scheme leads to the generation of low order harmonics if used in the same way as for a three-phase machine. However, by adding another set of hysteresis controller this problem can be solved [Hatua and Ranganathan (2005), Levi (2008)]. However, the addition of an extra controller complicates the control and removes the main advantage of the DTC over the FOC, which is simplicity [Levi (2008)]. Lastly, the PTC is a suitable alternative to DTC for five-phase machines because it offers faster speed response and better torque dynamics compared to DTC [Barrero and Duran (2016)].

2.5 CURRENT CONTROL SCHEMES FOR MULTIPHASE MACHINES

The dominant high performance control technique, FOC, is typically based on the use of the VSD [Levi (2008)], which concentrates the complete electromechanical energy conversion into a single two-dimensional subspace of the machine, regardless of the phase number. In balanced (i.e. healthy) operation the non-zero currents appear only in the flux/torque producing two-dimensional subspace,

while currents in all the other subspaces are controlled to zero [Che et al. (2014a)]. In the case of a fault or if unbalanced operation of the machine is desirable, it becomes necessary to operate with non-zero currents in the other two-dimensional subspaces [Tani et al. (2013), Che et al. (2014a), Duran et al. (2015)]. To devise a suitable control strategy, an appropriate setting of the current references for the auxiliary subspaces is required [Che et al. (2012b), Tani et al. (2013), Che et al. (2014c), Hu et al. (2014), Liu et al. (2016)]. This control scheme allows the stator currents and power flow of the multiphase machines to be flexibly controlled. It is important to have balanced currents among the multiple winding sets within a machine, so that problems like a reduction of the machine's expected lifetime, reduced performance and efficiency can be avoided. Furthermore, acoustic noise and torque pulsations increase as the degree of current imbalance increases.

In [Tani et al. (2013), Mengoni et al. (2016)] a quadruple three-phase machine, which is supplied using four inverters, is implemented as a starter-generator for aerospace applications. In these applications, a high-level redundancy is a necessity and to achieve this a current control scheme is developed. The IRFOC scheme has been modified in such a way that the control of the auxiliary currents is used to remove the imbalance between the different winding sets and to compensate the dead-time effect and the inverter non-linearity. In this algorithm, the current sharing coefficients of the quadruple three-phase machine are equal, and the auxiliary (fifth, seventh and eleventh harmonic) current harmonics are set to zero. When the degree of the current's imbalance is small, the current sharing coefficients could be seen as instantaneous power sharing coefficients. The management of the current amplitudes among the quadruple inverters is accomplished by using the auxiliary currents, which are considered as degrees of freedom. Nevertheless, the rotor flux and the torque are controlled using *d-q* components of the stator current in the synchronously rotating common reference frame. The fifth and eleventh current harmonic are controlled in another reference frame, which is an anti-synchronously rotating reference frame. This is so since they are proportional to the conjugate of the fundamental output current vector. On the other hand, the seventh current harmonic rotates in the same direction as the fundamental output current vector and hence the same synchronous reference frame is used as for the first harmonic.

Current balancing techniques for asymmetrical six-phase machines have been developed and implemented in [Hu et al. (2014)] and [Che et al. (2014c)]. The main difference between these two papers is the consideration of the fifth and seventh harmonics (produced due to the non-sinusoidal back electromotive force (EMF) and the non-linearity of the VSI, which are considered in [Hu et al. (2014)] but not by [Che et al. (2014c)]. However, [Hu et al. (2014)] considers the six-phase permanent magnet machine, while [Che et al. (2014c)] considers the six-phase induction machine. Although the performance of the permanent magnet machine utilising this control scheme is excellent, a small impact is noticeable in the torque performance during the transient state. The proposed scheme yielded the possibility for larger imbalance compensation; however, the complexity of the system is increased

compared to [Che et al. (2014c)]. The authors of [Liu et al. (2016)] use the symmetrical component theory to detect the imbalance between the currents and propose a novel RFOC method. By implementing the proposed scheme, the torque ripple is reduced thus increasing the motor's lifetime. The proposed RFOC and the conventional RFOC schemes are tested using symmetrical five-phase and nine-phase induction machines. As a result, the current imbalance is reduced from 13.86% to 1.62% for the symmetrical five-phase drive, while for the nine-phase drive it is reduced from 9.48% to 1.89% by utilising the proposed RFOC approach.

2.6 POWER SHARING AMONG WINDING SETS

The utilisation of multiple energy sources supplying a single multiple three-phase machine has gained interest among researchers recently. Hybrid energy storage systems (HESSs) based on battery and super-capacitors is a practical solution to improve the power and energy density of the energy storage system on EVs [Kuperman et al. (2013), Kollimalla et al. (2014), Hu et al. (2016a), Hu et al. (2016b), Hu et al. (2018)]. By utilising this combination of HESSs, the battery will provide the average load demand and the super-capacitors will provide the dynamic load current [Hu et al. (2018)]. There are several configurations where HESSs can be connected. Dual three-phase machines are a common choice for utilising this hybrid energy storage system, where each three-phase winding set is connected to a different energy source. The benefits of utilising the well-established three-phase power electronics technologies and the fault-tolerance capabilities plus the ability of being supplied by different energy sources is a distinctive feature of the multiple three-phase machines. Although batteries and super-capacitors are a viable option for EVs, other energy sources can also be integrated such as Fuel-cells and PV cells. Depending on the application, the HESSs' sources can be chosen. Usually these machines are controlled using multiple vector control which utilises the MS modelling approach. The ability to control each three-phase winding set separately is the main advantage of multiple vector control. However, the mutual coupling between the winding sets is the main disadvantage of this control scheme as mentioned earlier. The alternative is to control the machine using vector control utilising the VSD for multiple three-phase machines. The machine model will be completely decoupled after applying the VSD transformation. Through controlling α-β currents and the auxiliary currents, the ability to control the winding sets' current separately is possible. The power sharing control scheme utilising the VSD modelling approach for multiple three-phase machines has been introduced in [Zoric et al. (2018)]. The power sharing scheme focused on sharing the motoring power only, in other words, simultaneous motoring and generation between the different winding sets of the machine was not investigated.

There are several practical applications of the multiple three-phase machines such as, more-electric aircraft [Grandi et al. (2010), Tani et al. (2013), Mengoni et al. (2016)] and electric vehicles (EVs) [Subotic et al. (2016a), Subotic et al. (2016b), Subotic et al. (2016c), Subotic et al. (2016d)]. In the latter application, the electrical power generation and distribution systems are expected to rise from

the conventional low dc voltage to a higher dc voltage level in the near future. This will reduce the system losses and size as well [Scarcella et al. (2016)]. Furthermore, new starter-alternator topologies with a different number of turns per winding layer are introduced in [Scarcella et al. (2016)], the motivation being to accommodate multiple dc voltage levels (dc-bus voltage level of the corresponding VSIs), present in such systems. The starter-alternator is a multiple-winding three-phase induction machine, where each three-phase winding represents a sub-motor. The authors used a multiple vector control scheme in order to achieve multidirectional power flow between the multiple three-phase sub-motors. Obviously, multiple three-phase machines can also be categorised as a type of multiphase machine. However, multiple vector control is not the best approach to control multiphase machines as mentioned earlier.

Based on the survey papers [Levi (2008), Barrero and Duran (2016), Duran and Barrero (2016), Levi (2016)] in the last three years, there have been several attempts to provide motoring and generation at the same time as in [Scarcella et al. (2016), Zabaleta et al. (2018)]. Such work would enable the realisation of a dual-function distributed winding machine with multiple electrical inputs/outputs. Achievement of the stated goal may be easier with permanent magnet machines of modular design, due to the absence of the magnetic coupling between stator phases. Such a concentrated winding six-phase machine is considered in [Mese et al. (2016)] for low-power hybrid electric vehicle accessory drives. The specifics of the application mean that the role of the two windings is fixed. One of them does the generation in all operating regimes, while the other either motors or is idle, depending on the status of the ICE.

2.7 FAULT TOLERANCE

Fault-tolerant operation of multiple three-phase machines is of great interest for critical industrial applications such as wind farms and electric aircraft. Furthermore, continuous operation of remote wind energy conversion systems is highly desirable for stakeholders because interrupted operation can result in a significant loss of energy and revenue. Due to their high reliability, multiple three-phase machines represent an obvious solution for these applications. A fault of one or more semiconductor switches of the VSI is considered as an inverter fault whereas a short or open connection of the three-phase winding set phases will be considered as a machine fault.

An accurate fault detection method and post fault machine model must be considered first in order to implement an effective fault tolerant control algorithm. In [Apsley and Williamson (2006)] the stator windings of the machine are represented as a set of coils where the impact of each coil on the back MMF is calculated and its harmonic content analysed. This approach is quite complex to realise in real-time applications. Another approach to detect faults for odd phase number multiphase machine is proposed in [Zarri et al. (2011)]. The approach is based on determining the type of imbalance between the phases' currents such that the faulty phase can be detected.

Fault tolerance operation can be achieved for multiple three-phase machines more easily than for multiphase machines since a simple disconnection of a three-phase voltage source inverter is an obvious solution. Different performance can be obtained under fault tolerance operation depending on the winding configuration which provides different impact on magneto-motive force as investigated in [Alberti and Bianchi (2012)] for dual three-phase machines. The authors emulated the open-circuit fault and short circuit fault for dual three-phase machines with different winding configurations and compared the obtained experimental results for each one of them. They have found that the no-load current increased to 1.8 times the no-load current during the healthy operations for all winding configurations when one winding set is disconnected. However, the under-load test produced different results for each configuration under open-circuit fault and short circuit fault. Another approach of achieving the fault tolerance operation for multiple three-phase machines is by supplying each three-phase winding set with two parallel connected VSIs [Duran et al. (2016), Gonzalez-Prieto et al. (2016)]. If a fault occurs in one of the phase's legs, half of the rated current can be supplied using the leg from the parallel VSI. The suitable current references of the machine under post-fault operation is calculated using optimisation software. The mechanical impact on the machines under fault tolerance operation was not considered. Unequal flux distribution among the machine's circumference will lead to a vibration of the machine. To compensate for the lost phases, the machine magneto-motive force should be kept at rated value. This means increasing the healthy phase's currents. The analysis for three-, five- and seven-phases machines have been shown in [Fu and Lipo (1994)]. Using this method means an increment in the copper losses of the healthy phases. In [Apsley (2010)] two strategies for post-fault operation of a six-phase machine are developed. The first is to minimise the copper losses and the other equalizes the currents in the healthy phases. Reducing torque ripples in the post-fault operation for six-phase machines is proposed in [Kianinezhad et al. (2008)]. The work investigates post-fault operation with up to three phases open. In [Tani et al. (2012)] three different strategies have been proposed for post-fault operation with open-phase in odd phase number multiphase machines. The first targets minimum copper losses while the second minimum current amplitude. The second approach achieves minimum torque oscillations. Another approach to operate multiphase machines in post fault operation is to control the machine using a model that excludes the faulty phases. This approach is used for a six-phase machine in [Deilamani et al. (2011)] and for a five-phase machine in [Guzmán et al. (2012)].

2.8 SYNTHETIC LOADING

To validate the design of a newly developed machine, multiple tests should be conducted. For example, in order to find the efficiency of the machine at different operating points over the wide range of speed and torque, full-load test or the back-to-back test is usually conducted first. In this way, the efficiency and the temperature rise curve can be obtained before the machine is placed into production. The back-to-back configuration is obtained by coupling the tested machine's shaft with another machine's shaft using a mechanical coupling. The back-to-back configuration has its limitations such as

time consumption, high cost and required resources to align the coupled machines. Other alternatives to perform the full-load test, without the need to couple the tested machine with another one, have been proposed in the literature such as the two-frequency method [Meyer and Lorenzen (1979)], phantom loading [Fong (1972)] and the inverter driven method [Sheng and Grantham (1994), Soltani et al. (2002)]. The proposed alternatives are equivalent to the back-to-back technique in terms of stator currents and effective voltages [Ho and Fu (2001)]. However, these alternative methods do not have ability to recirculate the power, which is an important feature of the back-to-back configuration. During the back-to-back configuration test, the power withdrawn from the grid is equal only to the losses of the machines and their converters. On the other hand, for the above mentioned alternatives used power is equal to the rated power of the machine under the test. Nevertheless, the back-to-back configuration way of testing is still very expensive for the electrical machines with high power rating (for example a few MW wind turbines).

Another alternative, that eliminates mechanical coupling and the usage of another machine, has been proposed by [Luise et al. (2012a), Luise et al. (2012b)] for the interior permanent magnet machine. The analysed machine has four three-phase sections. For testing purposes, the opposite sections were connected in parallel and supplied by two three-phase converters with a common dc-link. The first converter is controlled using the speed as a control variable, while the second converter used the torque as a control variable. This system can be also seen as a multiphase machine (twelve-phase machine) controlled using multiple *d-q* (or multi-stator, MS) control approach.

In [Zabaleta et al. (2018)] the basic idea of [Luise et al. (2012a), Luise et al. (2012b)] has been extended to six-phase permanent magnet machine. The implementation of the multiple vector control in [Luise et al. (2012a), Luise et al. (2012b)] was straightforward due to the construction of the machine (four three-phase sections). On the other hand, the proposed regenerative test in [Zabaleta et al. (2018)] is more involved due to the different construction (coupling is present). The winding is distributed with zero phase shift between the three-phase winding sets which requires full decoupling compensation.

Recent literature surveys [Levi (2008), Barrero and Duran (2016), Duran and Barrero (2016), Levi (2016)] show that the main interest in multiphase systems exists in the electric transportation (locomotive traction, electric ship propulsion, EVs, etc.) as discussed in [Subotic et al. (2015), Subotic et al. (2016b), Subotic et al. (2016a)]. More-electric and full electric aircraft developments are considered in [Tani et al. (2013), Mengoni et al. (2016)] whereas remote offshore wind energy generation is investigated in [Ditmanson et al. (2014)]. For safety-critical applications (such as an electric aircraft) solutions with modular permanent magnet machine design and single-phase H-bridge supply of each phase are preferred. The dominant solution for all the other applications is a multiphase machine with distributed winding configuration (near-sinusoidal magneto-motive force distribution) and multiphase bridge power electronic converter [Tani et al. (2013), Mengoni et al. (2016)]. Machines

of this construction (synchronous or induction) are characterised with strong coupling between the phases, which makes the achievement of the postulated goals (synthetic loading, as well as independent power flow control, with both positive and negative sign, in various sub-systems) difficult to achieve with the current knowledge.

2.9 SUMMARY

In this chapter, a literature review of the multiphase machines and control schemes is presented. The literature review starts with revising multiphase machines' categories and advantages. Some of the early works about the multiphase machines are surveyed first. Afterwards, various aspects are revisited such as design, modelling, control and power supply options. Next, the modulation schemes for two level and multi-level multiphase VSIs are surveyed. Then, two modelling approaches (VSD and MS) of the multiphase machines are discussed. Furthermore, the different high-performance speed/torque control methods such as DTC, PTC, MPC and FOC are reviewed. A brief survey about current control methods for multiple three-phase machines has been included along with a review of the power sharing methods among single and double winding machines. Since this research will consider some aspects of fault tolerance, a survey on fault tolerance schemes for multiphase machines is included. Finally, the synthetic loading of three-phase and multiphase machines is examined in order to establish the uniqueness of the approach taken in this thesis.

CHAPTER 3

CURRENT SHARING FOR SYMMETRICAL MULTIPLE THREE-PHASE INDUCTION MACHINES

3.1 INTRODUCTION

This chapter considers design of a control scheme for current sharing between multiple three-phase winding sets within a symmetrical multiphase induction machine. A general *n*-phase induction machine model and control scheme are derived first, followed by the derivation of the current sharing technique between the multiple winding sets. The machine control scheme is developed based on the well-known indirect rotor flux-oriented control (IRFOC) scheme for the three-phase induction machines.

The chapter is organized as follows: In Section 3.2 a generalised mathematical modelling approach of the symmetrical multiphase induction machines is introduced. A few assumptions have been considered here to simplify the modelling and simulation process. Then, in section 3.3, Clarke's decoupling transformation for multiphase induction machines is introduced. The decoupling transformation decouples the machine flux/torque producing subspace from the losses producing subspaces. Next, in section 3.4, the common reference frame, or the rotational transformation, is presented, where the time-dependent terms introduced by Clarke's decoupling transformation are eliminated. In section 3.5, the generalised modelling of the multiple three-phase machines is introduced. Furthermore, introduced transformations are used to implement the IRFOC scheme of the multiphase induction machine, which is explained in section 3.6. The IRFOC scheme controls electromechanical energy subspace only. However, in order to minimise the losses and also control the current amplitude in each winding set, the auxiliary currents of the machine need to be controlled as well. Accordingly, section 3.7 presents the derivation of the current sharing scheme between the different winding sets by controlling the auxiliary currents and the electromechanical subspace simultaneously. Next, the machine model and control system are validated using Matlab/Simulink. The simulation and experimental results for a symmetrical triple three-phase machine (i.e. nine-phase machine), at different operating scenarios and with different control schemes, are presented in section 3.8 and 3.9, respectively. Finally, a summary of the chapter is given in section 3.10.

3.2 MODELLING OF MULTIPHASE INDUCTION MACHINES

Induction machines are widely utilised in industrial applications. Multiphase, as well as three-phase, induction machines operate based on the principle of the rotating field. The field is created by the spatially shifted machine's phases by an angle equal to the phase shift of the supplying multiphase

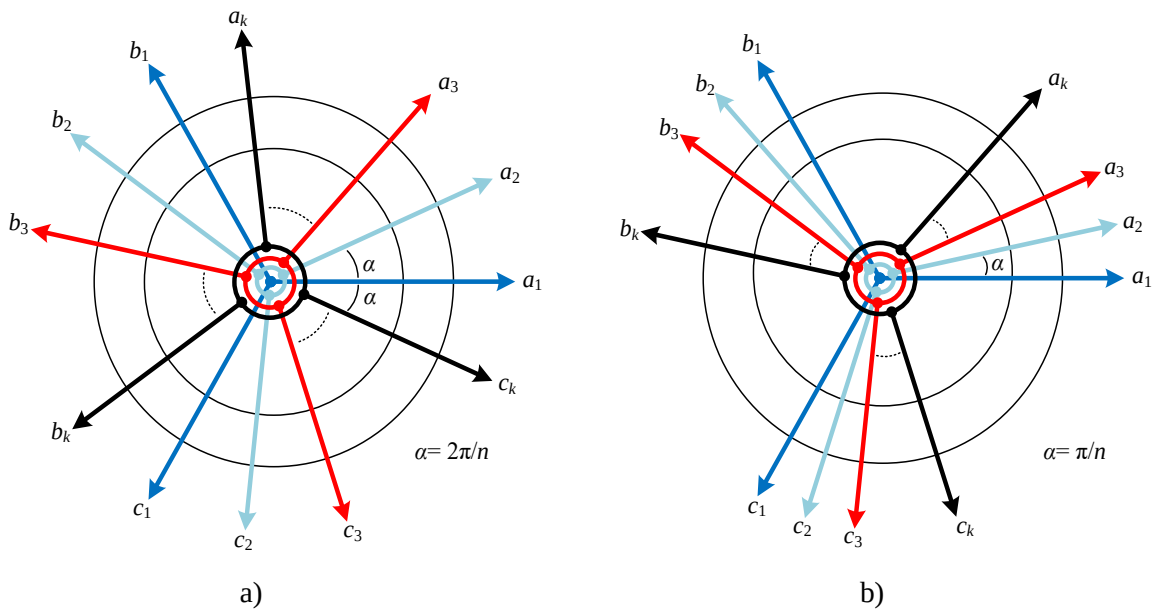

Fig. 3.1: Illustration of the a) symmetrical and b) asymmetrical stator magnetic axes for *n*-phase induction machine with multiple isolated neutral points.

currents. The fundamental harmonic of the supply is responsible for generation of the rotating field which rotates at the synchronous speed. However, the rotor of the induction machine rotates at the speed which is different from the speed of the rotating field (synchronous speed); thus induction machines are often termed as asynchronous machines [Levi et al. (2007)]. There are two different types of multiphase induction machines, symmetrical and asymmetrical multiphase machines, as illustrated in Fig. 1.1 (*n* represents the number of phases of the machine). The current sharing scheme introduced in this chapter is developed for the symmetrical multiphase (multiple three-phase) induction machines only.

In recent years, different mathematical models and mathematical transformations for the phase variables of the multiphase induction machines have been introduced [Singh (2002), Levi et al. (2007), Levi et al. (2008)]. The aim of these transformations is to simplify and to develop the machine's mathematical model, which describes its behaviour and the electromechanical energy conversion, using the equations with time invariant parameters only. This is desirable because in the original phase-variables reference frame, the inductances are time dependent, which significantly complicates modelling and especially control. In order to simplify the equations and convert the induction machine into its dc machine equivalent, fictitious variables are introduced by these transformations to decouple the control of the machine's flux and torque. In order to model the machine, and simplify the phase-variables model, the model is developed based on the following assumptions [Levi et al. (2007), Levi et al. (2008)].

1- The spatial shift between any two consecutive phases is equal to $\alpha = 2\pi/n$. This angle is in electrical degrees, i.e. it is assumed that the machine is first reduced to a single-pole pair machine. Hence, the analysed machine is symmetrical *n*-phase machine.

2- Identical and symmetrical windings of the individual phases are assumed.
3- The design of the winding ensures sinusoidal distribution of the flux around the air-gap (all the non-fundamental harmonics are neglected).
4- The impact of the stator and rotor slotting is neglected so that the air-gap is considered uniform and circular.
5- The resistance of the stator and rotor winding is assumed to be constant (skin effect and temperature variation are neglected).
6- The leakage inductance is assumed to be constant.
7- The magnetizing characteristic of the ferromagnetic materials is linearized. Thus, the mutual inductances are considered to be constant.
8- The parasitic capacitance, hysteresis and eddy current are neglected. Thus, corresponding losses are neglected also.
9- For simplicity, the rotor phase number is considered to equal the phase number of the stator.

Based on the previous assumptions, a generalised mathematical model, for an *n*-phase symmetrical induction machine, in the phase-variable reference frame, will be presented first. Later on, in this chapter, a symmetrical nine-phase induction machine will be considered, and a decoupled model will be developed starting from the generalised model.

The voltage equilibrium equations of the stator and rotor follow from the simple application of Kirchhoff's law due to the resistive-inductive nature of the windings, as in the following equations:

$$[v_s] = [R_s][i_s] + \frac{\mathrm{d}[\psi_s]}{\mathrm{d}t} \tag{3.1}$$

$$[v_r] = [R_r][i_r] + \frac{\mathrm{d}[\psi_r]}{\mathrm{d}t} \tag{3.2}$$

Where *v, R, i* and ψ stand for the instantaneous values of the phase-to-neutral voltage, winding resistance, phase current and the flux-linkage, respectively. The *s* and *r* in index represent the variables belonging to the stator or the rotor, respectively. Equations (3.1) and (3.2) are written in the matrix form. The voltage, current and flux-linkage matrices are expressed as follows:

$$[v_s] = \begin{bmatrix} v_{1s} & v_{2s} & v_{3s} & \cdots & v_{ns} \end{bmatrix}^T \tag{3.3}$$

$$[v_r] = \begin{bmatrix} v_{1r} & v_{2r} & v_{3r} & \cdots & v_{nr} \end{bmatrix}^T \tag{3.4}$$

$$[i_s] = \begin{bmatrix} i_{1s} & i_{2s} & i_{3s} & \cdots & i_{ns} \end{bmatrix}^T \tag{3.5}$$

$$[i_r] = \begin{bmatrix} i_{1r} & i_{2r} & i_{3r} & \cdots & i_{nr} \end{bmatrix}^T \tag{3.6}$$

$$\left[\psi_s\right]=\left[\psi_{1s} \quad \psi_{2s} \quad \psi_{3s} \quad \cdots \quad \psi_{ns}\right]^T \tag{3.7}$$

$$\left[\psi_r\right]=\left[\psi_{1r} \quad \psi_{2r} \quad \psi_{3r} \quad \cdots \quad \psi_{nr}\right]^T \tag{3.8}$$

The resistance matrices are defined as:

$$\left[R_s\right]=\begin{bmatrix} R_{1s} & 0 & 0 & \cdots & 0 \\ 0 & R_{2s} & 0 & \cdots & 0 \\ 0 & 0 & R_{3s} & \cdots & 0 \\ \vdots & \vdots & \vdots & \ddots & \vdots \\ 0 & 0 & 0 & \cdots & R_{ns} \end{bmatrix} \tag{3.9}$$

$$\left[R_r\right]=\begin{bmatrix} R_{1r} & 0 & 0 & \cdots & 0 \\ 0 & R_{2r} & 0 & \cdots & 0 \\ 0 & 0 & R_{3r} & \cdots & 0 \\ \vdots & \vdots & \vdots & \ddots & \vdots \\ 0 & 0 & 0 & \cdots & R_{nr} \end{bmatrix} \tag{3.10}$$

Since the rotor bars are short-circuited in the squirrel-cage induction machines, the rotor voltages in equation (3.4) are equal to zero. The resistance matrices in equation (3.9) and (3.10) are diagonal matrices. Since the *n* phases have identical winding, one can write: $R_{1s} = R_{2s} = R_{3s} = \ldots = R_{ns} = R_s$, and $R_{1r} = R_{2r} = R_{3r} = \ldots = R_{nr} = R_r$. The flux-linkage in equations (3.7) and (3.8) is dependent on the rotor and stator currents. This relation is given by the following equations:

$$\left[\psi_s\right]=\left[L_s\right]\left[i_s\right]+\left[L_{sr}\right]\left[i_r\right] \tag{3.11}$$

$$\left[\psi_r\right]=\left[L_r\right]\left[i_r\right]+\left[L_{sr}\right]^T\left[i_s\right] \tag{3.12}$$

The inductance matrices introduced in (3.11) and (3.12), $[L_s]$, $[L_r]$ and $[L_{sr}]$ are the stator inductance matrix, rotor inductance matrix and the mutual stator-to-rotor inductance matrix, respectively. The rotor-to-stator mutual inductance matrix, $[L_{rs}]$, is equivalent to the transpose matrix of the stator-to-rotor matrix $[L_{sr}]$, as presented in equation (3.12). The inductance matrices of the stator and the rotor have only constant coefficients due to the fixed mutual position of the windings and due to the constant parameters' assumptions. These matrices are obtainable as follows:

$$\left[L_s\right]=\begin{bmatrix} L_{11s} & L_{12s} & L_{13s} & \cdots & L_{1ns} \\ L_{21s} & L_{22s} & L_{23s} & \cdots & L_{2ns} \\ L_{31s} & L_{32s} & L_{33s} & \cdots & L_{3ns} \\ \vdots & \vdots & \vdots & \ddots & \vdots \\ L_{n1s} & L_{n2s} & L_{n3s} & \cdots & L_{nns} \end{bmatrix} \tag{3.13}$$

$$\left[L_r\right]=\begin{bmatrix} L_{11r} & L_{12r} & L_{13r} & \cdots & L_{1nr} \\ L_{21r} & L_{22r} & L_{23r} & \cdots & L_{2nr} \\ L_{31r} & L_{32r} & L_{33r} & \cdots & L_{3nr} \\ \vdots & \vdots & \vdots & \ddots & \vdots \\ L_{n1r} & L_{n2r} & L_{n3r} & \cdots & L_{nnr} \end{bmatrix} \tag{3.14}$$

The self-inductance (diagonal) terms introduced in (3.13) are all equal, such that $L_{11s} = L_{22s} = \ldots = L_{nns}$, and this value is equal to $L_{ls}+M$, where L_{ls} is the leakage inductance of the stator and M is the maximum value of the stator-to-rotor mutual inductance. The same applies to rotor; all diagonal terms in (3.14) are equal to $L_{lr}+M$, where L_{lr} is the leakage inductance of the rotor. The other inductance coefficients have different values i.e. to be more specific, $(n–1)/2$ different values. Now, (3.13) and (3.14) can be rewritten as follows:

$$\left[L_s\right]=\begin{bmatrix} L_{ls}+M & M\cos(\alpha) & M\cos(2\alpha) & \cdots & M\cos((n-1)\alpha) \\ M\cos((n-1)\alpha) & L_{ls}+M & M\cos(\alpha) & \cdots & M\cos((n-2)\alpha) \\ M\cos((n-2)\alpha) & M\cos((n-1)\alpha) & L_{ls}+M & \cdots & M\cos((n-3)\alpha) \\ \vdots & \vdots & \vdots & \ddots & \vdots \\ M\cos(\alpha) & M\cos(2\alpha) & M\cos(3\alpha) & \cdots & L_{ls}+M \end{bmatrix} \tag{3.15}$$

$$\left[L_r\right]=\begin{bmatrix} L_{lr}+M & M\cos(\alpha) & M\cos(2\alpha) & \cdots & M\cos((n-1)\alpha) \\ M\cos((n-1)\alpha) & L_{lr}+M & M\cos(\alpha) & \cdots & M\cos((n-2)\alpha) \\ M\cos((n-2)\alpha) & M\cos((n-1)\alpha) & L_{lr}+M & \cdots & M\cos((n-3)\alpha) \\ \vdots & \vdots & \vdots & \ddots & \vdots \\ M\cos(\alpha) & M\cos(2\alpha) & M\cos(3\alpha) & \cdots & L_{lr}+M \end{bmatrix} \tag{3.16}$$

From (3.15) and (3.16) one can see that stator and rotor inductance matrices $[L_s]$ and $[L_r]$, consist of constant terms only. On the other hand, the stator-to-rotor mutual inductance $[L_{sr}]$ matrix has no constant coefficients. This is because the rotor is in a continuous rotation while the stator windings are stationary. Thus, the stator-to-rotor inductance matrix is a time-dependent matrix with varying coefficients . The instantaneous angular position of the rotor magnetic axis 1r to the stator magnetic axis 1s (Fig. 3.2) is called the electrical position of the rotor θ_e. It is related to the electrical speed of rotation, ω_e, as:

$$\theta_e = \int \omega_e \mathrm{d}t + \theta_{e0} \tag{3.17}$$

where θ_{e0} is the initial angle between axes 1r and 1s, and in most of the cases it can be assumed to be 0. The stator-to-rotor mutual inductance matrix can be described with only the first order harmonics due to the assumption of sinusoidal distribution of the flux around the air-gap. As a result, the stator-to-rotor inductance matrix can be written as follows:

$$\left[L_{sr}\right]=M\begin{bmatrix}\cos\theta_e & \cos(\theta_e+\alpha) & \cos(\theta_e+2\alpha) & \cdots & \cos(\theta_e+(n-1)\alpha)\\ \cos(\theta_e+(n-1)\alpha) & \cos\theta_e & \cos(\theta_e+\alpha) & \cdots & \cos(\theta_e+(n-2)\alpha)\\ \cos(\theta_e+(n-2)\alpha) & \cos(\theta_e+(n-1)\alpha) & \cos\theta_e & \cdots & \cos(\theta_e+(n-3)\alpha)\\ \vdots & \vdots & \vdots & \ddots & \vdots\\ \cos(\theta_e+\alpha) & \cos(\theta_e+2\alpha) & \cos(\theta_e+3\alpha) & \cdots & \cos\theta_e\end{bmatrix} \tag{3.18}$$

The previous set of equations (3.1) – (3.18) represent a complete description of the electrical subsystem of a symmetrical *n*-phase induction machine. Conversely, in order to describe the mechanical subsystem of the multiphase induction machine, Newton's second law for rotation can be written:

$$T_e - T_l = J\frac{\mathrm{d}\omega_m}{\mathrm{d}t} \tag{3.19}$$

where T_e represents the electromagnetic torque, T_l stands for the load torque, J is the inertia of the multiphase machine, and ω_m is the mechanical speed of rotation. Additionally, ω_m is equal to the electrical speed of rotation ω_e divided by the number of pole pairs P of the multiphase machine, so that:

$$\omega_m = \frac{\omega_e}{P} \tag{3.20}$$

Thus, looking back at $[L_{sr}]$ in (3.18), and by considering (3.17) and (3.19), one can say that it depends on mechanical speed of the rotor ω_m and P. Rewriting (3.19) in terms of the electrical speed of rotation, will yield:

$$T_e - T_l = \frac{J}{P}\frac{\mathrm{d}\omega_e}{\mathrm{d}t} \tag{3.21}$$

The electro-mechanical energy conversion is a result of interaction between the electrical and mechanical subsystem of the machine. The electromagnetic torque T_e can be expressed as:

$$T_e = P\frac{1}{2}\left[i\right]^T\frac{\mathrm{d}\left[L\right]}{\mathrm{d}\theta_e}\left[i\right] \tag{3.22}$$

where $[L]$ and $[i]$ are the total inductance matrix and total current matrix of the system (machine). They are defined as:

$$\left[L\right]=\begin{bmatrix}[L_s] & [L_{sr}]\\ [L_{rs}] & [L_r]\end{bmatrix} \tag{3.23}$$

$$\left[i\right]=\begin{bmatrix}\left[i_s\right]^T & \left[i_r\right]^T\end{bmatrix}^T \tag{3.24}$$

Equation (3.22) can be rewritten in a simpler form, since the stator and rotor matrices (3.15) and (3.16) have constant terms (which do not change with respect to the rotor position, as in (3.18)). Additionally,

for the final simplification one should take into account that $[L_{rs}]=[L_{sr}]^T$, which leads to [Levi et al. (2007)]:

$$T_e = P\left[i_s\right]^T \frac{\mathrm{d}\left[L_{sr}\right]}{\mathrm{d}\theta_e}\left[i_r\right] \tag{3.25}$$

The previous set of equations, (3.1) through (3.25), represents a complete generalised mathematical model of a symmetrical *n*-phase induction machine in terms of the phase variables. So far, the developed model contains 2*n*+1 differential equations: 2*n* voltage equilibrium equations ((3.1) and (3.2)) and the mechanical equilibrium equation ((3.22) or (3.25)). Hence, if for example, a twelve-phase induction machine is considered, 25 first order differential equations with time varying coefficients are required to be solved. In order to simplify the mathematical model of the multiphase machines, fictitious variables from the original phase-variables can be obtained through the mathematical transformations. A number of transformations have been proposed in the last century [Levi et al. (2007)]. All these transformations are practically special cases of the general discrete Fourier's transformation (DFT) [Dordevic (2013)]. The following section will introduce the generalised decoupling mathematical transformation for a symmetrical *n*-phase induction machine. This transformation is known as Clarke's decoupling transformation.

3.3 CLARKE'S DECOUPLING TRANSFORMATION

Implementation of Clarke's decoupling transformation produces (*n*–2)/2 two-dimensional subspaces (planes) and two single-dimensional quantities for a symmetrical *n*-phase machine with an even number of phases, and (*n*–1)/2 two-dimensional subspaces and one single-dimensional quantity for an odd number of phases [Levi (2008), Levi et al. (2007)]. The two-dimensional subspaces are perpendicular to each other and every subspace consists of two perpendicular axes. In other words, a complete decoupled model subspaces for an *n*-phase machine is obtained using Clarke's decoupling transformation. Also, note that the total dimension of the system is unchanged and it is still *n* (*n* variables are mapped onto *n* axes). Application of Clarke's decoupling matrix will yield a simplified machine model compared to the phase-variable model introduced in the previous section. In order to transfer the multiphase machine phase-variable model into the decoupled model, the following equation defines the correlation between the original phase variables and the newly introduced fictitious variables:

$$\left[\, f_{\alpha\beta,x_1y_1,\ldots 0_+0_-} \,\right]_{n\times 1} = [C]_{n\times n}\left[\, f_{1,2,\ldots n} \,\right]_{n\times 1} \tag{3.26}$$

In (3.26), $[\, f_{\alpha\beta,x_1y_1,\ldots 0_+0_-} \,]_{n\times 1}$ represents the new fictitious variables matrix after the transformation. Matrix $[C]_{n\times n}$ represents Clarke's decoupling transformation matrix and $[f_{1,2,\ldots n}]_{n\times 1}$ represents the original variables in the phase-variables model. Variable *f* can be any variable such as voltage, current or the

flux-linkage for the stator or for the rotor. The transformation matrix [*C*] for a symmetrical *n*-phase machine with even number of phases and a single neutral point is defined as:

$$[C]=\sqrt{\frac{2}{n}}\left[\begin{array}{c|ccccccc}
\alpha & 1 & \cos(\alpha) & \cos(2\alpha) & \cos(3\alpha) & \cdots & \cos((n-1)\alpha) \\
\beta & 0 & \sin(\alpha) & \sin(2\alpha) & \sin(3\alpha) & \cdots & \sin((n-1)\alpha) \\
x_1 & 1 & \cos(2\alpha) & \cos(4\alpha) & \cos(6\alpha) & \cdots & \cos(2(n-1)\alpha) \\
y_1 & 0 & \sin(2\alpha) & \sin(4\alpha) & \sin(6\alpha) & \cdots & \sin(2(n-1)\alpha) \\
x_2 & 1 & \cos(3\alpha) & \cos(6\alpha) & \cos(9\alpha) & \cdots & \cos(3(n-1)\alpha) \\
y_2 & 0 & \sin(3\alpha) & \sin(6\alpha) & \sin(9\alpha) & \cdots & \sin(3(n-1)\alpha) \\
\vdots & \vdots & \vdots & \vdots & \vdots & \ddots & \vdots \\
x_{\frac{n-4}{2}} & 1 & \cos\left(\left(\frac{n-2}{2}\right)\alpha\right) & \cos\left(2\left(\frac{n-2}{2}\right)\alpha\right) & \cos\left(3\left(\frac{n-2}{2}\right)\alpha\right) & \cdots & \cos\left((n-1)\left(\frac{n-2}{2}\right)\alpha\right) \\
y_{\frac{n-4}{2}} & 0 & \sin\left(\left(\frac{n-2}{2}\right)\alpha\right) & \sin\left(2\left(\frac{n-2}{2}\right)\alpha\right) & \sin\left(3\left(\frac{n-2}{2}\right)\alpha\right) & \cdots & \sin\left((n-1)\left(\frac{n-2}{2}\right)\alpha\right) \\
0_+ & \frac{1}{\sqrt{2}} & \frac{1}{\sqrt{2}} & \frac{1}{\sqrt{2}} & \frac{1}{\sqrt{2}} & \cdots & \frac{1}{\sqrt{2}} \\
0_- & \frac{1}{\sqrt{2}} & \frac{-1}{\sqrt{2}} & \frac{1}{\sqrt{2}} & \frac{-1}{\sqrt{2}} & \cdots & \frac{-1}{\sqrt{2}}
\end{array}\right] \tag{3.27}$$

The decoupling matrix (3.27) can be applied on the stator and rotor variables. All the matrix coefficients are time invariant. The multiplication coefficient in front of the matrix is related to the power of the new machine model. By selecting this coefficient as $\sqrt{2/n}$, the power of the decoupled machine model will be the same as that of the original machine model. Hence, this choice represents the power-invariant form of the transformation, but the other options are also possible. The difference between the decoupling transformation matrix for a symmetrical multiphase machine with an even or with an odd number of phases is the following. If *n* is an odd number, the last row of the transformation matrix 0_- should be eliminated. Also, the number of *x*-*y* planes will be (*n*–3)/2 instead of (*n*–4)/2. The first subspace of the decoupled model *α*-*β* defines the flux and torque producing subspace because the coupling term between the stator-to-rotor will only appear in this subspace, as will be shown later on [Levi et al. (2007)]. Application of Clarke's decoupling transformation (3.27) to the voltage equilibrium equations (3.1) and (3.2) and the electromagnetic torque equation (3.25) for multiphase machines comprising an odd number of phases, results in the following equations. Obtained stator equations are:

$$v_{\alpha s}=R_s i_{\alpha s}+\frac{\mathrm{d}\psi_{\alpha s}}{\mathrm{d}t}=R_s i_{\alpha s}+\left(L_{ls}+L_m\right)\frac{\mathrm{d}i_{\alpha s}}{\mathrm{d}t}+L_m\frac{\mathrm{d}}{\mathrm{d}t}\left(i_{\alpha r}\cos\theta_e-i_{\beta r}\sin\theta_e\right) \tag{3.28}$$

$$v_{\beta s}=R_s i_{\beta s}+\frac{\mathrm{d}\psi_{\beta s}}{\mathrm{d}t}=R_s i_{\beta s}+\left(L_{ls}+L_m\right)\frac{\mathrm{d}i_{\beta s}}{\mathrm{d}t}+L_m\frac{\mathrm{d}}{\mathrm{d}t}\left(i_{\alpha r}\sin\theta_e+i_{\beta r}\cos\theta_e\right) \tag{3.29}$$

$$v_{x_k s}=R_s i_{x_k s}+\frac{\mathrm{d}\psi_{x_k s}}{\mathrm{d}t}=R_s i_{x_k s}+L_{ls}\frac{\mathrm{d}i_{x_k s}}{\mathrm{d}t} \tag{3.30}$$

$$v_{y_k s} = R_s i_{y_k s} + \frac{\mathrm{d}\psi_{y_k s}}{\mathrm{d}t} = R_s i_{y_k s} + L_{ls} \frac{\mathrm{d}i_{y_k s}}{\mathrm{d}t} \tag{3.31}$$

$$v_{0s} = R_s i_{0s} + \frac{\mathrm{d}\psi_{0s}}{\mathrm{d}t} = R_s i_{0s} + L_{ls} \frac{\mathrm{d}i_{0s}}{\mathrm{d}t} \tag{3.32}$$

In (3.30) and (3.31), index k represents a particular x-y plane, and since a machine with an odd number of phases is considered, $k \in 1$ to $(n–3)/2$. The rotor equations in the new α-β frame will have the following form:

$$v_{\alpha r} = 0 = R_r i_{\alpha r} + \frac{\mathrm{d}\psi_{\alpha r}}{\mathrm{d}t} = R_r i_{\alpha r} + \left(L_{lr} + L_m\right)\frac{\mathrm{d}i_{\alpha r}}{\mathrm{d}t} + L_m \frac{\mathrm{d}}{\mathrm{d}t}\left(i_{\alpha s}\cos\theta_e + i_{\beta s}\sin\theta_e\right) \tag{3.33}$$

$$v_{\beta r} = 0 = R_r i_{\beta r} + \frac{\mathrm{d}\psi_{\beta r}}{\mathrm{d}t} = R_r i_{\beta r} + \left(L_{\mathrm{lr}} + L_m\right)\frac{\mathrm{d}i_{\beta r}}{\mathrm{d}t} + L_m \frac{\mathrm{d}}{\mathrm{d}t}\left(-i_{\alpha s}\sin\theta_e + i_{\beta s}\cos\theta_e\right) \tag{3.34}$$

$$v_{x_k r} = 0 = R_r i_{x_k r} + \frac{\mathrm{d}\psi_{x_k r}}{\mathrm{d}t} = R_r i_{x_k r} + L_{lr} \frac{\mathrm{d}i_{x_k r}}{\mathrm{d}t} \tag{3.35}$$

$$v_{y_k r} = 0 = R_r i_{y_k r} + \frac{\mathrm{d}\psi_{y_k r}}{\mathrm{d}t} = R_r i_{y_k r} + L_{lr} \frac{\mathrm{d}i_{y_k r}}{\mathrm{d}t} \tag{3.36}$$

$$v_{0r} = 0 = R_r i_{0r} + \frac{\mathrm{d}\psi_{0r}}{\mathrm{d}t} = R_r i_{0r} + L_{lr} \frac{\mathrm{d}i_{0r}}{\mathrm{d}t} \tag{3.37}$$

Again, index k indicates the auxiliary plane number, $k \in 1$ to $(n–3)/2$. Finally, after the transformation into α-β coordinate system is done, the electromagnetic torque equation of (3.25), becomes:

$$T_e = PL_m\left(\cos\theta_e\left(i_{\alpha r} i_{\beta s} - i_{\beta r} i_{\alpha s}\right) - \sin\theta_e\left(i_{\alpha r} i_{\alpha s} + i_{\beta r} i_{\beta s}\right)\right) \tag{3.38}$$

In the equations (3.28) to (3.38), L_m is the per-phase equivalent circuit magnetizing inductance and it is equal to $L_m = (n/2)M$. The electromagnetic torque equation (3.38) shows that the developed torque can be obtained from the α-β components of the rotor and stator currents only, while the x-y components and the zero sequence components do not contribute to the developed torque. Thus, a simplified and fully decoupled model can be obtained from the previous equations (3.28) through (3.38). If the multiphase machine is supplied with an ideal symmetrical and balanced sinusoidal source, the electromagnetic subsystem of the transformed model can be resolved into four first order differential equations instead of the $2n$ in the original phase-variables model. Consequently, a considerable amount of simplification is offered by the transformed model. However, the major drawback of the transformed model is presented in the nonlinearity of the system and the time-dependent coefficients of the differential equations. In order to eliminate the time-dependent coefficients, another transformation is a necessity.

3.4 ROTATIONAL TRANSFORMATION

The application of the rotational transformation is aimed to eliminate the time-dependent terms after the application of the decoupling transformation in the previous section. The fictitious variables obtained from Clarke's decoupling transformation α-β will be replaced with new fictitious variables after the implementation of the rotational transformation (d-q). The rotational transformation is applied only to α-β plane, because the time-dependent terms (stator-to-rotor coupling) appear only in this plane. In Clarke's decoupled model stator windings are stationary, while the rotor windings are rotating with the same speed as the rotor. However, after transferring the Clarke's model into the rotational model, or what is known as the common reference frame, the stator and rotor windings are rotating at the same speed. The speed at which the common reference frame (d-q) rotates can be arbitrary and will be denoted as ω_a. The instantaneous position of the d-axis with respect to the first stator winding, $\theta_{s,}$, which is utilized to transfer the stator variables to the common reference frame, can be obtained from the arbitrary speed as in the following equation:

$$\theta_s = \int \omega_a \mathrm{d}t \tag{3.39}$$

Unlike the Clarke's transformation, now the stator and rotor quantities are not multiplied by the same matrix. The instantaneous position of the d-axis with respect to the first rotor winding, θ_r, can be obtained by subtracting the instantaneous position of the rotor's first winding (with respect to the first winding of the stator) from the position of the common reference frame, as illustrated in Fig. 3.2. It can be obtained by the following equation:

$$\theta_r = \theta_s - \theta_e = \int (\omega_a - \omega_e)\mathrm{d}t \tag{3.40}$$

The d-q axes are orthogonal to each other, as shown in Fig. 3.2, thus they are fully decoupled. The rotational transformation is applied according to:

$$\left[f_{dq,x_1y_1,\ldots 0_+0_-} \right]_{n\times 1} = [D]_{n\times n} \left[f_{\alpha\beta,x_1y_1,\ldots 0_+0_-} \right]_{n\times 1} \tag{3.41}$$

where $[D]_{n\times n}$ represents the rotational transformation matrix. The rotational matrix depends on whether the variables are belonging to the stator or rotor. The following matrices represent the transformation matrix of the stator and rotor quantities, respectively:

$$[D_s] = \begin{matrix} d_s \\ q_s \\ x_{1s} \\ y_{1s} \\ \vdots \\ 0_s \end{matrix} \begin{bmatrix} \cos\theta_s & \sin\theta_s & 0 & 0 & \cdots & 0 \\ -\sin\theta_s & \cos\theta_s & 0 & 0 & \cdots & 0 \\ 0 & 0 & 1 & 0 & \cdots & 0 \\ 0 & 0 & 0 & 1 & \cdots & 0 \\ \vdots & \vdots & \vdots & \vdots & \ddots & \vdots \\ 0 & 0 & 0 & 0 & \cdots & 1 \end{bmatrix} \tag{3.42}$$

$$[D_r] = \begin{array}{c} \\ d_r \\ q_r \\ x_{1r} \\ y_{1r} \\ \vdots \\ 0_r \end{array} \begin{bmatrix} \cos\theta_r & \sin\theta_r & 0 & 0 & \cdots & 0 \\ -\sin\theta_r & \cos\theta_r & 0 & 0 & \cdots & 0 \\ 0 & 0 & 1 & 0 & \cdots & 0 \\ 0 & 0 & 0 & 1 & \cdots & 0 \\ \vdots & \vdots & \vdots & \vdots & \ddots & \vdots \\ 0 & 0 & 0 & 0 & \cdots & 1 \end{bmatrix} \tag{3.43}$$

Equations describing α-β components of the decoupled model (3.28), (3.29), (3.33) and (3.34), after application of the rotational transformation, yield the following equations:

$$v_{ds} = R_s i_{ds} + \frac{\mathrm{d}\psi_{ds}}{\mathrm{d}t} - \omega_a \psi_{qs} \tag{3.44}$$

$$v_{qs} = R_s i_{qs} + \frac{\mathrm{d}\psi_{qs}}{\mathrm{d}t} + \omega_a \psi_{ds} \tag{3.45}$$

$$v_{dr} = 0 = R_r i_{dr} + \frac{\mathrm{d}\psi_{dr}}{\mathrm{d}t} - (\omega_a - \omega_e)\psi_{qr} \tag{3.46}$$

$$v_{qr} = 0 = R_r i_{qr} + \frac{\mathrm{d}\psi_{qr}}{\mathrm{d}t} + (\omega_a - \omega_e)\psi_{dr} \tag{3.47}$$

where:

$$\psi_{ds} = (L_{ls} + L_m) i_{ds} + L_m i_{dr} \tag{3.48}$$

$$\psi_{qs} = (L_{ls} + L_m) i_{qs} + L_m i_{qr} \tag{3.49}$$

$$\psi_{dr} = (L_{lr} + L_m) i_{dr} + L_m i_{ds} \tag{3.50}$$

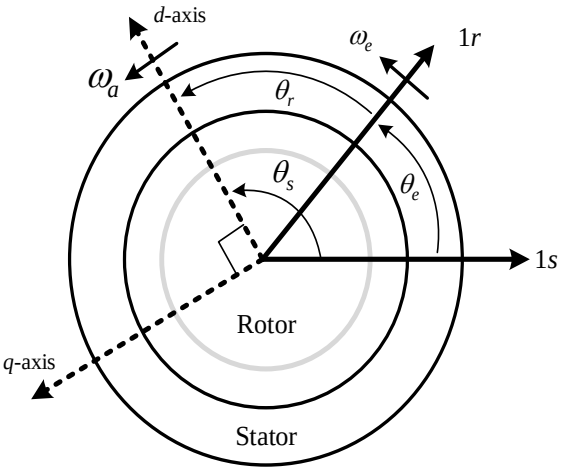

Fig. 3.2. Magnetic axes of the common reference frame for multiphase induction machine.

$$\psi_{qr} = \left(L_{lr} + L_m\right) i_{qr} + L_m i_{qs} \tag{3.51}$$

The electromagnetic torque T_e from (3.38), after the transformation becomes:

$$T_e = PL_m \left(i_{dr} i_{qs} - i_{ds} i_{qr}\right) \tag{3.52}$$

It can be noted from the voltage equilibrium equations in the common reference frame (3.44) through (3.47) that the speed of the stator and rotor fictitious windings (which are attached to new introduced *d-q* reference frame) is different from the speed of the stator and rotor original phase variables reference frames. In the common reference frame, both stator and rotor fictitious windings are rotating with the same speed, the arbitrary speed ω_a, while in the original phase variables model, the stator windings are stationary and the rotor windings rotate with the speed of the rotor. This is obviously demonstrated in the voltage equilibrium equations (3.44) – (3.47), in a common reference frame. Furthermore, the time-dependent terms introduced in voltage equilibrium equations in the stationary reference frame (after Clarke's transformation) and consequently in the electromagnetic torque equation (3.38), have been completely eliminated after the implementation of the rotational transformation. Due to the elimination of the time dependent terms in the voltage equilibrium equations, a significant simplification is introduced in the multiphase induction machine model in the common reference frame.

The electromagnetic torque can be expressed using different machine parameters. By changing the variables and finding the correlations of the *d-q* currents and flux-linkages, the following alternative forms can be obtained:

$$T_e = P\left(\psi_{ds}\, i_{qs} - \psi_{qs}\, i_{ds}\right) \tag{3.53}$$

$$T_e = P\frac{L_m}{L_r}\left(\psi_{dr}\, i_{qs} - \psi_{qr}\, i_{ds}\right) \tag{3.54}$$

Fig. 3.3 illustrates the fictitious *d-q* windings of the rotor and stator of any *n*-phase machine. It is obvious from the figure that the rotor and stator *d*-axes are rotating at the same arbitrary speed, ω_a. On the other hand, the original phase-variables reference frames (represented by the first axis of the stator and rotor 1*s* and 1*r*, in Fig. 3.3) have different speeds in the original phase variables reference frame. A different common reference frame can be chosen depending on the application of the multiphase machine. This is achievable by appropriate selection of the arbitrary speed ω_a. For instance, the arbitrary speed can be chosen as zero defining stationary reference frame, or as ω_{syn}, defining synchronous reference frame. For development of high-performance induction motor drive control schemes, a common choice would be that ω_a is equal to the speed of rotation of stator, air-gap or rotor rotating field. Based on that, different control schemes can be implemented such as the vector control scheme also

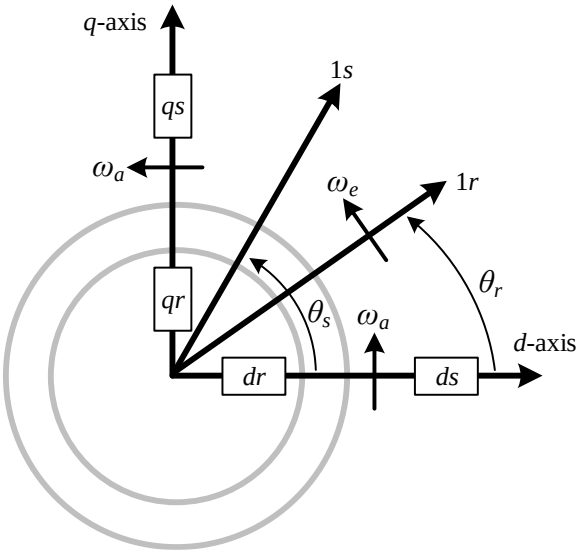

Fig. 3.3. The rotor and stator fictitious *d*-*q* windings obtained after the rotational transformation.

known as the field-oriented control (FOC) where the arbitrary speed is chosen to be equal to the stator, air-gap or the rotor rotating field [Levi et al. (2007), Levi et al. (2008)].

3.5 MODELLING OF MULTIPLE THREE-PHASE INDUCTION MACHINES

The previous sections have considered the mathematical modelling of multiphase induction machines with a single neutral point. However, there are numerous industrial applications where a multiphase induction machine consists of multiple three-phase windings with isolated neutral points. This type of multiphase machine offers a more fault tolerant and more reliable solution compared to the multiphase machines with a single neutral point from the power electronics point of view [Grandi et al. (2010), Levi et al. (2008), Tani et al. (2013), Che et al. (2014a), Tani et al. (2014), Mengoni et al. (2016)]. If in a multiphase machine, with n stator phases, the windings are divided into k winding sets with a phases in each winding set, then $n = ak$ where k represents the number of isolated neutral points or the number of winding sets. For instance, Fig. 3.4 illustrates the magnetic axes of a symmetrical nine-phase machine with three isolated neutral points. Each winding set consists of three phases, *a*, *b* and *c*, shifted by 120º (i.e. $2\pi/a$) and the spatial shift between consecutive phases is equal to $2\pi/n$. Indices 1, 2, 3 (in the general case until k), in Fig. 3.4, represent the winding set number. The modelling principles provided in previous sections remain the same for multiphase induction machines with multiple isolated neutral points. However, since the zero-sequence current cannot flow in any of the winding sets, the a-th current harmonic cannot exist. This will reduce the number of x-y planes in (3.27) by one, if a symmetrical nine-phase machine is considered, and the total number of zero axes will be three, i.e. k in general case. The following equation provides Clarke's transformation matrix for a symmetrical nine-phase induction machine with a single neutral point:

$$[C]=\sqrt{\frac{2}{9}}\begin{bmatrix}
 & a & b & c & d & e & f & g & h & i \\
\alpha & 1 & \cos(\alpha) & \cos(2\alpha) & \cos(3\alpha) & \cos(4\alpha) & \cos(5\alpha) & \cos(6\alpha) & \cos(7\alpha) & \cos(8\alpha) \\
\beta & 0 & \sin(\alpha) & \sin(2\alpha) & \sin(3\alpha) & \sin(4\alpha) & \sin(5\alpha) & \sin(6\alpha) & \sin(7\alpha) & \sin(8\alpha) \\
x_1 & 1 & \cos(2\alpha) & \cos(4\alpha) & \cos(6\alpha) & \cos(8\alpha) & \cos(10\alpha) & \cos(12\alpha) & \cos(14\alpha) & \cos(16\alpha) \\
y_1 & 0 & \sin(2\alpha) & \sin(4\alpha) & \sin(6\alpha) & \sin(8\alpha) & \sin(10\alpha) & \sin(12\alpha) & \sin(14\alpha) & \sin(16\alpha) \\
x_2 & 1 & \cos(3\alpha) & \cos(6\alpha) & \cos(9\alpha) & \cos(12\alpha) & \cos(15\alpha) & \cos(18\alpha) & \cos(21\alpha) & \cos(24\alpha) \\
y_2 & 0 & \sin(3\alpha) & \sin(6\alpha) & \sin(9\alpha) & \sin(12\alpha) & \sin(15\alpha) & \sin(18\alpha) & \sin(21\alpha) & \sin(24\alpha) \\
x_3 & 1 & \cos(4\alpha) & \cos(8\alpha) & \cos(12\alpha) & \cos(16\alpha) & \cos(20\alpha) & \cos(24\alpha) & \cos(28\alpha) & \cos(32\alpha) \\
y_3 & 0 & \sin(4\alpha) & \sin(8\alpha) & \sin(12\alpha) & \sin(16\alpha) & \sin(20\alpha) & \sin(24\alpha) & \sin(28\alpha) & \sin(32\alpha) \\
0 & \frac{1}{\sqrt{2}} & \frac{1}{\sqrt{2}} & \frac{1}{\sqrt{2}} & \frac{1}{\sqrt{2}} & \frac{1}{\sqrt{2}} & \frac{1}{\sqrt{2}} & \frac{1}{\sqrt{2}} & \frac{1}{\sqrt{2}} & \frac{1}{\sqrt{2}}
\end{bmatrix} \tag{3.55}$$

If three isolated neutral points are present, the matrix becomes:

$$[C]=\sqrt{\frac{2}{9}}\begin{bmatrix}
 & a_1 & a_2 & a_3 & b_1 & b_2 & b_3 & c_1 & c_2 & c_3 \\
\alpha & 1 & \cos(\alpha) & \cos(2\alpha) & \cos(3\alpha) & \cos(4\alpha) & \cos(5\alpha) & \cos(6\alpha) & \cos(7\alpha) & \cos(8\alpha) \\
\beta & 0 & \sin(\alpha) & \sin(2\alpha) & \sin(3\alpha) & \sin(4\alpha) & \sin(5\alpha) & \sin(6\alpha) & \sin(7\alpha) & \sin(8\alpha) \\
x_1 & 1 & \cos(2\alpha) & \cos(4\alpha) & \cos(6\alpha) & \cos(8\alpha) & \cos(10\alpha) & \cos(12\alpha) & \cos(14\alpha) & \cos(16\alpha) \\
y_1 & 0 & \sin(2\alpha) & \sin(4\alpha) & \sin(6\alpha) & \sin(8\alpha) & \sin(10\alpha) & \sin(12\alpha) & \sin(14\alpha) & \sin(16\alpha) \\
x_2 & 1 & \cos(4\alpha) & \cos(8\alpha) & \cos(12\alpha) & \cos(16\alpha) & \cos(20\alpha) & \cos(24\alpha) & \cos(28\alpha) & \cos(32\alpha) \\
y_2 & 0 & \sin(4\alpha) & \sin(8\alpha) & \sin(12\alpha) & \sin(16\alpha) & \sin(20\alpha) & \sin(24\alpha) & \sin(28\alpha) & \sin(32\alpha) \\
0_1 & \sqrt{3/2} & 0 & 0 & \sqrt{3/2} & 0 & 0 & \sqrt{3/2} & 0 & 0 \\
0_2 & 0 & \sqrt{3/2} & 0 & 0 & \sqrt{3/2} & 0 & 0 & \sqrt{3/2} & 0 \\
0_3 & 0 & 0 & \sqrt{3/2} & 0 & 0 & \sqrt{3/2} & 0 & 0 & \sqrt{3/2}
\end{bmatrix} \tag{3.56}$$

As already mentioned, the difference between (3.55) and (3.56) is in the absence of the 3rd harmonic plane (the second *x*-*y* plane, x_2-y_2) in (3.56), because the zero-sequence current cannot flow in the isolated three-phase winding sets. This plane as well as the zero axis, are replaced by the corresponding zero axes for each of *k* three-phase winding sets. The rotational transformation of the multiphase machine with multiple isolated neutral points is the same as for the single neutral point. Note that when multiple isolated neutral points are present, the number of voltage equilibrium equations, such as those in (3.28) through (3.37), will be reduced to $2\cdot(n–k)$. Similarly, as in previous section a fully decoupled

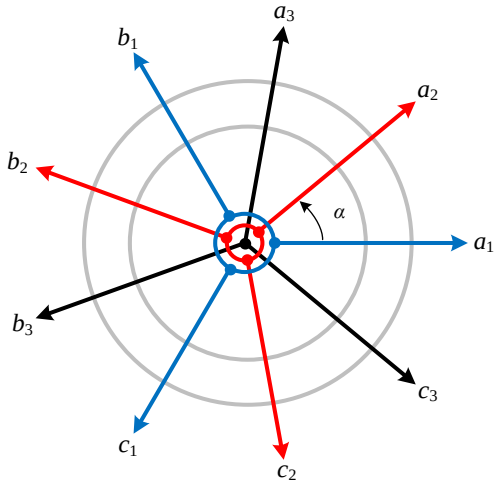

Fig. 3.4: Stator magnetic axes of a symmetrical nine-phase machine with three isolated neutral points.

machine model can be obtained, which can be further used for the development of closed-loop control schemes (such as FOC) for the multiphase machine with multiple isolated neutral points.

3.6 FIELD-ORIENTED CONTROL (FOC)

Many industrial applications employ variable speed electric drives. From the simplest application to the most sophisticated ones, the controlled variables change depending on the application. Speed, position and torque are the most commonly controlled variables. However, the electromagnetic torque is the utmost controlled variable. A controlled torque will provide a controlled transition from one operation speed to another with a smaller settling time compared to the open-loop control. Such variable speed electric drives with a controllable transient and steady-state are called the high-performance electric drives. In order to control the electric drive in transient and steady-state, the instantaneous position of the rotor shaft is always required [Levi et al. (2007)]. Fig. 3.5 illustrates the closed-loop control of *n*-phase high-performance variable speed electric drive. The schematic is equally applicable to any electric machine category such as permanent magnet, synchronous reluctance or induction machines. Electromagnetic torque is proportional to the product of the flux producing current (i_d^*) and the torque producing current (i_q^*). Usually, i_d^* is kept constant; nevertheless, this is not always the case [Levi et al. (2007)]. The torque producing current is the output of the torque controller. However, this controller can usually be eliminated because i_q^* can be obtained from the output of the speed controller multiplied by a scaling factor. Note that in Fig. 3.5 only *d-q* current controllers are shown for simplicity. However, in practice the auxiliary *x-y* currents should be controlled as well.

A cascaded controller structure is implemented in Fig. 3.5 and in most cases these controllers are proportional-integral (PI) ones. This cascaded structure is governed by equations (3.17) and (3.21). The machine's stator currents are used in the control algorithms since the electromagnetic torque is governed by the currents rather than the voltages. Thus, the power electronic inverter is a current controlled inverter [Levi et al. (2007)].

The high-performance electric drives require fully decoupled control of the flux and torque of the ac machines, as is the case in the dc machines. In dc machines the torque is inherently decoupled from the flux and directly controllable by the armature current. This is so, due to the construction of the dc machines and the specific design of the commutator. Therefore, in order to apply a fully decoupled control, it is essential to convert the ac machine model into its dc machine equivalent. This control scheme is called field-oriented control – FOC, or vector control, where two fictitious currents produce a decoupled control of the torque and flux of the ac machine. In contrast to the dc machines, these fictitious currents are rotating with synchronous speed in the ac machines. The synchronous speed is the speed of the rotating field at the steady-state operation. However, during the transient state there will be three different fluxes with three different speeds.

The most complex FOC scheme is the one applied to the induction machines because even though the position of the rotor is measurable, the exact position of the rotating field is difficult to measure. The FOC scheme is developed based on the rotational transformation model (*d*-*q* model) of the multiphase induction machine, represented by equations (3.44) through (3.54). The correlation between the original phase-variables model and the rotational transformation model is governed by the Clarke's decoupling transformation matrix [*C*] and the rotational transformation matrix [*D*]. Since the rotor is rotating with a speed different from the speed of the rotating field, or in other words it rotates asynchronously, the measured rotor position is not used by the rotational transformation matrices [Levi et al. (2007)].

In order to convert the induction machine into its dc machine equivalent, it is important to select the common reference frame in such a way that the *q*-component of the stator or rotor flux-linkage is equal to zero. This is possible, for example, by aligning the *d*-axis of the common reference frame with the flux-linkage of the rotor or the stator. However, aligning the *d*-axis to the stator flux-linkage will lead to a more complex FOC scheme. Therefore, the most applicable FOC scheme in the industrial applications is the FOC where the *d*-axis of the common reference frame is aligned to the rotor flux-linkage or what is usually called rotor flux-oriented control – RFOC. The characteristics of the common reference frame transformation matrix [D_s] now can be considered as follows:

$$\theta_s = \phi_r \qquad \omega_r = \frac{\mathrm{d}\phi_r}{\mathrm{d}t} \qquad \omega_a = \omega_r \tag{3.57}$$

where ϕ_r and ω_r represent the rotor field instantaneous position and speed of the rotor field, respectively. Thus, the transformation angle in equation (3.42) becomes equal to the angle of the rotor (rotating) field ϕ_r. As mentioned earlier, by aligning the *d*-axis to the *d*-component of the rotor flux-linkage, the *q*-component of the rotor flux-linkage will be equal to zero. Therefore:

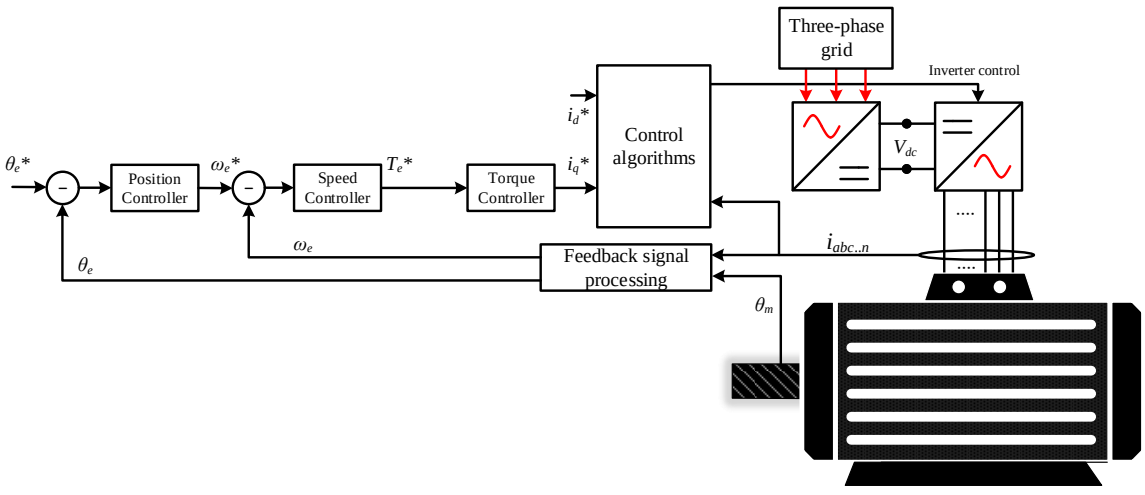

Fig. 3.5: Schematic of *n*-phase high-performance variable speed electric drive principle.

$$\psi_{dr} = \psi_r \qquad \psi_{qr} = 0 \qquad \frac{\mathrm{d}\psi_{qr}}{\mathrm{d}t} = 0 \tag{3.58}$$

Now, rewriting the rotor voltage equations (3.46) and (3.47) in the common reference frame, after implementing the described rotational transformation, will yield the following equations:

$$v_{dr} = 0 = R_r i_{dr} + \frac{\mathrm{d}\psi_r}{\mathrm{d}t} \tag{3.59}$$

$$v_{qr} = 0 = R_r i_{qr} + \left(\omega_r - \omega_e\right)\psi_r \tag{3.60}$$

Starting from rotor flux equations (3.50) and (3.51), the *d* and *q* rotor currents in the common reference frame can be expressed as follows:

$$\psi_r = \left(L_{lr} + L_m\right) i_{dr} + L_m i_{ds} \qquad \rightarrow \qquad i_{dr} = \frac{\psi_r - L_m i_{ds}}{L_r} \tag{3.61}$$

$$0 = \left(L_{lr} + L_m\right) i_{qr} + L_m i_{qs} \qquad \rightarrow \qquad i_{qr} = \frac{L_m}{L_r} i_{qs} \tag{3.62}$$

Substituting (3.61) and (3.62) into (3.59) and (3.60) will yield the model of a current-fed rotor flux-oriented induction machine:

$$\psi_r + T_r \frac{\mathrm{d}\psi_r}{\mathrm{d}t} = L_m i_{ds} \tag{3.63}$$

$$\left(\omega_r - \omega_e\right)\psi_r T_r = L_m i_{qs} \tag{3.64}$$

$$T_e = P\left(L_m / L_r\right)\psi_r i_{qs} \tag{3.65}$$

where $T_r = L_r/R_r$, is the rotor time constant. From (3.65), it is noticeable that by maintaining a constant rotor flux ψ_r, the electromagnetic torque T_e can be controlled by changing the *q*-component current of the stator, i_{qs}. Thus, the torque producing current is the i_{qs} and it is determined by the reference *q*-axis current of the stator. On the other hand, the flux producing current is the *d*-axis current of the stator as noticeable from (3.63). By expressing i_{qs} from (3.64) and substituting it into (3.65), the torque of the machine can be expressed in terms of the slip speed $\omega_{sl} = (\omega_r - \omega_e)$, as:

$$T_e = P\left(\frac{\psi_r^2}{R_r}\right)\omega_{sl} \tag{3.66}$$

It is noticeable from (3.66) that there is a linear relationship between the electromagnetic torque and the slip speed ω_{sl}. Theoretically this means that there is no pull-out torque, but in practice the torque is governed by the maximum stator voltages and current limits. In the steady state operation, the rotor flux-

linkage is constant and it is governed by the *d*-component of the stator current i_{ds} [Levi et al. (2007)]. Rewriting (3.63) for steady state operation yields the following:

$$\psi_r = L_m i_{ds} \tag{3.67}$$

The rotor flux-linkage reference should be equal to the magnetizing flux during no-load condition of the multiphase machine.

An illustration of the rotating common reference frame of a multiphase induction machine, where the stator current *d*-axis is firmly attached to the rotor flux-linkage axis (hence, rotor flux reference frame), is presented in Fig. 3.6. Based on this figure, one can see that the stator's current space vector i_s is defined as follows:

$$i_s = \sqrt{i_{ds}^2 + i_{qs}^2}\, e^{j\delta} = i_{ds} + j i_{qs} \tag{3.68}$$

where:

$$i_{ds} = i_s \cos\delta \qquad i_{qs} = i_s \sin\delta \tag{3.69}$$

Measuring the rotor flux-linkage position ϕ_r in a multiphase induction machine is not an easy job. Therefore, it is better to estimate it utilising the measurable variables of the induction machine [Levi et al. (2007)]. This estimation can be achieved by using equation (3.64) and the slip speed reference as follows. If the slip of the machine is equal to the reference slip one can write:

$$\omega_r = \omega_e + \omega_{sl}^* \tag{3.70}$$

$$\phi_r = \int \omega_r \mathrm{d}t = \int \left(\omega_e + \omega_{sl}^*\right) \mathrm{d}t = \theta_e + \int \omega_{sl}^* \mathrm{d}t \tag{3.71}$$

Further, for the reference values, based on (3.64) one can write:

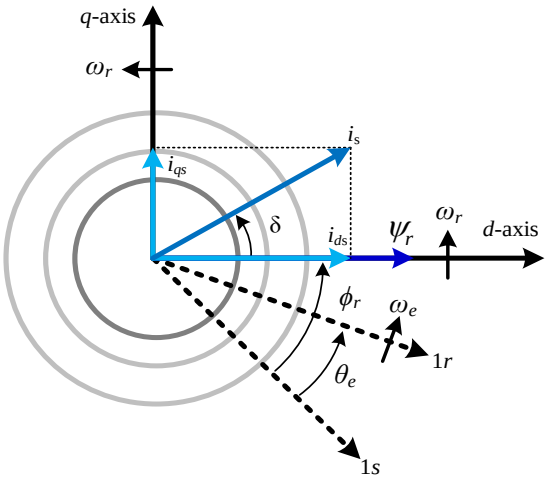

Fig. 3.6: The rotating common reference frame of a multiphase induction machine where the rotor flux-linkage is firmly attached to *d*-axis (rotor flux reference frame).

$$\omega_{sl}^{*} = \frac{L_m i_{qs}^{*}}{T_r \psi_r^{*}} \tag{3.72}$$

By substituting (3.67) into (3.72), the relationship between i_{qs} and the slip speed can be obtained as:

$$\omega_{sl}^{*} = \frac{i_{qs}^{*}}{T_r i_{ds}^{*}} = SG \cdot i_{qs}^{*} \tag{3.73}$$

where *SG* stands for the slip gain constant and is defined as: $SG = 1/(T_r \cdot i_{ds}^{*})$. By estimating the rotor flux position, RFOC is not directly measuring the position. Thus, this scheme is called indirect rotor field-oriented control (IRFOC). The block diagram of IRFOC for a multiphase induction machine is illustrated in Fig. 3.7. Note that in Fig. 3.7, the outer speed control loop is also shown (again, for simplicity the *x*-*y* current controllers are not included).

Operating the IRFOC scheme in the common reference frame requires considering the stator's voltage equations and the flux-linkage equations in the common reference frame. Substituting (3.48) and (3.49) into (3.44) and (3.45) and expressing (3.48) and (3.49) in terms of rotor flux-linkage equations (3.50) and (3.51) and in terms of the stator's currents, will produce the following equations:

$$v_{ds} = R_s i_{ds} + \sigma L_s \frac{\mathrm{d}i_{ds}}{\mathrm{d}t} + \frac{L_m}{L_r}\frac{\mathrm{d}\psi_r}{\mathrm{d}t} - \omega_r \sigma L_s i_{qs} \tag{3.74}$$

$$v_{qs} = R_s i_{qs} + \sigma L_s \frac{\mathrm{d}i_{qs}}{\mathrm{d}t} + \omega_r \frac{L_m}{L_r}\psi_r + \omega_r \sigma L_s i_{ds} \tag{3.75}$$

where L_s and L_r are the stator and rotor total inductance ($L_s = L_{ls} + L_m$ and $L_r = L_{lr} + L_m$), and σ is the total leakage coefficient and is defined as:

$$\sigma = 1 - \frac{L_m^2}{L_s L_r} \tag{3.76}$$

It is obvious from (3.74) and (3.75) that the stator's voltage equations are not fully decoupled, because the term of the *d*-component stator's current appear in the *q*-component stator's voltage and vice versa.

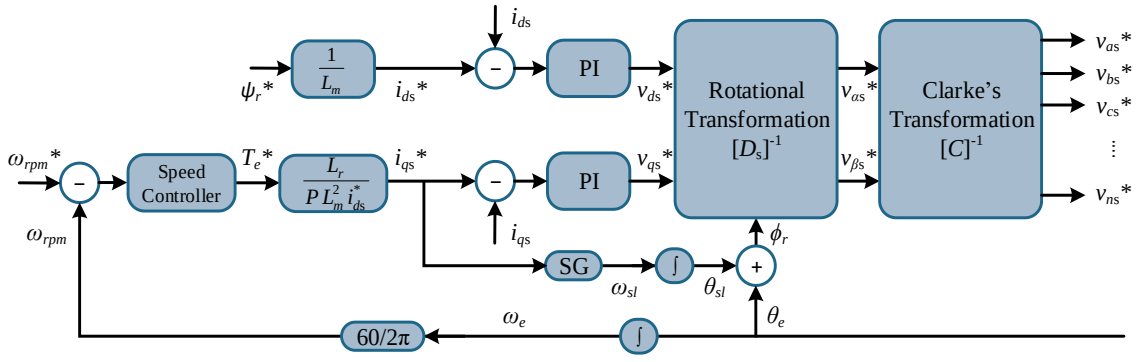

Fig. 3.7: IRFOC for multiphase induction machines.

This cross-coupling needs to be considered if the induction machine is required to be controlled in the rotor field reference frame. So, by redefining the voltage of the stator, the following equations are obtained:

$$v'_{ds} = R_s i_{ds} + L'_s \frac{\mathrm{d}i_{ds}}{\mathrm{d}t} \tag{3.77}$$

$$v'_{qs} = R_s i_{qs} + L'_s \frac{\mathrm{d}i_{qs}}{\mathrm{d}t} \tag{3.78}$$

where $L_s{}' = \sigma L_s$. The stator's reference values at the common reference frame are obtained as follows:

$$v^*_{ds} = v'_{ds} + e_d \tag{3.79}$$

$$v^*_{qs} = v'_{qs} + e_q \tag{3.80}$$

where e_d and e_q are the auxiliary variables needed to be added in order to obtain a fully decoupled control scheme. These variables are defined as:

$$e_d = \frac{L_m}{L_r} \frac{\mathrm{d}\psi_r}{\mathrm{d}t} - \omega_r L'_s i_{qs} \tag{3.81}$$

$$e_q = \omega_r \frac{L_m}{L_r} \psi_r + \omega_r L'_s i_{ds} \tag{3.82}$$

Since a constant flux is maintained during the operation of the induction machine (assuming that the machine is not operating in the field weakening region), the rotor flux linkage derivative is zero. Also, substituting (3.67) into (3.82) will yield to simplification of the auxiliary variables to:

$$e_d = -\omega_r L'_s i_{qs} \tag{3.83}$$

$$e_q = \omega_r L_s i_{ds} \tag{3.84}$$

Fig. 3.8 illustrates the IRFOC scheme for multiphase induction machine with cross-coupling decoupling (e_d and e_q) controller included. Again, the block diagram is shown with the outer speed control loop and no *x-y* current controllers.

Due to the non-ideal characteristics of the multiphase machine and power electronics converter in practice (such as the dead-time effect and asymmetries of the windings), controlling the *d-q* currents only with IRFOC is not sufficient. Therefore, the other *x-y* plane currents (auxiliary currents) need to be controlled along with the *d-q* plane.

3.7 CURRENT SHARING FOR MULTIPLE THREE-PHASE MACHINES

In the common reference frame of the multiphase induction machines, with sinusoidal magneto-motive force (mmf) distribution, the only torque and flux producing plane, actually contributing to the electromechanical energy conversion, is the *d-q* plane. The other planes are loss-producing sub-spaces. Thus, the *x-y* plane currents should be always controlled to zero, to eliminate the effects of non-ideal characteristics of the machine or the power electronics converter [Che et al. (2014a), Che et al. (2014c), Hu et al. (2014), Liu et al. (2016)]. However, post-fault techniques can utilise these currents to control the current's amplitude of the winding sets during the post-fault operating condition [Tani et al. (2013), Mengoni et al. (2016)]. The post-fault operation due to a fault of one or more inverters (when each winding set is supplied by an individual inverter) can be achieved by changing the sharing coefficients of the stator currents for each winding set. The current sharing control strategy will be discussed shortly in this section. However, Clarke's transformation for each winding set and for the whole machine have to be introduced first and the links between the original and the transformed variable, as well as between the transformed variables in the two different reference frames, have to be established.

Among the multiphase induction machines, multiple three-phase machines are attractive due to the availability of the well-established three-phase technology and their fault-tolerance capabilities. Since the neutral points of the winding sets are isolated, the zero-sequence current cannot flow and the 3rd harmonic does not exist. In order to control the auxiliary currents in a multiple three-phase machine, the machine can be decomposed into k three-phase winding sets (with a phase shift between the consecutive phases equal to $\alpha=2\pi/3$). Using the knowledge from three-phase theory, 3×3 Clarke's transformation [C_3], can be applied to each winding set (i = 1 to k). This modelling approach of multiphase machines will be termed here as the multi-stator (MS) modelling approach. Applying Clarke's transformation to each winding set will define α_i-β_i-o_i components for each set. When defining Clarke's transformation matrix for each winding set, the angular displacement of the set must be taken into account. Based on (3.27), Clarke's transformation matrix for each winding set can be defined as:

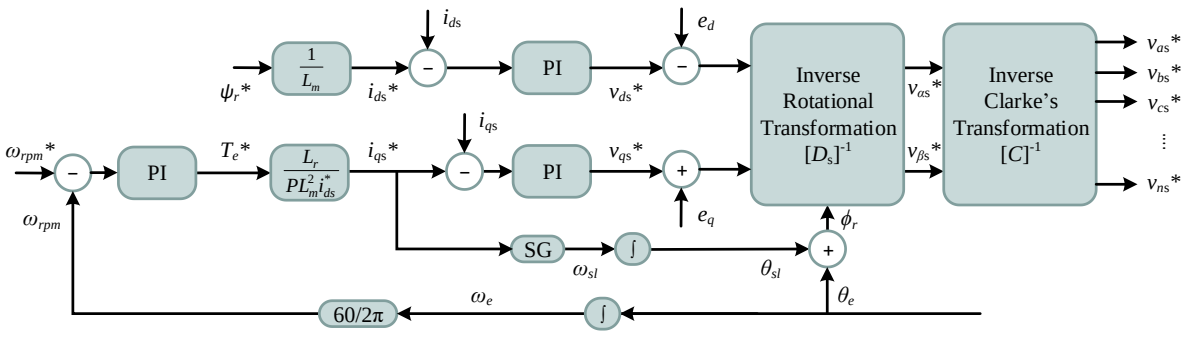

Fig. 3.8: IRFOC schematics with cross-coupling decoupling controllers.

$$\left[C_{3,i}\right]=\sqrt{\frac{2}{3}}\begin{bmatrix}\cos(\delta) & \cos\left(\delta+2\pi/3\right) & \cos\left(\delta+4\pi/3\right)\\ \sin(\delta) & \sin\left(\delta+2\pi/3\right) & \sin\left(\delta+4\pi/3\right)\\ 1/\sqrt{2} & 1/\sqrt{2} & 1/\sqrt{2}\end{bmatrix} \tag{3.85}$$

where δ represents the angular displacement of the *i*-th winding set with respect to the first winding set (i = 1 to k). For symmetrical multiple three-phase machine with k winding sets:

$$\delta\in\left\{0 \quad \alpha \quad 2\alpha \quad \cdots \quad (k-1)\alpha\right\} \qquad \text{or} \qquad \delta=(i-1)\alpha \tag{3.86}$$

The multiple three-phase machine can also be observed as a single n-phase machine and modelled as in section 3.5. Therefore, $n\times n$ Clarke's transformation, $[C_n]$, can be directly applied onto the full set of n phase currents defining decoupled phase current components: α, β, x_1, y_1, x_2, y_2, …, 0_1, 0_2, …, 0_k. This multiphase machine modelling approach will be termed as the vector space decomposition (VSD) approach. To define $[C_n]$ for the considered case of a symmetrical multiple three-phase machine, equation (3.56) can be rearranged and generalised for n-phase machines with k three-phase winding sets (and hence k isolated neutral points), as follows:

$$[C_n]=\sqrt{\frac{2}{n}}\left[\begin{array}{c|ccccccccc}
 & a_1 & b_1 & c_1 & a_2 & b_2 & c_2 & \cdots & a_k & b_k & c_k \\ \hline
\alpha & 1 & \cos(k\alpha) & \cos(2k\alpha) & \cos(\alpha) & \cos((k+1)\alpha) & \cos((2k+1)\alpha) & \cdots & \cos((k-1)\alpha) & \cos\left((k-1)\alpha+\frac{2\pi}{3}\right) & \cos\left((k-1)\alpha+\frac{4\pi}{3}\right) \\
\beta & 0 & \sin(k\alpha) & \sin(2k\alpha) & \sin(\alpha) & \sin((k+1)\alpha) & \sin((2k+1)\alpha) & \cdots & \sin((k-1)\alpha) & \sin\left((k-1)\alpha+\frac{2\pi}{3}\right) & \sin\left((k-1)\alpha+\frac{4\pi}{3}\right) \\
x_1 & 1 & \cos 2(k\alpha) & \cos 2(2k\alpha) & \cos 2(\alpha) & \cos 2((k+1)\alpha) & \cos 2((2k+1)\alpha) & \cdots & \cos 2((k-1)\alpha) & \cos 2\left((k-1)\alpha+\frac{2\pi}{3}\right) & \cos 2\left((k-1)\alpha+\frac{4\pi}{3}\right) \\
y_1 & 0 & \sin 2(k\alpha) & \sin 2(2k\alpha) & \sin 2(\alpha) & \sin 2((k+1)\alpha) & \sin 2((2k+1)\alpha) & \cdots & \sin 2((k-1)\alpha) & \sin 2\left((k-1)\alpha+\frac{2\pi}{3}\right) & \sin 2\left((k-1)\alpha+\frac{4\pi}{3}\right) \\
x_2 & 1 & \cos 4(k\alpha) & \cos 4(2k\alpha) & \cos 4(\alpha) & \cos 4((k+1)\alpha) & \cos 4((2k+1)\alpha) & \cdots & \cos 4((k-1)\alpha) & \cos 4\left((k-1)\alpha+\frac{2\pi}{3}\right) & \cos 4\left((k-1)\alpha+\frac{4\pi}{3}\right) \\
y_2 & 0 & \sin 4(k\alpha) & \sin 4(2k\alpha) & \sin 4(\alpha) & \sin 4((k+1)\alpha) & \sin 4((2k+1)\alpha) & \cdots & \sin 4((k-1)\alpha) & \sin 4\left((k-1)\alpha+\frac{2\pi}{3}\right) & \sin 4\left((k-1)\alpha+\frac{2\pi}{3}\right) \\
\vdots & \vdots & \vdots & \vdots & \vdots & \vdots & \vdots & \ddots & \vdots & \vdots & \vdots \\
x_{\frac{n-(k+2)}{2}} & 1 & \cos(hk\alpha) & \cos(2hk\alpha) & \cos(h\alpha) & \cos((k+1)h\alpha) & \cos((2k+1)h\alpha) & \cdots & \cos((k-1)h\alpha) & \cos\left((k-1)h\alpha+\frac{2\pi}{3}\right) & \cos\left((k-1)h\alpha+\frac{4\pi}{3}\right) \\
y_{\frac{n-(k+2)}{2}} & 0 & \sin(hk\alpha) & \sin(2hk\alpha) & \sin(h\alpha) & \sin((k+1)h\alpha) & \sin((2k+1)h\alpha) & \cdots & \sin((k-1)h\alpha) & \sin\left((k-1)h\alpha+\frac{2\pi}{3}\right) & \sin\left((k-1)h\alpha+\frac{4\pi}{3}\right) \\
0_1 & \sqrt{\frac{k}{2}} & \sqrt{\frac{k}{2}} & \sqrt{\frac{k}{2}} & 0 & 0 & 0 & \cdots & 0 & 0 & 0 \\
0_2 & 0 & 0 & 0 & \sqrt{\frac{k}{2}} & \sqrt{\frac{k}{2}} & \sqrt{\frac{k}{2}} & \cdots & 0 & 0 & 0 \\
\vdots & \vdots & \vdots & \vdots & \vdots & \vdots & \vdots & \ddots & \vdots & \vdots & \vdots \\
0_k & 0 & 0 & 0 & 0 & 0 & 0 & \cdots & \sqrt{\frac{k}{2}} & \sqrt{\frac{k}{2}} & \sqrt{\frac{k}{2}}
\end{array}\right] \tag{3.87}$$

where $h = (n\text{-}1)/2$. For current sharing, i.e. for controlling the currents of each winding set directly from the VSD reference frame, links between these two modelling approaches, VSD and MS, have to be established. By using Clarke's decoupling transformations for the three-phase winding sets $[C_{3,i}]$, the contribution of each winding set to the decoupled phase currents [defined by (3.87)] can be obtained. In other words, the links between α_1, β_1, o_1, α_2, β_2, o_2, α_k, β_k, o_k and α, β, x_1, y_1, x_2, y_2, …, 0_1, 0_2, …, 0_k, can be established. From Clarke's transformation matrix applied to each winding set, one can write:

$$\begin{bmatrix} i_{a1} \\ i_{b1} \\ i_{c1} \end{bmatrix} = \left[C_{3,1}\right]^{-1} \begin{bmatrix} i_{\alpha 1} \\ i_{\beta 1} \\ i_{o1} \end{bmatrix} \qquad \begin{bmatrix} i_{a2} \\ i_{b2} \\ i_{c2} \end{bmatrix} = \left[C_{3,2}\right]^{-1} \begin{bmatrix} i_{\alpha 2} \\ i_{\beta 2} \\ i_{o2} \end{bmatrix} \quad \cdots \quad \begin{bmatrix} i_{ak} \\ i_{bk} \\ i_{ck} \end{bmatrix} = \left[C_{3,k}\right]^{-1} \begin{bmatrix} i_{\alpha k} \\ i_{\beta k} \\ i_{ok} \end{bmatrix} \tag{3.88}$$

The phase currents can be represented in matrix form as:

$$\left[i_{ph}\right] = \left[i_{a1} \quad i_{b1} \quad i_{c1} \;\vdots\; i_{a2} \quad i_{b2} \quad i_{c2} \;\vdots\; \cdots \;\vdots\; i_{ak} \quad i_{bk} \quad i_{ck}\right]^T \tag{3.89}$$

The phase currents in (3.89) are intentionally shown as a vertical stack of the currents in each winding set. Now, if each sub-stack is substituted by (3.88), direct links between phase currents a_1, b_1, c_1, a_2, b_2, c_2, …, a_k, b_k, c_k and current projections for each set α_1, β_1, o_1, α_2, β_2, o_2, …, α_k, β_k, o_k, will be established. To demonstrate this a triple three-phase induction machine will be used:

$$\left[i_{ph9}\right] = \begin{bmatrix} i_{a1} \\ i_{b1} \\ i_{c1} \\ i_{a2} \\ i_{b2} \\ i_{c2} \\ i_{a3} \\ i_{b3} \\ i_{c3} \end{bmatrix} = \begin{bmatrix} \left[\mathrm{C}_{3,1}\right]^{-1} & [0]_{3\times 3} & [0]_{3\times 3} \\ [0]_{3\times 3} & \left[\mathrm{C}_{3,2}\right]^{-1} & [0]_{3\times 3} \\ [0]_{3\times 3} & [0]_{3\times 3} & \left[\mathrm{C}_{3,3}\right]^{-1} \end{bmatrix} \cdot \begin{bmatrix} i_{\alpha 1} \\ i_{\beta 1} \\ i_{o1} \\ i_{\alpha 2} \\ i_{\beta 2} \\ i_{o2} \\ i_{\alpha 3} \\ i_{\beta 3} \\ i_{o3} \end{bmatrix} \tag{3.90}$$

By calculating and substituting the values of $[C_{3,i}]^{-1}$ (i = 1 to 3), one gets:

$$\left[i_{ph9}\right] = \begin{bmatrix} \left[\mathrm{C}_{3,1}\right]^{-1} & [0]_{3\times 3} & [0]_{3\times 3} \\ [0]_{3\times 3} & \left[\mathrm{C}_{3,2}\right]^{-1} & [0]_{3\times 3} \\ [0]_{3\times 3} & [0]_{3\times 3} & \left[\mathrm{C}_{3,3}\right]^{-1} \end{bmatrix} \cdot \begin{bmatrix} i_{\alpha 1} \\ i_{\beta 1} \\ i_{o1} \\ i_{\alpha 2} \\ i_{\beta 2} \\ i_{o2} \\ i_{\alpha 3} \\ i_{\beta 3} \\ i_{o3} \end{bmatrix} = \begin{bmatrix} 0.816 i_{\alpha 1} + 0.577 i_{o1} \\ -0.408 i_{\alpha 1} + 0.707 i_{\beta 1} + 0.577 i_{o1} \\ -0.408 i_{\alpha 1} - 0.707 i_{\beta 1} + 0.577 i_{o1} \\ 0.626 i_{\alpha 2} + 0.525 i_{\beta 2} + 0.577 i_{o2} \\ -0.767 i_{\alpha 2} + 0.279 i_{\beta 2} + 0.577 i_{o2} \\ 0.142 i_{\alpha 2} - 0.804 i_{\beta 2} + 0.577 i_{o2} \\ 0.142 i_{\alpha 3} + 0.804 i_{\beta 3} + 0.577 i_{o3} \\ -0.767 i_{\alpha 3} - 0.279 i_{\beta 3} + 0.577 i_{o3} \\ 0.626 i_{\alpha 3} - 0.525 i_{\beta 3} + 0.577 i_{o3} \end{bmatrix} \tag{3.91}$$

Indeed (3.91) shows direct links between phase variables and the MS approach α_i-β_i-o_i variables. By multiplying the machine's phase currents matrix $[i_{ph}]$ by the generalised Clarke's transformation matrix (3.87), the decoupled phase currents $[i_{VSD}]$ can be defined:

$$\left[i_{VSD}\right]=\begin{bmatrix} i_{\alpha} \\ i_{\beta} \\ \hdashline i_{x1} \\ i_{y1} \\ \vdots \\ i_{x(n-(k+2)/2)} \\ i_{y(n-(k+2)/2)} \\ \hdashline i_{01} \\ \vdots \\ i_{0k} \end{bmatrix}=\left[C_n\right]\cdot\left[i_{ph}\right] \tag{3.92}$$

Clarke's transformation for the triple three-phase induction machine with symmetrical spatial displacement is given in (3.56). However, the columns of (3.56) should be reordered now, in order to follow the notation used in (3.87): a_1, b_1, c_1, a_2, b_2, c_2, a_3, b_3, c_3. After substituting the values of $[C_9]$ and $[i_{ph}]$ from (3.91) into (3.92), and after some maths, the links between α, β, x_1, y_1, x_2, y_2, …, 0_1, 0_2, …, 0_k and α_1, β_1, o_1, α_2, β_2, o_2, α_k, β_k, o_k, i.e. between the VSD and MS approaches, are obtained:

$$\left[i_{VSD}\right]=\begin{bmatrix} i_{\alpha} \\ i_{\beta} \\ i_{x_1} \\ i_{y_1} \\ i_{x_2} \\ i_{y_2} \\ i_{01} \\ i_{02} \\ i_{03} \end{bmatrix}=\begin{bmatrix} \frac{i_{\alpha1}+i_{\alpha2}+i_{\alpha3}}{\sqrt{3}} \\ \frac{i_{\beta1}+i_{\beta2}+i_{\beta3}}{\sqrt{3}} \\ \frac{2\sqrt{3}i_{\alpha1}-\sqrt{3}i_{\alpha2}-\sqrt{3}i_{\alpha3}+3i_{\beta2}-3i_{\beta3}}{6} \\ \frac{3i_{\alpha2}-3i_{\alpha3}-2\sqrt{3}i_{\beta1}+\sqrt{3}i_{\beta2}+\sqrt{3}i_{\beta3}}{6} \\ \frac{2\sqrt{3}i_{\alpha1}-\sqrt{3}i_{\alpha2}-\sqrt{3}i_{\alpha3}-3i_{\beta2}+3i_{\beta3}}{6} \\ \frac{3i_{\alpha2}-3i_{\alpha3}+2\sqrt{3}i_{\beta1}-\sqrt{3}i_{\beta2}-\sqrt{3}i_{\beta3}}{6} \\ i_{o1} \\ i_{o2} \\ i_{o3} \end{bmatrix} \tag{3.93}$$

From (3.93), one can see that α current of the multiphase machine consists of α_i components of the three winding sets. The same applies to the β component – it is proportional to the sum of β_i components. However, the *x*-*y* plane currents are consisting of a combination of the α_i-β_i components of the triple winding sets. Thus, the *x*-*y* currents, which sometimes are not controlled to zero but are used to achieve a post-fault operation of the machine, can be controlled by controlling the α_i-β_i components of the individual sets. Also, (3.93) confirms that 0_i and o_i axes are in fact the same (which may be confirmed from (3.87), for n=9 and k=3, and (3.85)), but the used notation clearly distinguishes which modelling approach is used.

To what follows it is convenient to introduce and use space vector notation. Multiphase machine's current space vectors in the VSD approach, can be defined as:

$$\begin{aligned}\bar{i}_{\alpha\beta} &= i_\alpha + ji_\beta = I_{\alpha\beta}\angle\varphi_{\alpha\beta}\\ \bar{i}_{xy1} &= i_{x1} + ji_{y1} = I_{xy1}\angle\varphi_{xy1}\\ \bar{i}_{xy2} &= i_{x2} + ji_{y2} = I_{xy2}\angle\varphi_{xy2}\end{aligned} \tag{3.94}$$

The zero-sequence currents of the winding sets will not be considered here, because these currents cannot flow in the multiphase machines with isolated neutral points. The current space vectors for each winding set, when the MS approach is used, are defined as:

$$\begin{aligned}\bar{i}_{\alpha\beta1} &= i_{\alpha1} + ji_{\beta1} = I_{\alpha\beta1}\angle\varphi_{\alpha\beta1}\\ \bar{i}_{\alpha\beta2} &= i_{\alpha2} + ji_{\beta2} = I_{\alpha\beta2}\angle\varphi_{\alpha\beta2}\\ \bar{i}_{\alpha\beta3} &= i_{\alpha3} + ji_{\beta3} = I_{\alpha\beta3}\angle\varphi_{\alpha\beta3}\end{aligned} \tag{3.95}$$

By rewriting $[i_{VSD}]$ from (3.93) in terms of the space vectors from equation (3.94) and (3.95), the following equations are obtained:

$$\bar{i}_{\alpha\beta} = \tfrac{1}{\sqrt{3}}(i_{\alpha1} + ji_{\beta1}) + \tfrac{1}{\sqrt{3}}(i_{\alpha2} + ji_{\beta2}) + \tfrac{1}{\sqrt{3}}(i_{\alpha3} + ji_{\beta3}) \tag{3.96}$$

$$\bar{i}_{xy1} = \tfrac{1}{\sqrt{3}}(i_{\alpha1} - ji_{\beta1}) + \tfrac{\sqrt{3}}{6}\left(\left(-1+ j\sqrt{3}\right)i_{\alpha2} + \left(\sqrt{3}+ j\right)i_{\beta2}\right) + \tfrac{\sqrt{3}}{6}\left(\left(-1- j\sqrt{3}\right)i_{\alpha3} - \left(\sqrt{3}- j\right)i_{\beta3}\right) \tag{3.97}$$

$$\bar{i}_{xy2} = \tfrac{1}{\sqrt{3}}(i_{\alpha1} + ji_{\beta1}) + \tfrac{\sqrt{3}}{6}\left(\left(-1+ j\sqrt{3}\right)i_{\alpha2} - \left(\sqrt{3}+ j\right)i_{\beta2}\right) + \tfrac{\sqrt{3}}{6}\left(\left(-1- j\sqrt{3}\right)i_{\alpha3} + \left(\sqrt{3}- j\right)i_{\beta3}\right) \tag{3.98}$$

After some simplification of (3.96) – (3.98) one can show that the VSD current space vectors can be rewritten in terms of the winding set MS approach current's space vectors, as follows:

$$\bar{i}_{\alpha\beta} = \tfrac{1}{\sqrt{3}}(\bar{i}_{\alpha\beta1} + \bar{i}_{\alpha\beta2} + \bar{i}_{\alpha\beta3}) \tag{3.99}$$

$$\bar{i}_{xy1} = \tfrac{1}{\sqrt{3}}\left(\bar{i}^{*}_{\alpha\beta1} + \bar{i}^{*}_{\alpha\beta2}e^{j\frac{2\pi}{3}} + \bar{i}^{*}_{\alpha\beta3}e^{-j\frac{2\pi}{3}}\right) \tag{3.100}$$

$$\bar{i}_{xy2} = \tfrac{1}{\sqrt{3}}\left(\bar{i}_{\alpha\beta1} + \bar{i}_{\alpha\beta2}e^{j\frac{2\pi}{3}} + \bar{i}_{\alpha\beta3}e^{-j\frac{2\pi}{3}}\right) \tag{3.101}$$

Once the transformations and links between the various reference frames are established, the current sharing can be considered. The *α-β* plane is a flux/torque producing plane, hence the current component $\bar{i}_{\alpha\beta}$ is responsible for the electromechanical energy conversion. Equation (3.99) shows that the flux/torque producing current space vector $\bar{i}_{\alpha\beta}$ in a triple three-phase induction machine is equal to the vector sum of the $\bar{i}_{\alpha\beta i}$ space vectors produced by each winding set. Scaling factor $1/\sqrt{3}$ in front,

comes as a consequence of the power invariant Clarke's transformation. Equation (3.99) also confirms the fact that the total torque generated by a multiple three-phase machine is equal to the sum of the torques generated by each winding set. Now, in order to control the contribution of each set to the total flux/torque producing current, the current sharing coefficients will be introduced. To minimise the stator current losses [Tani et al. (2013), Zoric et al. (2018)], it will be assumed that all $\bar{i}_{\alpha\beta i}$ space vectors are aligned with $\bar{i}_{\alpha\beta}$ space vector. Therefore, the current sharing coefficients K_1, K_2 and K_3, of the different winding sets, are defined as:

$$\left|i_{\alpha\beta 1}\right| = \sqrt{3}\,K_1\left|i_{\alpha\beta}\right| \tag{3.102}$$

$$\left|i_{\alpha\beta 2}\right| = \sqrt{3}\;K_2\left|i_{\alpha\beta}\right| \tag{3.103}$$

$$\left|i_{\alpha\beta 3}\right| = \sqrt{3}\;K_3\left|i_{\alpha\beta}\right| \tag{3.104}$$

By substituting equations (3.102) – (3.104) into (3.99) – (3.101), it will yield the following:

$$\bar{i}_{\alpha\beta} = (K_1 + K_2 + K_3)\bar{i}_{\alpha\beta} \tag{3.105}$$

$$\bar{i}_{xy1} = \left(K_1 + K_2 e^{j\frac{2\pi}{3}} + K_3 e^{-j\frac{2\pi}{3}}\right)\hat{\bar{i}}_{\alpha\beta} \tag{3.106}$$

$$\bar{i}_{xy2} = \left(K_1 + K_2 e^{j\frac{2\pi}{3}} + K_3 e^{-j\frac{2\pi}{3}}\right)\bar{i}_{\alpha\beta} \tag{3.107}$$

The previous current sharing equations (3.105) – (3.107) are valid in the common reference frame only. However, in order to control the currents, an appropriate rotational transformation, for each plane, has to be used. By investigating the current sharing equations, one can see that the auxiliary current space vectors are not necessarily rotating in the same direction as the α-β current space vector. In fact, from (3.106) one can see that $\bar{i}_{xy1}$ current space vector is rotating in the opposite direction from the α-β current space vector (complex conjugate, $\hat{\bar{i}}_{\alpha\beta}$), while from (3.107), obviously, $\bar{i}_{xy2}$ current space vector is rotating in the same direction as $\bar{i}_{\alpha\beta}$. Thus, the current control should be implemented in different synchronous reference frames. Rotating reference frames into which α-β, x_1-y_1 and x_2-y_2 components are projected are named as: d-q, d_1-q_1 and d_2-q_2, respectively. Fig. 3.9 illustrates the reference frames involved in the current sharing strategy and their directions of rotation.

The block diagram of the modified IRFOC scheme with auxiliary currents control is illustrated in Fig. 3.10. As for the IRFOC scheme from Fig. 3.8, the torque and rotor flux control in Fig. 3.10 are achieved by regulating the i_{ds} and i_{qs} in the synchronous reference frame. In order to control the amplitude of the currents in each winding set, the auxiliary currents are controlled according to the

current sharing equations (3.105) – (3.107) and in the appropriate reference frame according to Fig. 3.9. The first auxiliary currents x_1-y_1 subspace needs to be controlled in the anti-synchronous reference frame. This means that it needs to be multiplied by the rotational transformation matrix with the angle multiplied by –1. The following equations represent the synchronous rotational transformation matrix and the anti-synchronous rotational transformation matrix, respectively:

$$\left[e^{j\phi_r} \right] = \left[\begin{array}{c|cc} & \alpha, x_2 & \beta, y_2 \\ \hline d, d_2 & \cos\phi_r & \sin\phi_r \\ q, q_2 & -\sin\phi_r & \cos\phi_r \end{array}\right] \tag{3.108}$$

$$\left[e^{-j\phi_r} \right] = \left[\begin{array}{c|cc} & x_1 & y_1 \\ \hline d_1 & \cos\phi_r & -\sin\phi_r \\ q_1 & \sin\phi_r & \cos\phi_r \end{array}\right] \tag{3.109}$$

Equations (3.108) and (3.109) are used for x_1-y_1 and x_2-y_2 current control as illustrated in Fig. 3.10. Also note that these equations are transpose matrices of each other (orthogonal matrices). Therefore, they are both used in different order to convert the reference frame from rotational to stationary or from stationary to rotational reference frame, (Fig. 3.10). The benefit of implementing these different rotational transformations is to achieve the zero steady-state error of current control which will reduce the losses as a consequence.

In order to have a balanced system the sharing coefficients need to be equal to each other, and equal to 1/3 (see (3.105)) and their sum should be equal to one. For a nine-phase machine with three isolated neutral points, the sum of the sharing coefficients should always be equal to 1 during motoring mode, thus:

$$K_1 + K_2 + K_3 = 1 \tag{3.110}$$

In practice, when choosing the values of K_1, K_2 and K_3, one should be very careful because the rated currents of the machine or the inverter switches, should not be exceeded. Therefore, the following equations should be considered also during the current sharing operation of the machine:

$$\left| i_{abc...n} \right| \le I_{rated} \tag{3.111}$$

where I_{rated} represents the maximum inverter or phase rated current. If a fault occurred in one of the winding sets, the faulty winding set current should be distributed evenly among the healthy winding sets taking into consideration I_{rated}. To validate the developed auxiliary current control scheme, a symmetrical nine-phase induction machine with three isolated neutral points was developed using Matlab/Simulink. The simulation results are presented in the following section.

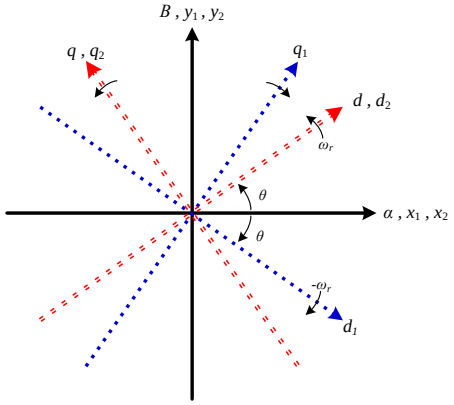

Fig. 3.9: Illustration of the reference frames involved in the current sharing strategy.

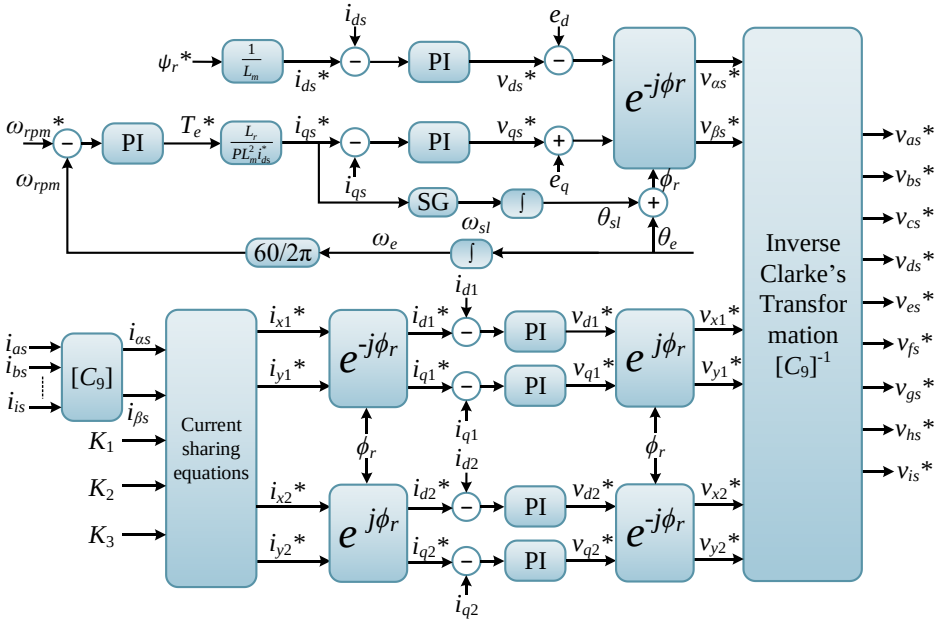

Fig. 3.10: Block diagram of IRFOC with current sharing control for triple three-phase induction machine.

3.8 SIMULATION RESULTS

A symmetrical nine-phase induction machine with three isolated neutral points is simulated in Matlab/Simulink using the phase variable model [Dordevic et al. (2010)]. The Clarke's decoupling transformation for a triple three-phase machine (as in (3.87) for n=9 and k=3) is implemented in the power invariant form. Afterward, the rotational transformation (as in (3.108) and (3.109)) is implemented in order to achieve a zero steady-state error of the regulated currents and to eliminate the time-dependent terms. In all cases the machine was supplied by a voltage source inverter (VSI). The voltage source inverter was modelled using an ideal switching. After the generation of the leg voltages

Table 3.1: The VSI's and nine-phase symmetrical induction machine's parameters.

P_{rated}	2.2 kW	P	1 (pair)
M	115.6 mH	R_s	4.85 Ω
L_{ls}	18 mH	R_r	1.82 Ω
L_{lr}	8.6 mH	L_s	538 mH
L_m	520 mH	L_r	528.6 mH
V_{dc}	750 V	f_s	5 kHz

references, the common mode voltage is subtracted to obtain the phase voltages. The Simulink model of the VSI is illustrated at appendix A. The parameters of the simulated machine and the VSI are illustrated in Table 3.1.

Different operating conditions are examined. Initially, the simulation is done by considering the triple three-phase machine supplied by three three-phase VSIs under open-loop condition. The results are shown in Fig. 3.11. The machine started with no load and reached the steady-state speed at approximately 0.7 sec. and then it was loaded with T_l = 5 Nm at t = 1.0 sec. The results show that the machine stator currents are balanced, and the amplitudes of the currents are the same for all winding

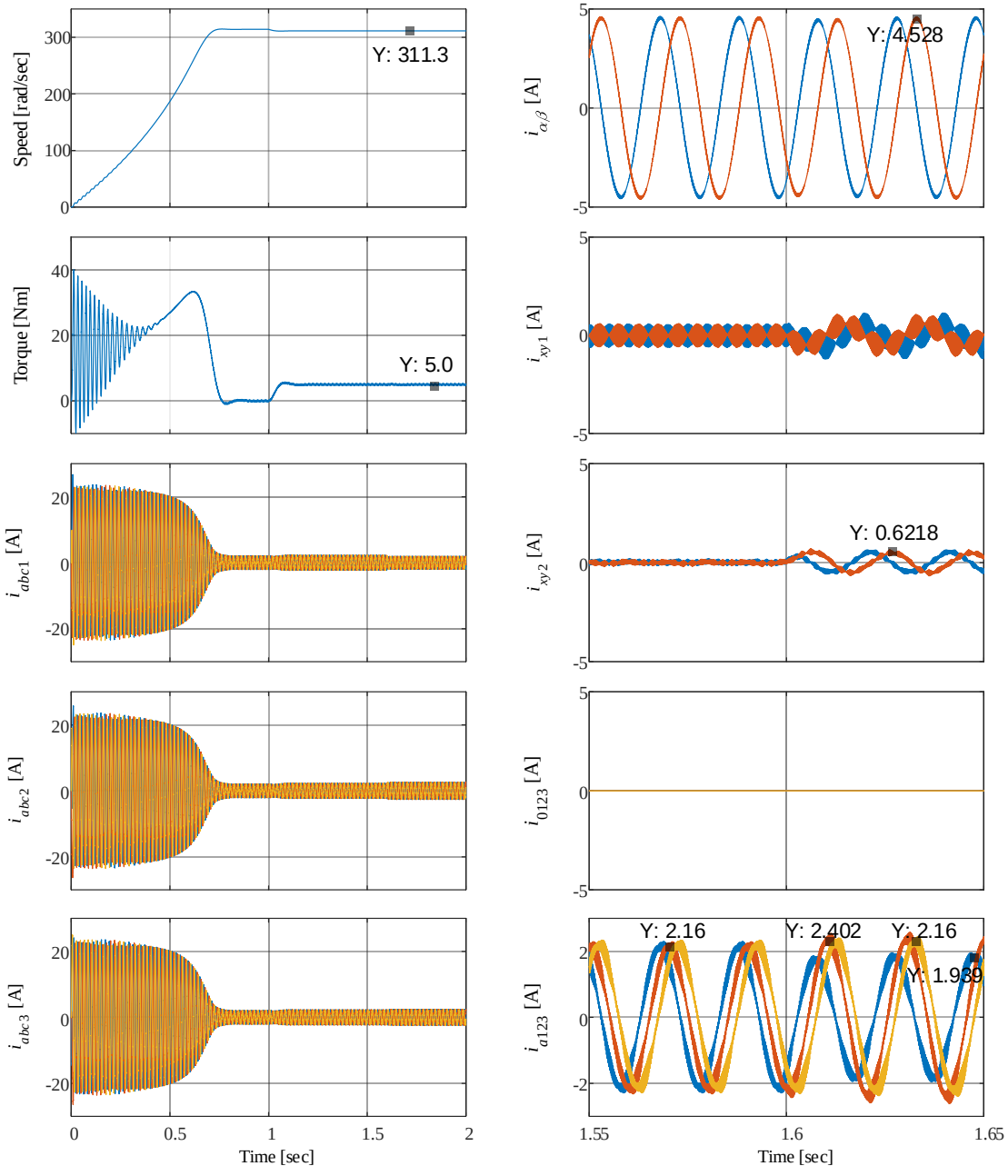

a) b)

Fig. 3.11: Simulation results for nine-phase induction machine with three isolated neutral points supplied by VSI in open-loop: (t = 0s – 1.6 sec balanced operation, t = 1.6 sec – 2 sec unbalanced operation). a) complete simulation, b) zoomed section between t = 1.55 sec – 1.65 sec.

sets. An expected reduction of speed is noticeable after applying the load torque at t = 1.0 sec. This test confirms proper development of the machine model. In order to test the machine running in open loop with an asymmetry in the winding sets, an asymmetry has been introduced in the first and the second winding set stator resistance, by adding 3 Ω to the original value of the first winding set and by subtracting 1 Ω from the second winding set original value. The asymmetry is initiated at t = 1.6 sec. The zoomed simulation results are illustrated in Fig. 3.11b.

It can be noticed that the currents become unbalanced once the asymmetry is added. The currents of the first winding sets (with asymmetry) are smaller than in the other winding sets. This is noticeable from the last subplot of Fig. 3.11b (i_{a123}), where i_{a1} = 1.93 A, i_{a2} = 2.40 A and i_{a3} = 2.16 A. Comparing the simulation results from Fig. 3.11b of the nine-phase machine with and without asymmetry shows that the machine auxiliary currents are zero during the balanced operation of the machine before 1.6 sec. On the contrary, the *x-y* currents components are present during unbalanced operation of the machine after 1.6 sec. as shown from Fig. 3.11b. Therefore, controlling only the machine's *α-β* currents is not enough to balance the machine's currents in the case of asymmetry in the windings.

Next, the machine is simulated under closed-loop control using the IRFOC including the current sharing algorithm. The implemented IRFOC scheme is illustrated in Fig. 3.10. The machine's flux and torque are controlled by regulating the *d-q* subspace currents. As can be seen from Fig. 3.10, the machine's currents are initially converted to the stationary reference frame and afterwards to the synchronous reference frame. The results are provided in Fig. 3.12. Once again, both cases, with and without asymmetry in the first and second winding sets stator resistances, were considered. The machine is accelerated to 1500 rpm and a load torque of 5 Nm is applied stepwise at t = 2.5 sec. One can see that the machine's currents are balanced between all the winding sets, and the machine's torque and flux producing current components are following their references (Fig. 3.12). The current sharing control algorithm presented in section 3.7 is implemented in Fig. 3.12 at t = 3.25 sec. The sharing coefficients were set to ($K_1 = K_2 = K_3 = 1/3$) initially and up to t = 3.25 sec. Subsequently, the sharing coefficients were changed ($K_1 = K_2 = 1/6$, $K_3 = 2/3$) during the period t = 3.25 sec – 3.5 sec. As a consequence, the amplitudes of i_{a1} and i_{a2} are equal and the amplitude of i_{a3} is four times larger, as can be seen from the last subplot of Fig. 3.12b (i_{a123}). Next, the current sharing coefficients were changed ($K_1 = K_2 = 1/4$, $K_3 = 1/2$) during the period t = 3.5 sec – 3.75 sec, and again the changes are directly reflected in the last subplot of Fig. 3.12b (i_{a123}) where the winding set currents are: i_{a1} = 1.74 A, i_{a2} = 1.74 A and i_{a3} = 3.35 A. Throughout the period between t = 3.75 sec – 4 sec the sharing coefficients were again changed ($K_1 = 1/4$, $K_2 = 1/2$, $K_2 = 1/4$) and here the winding set phase currents change correspondingly: i_{a1} = 1.74 A, i_{a2} = 3.35 A and i_{a3} = 1.74 A. These changes in the current sharing coefficients (3.25 sec – 4 sec) coincide with the machine operating with balanced winding sets. One can see that during the balanced operation of the machine, when the sharing coefficients are equivalent, the *x-y* subspace currents are zero. During the implementation of the current sharing strategy, after t = 3.25 sec, the current amplitude of the

winding sets is changing, while the total α-β currents remain unchanged. The x-y currents are changing according to the sharing coefficients K_i during the current sharing period.

During the time period t = 4 sec to t =5 sec the machine operates with unbalanced winding resistances as detailed earlier. The current sharing coefficients were changed according to the details provided at the top of Fig. 3.12b. When there is asymmetry introduced between the machine winding sets, the simulation results show that the current imbalance is not present anymore i.e. during the time when the sharing coefficients were set to ($K_1 = K_2 = K_3 = 1/3$) t = 4 sec to 4.25 sec. From Fig. 3.12b one

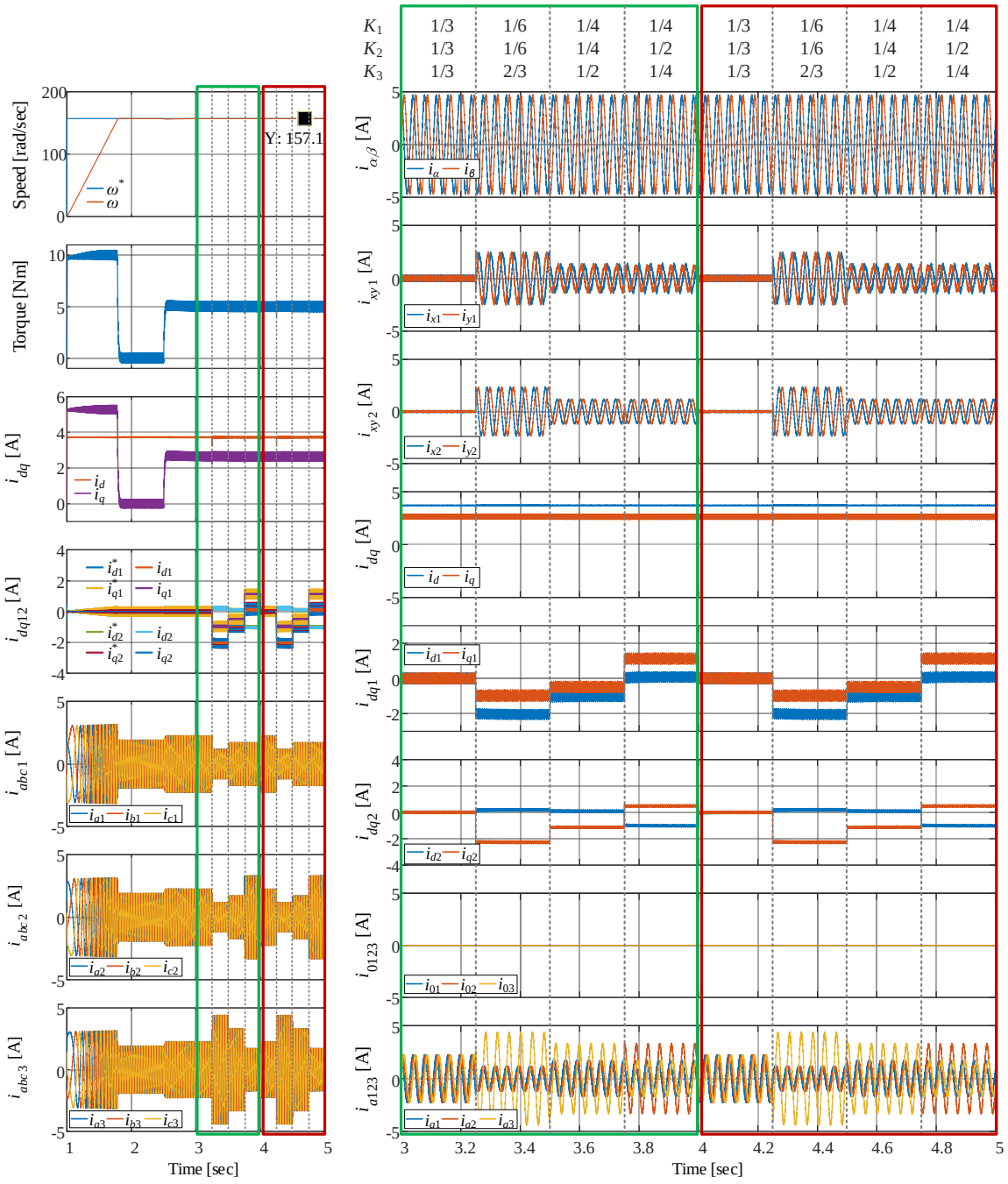

a) b)

Fig. 3.12: Simulation results for nine-phase induction machine controlled by IRFOC with and without asymmetry in the first and second winding sets. The green boxed area is without asymmetry while the red boxed area is with asymmetry. a) complete simulation, b) zoomed section between t = 3.0 sec – 5.0 sec.

can see that the currents in the first and third winding set have the same amplitude in all winding sets. Due to controlling the *x*-*y* currents to zero, the asymmetry of the machine's currents is eliminated. Having unbalanced currents between the winding sets can lead to decreased performance and efficiency of the drive system. In addition, the motor expected life will decrease. Also, according to [Liu et al. (2016)], in practice, this will increase the torque pulsation and the acoustic noise. Thus, the current balancing is an essential aspect of multiphase machines' control. The current sharing strategy can be

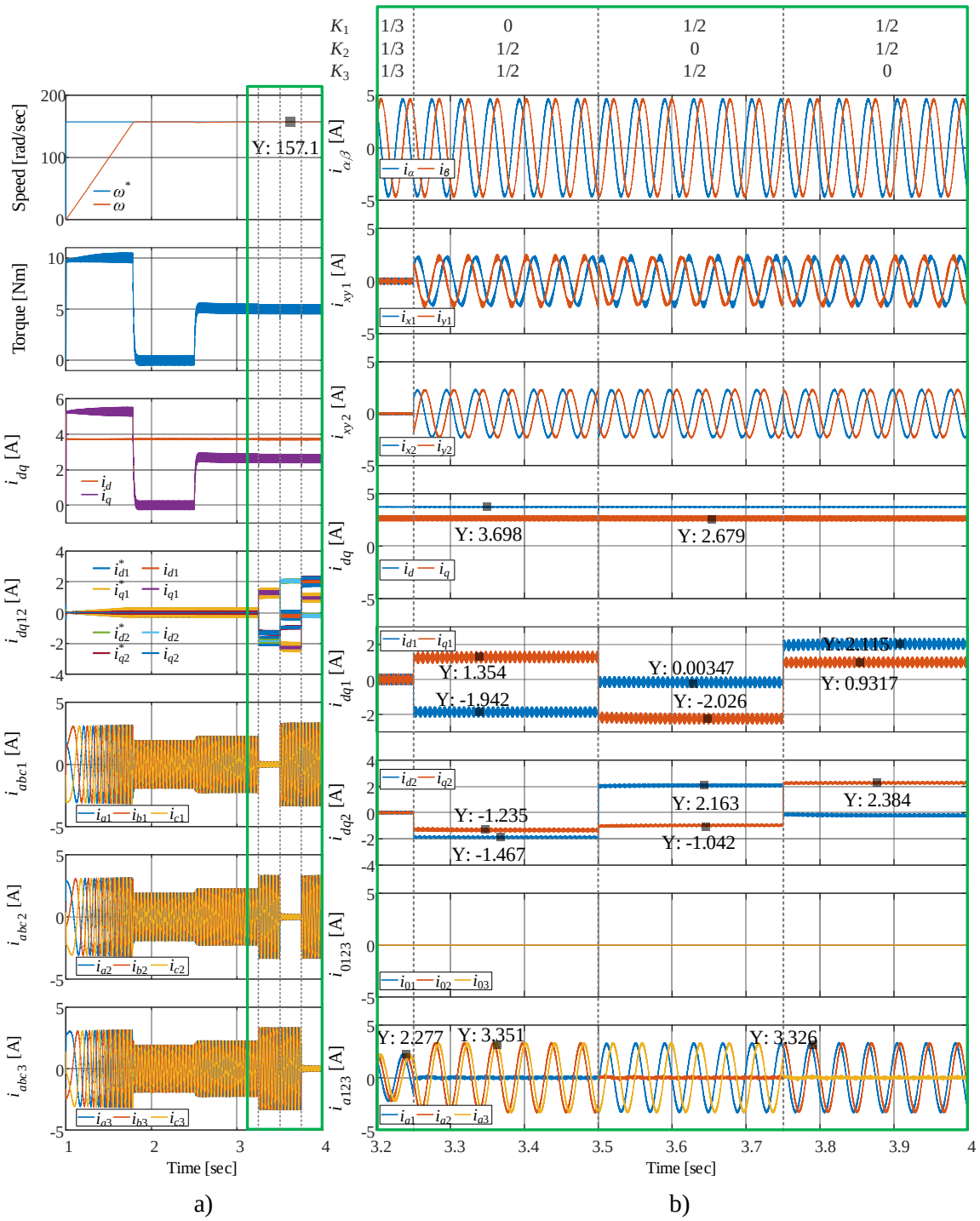

Fig. 3.13: Simulation results for nine-phase induction machine with three isolated neutral points controlled by IRFOC with auxiliary currents control working under post-fault. a) complete simulation, b) zoomed section between t = 3.2 sec – 4.0 sec.

implemented also when there is asymmetry in the machine windings. The results of the scenarios with different current sharing coefficients can be seen after t = 4.25 sec and are approximately identical to the previous results when the machine was simulated under symmetrical winding sets. This can be noticed by comparing the green and red boxed areas in Fig. 3.12b.

The current sharing control scheme can be utilised during the post-fault operation of the multiple three-phase induction machine. This can be achieved by manipulating the current sharing coefficients. For example, if one of the VSIs has a fault, the machine can still operate, albeit at a reduced capacity, while the faulty VSI is switched off. This scenario has been simulated in Fig. 3.13 where the first winding set's coefficient K_1 is set to zero at t = 3.25 sec. Afterward, the first set was put on again but the machine's second winding set's supply is switched off at t = 3.5 sec by setting K_2 to zero (Fig. 3.13b). Finally, the third winding set sharing coefficient K_3 is set to zero at t = 3.75 sec. In order to maintain the same machine performance, the required power is divided equally between the remaining two healthy winding sets. One can see that the machine's speed and torque are maintained the same in the post-fault operation. Also, note that the currents of the 'switched-off' winding sets are not exactly zero. This is so, because those winding sets are not physically disconnected, but their currents are controlled to zero, hence the ripple is present. Finally, note that for practical implementation of this algorithm the rated currents of the VSI's switches and the machine's rated currents should remain within the limit. Therefore, the current sharing coefficients should be appropriately reduced to satisfy these requirements.

3.9 EXPERIMENTAL RESULTS

The current sharing strategy presented in section 3.7 and simulated in section 3.8 is validated experimentally using a symmetrical nine-phase induction machine with three isolated neutral points. The machine parameters are presented in Table 3.1. Initially, the current sharing strategy is validated experimentally and the results are illustrated in Fig. 3.14. Then, the post-fault operation utilising the current sharing strategy is validated and the results are shown in Fig. 3.15.

The presented experimental results in Fig. 3.14a and Fig. 3.15a are recorded from dSPACE ControlDesk while the experimental results presented in Fig. 3.14b and Fig. 3.15b are screenshots of the oscilloscope. In Fig. 3.14 the experimental results of the current sharing strategy are implemented with the same condition of the simulation results in Fig. 3.12. The speed reference is set to 1500 rpm (157.1 rad/sec) and loaded using a self-excited DC generator with 5.22 Nm after reaching speed steady state. The sharing scenarios applied in Fig. 3.12 and Fig. 3.13 are applied to the nine-phase machine's experimental results as illustrated Fig. 3.14 and Fig. 3.15, respectively. In the first sharing scenario of the experimental results illustrated in Fig. 3.14 the sharing coefficients are changed to $K_1 = K_2 = 1/6$ and $K_3 = 2/3$ between t = 0.2 sec – 0.4 sec. It can be noticed from the last subplot of Fig. 3.14a that the third winding set current is four times the first and second winding sets' current. The d-q subspace currents are constant during the current sharing operation (t = 0.2 sec – 0.8 sec.). However, the x_i-y_i (d_i-q_i) are

changing according to the sharing coefficients. The experimental results match the simulation results during the same conditions, however, the experimental results have longer settling time of 0.1 sec, unlike the simulation results. Also, the current amplitude is slightly higher in the illustrated experimental results due to the higher load torque value (5.22 Nm) because applying the same load torque was not possible. In addition, additional vector PI regulators have been added to the auxiliary current controllers in parallel to eliminate the low order harmonics (5^{th}, 7^{th}, 11^{th}, 13^{th}, 29^{th} and 31^{st}) existing in the machine due to the

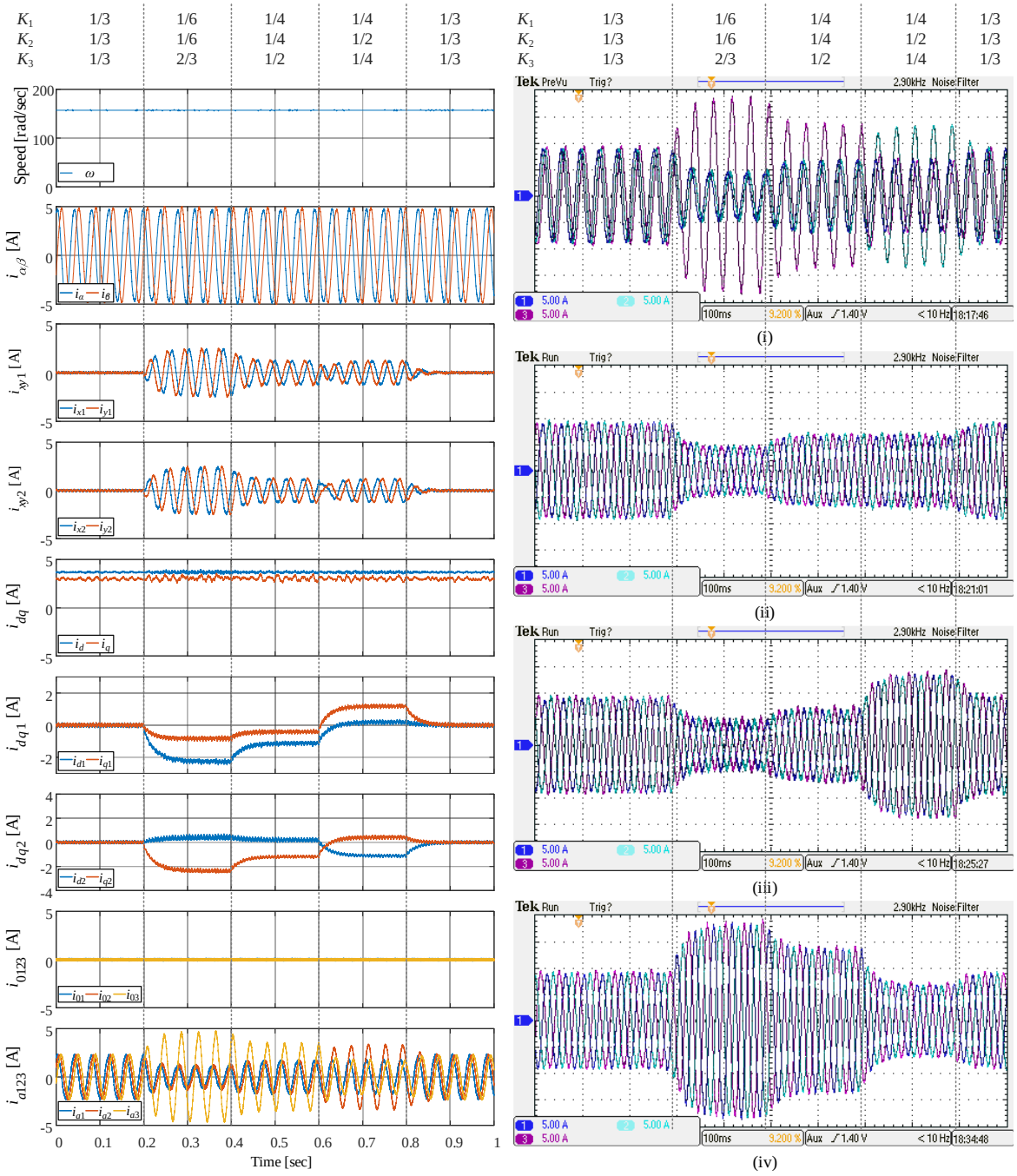

a) b)

Fig. 3.14: Experimental results for current sharing strategy of symmetrical nine-phase induction machine with three isolated neutral points (4 turns of wire were used for the oscilloscope current measurement). a) dSPACE recorder results b) Oscilloscope screenshots i) Ch1-i_{a1}, Ch2-i_{a2} and Ch3-i_{a3} current, ii) first set currents Ch1-i_{a1}, Ch2-i_{b1}, Ch3-i_{c1} iii) second set currents Ch1-i_{a2}, Ch2- i_{b2} and Ch3-i_{c2}. iv) third set currents Ch1-i_{a3}, Ch2- i_{b3} and Ch3-i_{c3}.

non-ideal design of the machine and due to the large dead-time of the VSI. The i_q current has a small ripple due to the existence of a small mechanical misalignment between the machine and the DC generator.

In the second sharing scenario presented in Fig. 3.14, the sharing coefficients are changed to K_1 = K_2 =1/4 and K_3 = 1/2 between t = 0.4 sec – 0.6 sec. As per the previous sharing scenario, the current ratio is following the sharing coefficients where the ratio between the third winding set current to the

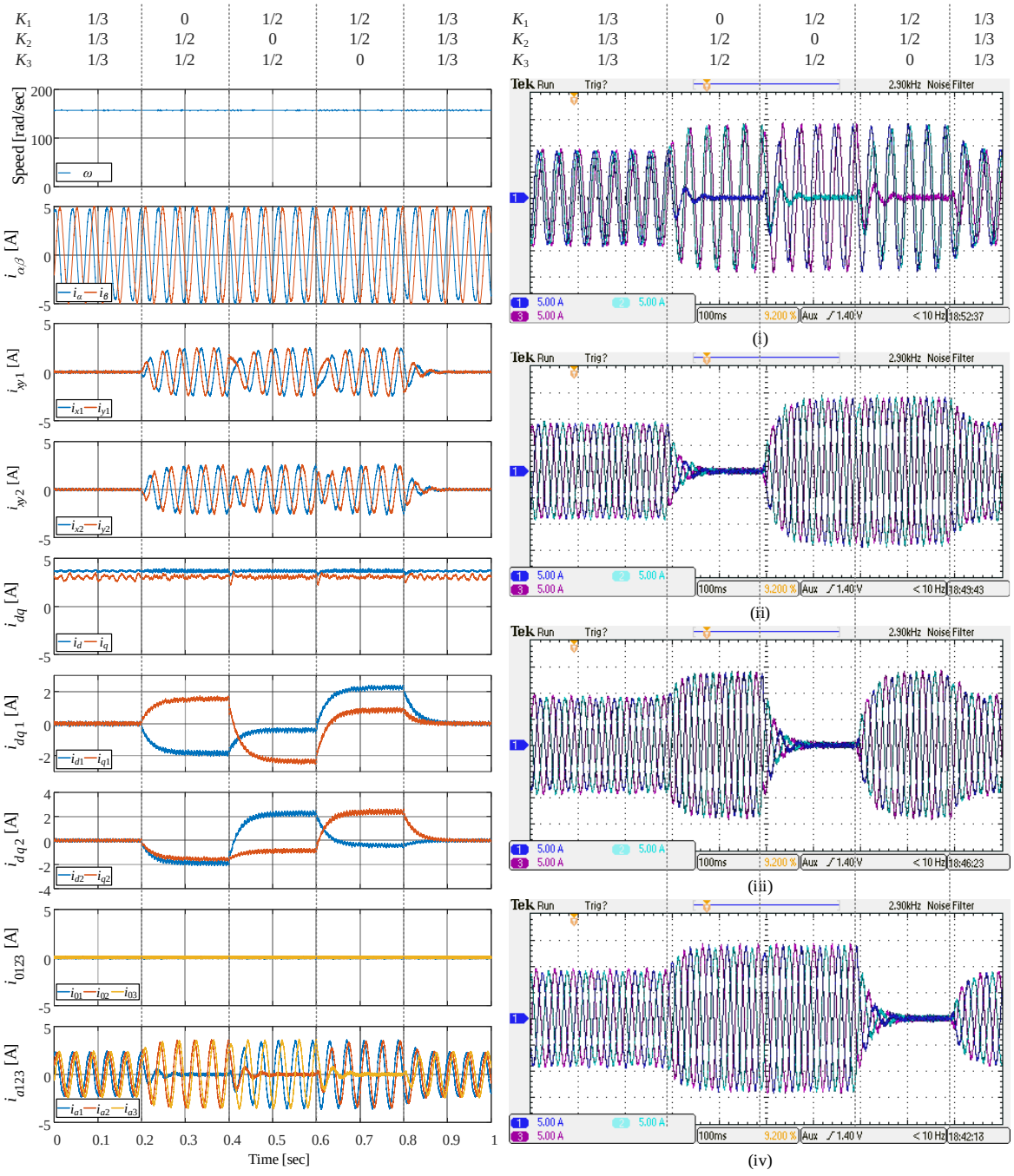

a) b)

Fig. 3.15: Experimental results for post-fault of a symmetrical nine-phase induction machine with three isolated neutral points using current sharing strategy (4 turns of wire were used for the oscilloscope current measurement). a) dSPACE recorder results b) Oscilloscope screenshots i) Ch1-i_{a1}, Ch2-i_{a2} and Ch3-i_{a3} current, ii) first set currents Ch1-i_{a1}, Ch2-i_{b1}, Ch3-i_{c1} iii) second set currents Ch1-i_{a2}, Ch2- i_{b2} and Ch3-i_{c2}. iv) third set currents Ch1-i_{a3}, Ch2- i_{b3} and Ch3-i_{c3}.

first and second winding sets currents is 2/1. The last current sharing scenario is implemented by changing the coefficients to K_1 = 1/4, K_2 = 1/2 and K_3 = 1/4 between t = 0.6 sec – 0.8 sec. The second winding current amplitude is twice the first and third winding set currents' amplitude during this scenario. This is clear from the last subplot of Fig. 3.14a (i_{a123}). In the last 0.2 sec (t = 0.8 sec – 1.0 sec), the machine is running in the normal condition where the auxiliary currents are controlled to zero by setting K_i to zeros. The same result is obtainable by equalising K_i to 1/3. Therefore, the currents' amplitude of the individual winding sets are equal. The winding sets' currents presented in Fig. 3.14b and Fig. 3.15b are measured using four turns of wire to increase the resolution of the measurement.

The second experiment of the current sharing strategy is performed to prove the ability of the current sharing strategy to operate the symmetrical nine-phase machine in post-fault operation. The experimental results illustrated in Fig. 3.15 are under the same conditions as the simulation results in Fig. 3.13 where the speed reference is set to 157.1 rad/sec and the load torque is equal to 5.22 Nm. Initially, the sharing coefficients are all set to 1/3 in the period from 0.0 sec – 0.2 sec. Then, the sharing strategy is applied by setting the sharing coefficients to 1/2 for the healthy winding sets and by shutting down one winding set (by setting its sharing coefficient to zero) each 0.2 sec, in the period from 0.2 sec – 0.8 sec. The first winding set is shutdown first by changing K_1 to zero. Afterwards, each 0.2 sec one of the winding sets is shutdown. Then the machine returns to the normal operation point when the sharing coefficients are set to 1/3. During post-fault operation of the machine the current in the running winding sets is roughly 1.5 times higher than during the normal operation of the machine. The experimental results of the post-fault operation of the nine-phase machines match the simulation results shown in Fig. 3.13.

3.10 SUMMARY

In this chapter a generalised mathematical modelling approach for the symmetrical multiphase induction machines is introduced. The modelling approach is based on a few assumptions and simplifications such as the linearization of the magnetising characteristics and neglecting the parasitic capacitances. Next, the generalised Clarke's decoupling transformation for the symmetrical multiphase machines was introduced. Usage of Clarke's transformation leads to a simplified mathematical model, compared to the phase variables model, which is decoupling the flux and torque producing plane from the loss producing (auxiliary) planes and zero-sequence axes. The rotational transformation is introduced, after the Clarke's decoupling transformation, in order to eliminate the time-dependent terms introduced by the Clarke's decoupling transformation. Then, the modelling approach of the multiple three-phase machines or multiphase machines with multiple isolated neutral points is discussed and the differences between these types of machines and the machines with a single neutral point were explained.

The field-oriented control for high-performance electric drives is derived for the multiphase induction machines. The main idea behind the field-oriented control is to convert the multiphase

induction machine to its dc machine equivalent. The best form of the FOC, to be utilised for induction machines, is the IRFOC scheme because the measurement of the position of the rotating field is not easy for these machines. Therefore, estimating the position of the rotating field is a better solution. The IRFOC scheme is used to control the multiphase induction machines. Due to the presence of non-ideal characteristics, such as asymmetry of the windings and dead-time effect, the auxiliary currents of the multiphase machines need to be controlled in addition to the flux/torque producing currents. The auxiliary currents can be used also to control the current amplitude in each winding set. This technique is called current sharing and it can control the induction machine current's amplitude (in each set) by simply changing the current sharing coefficients.

The current sharing method derivation is introduced and elaborated in this chapter. The introduced current sharing scheme is validated by the simulation and experimental results, presented at the end of the chapter. These results show the validity of the current sharing technique to control each winding set separately and therefore the power of the winding sets of the machine. Moreover, as presented, by setting the corresponding coefficient K_i to zero, the post-fault operation of the induction machines can be obtained by utilising the current sharing strategy.

CHAPTER 4

CURRENT SHARING FOR ASYMMETRICAL MULTIPLE THREE-PHASE INDUCTION MACHINES

4.1 INTRODUCTION

This chapter considers the design of a current sharing control scheme for the multiple three-phase asymmetrical induction machines. The general mathematical model and control for symmetrical *n*-phase induction machine were derived in Chapter 3. In this chapter, a generalised model of the asymmetrical multiple three-phase induction machine is derived first, followed by the derivation of the current sharing algorithm. As for the symmetrical machine, the current sharing scheme for asymmetrical machines is based on the IRFOC which has been derived in Chapter 3. Therefore, naturally, this chapter follows the organisation of the previous one, while putting more emphasis on the differences that come with the asymmetrical structure of the machine.

The organisation of the chapter is as follows. In section 4.2 a generalised mathematical modelling approach for the asymmetrical multiple three-phase induction machines is introduced. The same assumptions as those presented in Chapter 3 are used to simplify the mathematical modelling of the machine. Then, in section 4.3, vector space decomposition (VSD) transformation is introduced. VSD is Clarke's transformation equivalent which decouples the asymmetrical machine into a single flux/torque producing subspace and other subspaces, which produce losses, plus zero-sequence components. Next, in section 4.4, the generalised VSD is applied to a specific case of asymmetrical multiple three-phase machines with multiple neutral points. Section 4.5 presents the derivation of the current sharing scheme between the different winding sets for asymmetrical induction machine by controlling the auxiliary currents and the electromechanical subspace simultaneously. Next, the machine model and control system are validated using Matlab/Simulink. The simulation results of the asymmetrical nine-phase (triple three-phase) machine for different current sharing scenarios are presented in section 4.6. The experimental results for the asymmetrical machine are presented in section 4.7. Finally, the chapter's summary is made in section 4.8.

4.2 MODELLING OF ASYMMETRICAL MULTIPHASE INDUCTION MACHINES

The asymmetrical multiphase machines are operating based on the principle of the rotating field as for the symmetrical multiphase machines. They have to be supplied by the voltages which have an appropriate phase delay which corresponds to the magnetic axes of the machine. The asymmetrical multiphase machines were introduced to solve the problem of symmetrical multiphase machines where

the high pulsation in the torque waveform is present when supplied by a six-step modulated inverter. The torque pulsation causes excess mechanical vibration and poor performance during low speed and high torque operation [Nelson and Krause (1974)]. However, the development of the VSI with pulse width modulation has eliminated this problem. The main difference between these machine categories is the angular displacement between the winding sets. For instance, the angular displacement between the winding sets of the symmetrical *n*-phase machines is $\alpha=2\pi/n$. On the other hand, the angular displacement between consecutive winding sets of the asymmetrical machines is $\alpha=\pi/n$.

The mathematical model of an asymmetrical multiphase machine in principle is similar to the one of a symmetrical induction machine. The model can be derived in the same manner as in the previous chapter. However, the assumptions made in the previous chapter should be modified to consider the difference in the angular displacement between the winding sets of the machine. The electromechanical conversion equation is the same for symmetrical and asymmetrical configuration. However, the inductance matrices of the stator are different.

The asymmetrical induction machine general equations are exactly the same as for the symmetrical induction machine. Therefore, the equations (3.1) – (3.12) are also valid for the asymmetrical multiphase induction machine. The difference appears in the inductance matrices. Note that the model below is presented for multiple three-phase machine with *k* three-phase winding sets. The self-inductances of the stator and rotor ($[L_s]$ and $[L_r]$) contain only constant terms as expressed below:

$$\left[L_s\right]=\begin{bmatrix}\left[L_{s1}\right]_{k\times k} & \left[L_{s2}\right]_{k\times k} & \left[L_{s3}\right]_{k\times k}\\ \left[L_{s3}\right]_{k\times k} & \left[L_{s1}\right]_{k\times k} & \left[L_{s2}\right]_{k\times k}\\ \left[L_{s2}\right]_{k\times k} & \left[L_{s3}\right]_{k\times k} & \left[L_{s1}\right]_{k\times k}\end{bmatrix} \tag{4.1}$$

$$\left[L_r\right]=\begin{bmatrix} L_{lr}+M & M\cos(2\alpha) & M\cos(4\alpha) & \cdots & M\cos((2n-2)\alpha)\\ M\cos((2n-2)\alpha) & L_{lr}+M & M\cos(\alpha) & \cdots & M\cos((2n-4)\alpha)\\ M\cos((2n-4)\alpha) & M\cos((2n-2)\alpha) & L_{lr}+M & \cdots & M\cos((2n-6)\alpha)\\ \vdots & \vdots & \vdots & \ddots & \vdots\\ M\cos(2\alpha) & M\cos(4\alpha) & M\cos(6\alpha) & \cdots & L_{lr}+M\end{bmatrix} \tag{4.2}$$

where $\alpha=\pi/n$ and $[L_{s1}]$, $[L_{s2}]$ and $[L_{s3}]$ from (3.15) are defined as:

$$\left[L_{s1}\right]=\begin{bmatrix} L_{ls}+M & M\cos(\alpha) & \cdots & M\cos((k-2)\alpha) & M\cos((k-1)\alpha)\\ M\cos((2n-1)\alpha) & L_{ls}+M & \cdots & M\cos((k-3)\alpha) & M\cos((k-2)\alpha)\\ \vdots & \vdots & \ddots & \vdots & \vdots\\ M\cos((2n-(k-2))\alpha) & M\cos((2n-(k-3))\alpha) & \cdots & L_{ls}+M & M\cos(\alpha)\\ M\cos((2n-(k-1))\alpha) & M\cos((2n-(k-2))\alpha) & \cdots & M\cos((2n-1)\alpha) & L_{ls}+M\end{bmatrix} \tag{4.3}$$

$$\left[L_{s2}\right]=\begin{bmatrix} M\cos(\frac{2\pi}{3}) & M\cos(\frac{2\pi}{3}+\alpha) & \cdots & M\cos(\frac{2\pi}{3}+(k-2)\alpha) & M\cos(\frac{2\pi}{3}+(k-1)\alpha) \\ M\cos(\frac{2\pi}{3}-\alpha) & M\cos(\frac{2\pi}{3}) & \cdots & M\cos(\frac{2\pi}{3}+(k-3)\alpha) & M\cos(\frac{2\pi}{3}+(k-2)\alpha) \\ \vdots & \vdots & \ddots & \vdots & \vdots \\ M\cos(\frac{2\pi}{3}-(k-2)\alpha) & M\cos(\frac{2\pi}{3}-(k-3)\alpha) & \cdots & M\cos(\frac{2\pi}{3}) & M\cos(\frac{2\pi}{3}+\alpha) \\ M\cos(\frac{2\pi}{3}-(k-1)\alpha) & M\cos(\frac{2\pi}{3}-(k-2)\alpha) & \cdots & M\cos(\frac{2\pi}{3}-\alpha) & M\cos(\frac{2\pi}{3}) \end{bmatrix} \tag{4.4}$$

$$\left[L_{s3}\right]=\begin{bmatrix} M\cos(\frac{4\pi}{3}) & M\cos(\frac{4\pi}{3}+\alpha) & \cdots & M\cos(\frac{4\pi}{3}+(k-2)\alpha) & M\cos(\frac{4\pi}{3}+(k-1)\alpha) \\ M\cos(\frac{4\pi}{3}-\alpha) & M\cos(\frac{4\pi}{3}) & \cdots & M\cos(\frac{4\pi}{3}+(k-3)\alpha) & M\cos(\frac{4\pi}{3}+(k-2)\alpha) \\ \vdots & \vdots & \ddots & \vdots & \vdots \\ M\cos(\frac{4\pi}{3}-(k-2)\alpha) & M\cos(\frac{4\pi}{3}-(k-3)\alpha) & \cdots & M\cos(\frac{4\pi}{3}) & M\cos(\frac{4\pi}{3}+\alpha) \\ M\cos(\frac{4\pi}{3}-(k-1)\alpha) & M\cos(\frac{4\pi}{3}-(k-2)\alpha) & \cdots & M\cos(\frac{4\pi}{3}-\alpha) & M\cos(\frac{4\pi}{3}) \end{bmatrix} \tag{4.5}$$

Note that the stator is modelled as asymmetrical, while the rotor (which is assumed to be a squirrel cage rotor made of rotor bars) is in fact assumed to take a symmetrical structure. This simplifies the model but does not affect the generality of it.

The mutual inductance matrices between the stator and rotor are consisting of time-varying terms since the rotor is in constant movement and the stator is stationary. The matrices are dependent on the electrical position of the rotor θ_e, which is defined in (3.17). The mutual inductance matrix between the stator-to-rotor $[L_{sr}]$ and rotor-to-stator $[L_{rs}]$ is defined as follows:

$$\left[L_{sr}\right]=\begin{bmatrix} \left[L_{sr1}\right]_{k\times k} & \left[L_{sr2}\right]_{k\times k} & \left[L_{sr3}\right]_{k\times k} \\ \left[L_{sr3}\right]_{k\times k} & \left[L_{sr1}\right]_{k\times k} & \left[L_{sr2}\right]_{k\times k} \\ \left[L_{sr2}\right]_{k\times k} & \left[L_{sr3}\right]_{k\times k} & \left[L_{sr1}\right]_{k\times k} \end{bmatrix} \tag{4.6}$$

$$\left[L_{rs}\right]=\left[L_{sr}\right]^{T} \tag{4.7}$$

where $[L_{sr1}]$, $[L_{sr2}]$ and $[L_{sr3}]$ from (4.6) are defined as:

$$\left[L_{sr1}\right]=M\begin{bmatrix} \cos(\theta_e) & \cos(\theta_e+\alpha) & \cdots & \cos(\theta_e+(k-2)\alpha) & \cos(\theta_e+(k-1)\alpha) \\ \cos(\theta_e+(2n-1)\alpha) & \cos(\theta_e) & \cdots & \cos(\theta_e+(k-3)\alpha) & \cos(\theta_e+(k-2)\alpha) \\ \vdots & \vdots & \ddots & \vdots & \vdots \\ \cos(\theta_e+(2n-(k-2))\alpha) & \cos(\theta_e+(2n-(k-3))\alpha) & \cdots & \cos(\theta_e) & \cos(\theta_e+\alpha) \\ \cos(\theta_e+(2n-(k-1))\alpha) & \cos(\theta_e+(2n-(k-2))\alpha) & \cdots & \cos(\theta_e+(2n-1)\alpha) & \cos(\theta_e) \end{bmatrix} \tag{4.8}$$

$$\left[L_{sr2}\right]=M\begin{bmatrix} \cos(\theta_e+\frac{2\pi}{3}) & \cos(\theta_e+\frac{2\pi}{3}+\alpha) & \cdots & \cos(\theta_e+\frac{2\pi}{3}+(k-2)\alpha) & \cos(\theta_e+\frac{2\pi}{3}+(k-1)\alpha) \\ \cos(\theta_e+\frac{2\pi}{3}-\alpha) & \cos(\theta_e+\frac{2\pi}{3}) & \cdots & \cos(\theta_e+\frac{2\pi}{3}+(k-3)\alpha) & \cos(\theta_e+\frac{2\pi}{3}+(k-2)\alpha) \\ \vdots & \vdots & \ddots & \vdots & \vdots \\ \cos(\theta_e+\frac{2\pi}{3}-(k-2)\alpha) & \cos(\theta_e+\frac{2\pi}{3}-(k-3)\alpha) & \cdots & \cos(\theta_e+\frac{2\pi}{3}) & \cos(\theta_e+\frac{2\pi}{3}+\alpha) \\ \cos(\theta_e+\frac{2\pi}{3}-(k-1)\alpha) & \cos(\theta_e+\frac{2\pi}{3}-(k-2)\alpha) & \cdots & \cos(\theta_e+\frac{2\pi}{3}-\alpha) & \cos(\theta_e+\frac{2\pi}{3}) \end{bmatrix} \tag{4.9}$$

$$\left[L_{sr3}\right]=M\begin{bmatrix}\cos(\theta_e+\frac{4\pi}{3}) & \cos(\theta_e+\frac{4\pi}{3}+\alpha) & \cdots & \cos(\theta_e+\frac{4\pi}{3}+(k-2)\alpha) & \cos(\theta_e+\frac{4\pi}{3}+(k-1)\alpha)\\ \cos(\theta_e+\frac{4\pi}{3}-\alpha) & \cos(\theta_e+\frac{4\pi}{3}) & \cdots & \cos(\theta_e+\frac{4\pi}{3}+(k-3)\alpha) & \cos(\theta_e+\frac{4\pi}{3}+(k-2)\alpha)\\ \vdots & \vdots & \ddots & \vdots & \vdots\\ \cos(\theta_e+\frac{4\pi}{3}-(k-2)\alpha) & \cos(\theta_e+\frac{4\pi}{3}-(k-3)\alpha) & \cdots & \cos(\theta_e+\frac{4\pi}{3}) & \cos(\theta_e+\frac{4\pi}{3}+\alpha)\\ \cos(\theta_e+\frac{4\pi}{3}-(k-1)\alpha) & \cos(\theta_e+\frac{4\pi}{3}-(k-2)\alpha) & \cdots & \cos(\theta_e+\frac{4\pi}{3}-\alpha) & \cos(\theta_e+\frac{4\pi}{3})\end{bmatrix} \tag{4.10}$$

The above equations (4.1) – (4.10) represent the complete electrical subsystem of the asymmetrical multiphase machine. To describe the mechanical subsystem and the electro-mechanical energy conversion of an asymmetrical induction machine, the same equations as in Chapter 3 are also applicable here, (3.19) – (3.25). The mechanical subsystem of the machine can be described by Newton's second law for rotation as:

$$T_e - T_l = \frac{J}{P}\frac{\mathrm{d}\omega_e}{\mathrm{d}t} \tag{4.11}$$

The electro-mechanical energy conversion can be described by the following equations:

$$T_e = P\frac{1}{2}\left[i\right]^T\frac{\mathrm{d}\left[L\right]}{\mathrm{d}\theta_e}\left[i\right] \tag{4.12}$$

$$T_e = P\left[i_s\right]^T\frac{\mathrm{d}\left[L_{sr}\right]}{\mathrm{d}\theta_e}\left[i_r\right] \tag{4.13}$$

where [L] and [i] from (3.22) are defined as follows:

$$\left[L\right]=\begin{bmatrix}[L_s] & [L_{sr}]\\ [L_{rs}] & [L_r]\end{bmatrix} \tag{4.14}$$

$$\left[i\right]=\begin{bmatrix}\left[i_s\right]^T & \left[i_r\right]^T\end{bmatrix}^T \tag{4.15}$$

The complete mathematical model of the asymmetrical induction machine is represented by the above set of equations (4.1) – (4.15) plus the equation from Chapter 3 ((3.1) – (3.12)). The model in phase variables contains 2n+1 differential equation. To simplify the model, another form of the discrete Fourier transformation is utilised to decouple the asymmetrical machine into its dc machine equivalent. This special case is known as the vector space decomposition (VSD). A generalised VSD transformation is introduced in the following section for asymmetrical multiphase machines with multiple three-phase winding sets and a single neutral point.

4.3 VECTOR SPACE DECOMPOSITION TRANSFORMATION

Vector space decomposition transformation was introduced for asymmetrical six-phase machines in [Zhao and Lipo (1995)]. VSD, similar to Clarke's transformation, is based on the symmetrical

components' theory. After applying the transformation, the asymmetrical machine is decoupled into flux/torque producing subspace and loss producing subspaces plus the zero-sequence component(s). The transformation looks different depending on whether the machine winding sets are consisting of three, five or more phases. The most common and dominant configuration is with multiple three-phase winding sets. Therefore, this section will only consider the VSD transformation for the asymmetrical machines with multiple three-phase winding sets and with a single neutral point. The general case of this transformation has been analysed and presented in [Zoric et al. (2017)].

VSD will introduce new fictitious variables when it is applied to the phase variables such as stator or rotor voltages, currents or flux linkages. The following equation defines the relationship between the phase variables and the newly introduced VSD variables for an *n*-phase asymmetrical machine:

$$\left[f_{\alpha\beta,x_1y_1,\ldots 0_+0_-} \right]_{n\times 1} = \left[VSD\right]_{n\times n} \left[f_{1,2,\ldots n} \right]_{n\times 1} \tag{4.16}$$

where *f* can be any mentioned variable of the stator or the rotor. VSD transformation decouples the machine into orthogonal subspaces. This allows a separate control of the flux and torque of the asymmetrical multiphase machine. As for the Clarke's matrix transformation, the first subspace will have the fundamental harmonic of the machine (α-β subspace). The electro-mechanical energy conversion (flux/torque) occurs in this subspace. The loss-producing subspaces x_i-y_i are also present. The last component (for odd number of phases *n*) or last two components (for even number of phases *n*) of VSD variables represent the zero-sequence component(s). The generalised VSD transformation matrix $[VSD]_{n\times n}$ for asymmetrical multiphase machines with even number of phases *n* and a single neutral point is defined as:

$$\left[VSD\right]_{n\times n} = \sqrt{\frac{2}{n}} \left[\begin{array}{c|cccccc} \alpha & \cos([\theta_s]) & & & & & \\ \beta & \sin([\theta_s]) & & & & & \\ \hline x_1 & \cos(3\cdot[\theta_s]) & & & & & \\ y_1 & \sin(3\cdot[\theta_s]) & & & & & \\ x_2 & \cos(5\cdot[\theta_s]) & & & & & \\ y_2 & \sin(5\cdot[\theta_s]) & & & & & \\ \vdots & \vdots & & & & & \\ x_{\frac{n-4}{2}} & \cos((n-1)\cdot[\theta_s]) & & & & & \\ y_{\frac{n-4}{2}} & \sin((n-1)\cdot[\theta_s]) & & & & & \\ \hline 0_+ & \frac{1}{\sqrt{2}} & \frac{1}{\sqrt{2}} & \frac{1}{\sqrt{2}} & \frac{1}{\sqrt{2}} & \cdots & \frac{1}{\sqrt{2}} \\ 0_- & \frac{1}{\sqrt{2}} & \frac{-1}{\sqrt{2}} & \frac{1}{\sqrt{2}} & \frac{-1}{\sqrt{2}} & \cdots & \frac{-1}{\sqrt{2}} \end{array}\right] \tag{4.17}$$

where $[\theta_s]$ represents the angular displacement between the phases. For an asymmetrical machine $[\theta_s]$ can be expressed as follows (*k* is the number of three-phase winding sets):

$$[\theta_s]=\frac{\pi}{n}[0 \quad 1 \quad \cdots \quad k-2 \quad k-1 \mid 2k \quad 2k+1 \quad \cdots \quad 3k-2 \quad 3k-1 \mid 4k \quad 4k+1 \quad \cdots \quad 5k-2 \quad 5k-1] \quad (4.18)$$

Obviously, there is one α-β subspace in (4.17), (n–4)/2 x_i-y_i subspaces and two zero sequence components for an asymmetrical multiple three-phase machine with an even number of phases. On the other hand, when there is an odd number of phases, the matrix will be in the following form:

$$[VSD]_{n\times n}=\sqrt{\frac{2}{n}}\left[\begin{array}{c|c} \alpha & \cos([\theta_s]) \\ \beta & \sin([\theta_s]) \\ \hline x_1 & \cos(3\cdot[\theta_s]) \\ y_1 & \sin(3\cdot[\theta_s]) \\ x_2 & \cos(5\cdot[\theta_s]) \\ y_2 & \sin(5\cdot[\theta_s]) \\ \vdots & \vdots \\ x_{\frac{n-3}{2}} & \cos((n-2)\cdot[\theta_s]) \\ y_{\frac{n-3}{2}} & \sin((n-2)\cdot[\theta_s]) \\ \hline 0_+ & \frac{1}{\sqrt{2}} \quad \frac{1}{\sqrt{2}} \quad \frac{1}{\sqrt{2}} \quad \frac{1}{\sqrt{2}} \quad \cdots \quad \frac{1}{\sqrt{2}} \end{array}\right] \quad (4.19)$$

The angular displacement $[\theta_s]$ in (4.19) is the same as in (4.17) and is defined by (4.18). One can notice from (4.19) that the number of loss-producing (x_i-y_i) subspaces has changed to (n–3)/2. Also, the number of zero-sequence components is reduced to one only. The VSD matrices illustrated in (4.17) and (4.19) are in the power invariant form. The transformation can also be expressed in the amplitude invariant form if the coefficient in front is changed from $\sqrt{2/n}$ to 2/n and the zero sequence(s) terms are changed from $\pm 1/\sqrt{2}$ to ±1/2. The purpose of the previous matrices is to decouple the machine into flux/torque producing plane and the loss-producing planes. Furthermore, the transformations are uniquely mapping the odd-order harmonics into the created subspaces.

The application of the VSD matrices of (4.17) and (4.19) onto the stator and rotor voltage equilibrium equations, (4.1) and (4.2), will produce the same results as in Chapter 3 equations (3.28) – (3.37). The electromagnetic torque T_e equation after application of the VSD transformation (stationary reference frame) can be expressed as:

$$T_e = PL_m\left(\cos\theta_e\left(i_{\alpha r}i_{\beta s}-i_{\beta r}i_{\alpha s}\right)-\sin\theta_e\left(i_{\alpha r}i_{\alpha s}+i_{\beta r}i_{\beta s}\right)\right) \quad (4.20)$$

The electromagnetic torque expressed in (3.38) shows that the developed torque of the machine is dependent only on the α-β currents components of the stator and rotor. In order to eliminate the nonlinearity of the system and the time-dependent coefficients, the rotational transformation should be applied. This chapter will not discuss the rotational transformation since it is exactly the same as for the symmetrical multiphase machines. Application of the rotational transformation will provide a significant

simplification of the machine's model and control. The same set of equations as in Chapter 3, (3.44) – (3.51), describing the machine model in rotational reference frame will be valid for the asymmetrical machine as well. The electromagnetic torque T_e from (4.32) will be simplified further to (which is in fact the same as (3.52)):

$$T_e = PL_m\left(i_{dr}i_{qs} - i_{ds}i_{qr}\right) \tag{4.21}$$

The VSD transformations matrices (4.17) and (4.19) are considering the asymmetrical machines with a single neutral point. In the following section, the VSD transformation for an asymmetrical multiple three-phase machine with multiple neutral points will be introduced in a general form.

4.4 VSD Transformation with Multiple Neutral Points

The interest in the multiple three-phase machines has significantly increased recently. This is because of their fault tolerance capabilities and their utilisation of the well-established three-phase power electronics technologies [Che et al. (2014a), Che et al. (2014b), Che et al. (2014c)]. An illustration of the asymmetrical nine-phase machine with multiple neutral points is shown in Fig. 4.1. The construction of the VSD transformation matrix for these machines is the same as for the case with a single neutral point, but with two important differences. First, the number of zero axes will change to *k*, to correspond to the number of three-phase winding sets (and the number of isolated neutral points). Further, if each set is formed of *a* phases (*a*=3, for multiple three-phase case), *a*-th harmonics and its odd-multiples (third, ninth, fifteenth etc. harmonic, for *a*=3) will now map into zero-sequences. Hence, x_i-y_i subspaces corresponding to these harmonics (when single neutral point was present) will not exist any more. These subspaces are practically replaced by added zero components, still keeping the total number of axes after the transformation equal to *n*. VSD transformation matrix for asymmetrical multiple three-phase machine with *k* neutral points is given as:

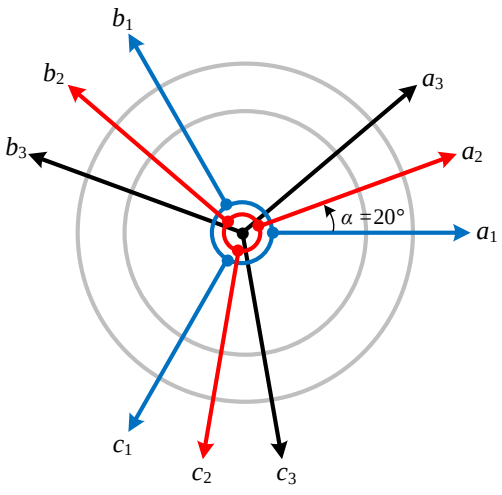

Fig. 4.1: Stator magnetic axes of an asymmetrical nine-phase machine with three isolated neutral points.

$$[VSD]_{n\times n}=\sqrt{\frac{2}{n}}\left[\begin{array}{c|ccc|ccc|c|ccc}
\alpha & \multicolumn{10}{c}{\cos([\theta_s])} \\
\beta & \multicolumn{10}{c}{\sin([\theta_s])} \\
\hline
x_1 & \multicolumn{10}{c}{\cos(5\cdot[\theta_s])} \\
y_1 & \multicolumn{10}{c}{\sin(5\cdot[\theta_s])} \\
x_2 & \multicolumn{10}{c}{\cos(7\cdot[\theta_s])} \\
y_2 & \multicolumn{10}{c}{\sin(7\cdot[\theta_s])} \\
\vdots & \multicolumn{10}{c}{\vdots} \\
x_{\frac{n-(k+2)}{2}} & \multicolumn{10}{c}{\cos((n-1)\cdot[\theta_s])} \\
y_{\frac{n-(k+2)}{2}} & \multicolumn{10}{c}{\sin((n-1)\cdot[\theta_s])} \\
\hline
0_1 & \sqrt{\frac{k}{2}} & \sqrt{\frac{k}{2}} & \sqrt{\frac{k}{2}} & 0 & 0 & 0 & \cdots & 0 & 0 & 0 \\
0_2 & 0 & 0 & 0 & \sqrt{\frac{k}{2}} & \sqrt{\frac{k}{2}} & \sqrt{\frac{k}{2}} & \cdots & 0 & 0 & 0 \\
\vdots & \vdots & \vdots & \vdots & \vdots & \vdots & \vdots & \ddots & \vdots & \vdots & \vdots \\
0_k & 0 & 0 & 0 & 0 & 0 & 0 & \cdots & \sqrt{\frac{k}{2}} & \sqrt{\frac{k}{2}} & \sqrt{\frac{k}{2}}
\end{array}\right] \tag{4.22}$$

Note that the way that the phases are arranged into a vector is changed now in (4.22). Rather than positioning phases according to their angle (a_1, a_2, …, a_k, b_1, b_2, …, b_k, c_1, c_2, …, c_k), they are now arranged set-by-set (a_1, b_1, c_1, a_2, b_2, c_2, …, a_k, b_k, c_k). Hence, $[\theta_s]$ is now defined as:

$$[\theta_s]=\frac{\pi}{n}\left[\begin{array}{ccc|ccc|ccc|c|ccc} 0 & 2k & 4k & 1 & 2k+1 & 4k+1 & 2 & 2k+2 & 4k+2 & \cdots & k-1 & 3k-1 & 5k-1 \end{array}\right] \tag{4.23}$$

The VSD matrix of (4.22) is applicable to asymmetrical multiple three-phase machines with an even number of phases. In case of an odd number of phases, the VSD matrix can be expressed as follows:

$$[VSD]_{n\times n}=\sqrt{\frac{2}{n}}\left[\begin{array}{c|ccc|ccc|c|ccc}
\alpha & \multicolumn{10}{c}{\cos([\theta_s])} \\
\beta & \multicolumn{10}{c}{\sin([\theta_s])} \\
\hline
x_1 & \multicolumn{10}{c}{\cos(5\cdot[\theta_s])} \\
y_1 & \multicolumn{10}{c}{\sin(5\cdot[\theta_s])} \\
x_2 & \multicolumn{10}{c}{\cos(7\cdot[\theta_s])} \\
y_2 & \multicolumn{10}{c}{\sin(7\cdot[\theta_s])} \\
\vdots & \multicolumn{10}{c}{\vdots} \\
x_{\frac{n-(k+2)}{2}} & \multicolumn{10}{c}{\cos((n-2)\cdot[\theta_s])} \\
y_{\frac{n-(k+2)}{2}} & \multicolumn{10}{c}{\sin((n-2)\cdot[\theta_s])} \\
\hline
0_1 & \sqrt{\frac{k}{2}} & \sqrt{\frac{k}{2}} & \sqrt{\frac{k}{2}} & 0 & 0 & 0 & \cdots & 0 & 0 & 0 \\
0_2 & 0 & 0 & 0 & \sqrt{\frac{k}{2}} & \sqrt{\frac{k}{2}} & \sqrt{\frac{k}{2}} & \cdots & 0 & 0 & 0 \\
\vdots & \vdots & \vdots & \vdots & \vdots & \vdots & \vdots & \ddots & \vdots & \vdots & \vdots \\
0_k & 0 & 0 & 0 & 0 & 0 & 0 & \cdots & \sqrt{\frac{k}{2}} & \sqrt{\frac{k}{2}} & \sqrt{\frac{k}{2}}
\end{array}\right] \tag{4.24}$$

In (4.24), $[\theta_s]$ is arranged by winding sets, as in (4.23). Application of the VSD transformation ((4.22) and (4.24)) will produce a decoupled model of the asymmetrical machine with multiple neutral points.

The same as for the other analysed configurations of machines, the first subspace (α-β subspace) is the flux/torque producing subspace, where the electro-mechanical energy conversion is occurring, and the x_i-y_i subspaces are the loss-producing subspaces. The number of auxiliary x_i-y_i planes in (4.22) and (4.24) is reduced to (n–(k+2))/2 compared to (n–4)/2 and (n–3)/2 in (4.17) and (4.19), respectively, where a single neutral point is present. As mentioned, the reduction in the number of x_i-y_i subspaces is countered by an increase in the number of zero-sequence components to k instead of two or one in (4.17) and (4.19), respectively. Each zero-sequence component in (4.22) and (4.24) is representing a zero-sequence component of one of the three-phase winding sets.

Applying the VSD transformation matrix ((4.22) or (4.24)) to the voltage equilibrium equations in the phase variables reference frame ((4.1) and (4.2)) will lead to differential equations with time-dependent terms as for the Clarke's transformation and the VSD transformation with single neutral point. The implementation of the rotational transformation is a necessary step to remove the time-dependent terms. The rotational transformation has been discussed in detail in section 3.4 of Chapter 3. The model of the multiphase induction machines in the common reference frame (after application of the rotational transformation) whether in symmetrical or asymmetrical configuration, with single or with multiple neutral points, is basically the same (with the mentioned difference in the number of auxiliary planes and zero axes). Hence repetition of the derivation is omitted. This, common reference frame modelling approach is regularly used for controlling the multiphase machines (for example, for IRFOC).

Controlling a multiple three-phase machine with symmetrical or asymmetrical configuration in essence is the same. The difference is in the application of the decoupling transformation matrices. Symmetrical machines are decoupled using Clarke's decoupling transformation whether they are in the single neutral point configuration (3.27), or in the multiple neutral points' configuration (3.87). On the contrary, the asymmetrical machines use the VSD transformation matrices to decouple the machine. The IRFOC scheme has been derived and discussed in detail for the symmetrical multiphase machines in section 3.6 of Chapter 3. The derivation is equally applicable to the asymmetrical multiphase machines taking into consideration the different decoupling transformations. The IRFOC schematic for asymmetrical multiphase induction machines with cross-coupling decoupling is illustrated in Fig. 4.2.

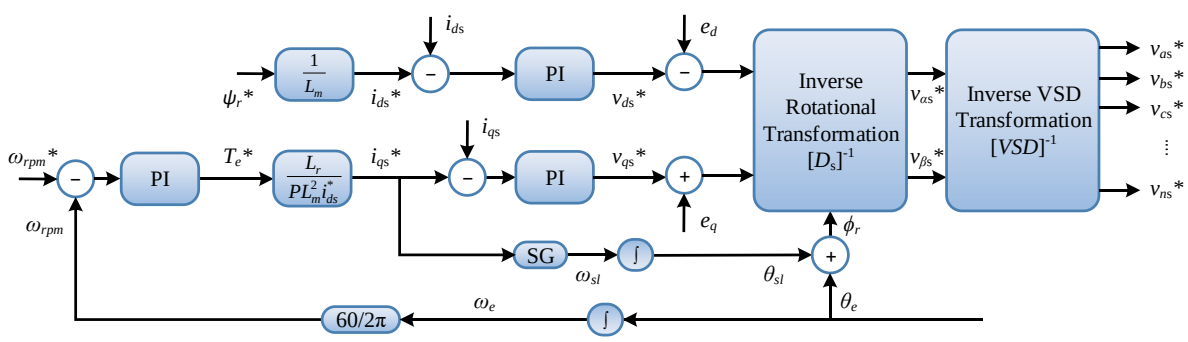

Fig. 4.2: IRFOC schematic for asymmetrical multiphase induction machine with cross-coupling decoupling controllers.

The difference between Fig. 4.2 and Fig. 3.8 is in the applied decoupling transformation as obvious from the schematics. The schematic presented in Fig. 4.2 does not consider any control of x_i-y_i subspaces. However, these subspaces are to be controlled in practice to compensate any asymmetries in the machine's windings or in the power electronics converter, as mentioned earlier in section 3.6. In addition, the loss-producing subspaces (x_i-y_i) can be utilised to perform full control of the current's amplitude of each winding set within a multiple three-phase machine as will be shown in the following section.

4.5 CURRENT SHARING FOR ASYMMETRICAL MULTIPLE THREE-PHASE MACHINES

The current sharing for symmetrical machines has been introduced in section 3.7 of Chapter 3. The current sharing strategy utilises IRFOC and auxiliary current control to achieve full control of the winding sets' currents' amplitude while utilising Clarke's decoupling transformation (3.87). The current amplitude can be controlled by using multi-stator (MS) vector control. In this modelling approach, the machine is considered as an aggregation of multiple three-phase machines. However, the main drawback of the MS method is the heavy coupling between the winding sets. Proper decoupling can become quite involved [Zabaleta et al. (2018)], and hence it is not favoured for control of the multiple three-phase machines. Instead, the VSD approach is recommended. The VSD approach considers the machine as a whole rather than as aggregation of three-phase machines. However, by utilising the VSD approach the ability to control the individual winding sets is lost and the machine is controlled by a single α-β subspace (rather than by three separate α-β planes as in MS approach). In section 3.7, a technique to control the individual winding sets' currents has been derived where the links between the Clarke's decoupling transformation and the MS modelling approach have been found. The current sharing strategy has been derived for a symmetrical multiple three-phase machine. In this section, following the same procedures as in section 3.7, the current sharing strategy for the asymmetrical multiple three-phase machine will be briefly derived.

In the MS approach, when using the three-phase Clarke's transformation, the angular displacement of the winding sets (with respect to the first one) should be considered. The Clarke's transformation for each winding set [$C_{3,i}$] is defined as:

$$\left[C_{3,i}\right]=\sqrt{\frac{2}{3}}\begin{bmatrix}\cos(\delta) & \cos\left(\delta+2\pi/3\right) & \cos\left(\delta+4\pi/3\right)\\ \sin(\delta) & \sin\left(\delta+2\pi/3\right) & \sin\left(\delta+4\pi/3\right)\\ 1/\sqrt{2} & 1/\sqrt{2} & 1/\sqrt{2}\end{bmatrix} \tag{4.25}$$

where δ represents the angular displacement between i-th winding set with respect to the first winding set. For an asymmetrical multiple three-phase machine with k winding sets, δ can be expressed as:

$$\delta\in\left\{0 \quad \alpha \quad 2\alpha \quad \cdots \quad \left(k-1\right)\alpha\right\} \qquad \text{or} \qquad \delta=\left(i-1\right)\alpha \tag{4.26}$$

where $\alpha = \pi/n$. In order to control the amplitude of the winding set currents, i.e. to perform current sharing, the links between the two modelling approaches should be found first. The same derivation of the current sharing strategy for symmetrical multiple three-phase machines can be repeated for the asymmetrical multiple three-phase machines.

After applying Clarke's transformation to the individual winding sets' (MS approach), phase currents can be expressed in the following way:

$$\begin{bmatrix} i_{a1} \\ i_{b1} \\ i_{c1} \end{bmatrix} = \left[C_{3,1}\right]^{-1} \begin{bmatrix} i_{\alpha 1} \\ i_{\beta 1} \\ i_{o1} \end{bmatrix} \qquad \begin{bmatrix} i_{a2} \\ i_{b2} \\ i_{c2} \end{bmatrix} = \left[C_{3,2}\right]^{-1} \begin{bmatrix} i_{\alpha 2} \\ i_{\beta 2} \\ i_{o2} \end{bmatrix} \quad \cdots \quad \begin{bmatrix} i_{ak} \\ i_{bk} \\ i_{ck} \end{bmatrix} = \left[C_{3,k}\right]^{-1} \begin{bmatrix} i_{\alpha k} \\ i_{\beta k} \\ i_{ok} \end{bmatrix} \tag{4.27}$$

Stacking together, currents in phase variables reference frame can be expressed as:

$$\left[i_{ph}\right] = \left[i_{a1} \quad i_{b1} \quad i_{c1} \,\vdots\, i_{a2} \quad i_{b2} \quad i_{c2} \,\vdots\, \cdots \,\vdots\, i_{ak} \quad i_{bk} \quad i_{ck}\right]^T \tag{4.28}$$

The phase currents shown in (4.40) are arranged by winding set. For simplicity, from now on an asymmetrical nine-phase machine with three isolated neutral points is taken as an example. By combining (4.39) and (4.40), for nine-phase case, one can write:

$$\left[i_{ph9\mathrm{A}}\right] = \begin{bmatrix} i_{a1} \\ i_{b1} \\ i_{c1} \\ i_{a2} \\ i_{b2} \\ i_{c2} \\ i_{a3} \\ i_{b3} \\ i_{c3} \end{bmatrix} = \begin{bmatrix} \left[\mathrm{C}(0)\right]^{-1} & [0]_{3\times 3} & [0]_{3\times 3} \\ [0]_{3\times 3} & \left[\mathrm{C}\left(\frac{\pi}{9}\right)\right]^{-1} & [0]_{3\times 3} \\ [0]_{3\times 3} & [0]_{3\times 3} & \left[\mathrm{C}\left(\frac{2\pi}{9}\right)\right]^{-1} \end{bmatrix} \cdot \begin{bmatrix} i_{\alpha 1} \\ i_{\beta 1} \\ i_{o1} \\ i_{\alpha 2} \\ i_{\beta 2} \\ i_{o2} \\ i_{\alpha 3} \\ i_{\beta 3} \\ i_{o3} \end{bmatrix} \tag{4.29}$$

On the other hand, from the VSD perspective (for asymmetrical nine-phase case) one has:

$$\left[i_{VSD9\mathrm{A}}\right] = \left[i_{\alpha} \quad i_{\beta} \,\vdots\, i_{x1} \quad i_{y1} \quad i_{x2} \quad i_{y2} \,\vdots\, i_{01} \quad i_{02} \quad i_{03}\right]^T = \left[VSD\right]_{9\times 9} \cdot \left[i_{ph9\mathrm{A}}\right]_{9\times 1} \tag{4.30}$$

where $[VSD]_{9\times 9}$ matrix is defined as in (4.22) or (4.24).

By substituting phase current $[i_{ph9A}]$ from (4.29) into (4.42) the links between VSD current (α-β, x_i-y_i, 0_1-0_k) and MS currents (α_i-β_i-o_i), for the asymmetrical nine-phase machine with three neutral points, can be obtained:

$$\left[i_{VSD9A}\right]=\begin{bmatrix} i_{\alpha} \\ i_{\beta} \\ \hdashline i_{x_1} \\ i_{y_1} \\ i_{x_2} \\ i_{y_2} \\ \hdashline i_{01} \\ i_{02} \\ i_{03} \end{bmatrix}=\left[VSD\right]_{9\times 9}\cdot\left[i_{ph9A}\right]_{9\times 1}=\begin{bmatrix} \frac{i_{\alpha 1}+i_{\alpha 2}+i_{\alpha 3}}{\sqrt{3}} \\ \frac{i_{\beta 1}+i_{\beta 2}+i_{\beta 3}}{\sqrt{3}} \\ \hdashline \frac{2\sqrt{3}i_{\alpha 1}-\sqrt{3}i_{\alpha 2}-\sqrt{3}i_{\alpha 3}+3i_{\beta 2}-3i_{\beta 3}}{6} \\ \frac{3i_{\alpha 2}-3i_{\alpha 3}-2\sqrt{3}i_{\beta 1}+\sqrt{3}i_{\beta 2}+\sqrt{3}i_{\beta 3}}{6} \\ \frac{2\sqrt{3}i_{\alpha 1}-\sqrt{3}i_{\alpha 2}-\sqrt{3}i_{\alpha 3}-3i_{\beta 2}+3i_{\beta 3}}{6} \\ \frac{3i_{\alpha 2}-3i_{\alpha 3}+2\sqrt{3}i_{\beta 1}-\sqrt{3}i_{\beta 2}-\sqrt{3}i_{\beta 3}}{6} \\ \hdashline i_{o1} \\ i_{o2} \\ i_{o3} \end{bmatrix} \tag{4.31}$$

The correlations between the MS and VSD approach for nine-phase asymmetrical machines with three isolated neutral points are obvious from (4.31). Looking back at the correlations between the MS and Clarke's decoupling transformation, for the symmetrical nine-phase machine with three neutral points, defined in (3.93), one can see that the correlations are exactly the same. In other words, although the machine's winding is different, the correlations between their currents in two different reference frames are the same.

Since the electromechanical energy conversion should be maintained, the current sharing should be implemented using the x_i-y_i subspaces currents. In order to simplify the equations, the current sharing strategy can be represented by the space vectors of the individual winding sets and VSD currents' space vectors. Repeating the same mathematical procedure from section 3.7, (3.93) through (3.107), the following results are obtained:

$$\overline{i}_{\alpha\beta}=(K_1+K_2+K_3)\overline{i}_{\alpha\beta} \tag{4.32}$$

$$\overline{i}_{xy1}=\left(K_1+K_2e^{j\frac{2\pi}{3}}+K_3e^{-j\frac{2\pi}{3}}\right)\overline{i}_{\alpha\beta} \tag{4.33}$$

$$\overline{i}_{xy2}=\left(K_1+K_2e^{j\frac{2\pi}{3}}+K_3e^{-j\frac{2\pi}{3}}\right)\overline{i}_{\alpha\beta} \tag{4.34}$$

(4.44) through (4.46) are valid in the stationary reference frame. Different rotational transformations for each subspace, in (4.44) – (4.46), should be considered. An illustration of the different rotational transformations for the different *x*-*y* subspaces is shown in Fig. 4.3.

The current sharing strategy for asymmetrical nine-phase machines can be obtained using IRFOC with auxiliary current control as illustrated in Fig. 4.4. The schematic is the same as in Fig. 3.10 for the symmetrical nine-phase machines apart from the different decoupling transformation. During the implementation of the current sharing, the sharing coefficients should always sum to 1. However, the

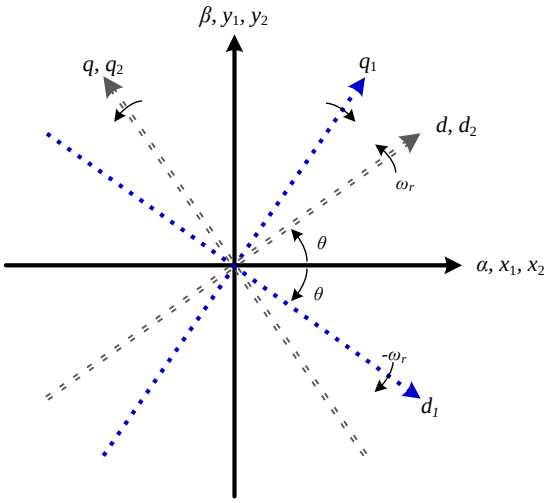

Fig. 4.3: Illustration of the reference frames involved in the current sharing strategy.

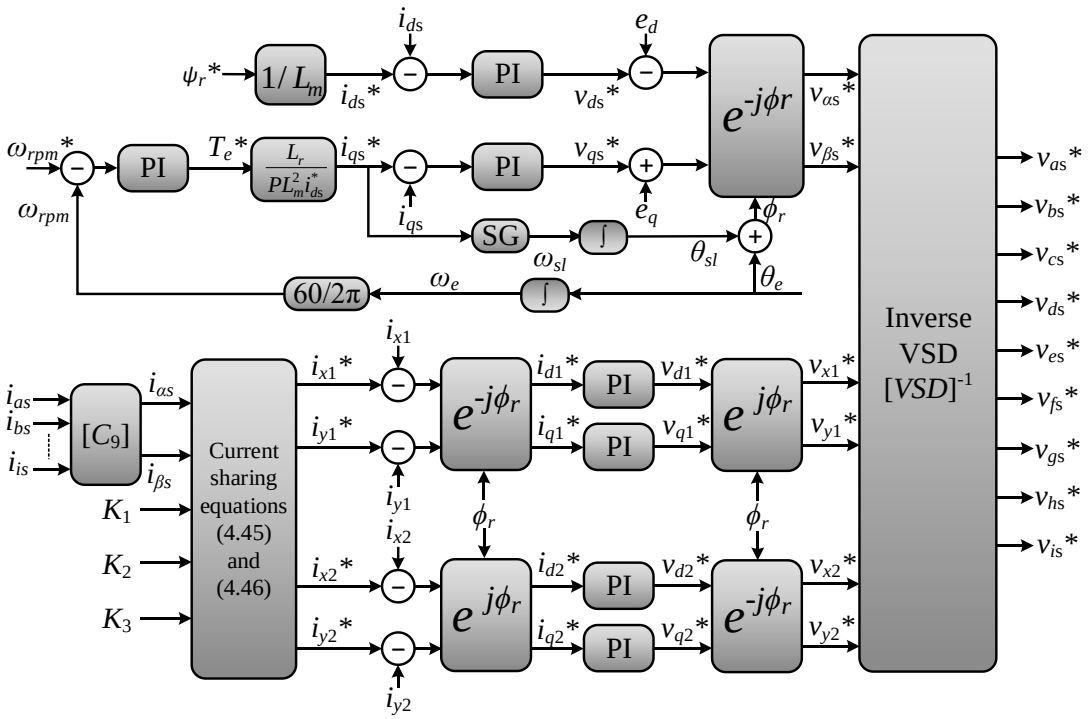

Fig. 4.4: IRFOC with current sharing control for asymmetrical triple three-phase induction machine.

rated current of the winding sets should be taken into consideration. The validation of the current sharing strategy illustrated in Fig. 4.4 using Matlab/Simulink is presented in the following section.

4.6 SIMULATION RESULTS

An asymmetrical nine-phase induction machine with three isolated neutral points has been simulated using Matlab/Simulink. The machine is modelled using the presented phase variables model, (4.1) – (4.15), in section 4.2, [Dordevic et al. (2010)]. The asymmetrical machine parameters are taken to be the same as the ones presented in Table 3.1. In order to test the current sharing algorithm, the

control scheme from Fig. 4.4 is implemented in Simulink. The rotational transformation is applied to each VSD subspace according to its direction of rotation (synchronous or anti-synchronous, Fig. 4.3) as in Fig. 4.4. The simulation results are illustrated in Fig. 4.5 – Fig. 4.6.

In Fig. 4.5 three current sharing scenarios are implemented, as will be specified shortly. Initially, the machine is magnetised for one second. Then, the machine is set for a speed reference of 157.1 rad/sec at t = 1 sec, as shown in Fig. 4.5a. After the machine reaches steady-state, it is loaded at t = 2.5 sec with

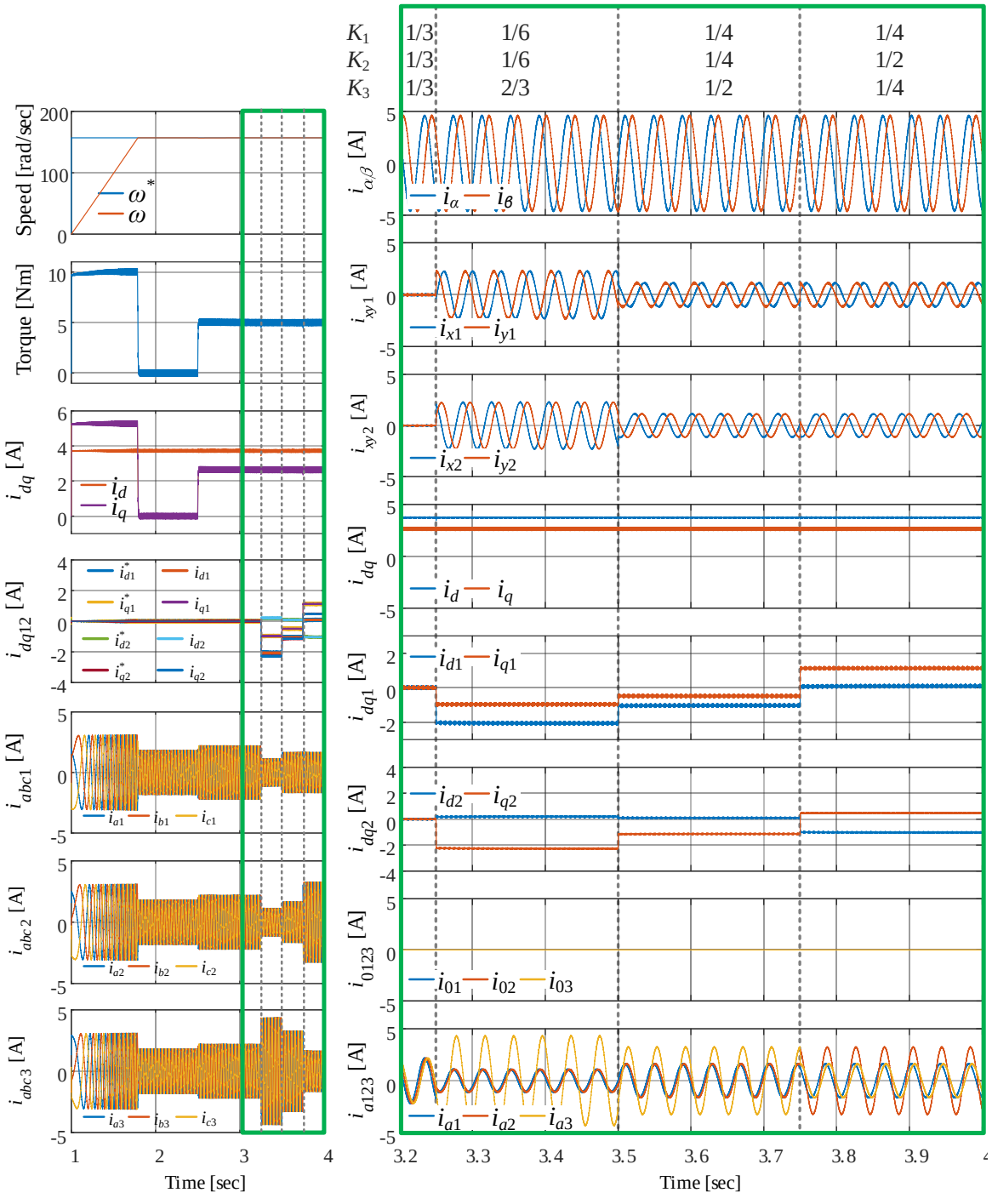

Fig. 4.5: Current sharing simulation results for an asymmetrical nine-phase induction machine. a) Complete simulation, b) zoomed section with current sharing between t = 3.2 sec – 4 sec.

T_l = 5 Nm. This is obvious from the torque subplot in Fig. 4.5a. The current sharing scenarios are implemented starting from t = 3.25 sec. To clearly show the waveforms in regular operation (3 sec – 3.25 sec) as well as during the current sharing operation (3.25 sec – 4 sec), timing waveforms from Fig. 4.5a are enlarged and shown in Fig. 4.5b. One can see, that regardless of current sharing presence, the electromechanical energy conversion is constant during the steady-state operation of the machine.

Prior to t = 3.25 sec the current sharing technique was not used, so K_i coefficients were all equal to 1/3. Then, the current sharing coefficients are changed to K_1 = 1/6, K_2 = 1/6, K_3 = 2/3, and are valid for the time range t = 3.25 sec – 3.5 sec, as illustrated in Fig. 4.5b. Accordingly, the third winding set's currents i_{a3} are four times the other winding sets' currents as obvious from the bottom subplot of Fig. 4.5b. From the top subplot one can see that the α-β currents are the same during balanced operation and during the current sharing scenario. However, the x_i-y_i currents are not zero during the current sharing as shown in Fig. 4.5b. In the next current sharing scenarios implemented between 3.5 sec – 3.75 sec, the sharing coefficients are set such that the third winding set (i_{a3}) will be twice the other winding sets' currents (i.e. K_1 = 1/4, K_2 = 1/4, K_3 = 1/2). Finally, between 3.75 sec – 4 sec the second winding set current (i_{a2}) is twice the amplitude of the other winding sets (again, see the last subplot in Fig. 3.12b) which is obtained by setting K_1 = 1/4, K_2 = 1/2, K_3 = 1/4. In all cases the machine's torque and α-β currents are constant, although the x_i-y_i currents are not zero; they have different values in each case. From the simulation results illustrated in Fig. 4.5, the current sharing strategy shown in Fig. 4.4 for the asymmetrical nine-phase machine with multiple three-phase machine has been validated.

The presented current sharing strategy, utilising VSD auxiliary currents, can be also used to operate a multiple three-phase machine in the post-fault operation region. This is proven by the simulation results illustrated in Fig. 4.6. Initially, the machine is magnetised for 1 sec. Then, the machine is accelerated to a speed of 157.1 rad/sec and then loaded with 5 Nm at t = 2.5 sec, as shown in Fig. 4.6a. Next, the current sharing strategy is implemented at t = 3.25 sec where one of the three winding sets is shut down completely for 0.25 sec. The last second of the simulation is enlarged and shown in Fig. 4.6b. The winding sets are shut down by setting their current sharing coefficients K_i to zero, causing the current of that set to be zero as well. This is obvious from the last subplot of Fig. 4.6b where the winding set currents (first of each set, i_{a1}, i_{a2} and i_{a3}) are illustrated. The first winding set is shut down at t = 3.25 sec by changing the coefficient K_1 to zero and increasing the current of the other winding sets (K_2 = K_3 = 1/2) to compensate the lost power of the first winding set. Then the second set only was shut down at 3.5 sec, and finally at 3.75 sec the third set was shut down. The current sharing coefficients used in each section are shown in the top row of Fig. 4.6b.

When a set is shut down, the amplitude of the current in the other two winding sets is increased from 2.125 A to 3.30 A during the post-fault operation as shown from the last subplots of Fig. 4.6b. The copper losses of the active winding sets are increased due to the increment of the winding sets' currents

during the post-fault operation. However, note that in practice the winding's rated current should be taken into consideration. If the rated current is reached, the torque of the machine should be reduced. In the simulation results illustrated in Fig. 4.6, the machine electromechanical conversion is kept constant, as can be seen from the speed and torque subplots in Fig. 4.6a. The *d-q* currents are constant during the balanced and post-fault operations. The x_i-y_i currents are not zero during the post-fault operation and they change according to (4.45) and (4.46). Therefore, by changing the current sharing coefficients K_i,

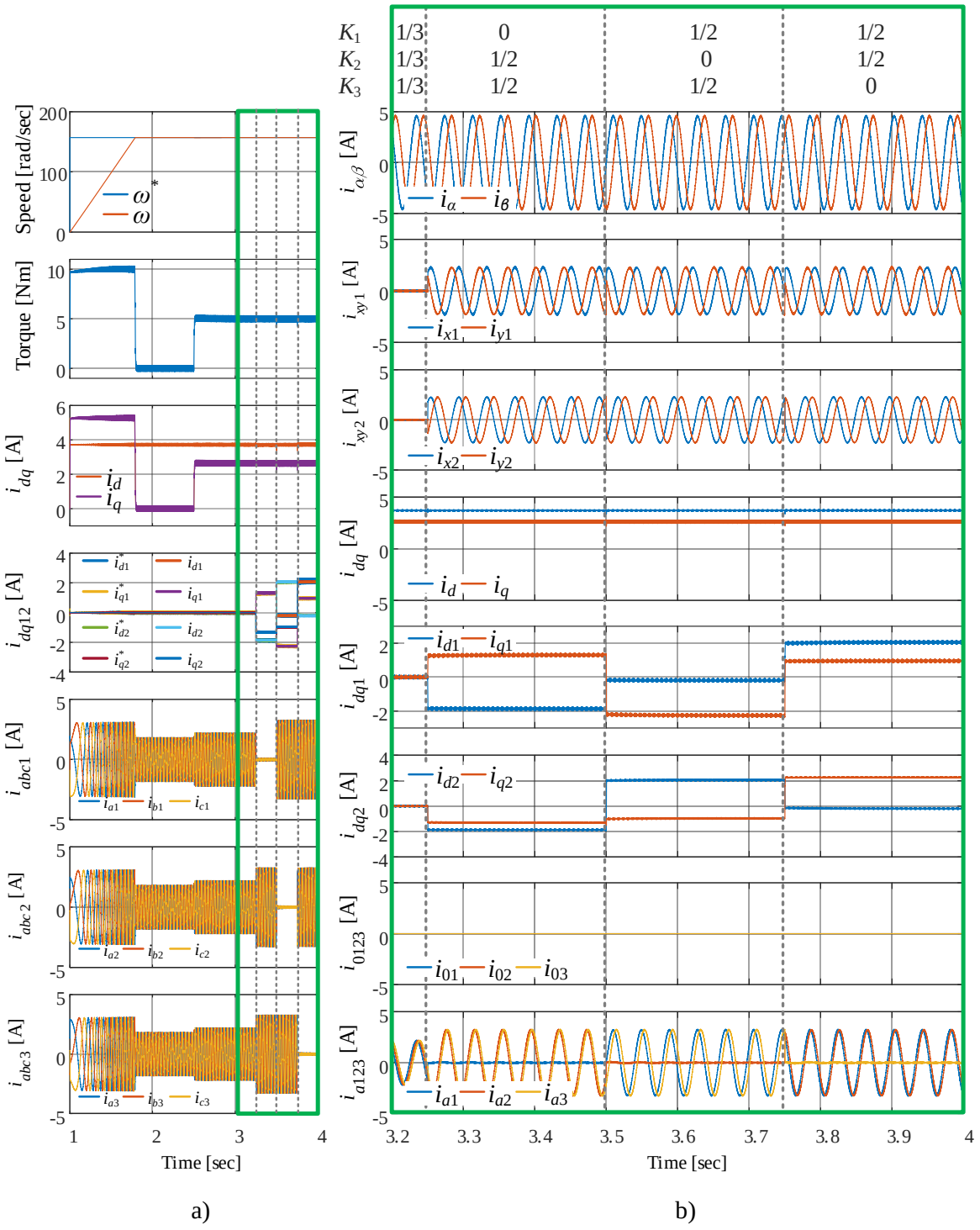

Fig. 4.6: Current sharing simulation results during post-fault operation. a) Complete simulation, b) zoomed section with current sharing between t = 3.2 sec – 4 sec.

the winding sets can be controlled independently, and the current sharing strategy can be utilised to operate the machine during post-fault operation.

4.7 EXPERIMENTAL RESULTS

The current sharing strategy presented in section 4.5 and simulated in section 4.6 is validated experimentally using an asymmetrical nine-phase induction machine with three isolated neutral points. The experimental setup is described in Appendix A. Note that the same nine-phase machine can be configured in symmetrical or asymmetrical configuration. Therefore, the same nine-phase induction machine, as the one used in Chapter 3, is used here as well. This is possible only if both, positive and negative, terminals of each phase are accessible (machine has 18 terminals in total), which is the case with the machine used. The reconfiguration can be accomplished in the following way. Positive terminals of the first winding set, of the symmetrical machine, are connected as usual to the first set of the VSI. Negative terminals are connected to each other forming a neutral point. If the magnetic axes of the third set (red set in Fig. 4.7) of the symmetrical machine are rotated by 180° then an asymmetrical configuration can be obtained (as shown in Fig. 4.7). Rotation of the magnetic axes can be obtained by swapping positive and negative winding terminals for this set. Therefore, negative terminals of the third (red) winding set of the machine are supplied from the VSI's second winding set terminals (while the positive terminals are forming a neutral point). Note also that changing the phase sequence is necessary as indicated in Fig. 4.7-right. Finally, the second winding set of the originally symmetrical machine becomes the third winding set of the asymmetrical machine. VSI terminals are again as usual connected to the positive terminals of this set, while the negative terminals are forming the neutral point. After this reconfiguration machine parameters remain the same, therefore the asymmetrical machine parameters are still the same as those presented in Table 3.1.

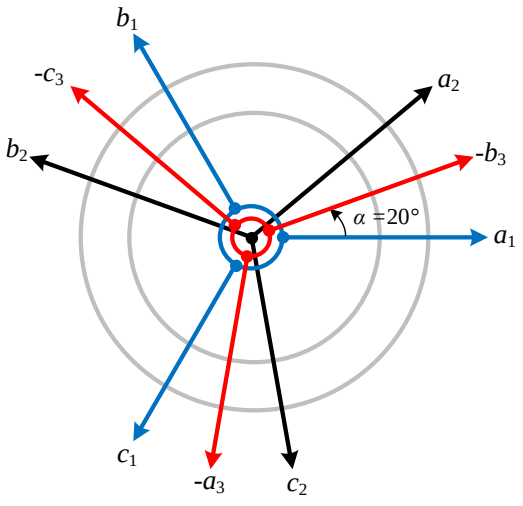

VSI terminals	→	Machine terminals
a_1	→	a_1
b_1	→	b_1
c_1	→	c_1
a_2	→	$-b_3$
b_2	→	$-c_3$
c_2	→	$-a_3$
a_3	→	a_2
b_3	→	b_2
c_3	→	c_2

Fig. 4.7: Symmetrical to asymmetrical nine-phase induction machine conversion.

Initially, the current sharing strategy for the asymmetrical nine-phase machine, corresponding to the simulation results in Fig. 4.5, is validated experimentally. Experimental results are shown in Fig. 4.8. Furthermore, the post-fault operation utilising the current sharing strategy is validated and the results are presented in Fig. 4.9 (corresponding simulation results are in Fig. 4.6). Presented experimental results in Fig. 4.8a and Fig. 4.9a are recorded by dSPACE ControlDesk while the experimental results presented in Fig. 4.8b and Fig. 4.9b are from the oscilloscope screenshots. Note

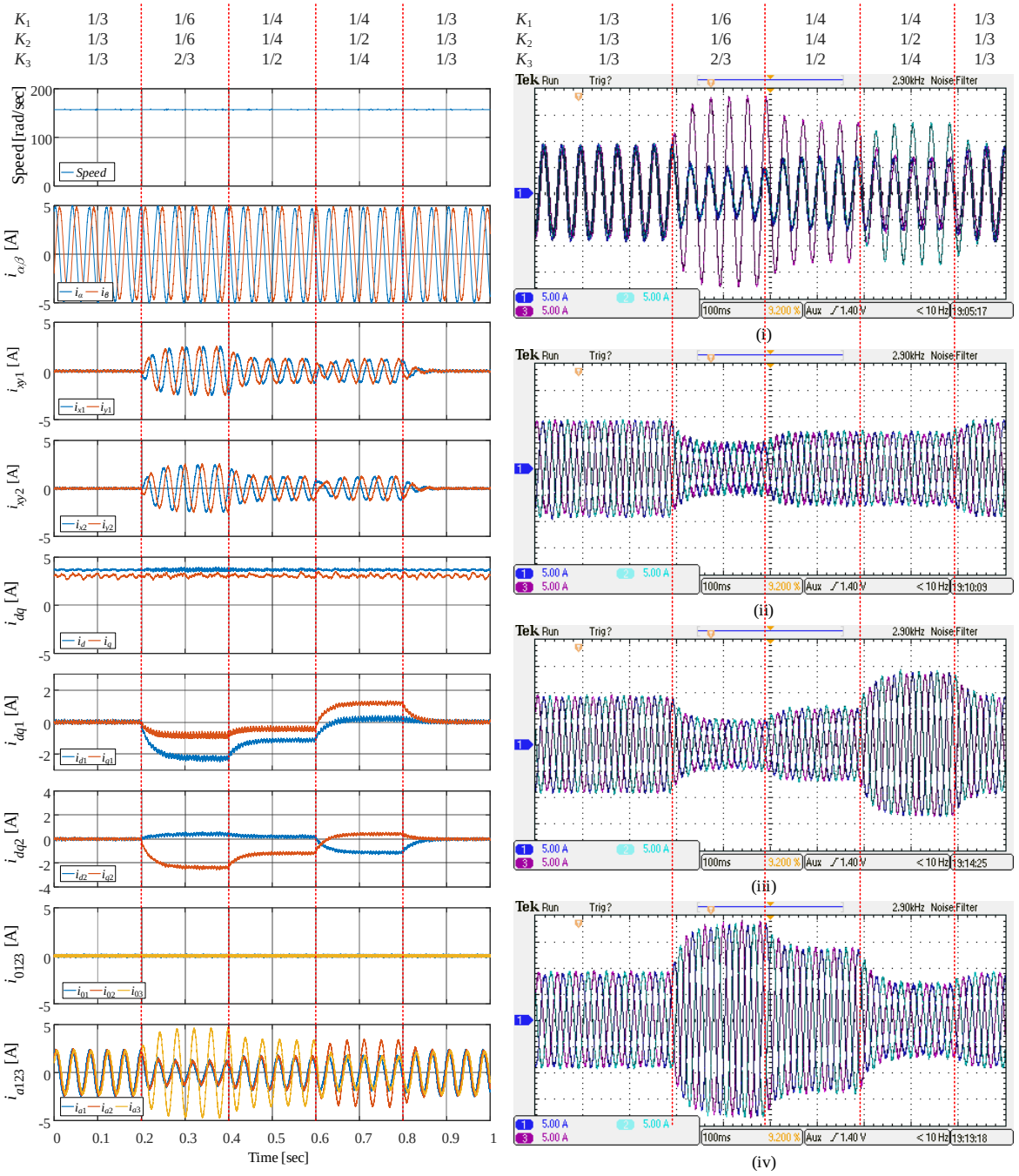

Fig. 4.8: Experimental results for current sharing strategy of an asymmetrical nine-phase induction machine with three isolated neutral points. a) Timing waveforms captured by dSpace ControlDesk. b) Oscilloscope screenshots: (i) i_{a1}, i_{a2}, i_{a3}, (ii) set-1 currents i_{a1}, i_{b1}, i_{c1}, (iii) set-2 currents i_{a2}, i_{b2}, i_{c2}, (iv) set-3 currents i_{a3}, i_{b3}, i_{c3}. Four turns of wire were used for oscilloscope current measurements.

that the winding sets' currents presented in Fig. 4.8b and Fig. 4.9b are measured using four turns of wire to increase the resolution of the measurement.

In Fig. 4.8 the experimental results of the current sharing strategy are implemented with the same sharing scenarios as in the simulation results in Fig. 4.5. The speed reference is set to 1500 rpm (157.1 rad/sec), and after the machine has reached the steady state it is loaded, using a permanent magnet

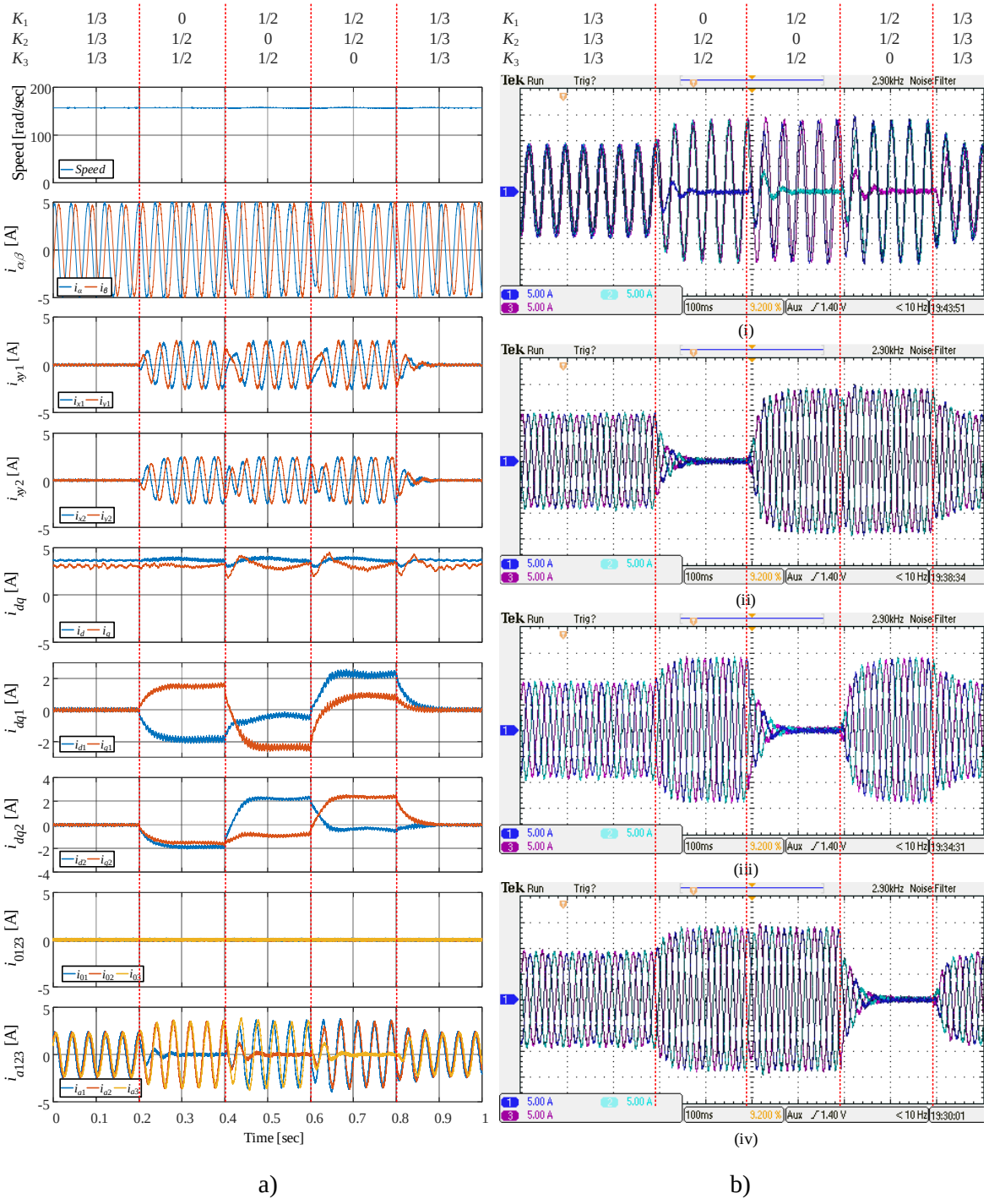

Fig. 4.9: Experimental results for post-fault of an asymmetrical nine-phase induction machine with three isolated neutral points using current sharing strategy. a) Timing waveforms captured by dSpace ControlDesk. b) Oscilloscope screenshots: (i) i_{a1}, i_{a2}, i_{a3}, (ii) set-1 currents i_{a1}, i_{b1}, i_{c1}, (iii) set-2 currents i_{a2}, i_{b2}, i_{c2}, (iv) set-3 currents i_{a3}, i_{b3}, i_{c3}. Four turns of wire were used for oscilloscope current measurements.

DC generator, with 5.17 Nm. The current sharing coefficients K_i, for each current sharing scenario are given at the top of Fig. 4.8. The current sharing operation is performed between t = 0.2 – 0.8 sec, while before and after regular operation (no current sharing) is performed $K_1 = K_2 = K_3 = 1/3$. Note that the regular operation can also be obtained by setting the current sharing coefficient K_i to 0. It can be noticed from the last subplot in Fig. 4.8a (i_{a1}, i_{a2} and i_{a3}) that the current ratios are always following the current sharing coefficients. For example, between t = 0.2 – 0.4 sec, K_1=1/6, K_2=1/6 and K_3=2/3 and hence the third winding set current is four times larger than the current in the first and second winding sets. The *d-q* subspace currents are constant during the current sharing operation (t = 0.2 – 0.8 sec). However, the x_i-y_i current (d_i-q_i, after the rotational transformation) changes according to the sharing coefficients. Experimental results match the simulation results during the same conditions. However, the experimental results have a much longer settling time of around 0.06 sec, unlike the simulation results. This can be reduced, by additional fine tuning of the current controllers. Also, the current amplitude is slightly higher in the illustrated experimental results due to the higher load torque value (5.17 Nm), as application of the same exact load torque was not possible. Also, for the practical implementation, additional vector PI regulators have been added in parallel to the auxiliary current controllers to eliminate the low order harmonics (5^{th}, 7^{th}, 11^{th}, 13^{th}, 29^{th} and 31^{st}). These harmonics were present in practice due to non-ideal design of the machine and due to relatively large dead-time of the VSI (6 μs). The i_q current has a small ripple due to the existence of a mechanical misalignment between the machine and the dc generator.

The second experiment of the current sharing strategy is performed to prove the ability of the current sharing strategy to operate the asymmetrical nine-phase machine in post-fault operation. The experimental results illustrated in Fig. 4.9 are under the same conditions as the simulation results in Fig. 4.6. The speed reference is set to 157.1 rad/sec and the load torque is equal to 5.17 Nm. The sharing coefficients are set to 1/3 between 0.0 – 0.2 sec to perform normal healthy operation. Then, during the period from 0.2 – 0.8 sec, the sharing strategy is applied by setting the sharing coefficients to 1/2 for the two healthy winding sets and by shutting down the third winding set by setting its sharing coefficient to zero. The choice of the set to be shut down is cyclically rotated each 0.2 sec. In last 0.2 sec of the experimental results the machine returns to the normal operation with no current sharing (i.e. when the sharing coefficients are all set to 1/3). The current sharing coefficients K_i are given on top of Fig. 4.9. During the post-fault operation of the machine the currents in the running winding sets are roughly 1.5 greater than during the normal operation of the machine to maintain the same torque. The experimental results of the post-fault operation of the nine-phase machine match the simulation results shown in Fig. 4.6.

4.8 SUMMARY

In this chapter, a generalised mathematical modelling approach for asymmetrical multiphase induction machines with multiple three-phase winding sets is presented. The mathematical model uses the same assumptions and simplifications as those utilised to model symmetrical multiphase machines in Chapter 3. Then, a generalised VSD transformation for the asymmetrical multiple three-phase machines with a single neutral point was introduced. The asymmetrical machine can be decoupled into several orthogonal subspaces. The first subspace is the fundamental harmonic subspace (α-β) which is the flux and torque producing subspace. The remaining subspaces are the losses-producing subspaces (x_i-y_i) plus the zero-sequence components. Then, VSD for asymmetrical multiple three-phase machines with multiple neutral points was introduced. The difference between the decoupling transformation for a single and multiple neutral points is explained. The mathematical model of the machine in the stationary reference frame (after applying VSD transformation) is the same as for the symmetrical machines in the stationary reference frame. Therefore, applying the rotational transformation provided the same model as for the symmetrical machine. Since the symmetrical and asymmetrical machines have the same model in the rotating reference frame, applying IRFOC for asymmetrical machines is the same as for the symmetrical machines which was derived in Chapter 3. The derivation of the current sharing strategy for the asymmetrical machine was presented at the end of the chapter along with the simulation and experimental results. As elaborated in the chapter, the current sharing scheme is done by utilising VSD and by finding the correlations of the MS and VSD modelling approach. It is shown that although they have different angular displacement, the current sharing equations for the asymmetrical and symmetrical nine-phase machines are exactly the same.

CHAPTER 5

POWER SHARING FOR MULTIPLE THREE-PHASE INDUCTION MACHINES

5.1 INTRODUCTION

This chapter considers the development of power sharing control among multiple three-phase winding sets within a single multiphase induction machine. Current sharing strategies for symmetrical and asymmetrical multiple three-phase machines have been introduced in the last two chapters (Chapter 3 and Chapter 4). In these chapters, the current sharing was utilised to control the amplitude of the winding sets' currents and to operate the machine in post-fault operation. In this chapter, the current sharing strategy is utilised to control the power flow between the different winding sets when they are connected to different energy sources. The energy can be transferred from one power source to another e.g. when there is a surge of energy, or in any other case when needed.

This chapter is organised as follows. In section 5.2 a general background about the multiple energy source solution supplying a single multiple three-phase machine is introduced. This is a viable solution especially for electric vehicles (EVs). Next, in section 5.3 the power sharing strategy based on the current sharing strategy, introduced in Chapter 3 and Chapter 4, is presented. The current's amplitude can be controlled by varying the *x-y* currents according to specific equations derived in the previous chapters. In this chapter, the amplitude and also the direction of current is changed to provide a multidirectional power flow control among the winding sets. However, the efficiency of the transferred power between the multiple three-phase sets is not optimal if the current sharing strategy illustrated in Chapter 3 and Chapter 4 is used. The sharing strategy in the previous chapters is achieved by sharing the flux and torque producing the currents equally. A more optimal and efficient solution for the power sharing is explained in section 5.4. The strategy is based on sharing the torque, rather than sharing the flux and torque producing currents together. In section 5.5, the power sharing strategies are validated through simulation, using Matlab/Simulink. An asymmetrical nine-phase induction machine is simulated and the power sharing strategies are compared in terms of the transferred power efficiency. The experimental results of both power sharing schemes are illustrated and compared in section 5.6. Although, the simulation and experimental results are presented for asymmetrical machines, the power sharing strategies are equally applicable to the symmetrical machines as well. Finally, the summary of the chapter is made in section 5.7.

5.2 MULTIPLE ENERGY SOURCES SUPPLYING A SINGLE MACHINE

The utilisation of multiple energy sources supplying a single three-phase machine appeared as a concept recently. Hybrid energy storage systems (HESSs) based on battery and super-capacitors are the practical solutions to improve the power and energy density of the energy storage system in EVs [Kuperman et al. (2013), Kollimalla et al. (2014), Hu et al. (2016a), Hu et al. (2016b), Hu et al. (2018)]. By utilising this combination of HESSs, the battery will provide the average load demand and the super-capacitor will provide the dynamic load current demand [Hu et al. (2018)]. There are several configurations how HESSs can be connected, as illustrated in Fig. 5.1. The dual three-phase machine is a common choice where the hybrid energy storage system can be utilised. In this case each three-phase winding set is connected to a different energy source. The benefits of utilising the well-established three-phase power electronics technologies and the fault-tolerance capabilities, plus the ability to be supplied by different energy sources are distinguishing features of the multiple three-phase machines. Although batteries and super-capacitors are viable options for EVs, other alternative energy sources can be integrated also, such as fuel-cells and/or PV cells. Depending on the application, the HESSs' sources can be chosen.

Multiple three-phase machines are usually controlled by multiple vector control schemes (based on the multi-stator, MS, modelling approach). The ability to control each three-phase winding set separately is the main advantage of multiple vector control schemes. However, the mutual coupling between the winding sets is the main disadvantage of this control scheme as mentioned earlier. The alternative is to control the machine using vector control algorithms and VSD transformation. By utilising an appropriate VSD transformation, the machine model can be completely decoupled. Through control of the α-β as well as the auxiliary x-y currents, the ability to control the winding sets' currents separately is possible, as illustrated in Chapter 3 and Chapter 4.

The current sharing scheme introduced in the previous chapters can be utilised to separate the control of dynamic load and the average load in EV applications. In addition, if another application is utilising fuel-cells or PV cells as HESS components, the power can be directed to the battery bank connected through one of the three-phase winding sets of the machine. Therefore, by certain manipulations of the current sharing coefficients, introduced in the previous chapters, the energy transfer can be done through the multiple three-phase machine itself, rather than by adding additional dc/dc converters to charge/discharge the batteries or the super-capacitor.

The winding sets of the multiple three-phase machine can run in motoring and/or in generation mode simultaneously. In Fig. 5.1, the three-phase machine is either in traction (motoring) or in regeneration (generation) mode. Therefore, the three-phase machine can run in a single mode unlike the multiple three-phase machine where the machine's winding sets can run in different modes of operation at the same time, as illustrated in Fig. 5.2. The twelve-phase machine (used just as an example)

illustrated in Fig. 5.2 is supplied by four different energy sources. The super-capacitors and the batteries can be charged or discharged. They can be used to store the regenerative energy during braking. On the other hand the fuel-cells and PV cells cannot sink the power and are providing the traction (motoring) power only. A combination of these energy sources can provide a viable solution for many applications such as EVs or electric ships. The electrical machine illustrated in Fig. 5.2 is an induction machine. However, the principle is valid regardless of the machine type (induction machine, synchronous machine, with interior permanent magnets IPM, synchronous reluctance SR, etc.). Because of its availability, in this chapter, only an induction machine with multiple three-phase winding sets configuration will be considered.

As mentioned, transferring the energy can be done by using multiple three-phase machines and the current sharing scheme from Chapter 3 and Chapter 4. The following section will introduce the power sharing (energy transfer) strategy among three-phase winding sets utilising the above mentioned current sharing scheme.

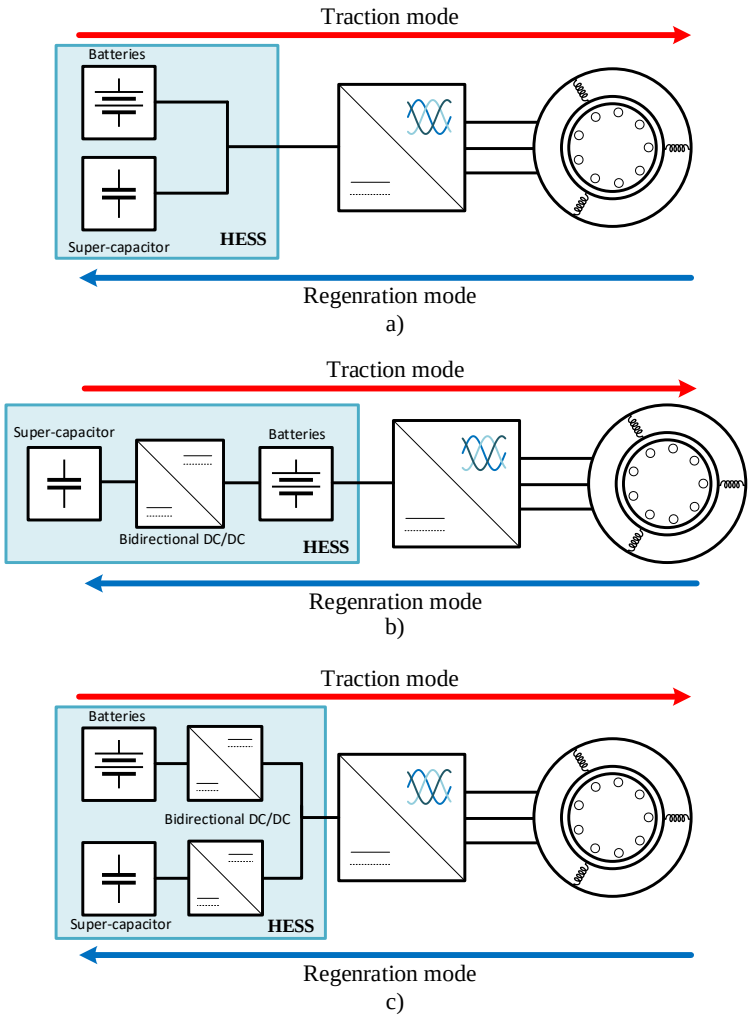

Fig. 5.1: Different HESSs configurations. a) Passive parallel configuration. b) Semi-active HESS configuration. c) Full active HESS configuration.

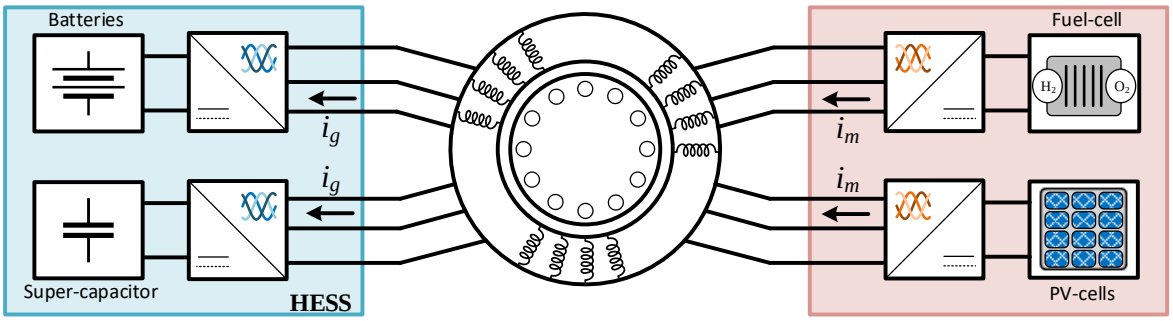

Fig. 5.2: Different HESS's energy sources connected to an asymmetrical twelve-phase induction machine.

5.3 POWER SHARING UTILISING CURRENT SHARING STRATEGY

The main aspect of sharing the power among the multiple three-phase winding sets is controlling the amplitude and direction of power flow for each winding set separately. This is easily achievable using multiple vector control. Multiple vector control uses the MS modelling approach to achieve the independent control of the winding sets' current amplitude and direction. However, due to the mutual coupling between the winding sets this is not a recommended method to control high performance multiphase machine drives. Therefore, vector control utilising VSD or Clarke's transformation for multiple three-phase machines is the more suitable solution. The machine is decoupled into several subspaces with only one α-β subspace. Therefore, the ability to control the amplitude and direction of the individual winding sets of the machine is not possible utilising VSD or Clarke's alone. A combination of both modelling approaches is introduced in Chapter 3 and Chapter 4. With that new approach, based on the links between MS and VSD modelling methods and by controlling α-β and x_i-y_i subspaces currents, the machine's winding sets can be controlled independently.

Note that the steps for establishing the links between the MS and VSD approaches from Chapter 3 and Chapter 4 are universal and can be applied for any other phase number or the winding arrangement. An example of derivation of those links for an asymmetrical fifteen-phase machine is given in Appendix B.

By changing the current sharing coefficients K_i (introduced in Chapter 3 and Chapter 4) the amplitude of the individual winding sets' currents are controllable using VSD. Thus, by changing the current sharing coefficients to any value, respecting the limit of the rated current, the power of each winding set is controlled. To change the winding set mode of operation between motoring and generation, a simple multiplication of the K_i with –1 will make the winding set operating in generation mode. Regardless of the mode of operation (i.e. sign of K_i), the following equation of the sharing coefficients K_i should always be satisfied:

$$K_1 + K_2 + \cdots + K_i = 1 \tag{5.1}$$

Therefore, the previously introduced current sharing strategy can be directly used for power flow control. However, as it will be shown later on in this chapter, the application of the power sharing strategy in this way is not recommended and it is not efficient since the same sharing coefficients K_i are used for both the active and reactive power of the individual winding sets. In other words, the sharing coefficients are multiplied equally by the flux (α) and torque (β) producing currents. Since the transfer should be for the active power, an alternative current sharing scheme to transfer the power efficiently should be developed. In the following section an efficient way to transfer the power and direct it to the required energy storage source is introduced.

5.4 EFFICIENT POWER SHARING STRATEGY

As mentioned, the power sharing strategy using the current sharing strategy introduced in the previous section is not recommended. The current sharing strategy is changing the amplitude of both flux and torque producing currents (α-β or d-q) of the individual winding sets by multiplying them by the same coefficient. The electromagnetic torque achieved in the air-gap, T_e, is a function of the transmitted active power P and the angular speed of the rotating magnetic field ω (because $P=T_e \cdot \omega$). The active power of the winding sets reaching the air-gap is equivalent to the input power of the winding set minus the copper losses and core losses of the winding sets. Therefore, the sharing of the power should be done by sharing the torque rather than the flux and torque of the individual winding sets.

The torque can be shared by controlling the torque producing current (i_{qi}) of the i-th winding set. The flux producing current (i_{di}) should be kept constant. Therefore, a necessity to separate the current sharing coefficients K_i into K_{di} and K_{qi} for the flux and torque producing currents appears here. This can be achieved using the scalar values of the auxiliary currents rather than their space vectors. For example, the scalar values of the auxiliary currents can be found from (3.93) for the nine-phase machines, while for the more complicated fifteen-phase case it can be found in Appendix B.

The absolute value of summation of K_{di} should be always equal to one, and the algebraic sum of K_{qi} should be equal to one. Rewriting the power sharing coefficients criteria to maintain the same torque and flux as follows:

$$\left|K_{d1} + K_{d2} + K_{d3}\right| = 1 \tag{5.2}$$

$$K_{q1} + K_{q2} + K_{q3} = 1 \tag{5.3}$$

As always, in practice one should be careful and the RMS value of the current should not exceed the rated value I_{rated} at any time.

$$I_{abc...n} \le I_{rated} \tag{5.4}$$

By changing the K_{qi} coefficients the winding set's power direction and amplitude can be altered accordingly. K_{di} coefficients should be always positive values and sum to one during the power sharing operation. When using separate sharing coefficients K_{di} and K_{qi} for the flux and torque producing currents, the equations for nine-phase case become (note that these equations correspond to (3.93) if common K_i current sharing coefficients are used):

$$i_{d1} = \frac{1}{6}\left(\sqrt{3}(2K_{d1} - K_{d2} - K_{d3})i_{ds} + 3(K_{q2} - K_{q3})i_{qs}\right) \tag{5.5}$$

$$i_{q1} = \frac{1}{6}\left(3(K_{d2} - K_{d3})i_{ds} - \sqrt{3}(2K_{q1} - K_{q2} - K_{q3})i_{qs}\right) \tag{5.6}$$

$$i_{d2} = \frac{1}{6}\left(\sqrt{3}(2K_{d1} - K_{d2} - K_{d3})i_{ds} - 3(K_{q2} - K_{q3})i_{qs}\right) \tag{5.7}$$

$$i_{q2} = \frac{1}{6}\left(3(K_{d2} - K_{d3})i_{ds} + \sqrt{3}(2K_{q1} - K_{q2} - K_{q3})i_{qs}\right) \tag{5.8}$$

The power sharing operation is done using IRFOC and the auxiliary currents control. The schematic for power sharing strategy is illustrated in Fig. 5.3. The scheme includes the scalar auxiliary (*x-y*) currents equations to control the amplitude and direction of the power. By controlling the torque producing currents of the individual winding sets, i.e. by controlling the sharing coefficients K_{qi}, the

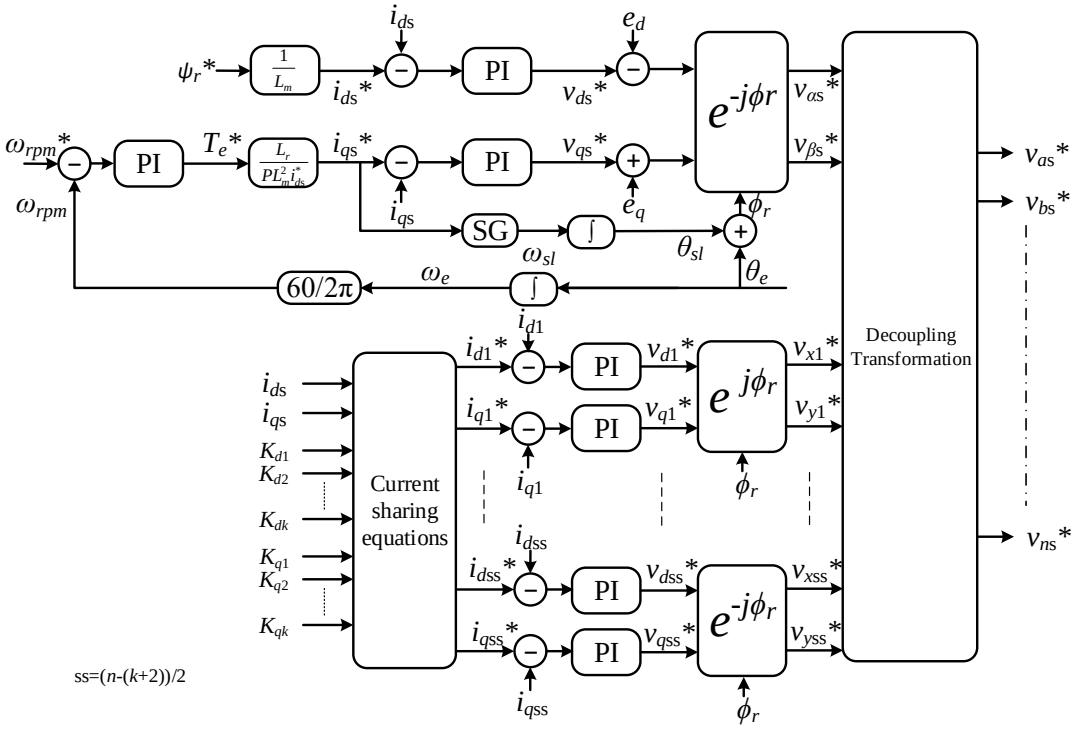

Fig. 5.3: Block diagram of IRFOC scheme with power sharing control using VSD for multiple three-phase induction machine.

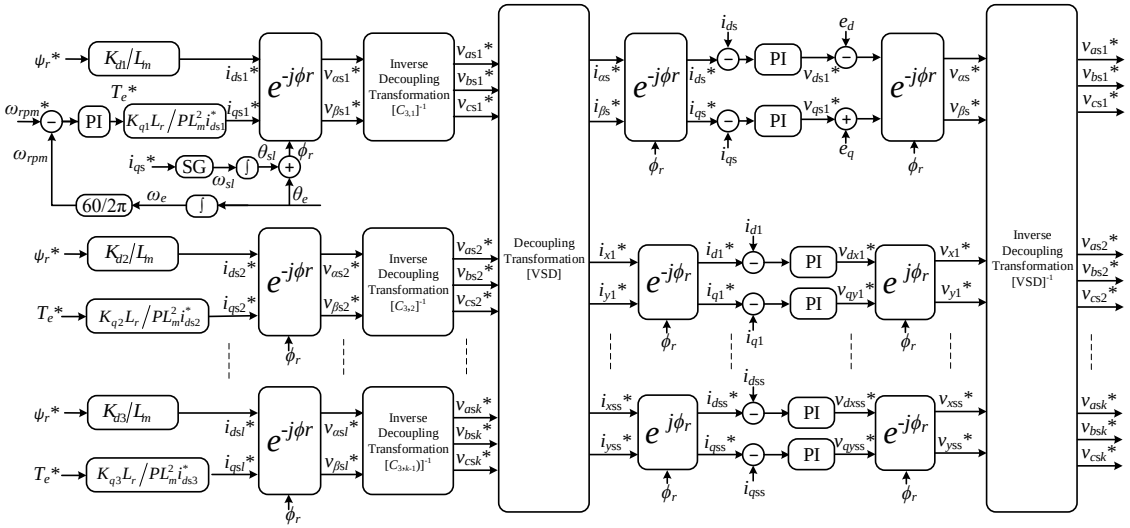

Fig. 5.4: Block diagram of IRFOC scheme with power sharing control using MS and VSD for asymmetrical multiple three-phase induction machine.

control of the active power direction and amount is achieved. The scheme is applicable to any multiple three-phase machines.

The utilisation of the auxiliary currents to control the power of the individual winding sets is not straightforward. This is because the correlations between the MS modelling approach and VSD modelling approach need to be defined, which requires heavy mathematical computations. For example, in the control algorithm in Fig. 5.3, "Current sharing equations" block is defined by the sharing equations shown in (5.5) to (5.8). To avoid these complex calculations, another easier approach to control the power flow of the individual winding sets is developed. This approach is shown in Fig. 5.4.

The new approach is utilising the MS modelling approach at the early stage of control, and then it converts the decoupled current references of the individual winding sets into its phase variables equivalent by multiplying them by the inverse decoupling transformation $[C_{3,1}]^{-1}$, $[C_{3,2}]^{-1}$, … (see Fig. 5.4). Then, transformation of the phase variable currents into the VSD reference frame is obtained by multiplying them by [*VSD*] ("Decoupling Transformation [VSD]" block in Fig. 5.4). Afterwards, the decoupled current is controlled in the rotational reference frame along with the auxiliary currents with the suitable rotational transformation of the *x-y* currents. Finally, the decoupled voltage references are converted into the phase variable reference frame by applying the "Inverse Decoupling Transformation $[VSD]^{-1}$" matrix as illustrated in Fig. 5.4. By applying this control scheme, the ability to control the winding sets individually is possible while maintaining the unique harmonic mapping of the machine currents and elimination of the coupling between the winding sets.

Note that both control schemes, one presented in Fig. 5.3 and the one in Fig. 5.4, are identical. The only difference is that, for the one in Fig. 5.3, offline complex mathematical calculations for obtaining the current sharing equations are needed. In the algorithm presented in Fig. 5.4 these calculations are left to the controller to be obtained. Hence, although the algorithm in in Fig. 5.4 may

look more direct for general implementation, it is not recommended for practical implementation if the execution time and the processor power are critical. In fact in this thesis the power sharing control schematic presented in Fig. 5.3 was used. The validation of the method is presented in the following section.

5.5 SIMULATION RESULTS

To validate the proposed power sharing scheme, illustrated in Fig. 5.3, an asymmetrical nine-phase machine has been simulated using Matlab/Simulink. Initially, the simulation is undertaken using the power sharing scheme utilising the current sharing strategy presented in Chapter 3 and Chapter 4. Then, the power sharing scheme with separated sharing coefficients for the flux and torque producing currents is simulated. The power efficiency is calculated and compared between the two approaches. The parameters of the nine-phase machine are provided in Table 3.1.

The power sharing utilising the current sharing scheme presented in the previous chapter (Fig. 4.4) is implemented in Matlab/Simulink and validated first. Initially, the machine is magnetised for one second, and then the reference speed is set to 157.1 rad/sec (1500 rpm). After the machine has reached steady state, it was loaded with 5 Nm at t = 2.5 sec, as obvious from the torque subplot in Fig. 5.5a. Next, three power sharing scenarios have been implemented starting from t = 3.25 sec, each lasting for 0.25 sec. The sharing scenarios are presented in Fig. 5.5b. The power is shared according to the sharing coefficients of the individual winding sets K_i. The sharing is achieved by multiplying the amplitude of the *x-y* currents references by the suitable K_i coefficients, i.e. by using the appropriate current sharing equations which are in this case for the asymmetrical nine-phase machine given by (4.44) – (4.46). The sharing coefficients are the same for the *d* and *q* currents (α-β subspace). The first scenario (between 3.25 sec and 3.5 sec) is achieved by setting the K_i coefficients to $K_1 = -1/3$, $K_2 = 2/3$ and $K_3 = 2/3$. The currents have changed according to the values of K_i. The currents i_{a2} and i_{a3} are doubled, compared to the original value, while i_{a1} maintained the same amplitude, but with an opposite direction, as illustrated in i_{a123} subplot of Fig. 5.5b. It can be noticed from the input powers of the winding sets P_{s123}, illustrated in the last subplot of Fig. 5.5b, that during this period the second and third winding set are operating in motoring mode while the first winding set is operating in generation mode.

The second power sharing scenario is simulated between t = 3.5 sec and 3.75 sec where the sharing coefficients are set to $K_1 = 2/3$, $K_2 = -1/3$ and $K_3 = 2/3$. Now, in this scenario, two winding sets (first and third) are running in motoring mode and the second is running in generation mode. The current of the first and third winding set is twice the current of the second winding set as expected and as illustrated in Fig. 5.5b.

The last scenario of the power sharing utilising the current sharing strategy is illustrated in Fig. 5.5b between t = 3.75 sec and 4 sec. The sharing coefficients are changed to $K_1 = 2/3$, $K_2 = 2/3$ and

$K_3 = -1/3$. The first and second winding sets are now running in motoring mode while the third winding set is in generation mode.

In each scenario after $t = 3.25$ sec one set is in generation mode (keeping the same current magnitude as before the sharing is applied), while the other two sets are in motoring mode (operating with twice larger current magnitude than before the sharing coefficients are applied). As can be seen from Fig. 5.5a, the speed and torque and hence the output power on the shaft, are maintained before and

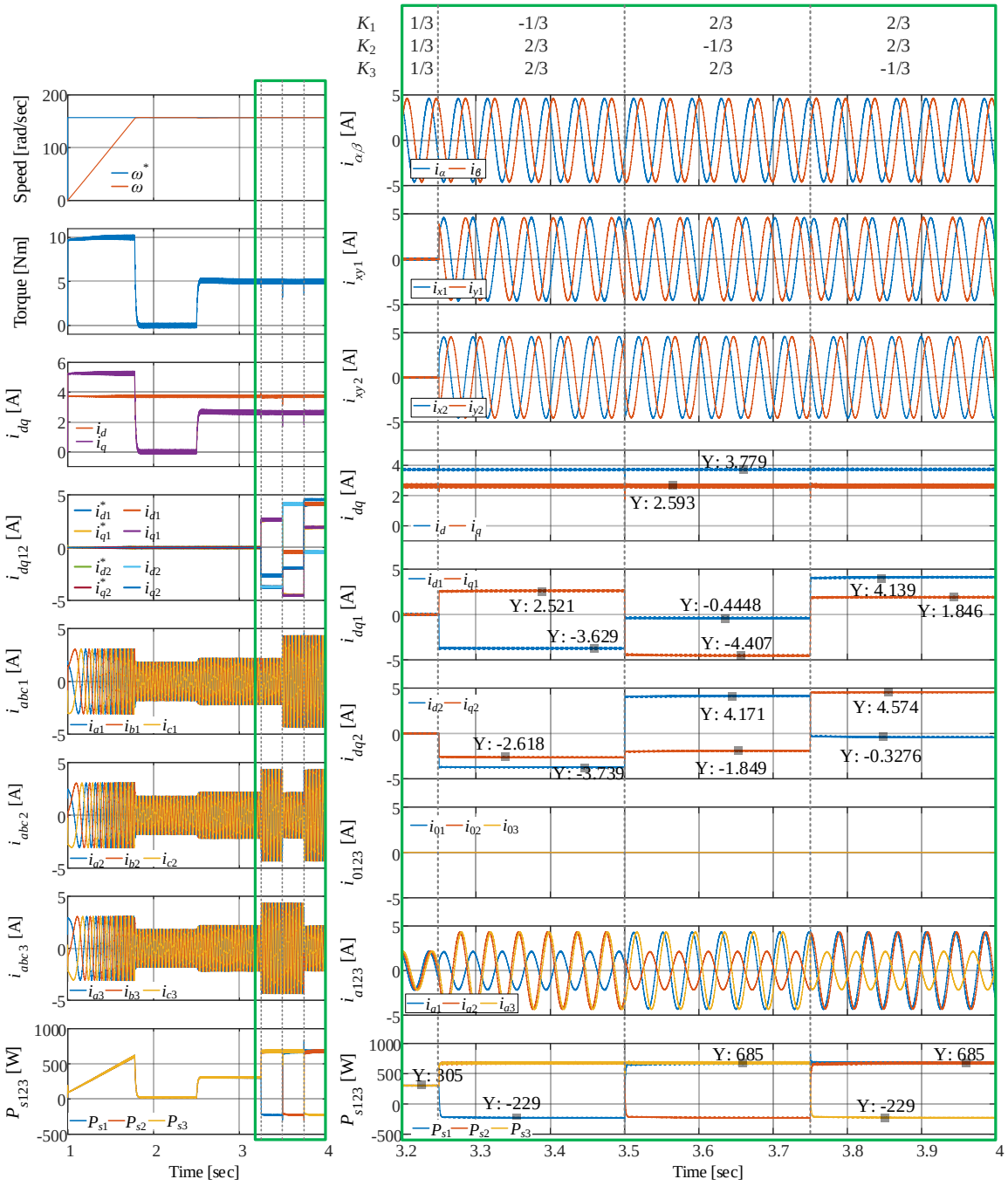

a) b)

Fig. 5.5: Simulation results of power sharing control using current sharing strategy for asymmetrical nine-phase induction machine. a) Complete simulation, b) zoomed section between $t = 3.2$ sec – 4 sec.

after the sharing is applied. The torque is kept at 5 Nm and the speed is kept at 157.1 rad/s hence the output power is $P_{out} = T\omega = 785.4$ W.

The input power of each winding set is illustrated in the last subplot of Fig. 5.5b. Before the sharing is applied, all winding sets are in motoring mode consuming the power of 305 W each, or 915 W in total. Once the sharing is applied, i.e. after $t = 3.25$ sec the power consumed by the two sets running in motoring mode is around 685 W each, while the transferred power to the second winding set running in generation mode is around –229 W. Hence, the total input power is 1141 W (685 W + 685 W – 229 W). One can see that, once the sharing has started, although keeping the output power constant, the input power has been significantly increased from 915 W to 1141 W. Therefore, the efficiency of the machine, calculated as delivered mechanical power over the total input power, which is now also used for power transfer between the windings, has significantly dropped from $\eta_1 = 785.4$ W/894.9 W = 87.8 % to $\eta_2 = 785.4$ W/1141 W = 68.83 %. This is a consequence of the significant increase of the copper losses. For example, the current in all windings before the sharing was applied was 1.52 A rms. After $t = 3.25$ sec the same value is kept in the winding operating in generation mode, while the current of the two windings operating in motoring mode has practically doubled and increased to 3.054 A rms. The value of $R_s = 4.85\ \Omega$ (see Table 3.1), enables one to easily calculate that the stator copper losses increased from 100.84 W to 305.03 W after the current sharing is applied. Therefore, the new, more efficient, method should aim to share the torque current component as required, but not to significantly increase the overall current magnitude (as it will obviously increase the copper losses in the machine). The simulation results with a new, more efficient, power sharing method are presented next.

The power sharing efficiency can be improved sharing the torque producing current only. The developed sharing scheme illustrated in Fig. 5.3 is separating the sharing coefficients among the *d* and *q* currents of the machine as discussed in section 5.4. The simulation results of this power sharing scheme are illustrated in Fig. 5.6. The sharing is achieved by changing the coefficients associated with the torque producing current K_{qi} of the individual winding sets. The sharing coefficients associated with the flux producing current K_{di} are kept constant and equal during the power sharing scenarios except when the winding set is shut down. The first sharing scenario is implemented between $t = 3.25$ sec and $t = 3.5$ sec and the sharing coefficients are set to $K_{q1} = -1/3$, $K_{q2} = K_{q3} = 2/3$, and $K_{d1} = K_{d2} = K_{d3} = 1/3$. Note that the values of K_{di} are kept the same for all scenarios. The ratio between the winding sets' currents is not following the ratio between the sharing coefficients K_{qi} and K_{di} as in the case of the power sharing utilising the current sharing strategy illustrated in Fig. 5.5. However, the efficiency of the transferred power is improved as demonstrated based on the last subplot of Fig. 5.6.

The second power sharing scenario is implemented between $t = 3.5$ sec and 3.75 sec by running the first and third winding sets in motoring mode and the second winding set in generation mode. The

coefficients are now adjusted to K_{q1} = 2/3, K_{q2} = –1/3, K_{q3} = 2/3, K_{d1} = K_{d2} = K_{d3} = 1/3. The enlarged simulation results are presented in Fig. 5.6.

Finally, in the last scenario the third set is operating in the generation mode, while the first two sets are in motoring mode. This scenario is implemented between t = 3.75 sec and t = 4 sec. The sharing coefficients in this mode are set to K_{q1} = 2/3, K_{q2} = 2/3, K_{q3} = –1/3 and K_{d1} = K_{d2} = K_{d3} = 1/3, as illustrated in Fig. 5.6b.

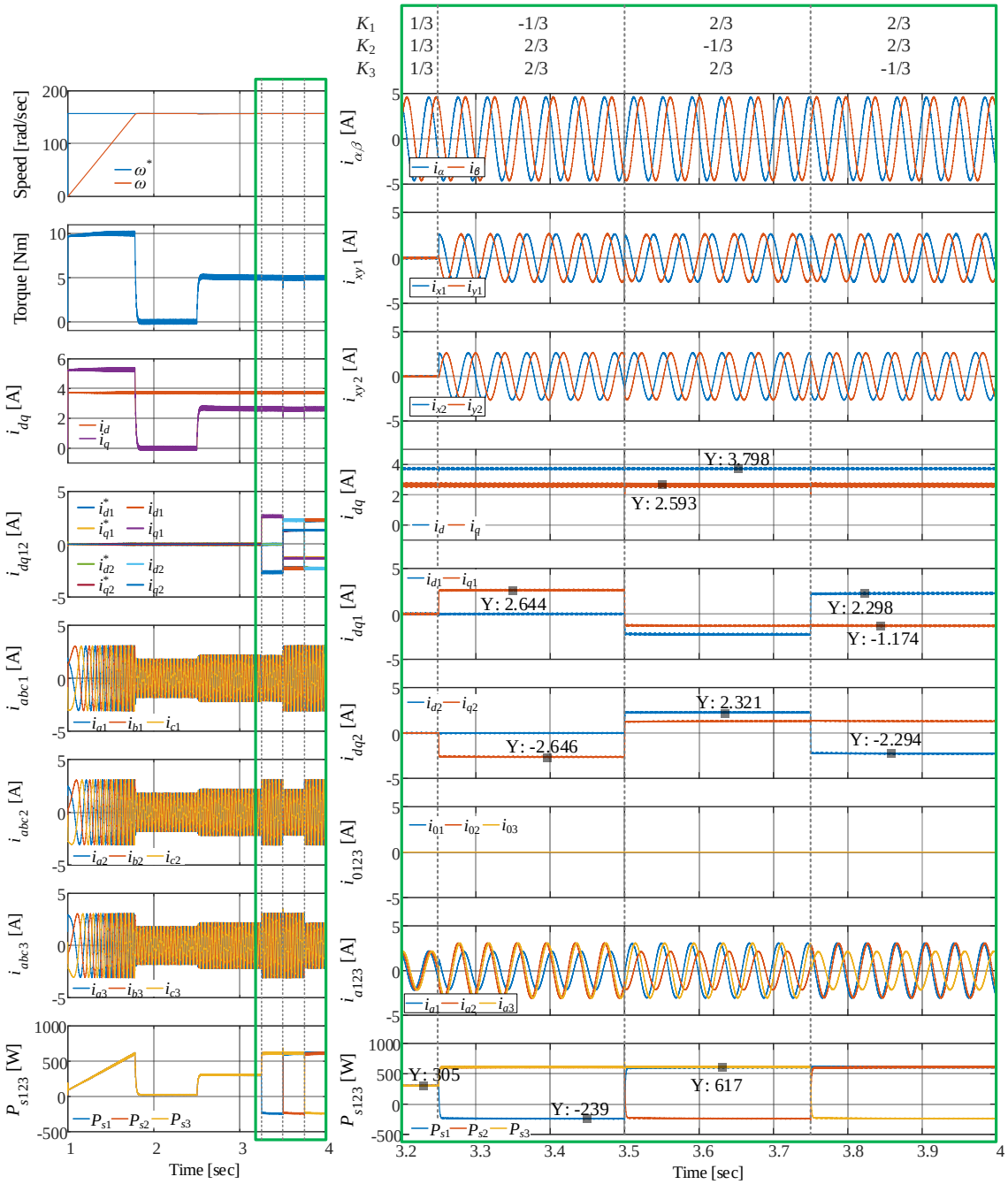

a) b)

Fig. 5.6: Simulation results of the proposed efficient power sharing control using for asymmetrical nine-phase induction machine. a) Complete simulation, b) zoomed section between t = 3.2 sec – 4 sec.

Again, before the sharing coefficients were applied the power consumed by each winding set was 305 W, meaning that the total machine input power was 915 W (see the bottom subplot in Fig. 5.6b). The machine is again maintaining the speed of 1500 rpm (157.1 rad/s) while loaded by 5 Nm. Hence the output power of the machine is 785.4 W before and after the sharing coefficients are applied. Once the sharing has started (after 3.25 sec), the power consumed by the windings operating in motoring mode has increased to 617 W, while the power of the set operating in generation mode is –239 W. Hence, the total input power into the machine is: 995 W (617 W + 617 W – 239 W). Comparing the values if the current sharing method is used (Fig. 5.5), one can see that the efficient power transfer scheme has reduced the input power of the motoring winding sets (from 700 W to 617 W per set) and increased the generated power by the generation winding sets (excluding the '–' sign, 239 W), while keeping the same electromechanical energy conversion at 5 Nm and speed of 1500 rpm. The efficiency of the machine now is η_3 = 785.4 W/995 W = 78.93%. Therefore, from this scenario it can be seen that the transferred power efficiency is improved compared to the last scenario utilising the current sharing strategy implemented in Fig. 5.5.

Once again it is worth mentioning that the ratio of the winding sets' currents is not following the ratio of the sharing coefficients K_{qi} and K_{di}, as was the case for the power sharing utilising the current sharing strategy illustrated in Fig. 5.5. For example, the rms values of the sets operating in motoring mode are 2.15 A rms and for the set operating in generation mode it is 1.52 A rms. So the ratio is not 2 any more. However, the ratio of the sharing coefficients still defines how much each winding set contributes to the value of the electromagnetic torque, i.e. to the output power.

5.6 EXPERIMENTAL RESULTS

To validate the proposed power sharing schemes discussed in sections 5.3 and 5.4, and to confirm the simulation results from the previous section, an asymmetrical nine-phase induction machine with three isolated neutral points is used. The experimental results are shown in Fig. 5.7 and Fig. 5.8. The power sharing results obtained using current sharing coefficients K_i are illustrated in Fig. 5.7, while Fig. 5.8 shows the experimental results of the efficient power sharing strategy using K_{di} and K_{qi}. For implementation of both algorithms real-time platform dSPACE was used. The asymmetrical nine-phase machine parameters are provided in Table 3.1.

Experimental results for the power sharing scheme, using the same sharing coefficients for the flux and torque producing currents, are illustrated in Fig. 5.7. The machine reference speed is set to 157.1 rad/sec and it is loaded using a dc generator with load torque of 5.22 Nm. The presented results correspond to the simulation result in Fig. 5.5. The same sharing scenarios are implemented for the simulation and experimental results. However, the duration of each scenario in the experimental results is reduced to 0.2 sec (instead of 0.25 sec used in simulation). Again, three power sharing scenarios have been implemented where two motoring winding sets have current sharing coefficients of 2/3 while the

third winding set in generation has a coefficient of –1/3. Initially and at the end of the shown time, the machine is running with no current sharing ($K_1 = K_2 = K_3 = 1/3$). The values of the current sharing coefficients for each segment are shown on top of Fig. 5.7. It is obvious from i_{a123} subplot of Fig. 5.7a, or from Fig. 5.7b (i), that the current ratio between the motoring winding sets and the one in generation, when applying the power sharing scenario, is 2/1. Also note that for settling in each sharing scenario it takes around 0.1 sec, hence the second half of the shown 0.2 sec for each scenario should be observed.

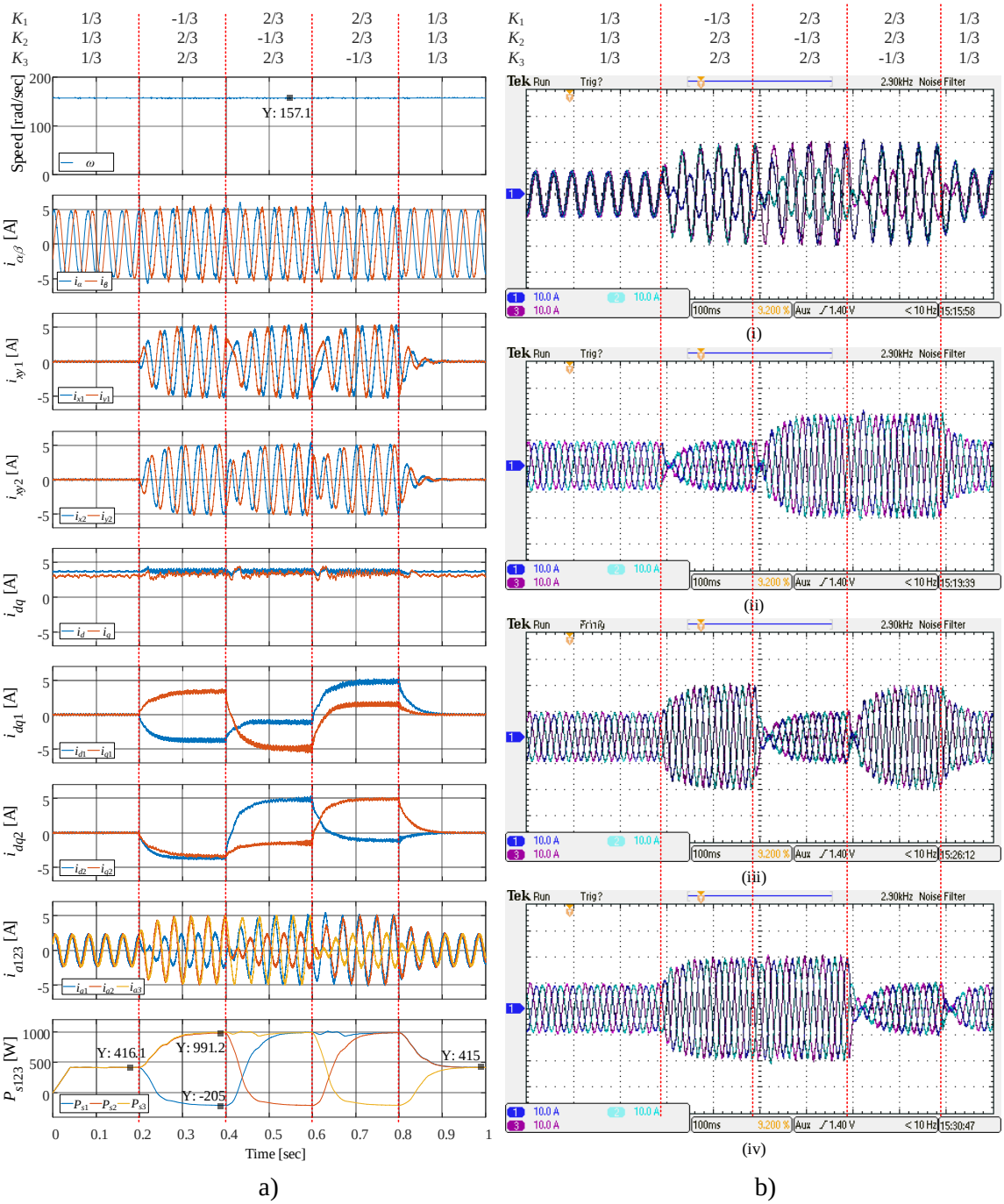

Fig. 5.7: Experimental results of power sharing control using current sharing strategy K_i for asymmetrical nine-phase induction machine. a) Timing waveforms captured by dSpace ControlDesk. b) Oscilloscope screenshots: (i) i_{a1}, i_{a2}, i_{a3}, (ii) set-1 currents i_{a1}, i_{b1}, i_{c1}, (iii) set-2 currents i_{a2}, i_{b2}, i_{c2}, (iv) set-3 currents i_{a3}, i_{b3}, i_{c3}. Four turns of wire were used for oscilloscope current measurements.

It is obvious from the bottom subplot in Fig. 5.7a, when no sharing is applied (all winding sets are in motoring) the input power of the machine is 416 + 416 + 416 = 1248 W. On the other hand, during the power sharing scenarios, the input power of the motoring winding sets is 991 + 991 = 1982 W, while the power of the set running in generation mode is –205 W. Hence the total input power when the sharing is applied is 1777 W. As explained before, significant increase of input power is expected in this mode when the same sharing coefficients are applied for both torque and flux current components.

Although there are vector PI controllers in the *x*-*y* subspaces to eliminate the low order harmonics of the machine, introduced by the dead-time of the VSIs and the non-ideal design of the machine, a presence of the low order harmonics is obvious in the winding sets' currents during the application of the power sharing strategy. This can be seen from the oscilloscope screenshots in Fig. 5.7b. Additionally, it can be noticed from the second subplot of Fig. 5.7a that there are unexpected low order harmonics present in $i_{\alpha\beta}$ currents during the power sharing operation between (t = 0.2 – 0.8 sec). Ideally $\alpha\beta$ currents should remain the same regardless of power sharing operation. These harmonics are not present in the simulation results (Fig. 5.5b, top subplot) and are the consequence of the non-ideal phenomena present in practice. These harmonics can be mitigated using additional vector PI regulator in the α-β plane.

In order to improve the transmitted power efficiency among the winding sets, the sharing of the active and reactive power should be separated. The separation of the power is done by sharing the torque producing current rather than both flux and torque producing currents as used by the previous method. The efficient power transfer scheme introduced in section 5.4 and simulated in Fig. 5.6 is validated experimentally in Fig. 5.8.

The same testing conditions implemented for the power sharing using K_i are used for the authentication of the efficient power transfer scheme illustrated in Fig. 5.8. Hence the reference speed is still 157.1 rad/sec and the load torque is 5.22 Nm. The machine starts and ends up in the motoring mode, while the three sharing scenarios are applied in the middle, each for 0.2 sec. Note that now only the values of K_{qi} are varied during the power sharing operation while K_{di} is maintained constant at 1/3. For the motoring, the winding sets *q*-sharing coefficient (K_{qi}) is set to 2/3 while for the generation winding set K_{qi} = –1/3. The power sharing coefficients are shown on top of Fig. 5.8. Note that with this method the ratio of the magnitudes of the currents in motoring and in the generation mode is not any more following the ratio of the coefficients and is not anymore 2/1. The reduction of the current magnitudes causes the reduction of the copper losses of the winding sets, and hence contributes to the increased efficiency.

The input power of the winding sets P_{s123}, shown in Fig. 5.8a bottom subplot, illustrates the validity of the approach to transfer the power more efficiently compared to the approach shown in Fig. 5.7. The withdrawn power of the motoring winding sets is now 853 + 853 = 1706 W, which is less than the previous method (1982 W). Also the generated power is –252 W, which is more (by absolute

value) than the generated power in the previous method (–205 W). Therefore the total input power is now 1454 W, which is significantly less than 1777 W obtained using the previous method. In both cases the output torque and speed (and hence power) are the same. Hence, the efficiency of transferred power has increased. As for the previous method, the low order harmonics appear in the α-β subspace currents during the power sharing operations as can be seen from the second subplot of Fig. 5.8a.

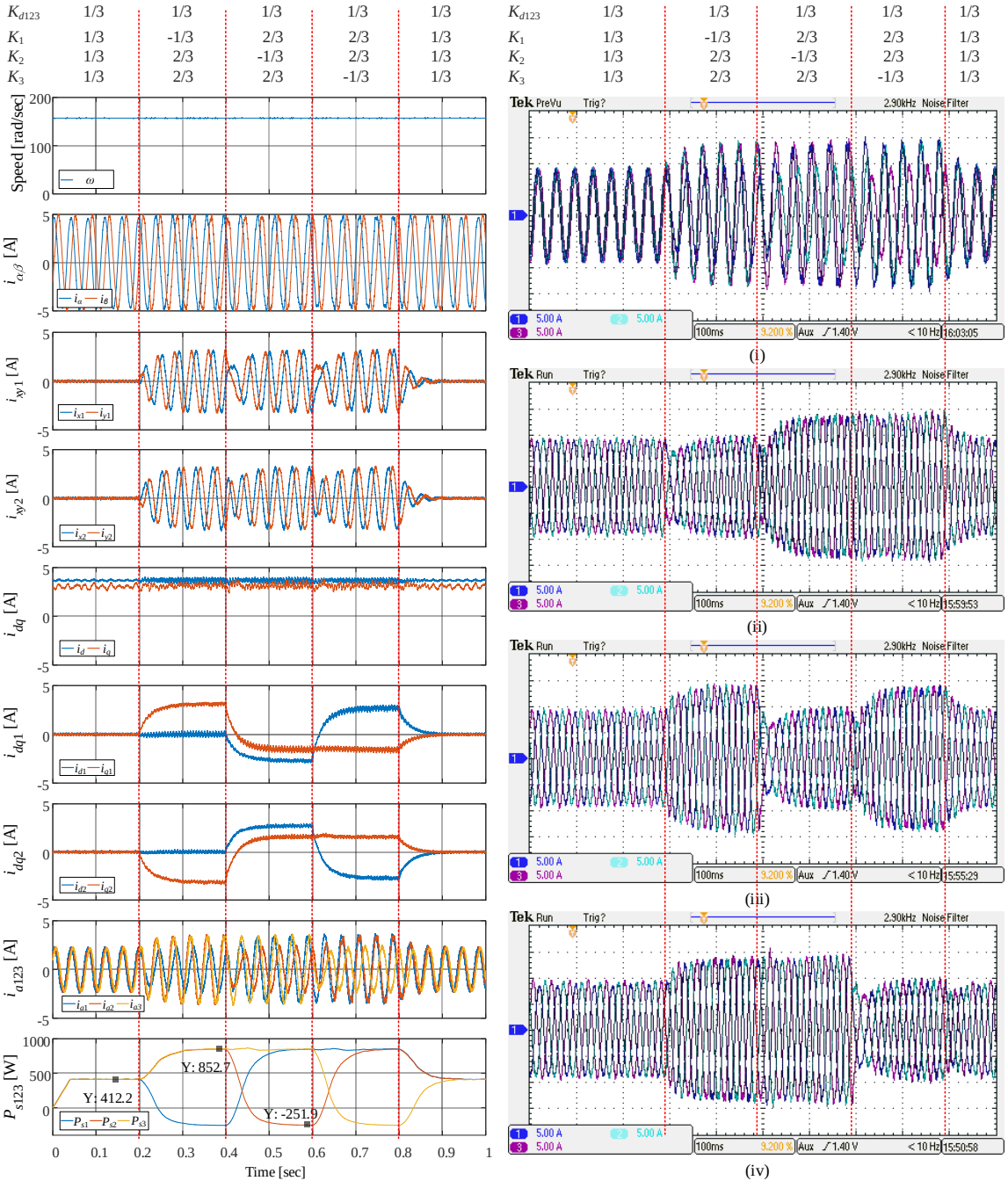

Fig. 5.8: Experimental results of efficient power sharing control using K_{di} and K_{qi} for asymmetrical nine-phase induction machine. a) Timing waveforms captured by dSpace ControlDesk. b) Oscilloscope screenshots: (i) i_{a1}, i_{a2}, i_{a3}, (ii) set-1 currents i_{a1}, i_{b1}, i_{c1}, (iii) set-2 currents i_{a2}, i_{b2}, i_{c2}, (iv) set-3 currents i_{a3}, i_{b3}, i_{c3}. Four turns of wire were used for oscilloscope current measurements.

The simulation results of the power sharing schemes are different compared to the experimental results since an ideal model of the nine-phase machine is used in simulation. The rotor friction and the core losses of the machine were not considered during the simulation results. In addition, a 5 Nm load was used in simulation, while in practice it was 5.22 Nm.

5.7 SUMMARY

In this chapter, the power sharing between winding sets of the multiple three-phase machine is introduced. Two power sharing approaches are discussed. The first approach is based on the current sharing approach presented in Chapter 3 and Chapter 4. The power sharing is achieved by using current sharing coefficients K_i applied to α and β (d and q) currents equally. The transferred power efficiency is not optimal using this approach. This is so because the flux producing current (i_α) is multiplied with the same coefficient as the torque producing current (i_β). The flux producing current does not contribute to the active power transferred to the air-gap. Therefore, the α current should not be shared in the same manner as the β current. A more efficient approach for power sharing is introduced by separating the sharing coefficients K_i among the torque and flux producing currents (K_{di} and K_{qi}). The copper losses are reduced in this way since the i_d current is kept constant during the power sharing operation and the normal operation of the machine. Both methods can be applied either to symmetrical or asymmetrical types of machine. An asymmetrical nine-phase induction machine is used for verification and simulated with the different power sharing scenarios. The simulation results of the two approaches proved the theoretical analysis. The efficiency of the transferred power is significantly improved using the separate sharing coefficients for d and q currents (K_{di} and K_{qi}) compared to the power sharing approach utilising a single current sharing coefficient for both flux and torque producing currents. To validate the theoretical analysis and the simulation results of the power sharing schemes, experimental validation of the power sharing schemes has been carried out on an asymmetrical nine-phase machine. The experimental results match the simulation results where the efficiency has been significantly improved using the method with separate sharing coefficients for the torque and flux producing current.

CHAPTER 6

POWER FLOW CONTROL AMONG DOUBLE-WINDING MULTIPLE THREE-PHASE MACHINES' WINDING SETS

6.1 INTRODUCTION

This chapter presents two vector control schemes for double-winding multiple three-phase induction machines with symmetrical and asymmetrical configuration. Double-winding multiphase machine is defined here as a multiphase machine where each phase winding has its corresponding (double) winding set spatially shifted by zero electrical degrees. Hence, an *n*-phase double-winding multiphase machine can be considered as consisting of two *n*/2-phase multiphase sub-machines sharing the same stator slots. The developed schemes introduce the ability to control the power flow among the multiple winding sets. The power flow control introduced in Chapter 5 was for symmetrical and asymmetrical machines with multiple three-phase winding sets, but with no double-winding. In this chapter, the power flow control for multiple three-phase winding sets within double-winding multiphase machine is introduced utilising vector control and multiple vector control schemes to provide the multidirectional power flow control of each winding set separately. The energy can be transferred from one winding sets to another using the developed scheme within the same sub-motor or from one sub-motor to another.

This chapter is organised as follows. In Section 0 a general background about double-winding multiple three-phase machines is introduced. By having a different turns ratio for each sub-motor different dc-bus voltage levels can be used. This will provide different voltage level for each sub-motor according to the turn's ratio of each one of them. Next, in section 6.3 the mathematical modelling of the double-winding multiple three-phase machines is presented. The double-winding three-phase machines can be mathematically modelled as a summation of the sub-motors and by considering the coupling between them. In section 6.4, the control strategies developed to perform multidirectional power flow control of the double-winding multiple three-phase machines are presented. The schemes are developed for twelve-phase induction machines, i.e. six-phase machines with double-winding, with four three-phase winding sets. Two approaches are developed to control the power flow of the winding sets. The first approach is developed based on current sharing strategy while the second one is based on the efficient power sharing strategy from Chapter 5. To validate the developed vector control schemes for the double-winding machines, a twelve-phase machine with dual six-phase winding was simulated using Matlab/Simulink in section 6.5. The power sharing approaches are compared based on transferred power efficiency. Finally, the summary of the chapter is made in section 6.6.

Original contributions of this Chapter have been presented at IEEE IECON 2017 conference in Beijing, China and published in [Abduallah at el. (2017)].

6.2 DOUBLE-WINDING MULTIPLE THREE-PHASE MACHINES

Some of the most common practical applications of the multiple three-phase induction machines are in more-electric aircrafts [Grandi et al. (2010), Tani et al. (2013), Mengoni et al. (2016)] and in electric vehicles, EVs [Subotic et al. (2016a), Subotic et al. (2016b), Subotic et al. (2016c), Subotic et al. (2016d)]. In the latter application, the electrical power generation and distribution systems are expected to raise from the conventional low dc voltage to a higher dc voltage level in the near future. This will reduce the system losses and size as well [Scarcella et al. (2016)]. Furthermore, new starter-alternator topologies with different numbers of turns per winding layer (sub-machine) are introduced in [Scarcella et al. (2016)]. The motivation behind this unusual structure is to accommodate multiple dc voltage levels (dc-bus voltage level of the corresponding VSIs), present in such a system. The introduced starter-alternator is a multiple-winding three-phase induction machine, where each three-phase winding represents a sub-motor. The authors used a multiple vector control scheme in order to achieve multidirectional power flow between the multiple three-phase sub-motors. Obviously, multiple three-phase machines, with single or double winding, can also be categorised as a type of multiphase machine. However, as mentioned before, multiple vector control is not the best approach to control multiphase machines. A more popular control method for multiphase machines is based on the VSD modelling approach. Therefore, the aim of this chapter is to develop vector control algorithm for multiple three-phase induction machines with double-winding. The scheme uses the additional degrees of freedom offered by the multiphase machine to control the currents' amplitude and power flow direction of each three-phase winding set independently. A simplified structure of a double-winding symmetrical and asymmetrical six-phase induction machine, which will be analysed in this chapter, is shown in Fig. 6.1. For simplicity, stator phases are illustrated by the magnetic axes. Blue and red colours are used to represent different layers within the same phase, i.e. sub-machine I and sub-machine II.

6.3 MATHEMATICAL MODEL OF DOUBLE-WINDING MULTIPLE THREE-PHASE MACHINES

The mathematical model of the analysed machine can be considered as a twelve-phase machine in phase variable form, but also as a summation of dynamic equations of the two separate six-phase induction sub-motors. The equivalence of these two models is proven by the simulation results shown in Fig. A.4 of Appendix A. This fact makes it possible to simplify control and is used to control this twelve-phase machine as two six-phase sub-motors, as demonstrated in the next section. Also, in order to simplify the equations, the model of the double-winding six-phase induction motor is derived here as a combination of two separate six-phase sub-motors sharing the same rotor. Stator and rotor voltage equilibrium equations, for each six-phase sub-motor, can be defined as:

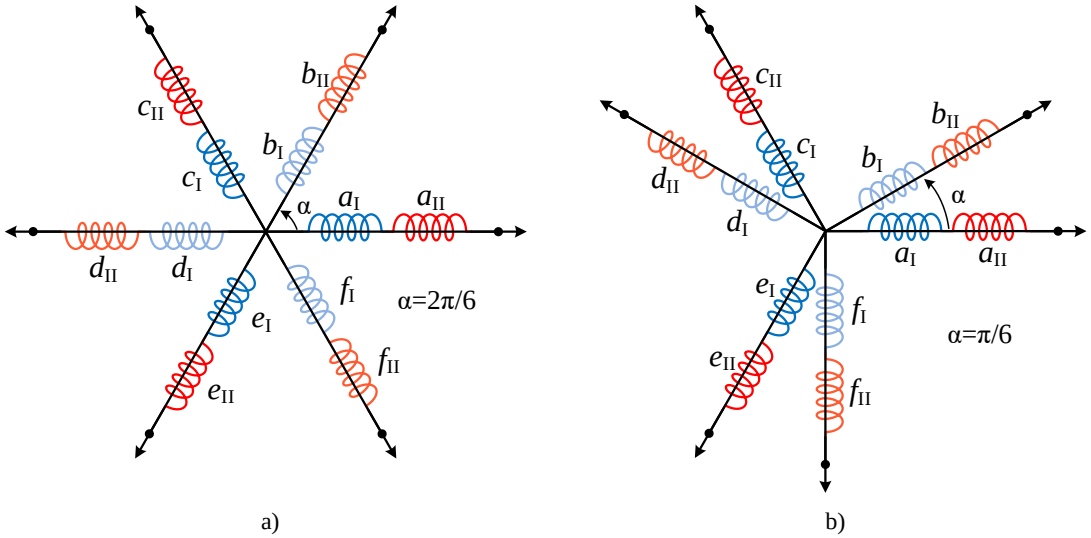

a) b)

Fig. 6.1: Spatial position of the a) symmetrical and b) asymmetrical six-phase double-winding induction machine stator's magnetic axes.

$$[v_{sk}] = [R_{sk}][i_{sk}] + \frac{\mathrm{d}[\psi_{sk}]}{\mathrm{d}t} \tag{6.1}$$

$$[v_{rk}] = [R_{rk}][i_{rk}] + \frac{\mathrm{d}[\psi_{rk}]}{\mathrm{d}t} \tag{6.2}$$

In (6.1), $[v_{sk}] = [v_{sak}\ v_{sbk}\ v_{sck}\ v_{sdk}\ \dots\ v_{snk}]^T$, $[i_{sk}] = [i_{sak}\ i_{sbk}\ i_{sck}\ i_{sdk}\ \dots\ i_{snk}]^T$, $[\psi_{sk}] = [\psi_{sak}\ \psi_{sbk}\ \psi_{sck}\ \psi_{sdk}\ \dots\ \psi_{snk}]^T$, represent stator phase voltages, currents and flux linkages, respectively. Index k is used to indicate sub-motor (k = I or II). Matrix $[R_{sk}]$ represents stator resistance matrix, of each sub-motor. It is a diagonal matrix, where all elements on the main diagonal are equal to R_s due to the assumed machine's symmetry. Equation (6.2) is of the same form as (6.1), but it is given for rotor variables, hence r in index instead of s. Note that division of the rotor into two sub-motors does not physically exist. For instance, if the rotor currents are taken as an example, $[i_{rI}]$ and $[i_{rII}]$ would represent the rotor currents produced by each sub-motor. The flux-linkage equations for each sub-motor are defined as follows:

$$[\psi_{sk}] = [L_{sk}][i_{sk}] + [L_{srk}][i_{rk}] \tag{6.3}$$

$$[\psi_{rk}] = [L_{rk}][i_{rk}] + [L_{srk}]^T[i_{sk}] \tag{6.4}$$

where $[L_{sk}]$ and $[L_{rk}]$ represent stator and rotor self-inductance matrices and $[L_{srk}]$ represents stator-to-rotor inductance, for k-th (k = I or II) sub-motor. These inductances are defined as in (3.15) through (3.18) for symmetrical machines and as in (4.13) through (4.22) for asymmetrical machines. The electromagnetic torque T_e can be calculated as:

$$T_e = P\left[i_s\right]^T \frac{\mathrm{d}\left[L_{sr}\right]}{\mathrm{d}\theta_e}\left[i_r\right] \tag{6.5}$$

where $[i_s]$ represents the sum of $[i_{s\mathrm{I}}]$ and $[i_{s\mathrm{II}}]$, and $[i_r]$ represents the sum of $[i_{r\mathrm{I}}]$ and $[i_{r\mathrm{II}}]$. In other words, T_e can be calculated by summing the electrometric torque produced by each sub-motor. The same approach was applied in [Scarcella et al. (2016)]. Hence, the electromagnetic torque can be expressed as follows for double-winding machines:

$$T_e = P\left(\left[i_{s\mathrm{I}}\right]^T \frac{\mathrm{d}\left[L_{sr\mathrm{I}}\right]}{\mathrm{d}\theta_e}\left[i_{r\mathrm{I}}\right] + \left[i_{s\mathrm{II}}\right]^T \frac{\mathrm{d}\left[L_{sr\mathrm{II}}\right]}{\mathrm{d}\theta_e}\left[i_{r\mathrm{II}}\right]\right) \tag{6.6}$$

Note that the parameters of the sub-motors are reliant on the turns ratio between the sub-motors [Scarcella et al. (2016)]. However, in this chapter it is assumed that the sub-motors are identical.

In order to implement the vector control, it is essential to convert the ac machine model into its dc machine equivalent where the flux and torque are decoupled. The fictitious flux and torque producing variables can be obtained from the phase variables reference frame through Clarke's decoupling transformation [Levi et al. (2007)]. The decoupling transformation can be obtained using (3.87) for symmetrical machines and (4.34) or (4.36) for asymmetrical machines. Here, a symmetrical six-phase machine with double-winding is considered as an example. Clarke's transformation for a symmetrical six-phase machine with two isolated neutral points, is defined as:

$$[C] = \sqrt{\frac{2}{6}}\begin{bmatrix} \alpha & 1 & \cos(\alpha) & \cos(2\alpha) & \cos(3\alpha) & \cos(4\alpha) & \cos(5\alpha) \\ \beta & 0 & \sin(\alpha) & \sin(2\alpha) & \sin(3\alpha) & \sin(4\alpha) & \sin(5\alpha) \\ x & 1 & \cos(2\alpha) & \cos(4\alpha) & \cos(6\alpha) & \cos(8\alpha) & \cos(10\alpha) \\ y & 0 & \sin(2\alpha) & \sin(4\alpha) & \sin(6\alpha) & \sin(8\alpha) & \sin(10\alpha) \\ 0_+ & 1 & 0 & 1 & 0 & 1 & 0 \\ 0_- & 0 & 1 & 0 & 1 & 0 & 1 \end{bmatrix} \tag{6.7}$$

The rotational transformation from (3.108) is applied only on the α-β components since the stator-to-rotor coupling terms appear only in this plane. The ω_a can be arbitrarily chosen and for the IRFOC algorithm. It is chosen to be equal to the rotational speed of the rotor-field. With this choice, the following relations can be obtained:

$$\theta_s = \phi_r \qquad \omega_r = \frac{\mathrm{d}\phi_r}{\mathrm{d}t} \qquad \omega_a = \omega_r \tag{6.8}$$

where ϕ_r and ω_r represent the rotor-field instantaneous position and the speed of the rotating field of the rotor, respectively.

6.4 CONTROL STRATEGY

The IRFOC algorithm can be applied to six-phase induction machines utilising previous decoupling and rotational transformations. As already discussed, due to the special construction of the considered twelve-phase (i.e. double-winding six-phase) machine, the control can be implemented by applying the IRFOC algorithm to each sub-motor individually [Scarcella et al. (2016)]. The traditional IRFOC can be reconfigured to suit this specific application. This will yield to a double vector control scheme to control each sub-motor independently. Nevertheless, in order to ensure that the flux of both sub-motors rotates at the same frequency and direction, the *d*-axis current components of the two sub-motors must be synchronised (aligned). The total flux should be maintained constant and divided among sub-motors according to their corresponding nominal flux values. In general, this is determined by the turns' ratio, but in this chapter sub-motors are assumed to be identical. Furthermore, the *q*-components of the stator currents are proportional to the electromagnetic torque produced by each sub-motor and also must be synchronised.

In IRFOC, in steady state, the *q*-component of the rotor flux-linkage will be equal to zero. Based on this, the IRFOC equations for each sub-motor can be found using (3.58) through (3.73). For a six-phase induction machine with double sub-motors, the slip speed can be found by adding the influence of i_{ds} and i_{qs} of the two sub-motors as in the following equation:

$$\omega_{sl}^{*} = \frac{i_{qsI}^{*} + (N_{sII}/N_{sI}) \cdot i_{qsII}^{*}}{((L_{mI} + L_{lr})/R_r) \cdot (i_{dsI}^{*} + (N_{sII}/N_{sI}) \cdot i_{dsII}^{*})} \tag{6.9}$$

where N_{sk} indicates the number of turns in each sub-motor. As already mentioned, in this chapter the simplest case where $N_{sI} = N_{sII}$ is considered. The magnetising inductance of the first sub-motor L_{mI} is equal to $(6/2)\cdot M_I$.

In order to utilise the double six-phase machines (e.g. in starter-alternator applications), the IRFOC algorithm for each sub-motor must share the same speed controller in order to ensure synchronisation of the rotating fields between the sub-motors. However, to obtain multidirectional power flow between them, the speed controller output (i_{qs}) should be multiplied by a suitable factor to control the current direction of each sub-motor as shown in Fig. 6.2. Introduced values G_I and G_{II} are the power sharing gains of the two sub-motors. Controlling these coefficients will allow the power sharing between the sub-motors. However, controlling the power flow direction for each winding set,

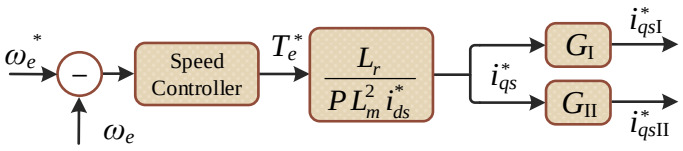

Fig. 6.2: Modified speed controller for six-phase induction machine with double-winding.

using these gains only, is not possible. Therefore, further modifications of the proposed IRFOC algorithm and introduction of current sharing coefficients for each winding set are necessary, as explained further.

As stated before, controlling the *d-q* currents with the IRFOC algorithm is not sufficient. Therefore, the other *x-y* currents (auxiliary currents) need to be controlled beside the *d-q* currents. This is common when controlling multiphase machines, and usually it is used to eliminate the non-ideal characteristics of the machine or the power electronics converter. Moreover, post-fault strategies utilise these currents to control the current's amplitude of the winding sets during the post-fault condition. Post-fault control due to a fault of one or more VSIs can be achieved by changing the sharing coefficients of the three-phase winding sets [Che et al. (2012a), Tani et al. (2013), Che et al. (2014c), Mengoni et al. (2016)].

In order to control the auxiliary currents in multiple three-phase machines, each three-phase winding set can be considered as a three-phase machine. The spatial displacement between each consecutive winding set in symmetrical induction machines is equal to $\alpha=2\pi/n$. Using the decoupling matrix for three-phase induction machines (3.85), the contribution of each winding set into the decoupled sub-motor's currents can be obtained. In order to get the decoupled currents of each winding set, the original phase variables current of each winding set should be multiplied by the three-phase decoupling transformation matrix (3.85), taking into consideration the spatial displacement of each winding set. Applying the current sharing strategy (which is illustrated in Section 3.7 for the nine-phase case), for the six-phase machine and using (3.85) and (6.7), the following relationships can be obtained for the first six-phase sub-motor:

$$\left[i_{VSD}\right]=\begin{bmatrix} i_{\alpha} \\ i_{\beta} \\ i_{x} \\ i_{y} \\ i_{0+} \\ i_{0-} \end{bmatrix}=[C]\left[i_{ph1}\right]=\begin{bmatrix} \frac{i_{\alpha 1}+i_{\alpha 2}}{\sqrt{2}} \\ \frac{i_{\beta 1}+i_{\beta 2}}{\sqrt{2}} \\ \frac{i_{\alpha 1}-i_{\alpha 2}}{\sqrt{2}} \\ \frac{-i_{\beta 1}+i_{\beta 2}}{\sqrt{2}} \\ i_{01} \\ i_{02} \end{bmatrix} \tag{6.10}$$

The corresponding equation to (6.10), for the nine-phase case in Section 3.7 is (3.93).

From (6.10), one can see that the stationary currents of the first sub-motor (the same applies for the second sub-motor) consist of α and β components of the two winding sets only. The six-phase sub-motors current space vectors can be defined as:

$$\begin{aligned}\bar{i}_{\alpha\beta} &= i_\alpha + ji_\beta = I_{\alpha\beta}\, e^{j\phi_{\alpha\beta}} \\ \bar{i}_{xy} &= i_x + ji_y = I_{xy}\, e^{j\phi_{xy}}\end{aligned} \tag{6.11}$$

The winding sets current space vectors can be defined as:

$$\begin{aligned}\bar{i}_{\alpha\beta 1} &= i_{\alpha 1} + ji_{\beta 1} = I_{\alpha\beta 1} e^{j\phi_{\alpha\beta 1}} \\ \bar{i}_{\alpha\beta 2} &= i_{\alpha 2} + ji_{\beta 2} = I_{\alpha\beta 2} e^{j\phi_{\alpha\beta 2}}\end{aligned} \tag{6.12}$$

Based on (6.10) through (6.12), the sub-motor current space vectors can be expressed in terms of the winding sets current space vectors, as:

$$\bar{i}_{\alpha\beta \mathrm{I}} = \tfrac{1}{\sqrt{2}}\left(\bar{i}_{\alpha\beta 1} + \bar{i}_{\alpha\beta 2}\right) \tag{6.13}$$

$$\bar{i}_{xy \mathrm{I}} = \tfrac{1}{\sqrt{2}}\left(\bar{i}_{\alpha\beta 1} - \bar{i}_{\alpha\beta 2}\right) \tag{6.14}$$

Note that (6.13) and (6.14) represent the space vector form of the previously given relationships in (6.10). The same set of equations can be defined for the second sub-motor (denoted with II) as well.

By introducing the current sharing coefficients K_1, K_2, K_3 and K_4 the winding set current space vectors can be rewritten in terms of the α-β space vectors for each sub-motor. The following relationships can be obtained for both sub-motors:

$$\begin{aligned}\bar{i}_{\alpha\beta 1} &= \sqrt{2}\, K_1\, \bar{i}_{\alpha\beta \mathrm{I}} \\ \bar{i}_{\alpha\beta 2} &= \sqrt{2}\, K_2\, \bar{i}_{\alpha\beta \mathrm{I}} \\ \bar{i}_{\alpha\beta 3} &= \sqrt{2}\, K_3\, \bar{i}_{\alpha\beta \mathrm{II}} \\ \bar{i}_{\alpha\beta 4} &= \sqrt{2}\, K_4\, \bar{i}_{\alpha\beta \mathrm{II}}\end{aligned} \tag{6.15}$$

where K_1, K_2, K_3 and K_4 represent the current sharing coefficients of the four winding sets. Note that the winding sets of the second sub-motor are denoted with indices 3 and 4 ($\bar{i}_{\alpha\beta 3}$ and $\bar{i}_{\alpha\beta 3}$). By substituting newly introduced current sharing coefficients of (6.15) into (6.13) and (6.14) the following relationships between the sub-motor α-β space vectors and the winding sets current space vectors can be obtained (note that the equations are given for the first sub-motor only, but equivalent equations can be given for the second sub-motor):

$$\begin{aligned}\bar{i}_{\alpha\beta \mathrm{I}} &= (K_1 + K_2)\bar{i}_{\alpha\beta \mathrm{I}} \\ \bar{i}_{xy \mathrm{I}} &= (K_1 - K_2)\bar{i}^{*}_{\alpha\beta \mathrm{I}}\end{aligned} \tag{6.16}$$

From (6.16), the currents of the winding sets can be controlled by changing the K coefficients. These equations are valid in the common reference frame. Unlike $\bar{i}_{\alpha\beta}$, $\bar{i}_{xy}$ should be controlled in the anti-synchronous reference frame [Che et al. (2014c)]. This will allow the control of the currents' amplitude of the winding sets in each sub-motor and consequently the power flow direction of each individual set.

However, the transfer of power from one sub-motor to another is not possible by using the current sharing coefficients only. Thus, the sub-motors' power sharing coefficients (G_{I} and G_{II}) should be integrated with the current sharing coefficients of the winding sets to obtain multidirectional power flow among the winding sets of the two sub-motors.

As obvious from (6.16), the summation of each sub-motor's current sharing coefficients should always be equal to one (K_1+K_2=1 for the first, and K_3+K_4=1 for the second sub-motor). Also, the sub-motor power sharing coefficients (G_{I} and G_{II}) must always sum to one, in order to maintain the same speed and torque. Fig. 6.3 illustrates the IRFOC schematic for the double-winding six-phase drive.

Although this schematic is valid for multidirectional power flow control among double-winding multiple three-phase machines, a more efficient power sharing approach has been introduced in section 5.4. Therefore, it is implemented next. The scheme is based on sharing the torque producing current (β) of each winding set rather than sharing the flux and torque producing currents (α-β). In this approach, the active power is shared only, rather than sharing the active and reactive power. The scheme is directly applicable to sub-windings of each sub-motor of a double-winding machine. It is also applicable for power sharing between the sub-motors, where the power sharing coefficients G_{I} and G_{II} are applied only to the q-current components of the sub-motors. The IRFOC scheme utilising the efficient power sharing scheme is illustrated in Fig. 6.4. By applying the efficient power sharing scheme for the double-winding six-phase machine, the number of sharing coefficients 'K' is increased to four coefficients, instead of

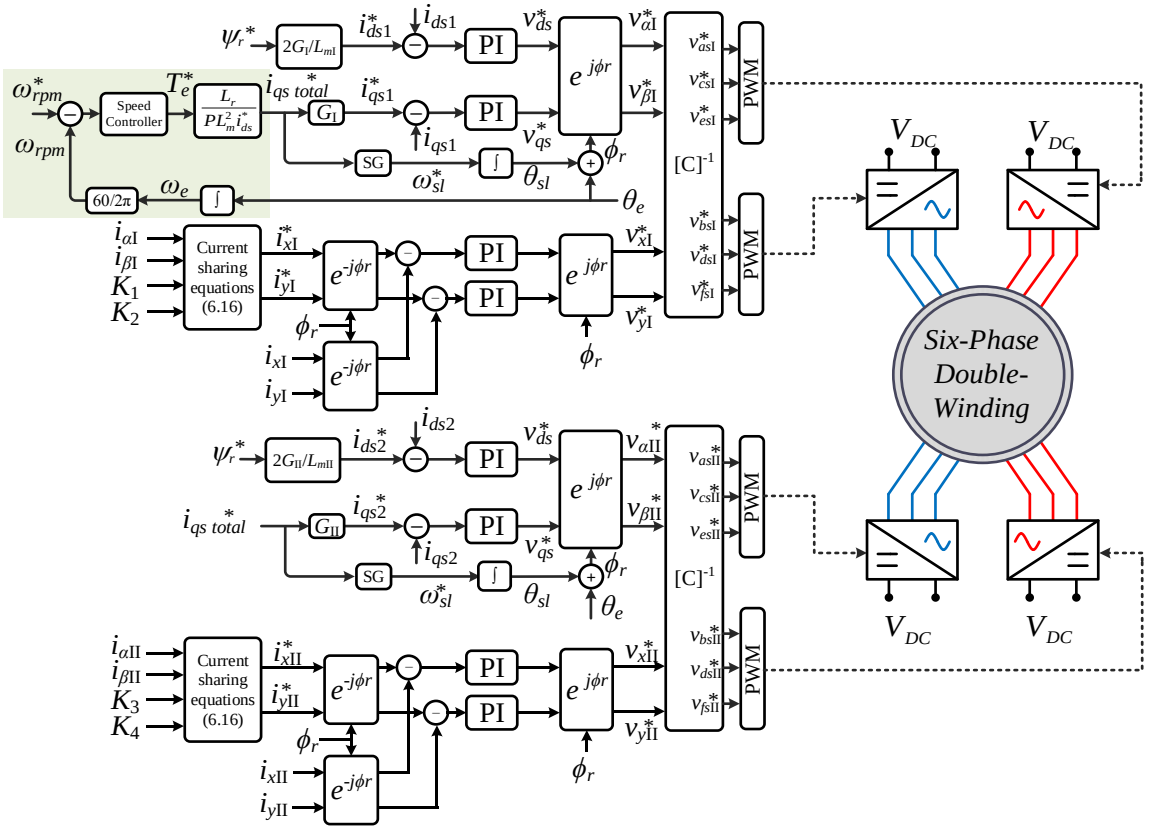

Fig. 6.3: IRFOC schematic with power sharing strategy for the double-winding six-phase induction machine.

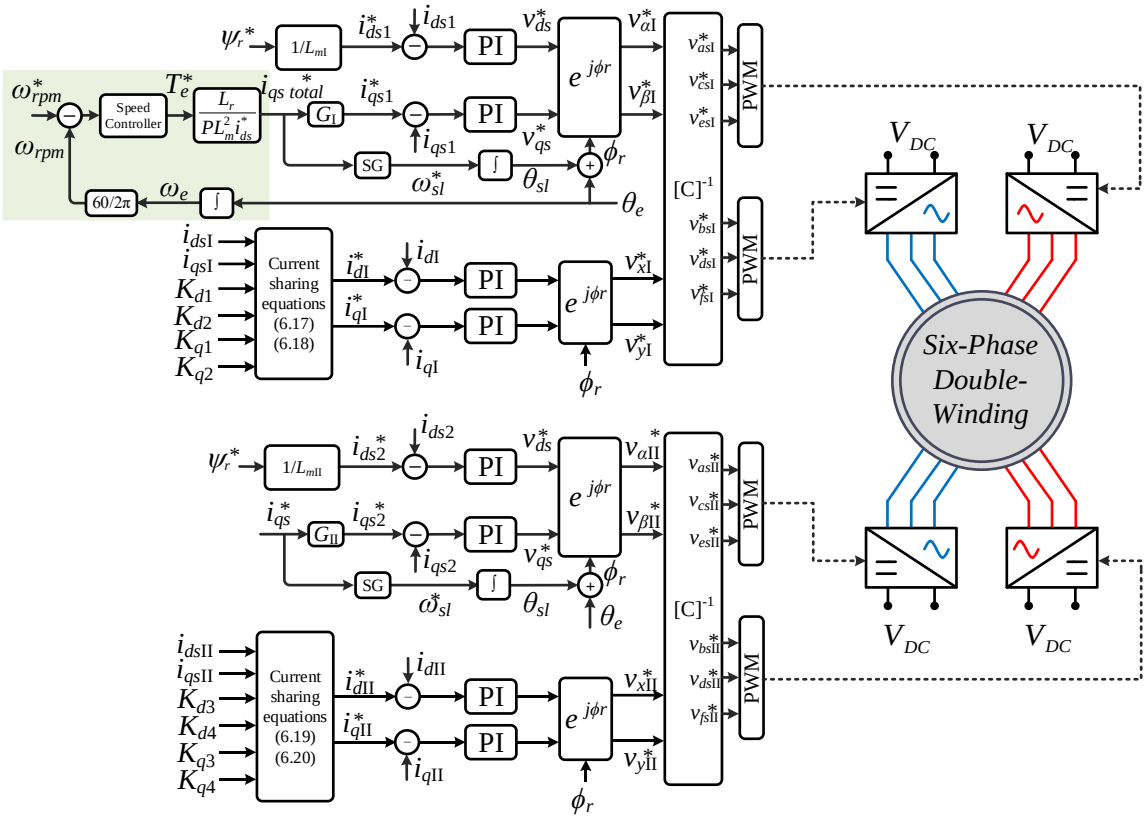

Fig. 6.4: IRFOC with efficient power sharing schematic for the double-winding six-phase induction machine.

two, per sub-motor. The power sharing equations, given by (6.10) and in complex form by (6.16), are changed to accommodate flux and torque producing currents for each individual winding set separately. The sharing coefficients are applied on *d* and *q* current components because sharing them in the stationary reference frame, with different sharing coefficients, would lead to asymmetry between the winding set currents themselves. The common sharing coefficients K_i are split into *d* and *q* axis coefficients K_{di} and K_{qi}. After doing so, it becomes:

$$i_{x\mathrm{I}} = \frac{1}{\sqrt{2}}\left(K_{d1} - K_{d2}\right) i_{ds\mathrm{I}} \tag{6.17}$$

$$i_{y\mathrm{I}} = \frac{1}{\sqrt{2}}\left(-K_{q1} + K_{q2}\right) i_{qs\mathrm{I}} \tag{6.18}$$

$$i_{x\mathrm{II}} = \frac{1}{\sqrt{2}}\left(K_{d3} - K_{d4}\right) i_{ds\mathrm{II}} \tag{6.19}$$

$$i_{y\mathrm{II}} = \frac{1}{\sqrt{2}}\left(-K_{q3} + K_{q4}\right) i_{qs\mathrm{II}} \tag{6.20}$$

The sharing coefficients illustrated in Fig. 6.4 should be shared according to the following equations:

$$\left|K_{d1}+K_{d2}\right|=1 \quad , \quad \left|K_{d3}+K_{d4}\right|=1 \tag{6.21}$$

$$K_{q1}+K_{q2}=1 \quad , \quad K_{q3}+K_{q4}=1 \tag{6.22}$$

More efficient power sharing strategy and multidirectional power flow control for each winding set can be obtained using this scheme. Both power sharing schemes are validated using Matlab/Simulink in the following section.

6.5 SIMULATION RESULTS

The proposed six-phase induction machine control strategies are validated using Matlab/Simulink. The parameters of the simulated double six-phase induction machine are presented in Table 6.1. Note that the parameters are given per sub-motor. The simulation results are illustrated in Fig. 6.5 through Fig. 6.8. The double six-phase machine is modelled and simulated as a twelve-phase machine in terms of phase variables considering all flux linkages between the windings. Hence, the phase shift between the consecutive phases in the phase variables model is: 0°, 0°, 60°, 60°, 120°, 120°, etc. This is done so because such a machine cannot be modelled (or controlled) by using a single decoupling transformation for a double-winding machine. The required transformation matrix would be of 12×12 size and would not be invertible. Also due to this fact, the machine is controlled as a summation of the two sub-motors i.e. as a double vector control, rather than as a single twelve-phase machine. The leakage flux (i.e. inductance) between the double six-phase sub-motors was considered in the simulation model.

The proposed multidirectional power flow control schemes illustrated in Fig. 6.3 and Fig. 6.4 are validated respectively. Initially, the first control scheme illustrated in Fig. 6.3, where the power sharing is done using the same coefficients for the flux and torque producing currents, is validated using Matlab/Simulink. The simulation results are shown in Fig. 6.5 and Fig. 6.6. Afterwards, the efficient power sharing scheme illustrated in Fig. 6.5, where the torque producing currents are shared in a different way than the flux producing currents, is validated with the same machine model. The simulation results of the efficient power sharing scheme are illustrated in Fig. 6.7 and Fig. 6.8.

In Fig. 6.5, initially the double six-phase machine is magnetised for 1 sec (not shown in the figure). After that the machine's speed reference is set to 99.5 rad/sec (1000 rpm) with T_l = 0 Nm. Once the machine reached the reference speed, it was loaded with 4 Nm at t = 1.8 sec, as can be seen from the top-right subplot of Fig. 6.5. Through this period, the power sharing coefficients of the sub-motors G_{I} and G_{II} are both equal, and kept at 0.5 till t = 2.5 sec. In the period, from 2.0 sec – 2.5 sec, the power

Table 6.1: VSI's and six-phase symmetrical sub-motor's parameters.

P_{rated}	1.1 kW	P	3 (pair)
$f_{switching}$	10 kHz	$R_{r,\,total}$	1.8 Ω
$L_{ls\,\mathrm{I,\,II}}$	8.1 mH	$R_{s\,\mathrm{I,\,II}}$	3.6 Ω
$L_{lr,\,total}$	11.5 mH	$M_{\mathrm{I,\,II}}$	68.33 mH
V_{DC}	400 V	$L_{m\,\mathrm{I,\,II}}$	205 mH

flow control within each sub-motor (but not between the sets belonging to different sub-motors) is validated first. The power transfer from the first to the second winding set of each sub-motor is performed by changing the current sharing coefficients of the winding sets ($K_{1,2}$ and $K_{3,4}$), as shown in Fig. 6.6a (enlarged view of Fig. 6.5). From Fig. 6.6a one can see that the amplitude of each winding set, within each sub-motor, can be precisely controlled according to the selected values of current sharing coefficients K_i. Note that here all the sets are operating in the motoring mode. It can be seen from Fig. 6.6a that the *d-q* currents of the sub-motors are constant through this period. However, the auxiliary *x-y* currents change according to the current sharing coefficients and the corresponding current sharing equations (6.16). The last two subplots of Fig. 6.6a illustrate, the first current of each of four three-phase winding sets of the machine, and the input power of each winding set $P_{inS1,2,3,4}$. The subplot with stator current illustrates the ability of the scheme to control the currents' amplitude of each winding set separately while maintaining the same torque and speed of the double-winding machine using the double vector control approach. The illustrated results prove the validity of the current sharing for each sub-motor.

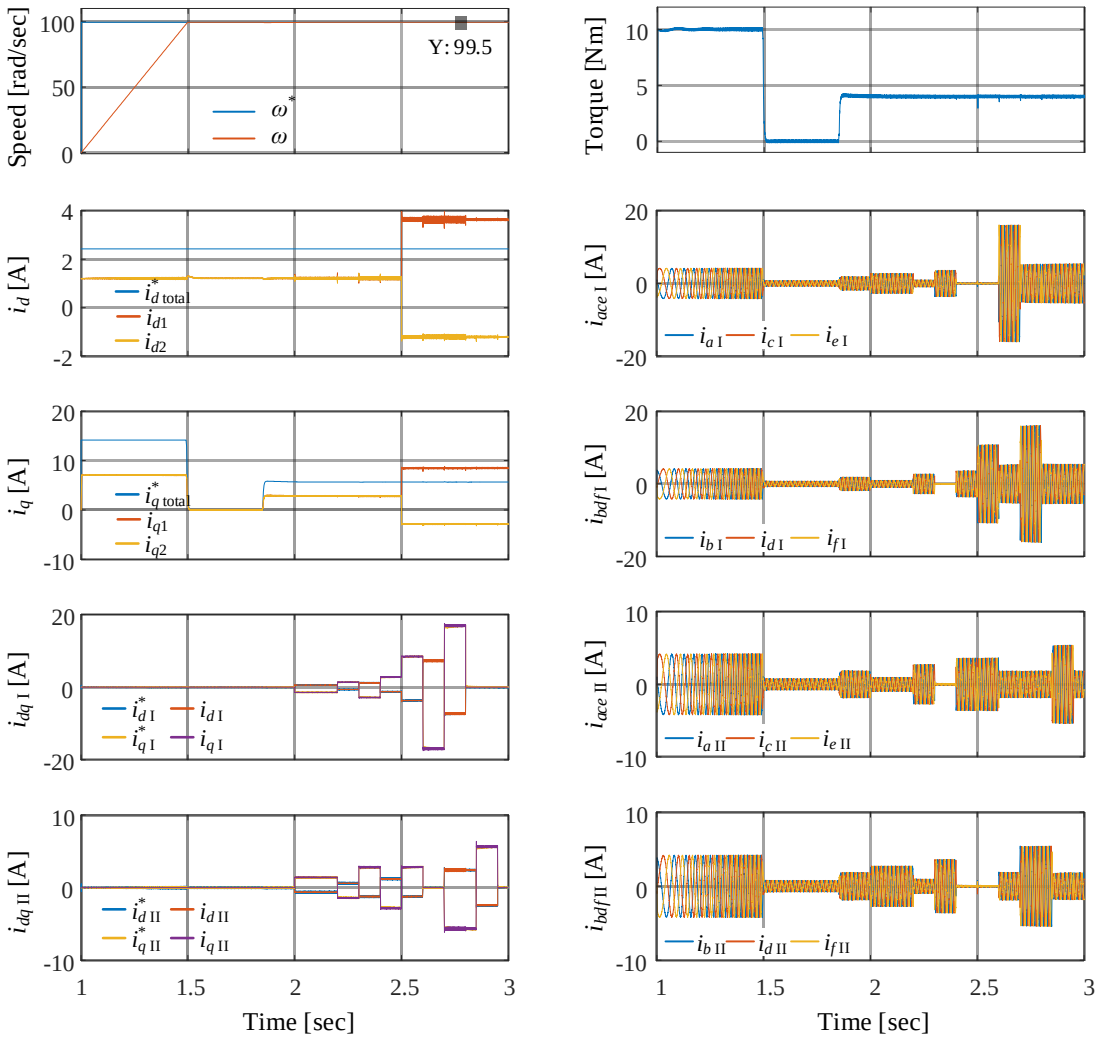

Fig. 6.5: Simulation results of multidirectional power sharing control for double-winding symmetrical six-phase induction machine.

However, the complete control algorithm should be able to transfer the power from the first to the second sub-motor and vice versa. Therefore, the power sharing coefficients G_{I} and G_{II} should be used as well. This mode of operation is shown between 2.5 sec and 3 sec, where the sub-motor coefficients G_{I} and G_{II} are set to 1.5 and –0.5, respectively. This scenario is shown in Fig. 6.6b (zoomed-in area of Fig. 6.5). The change of G_{I} and G_{II} coefficients is directly reflected in i_d and i_q subplots of Fig. 6.6b. Because G_{II} is set to a negative value, that means that during this period (from at 2.5 sec to 3 sec) the

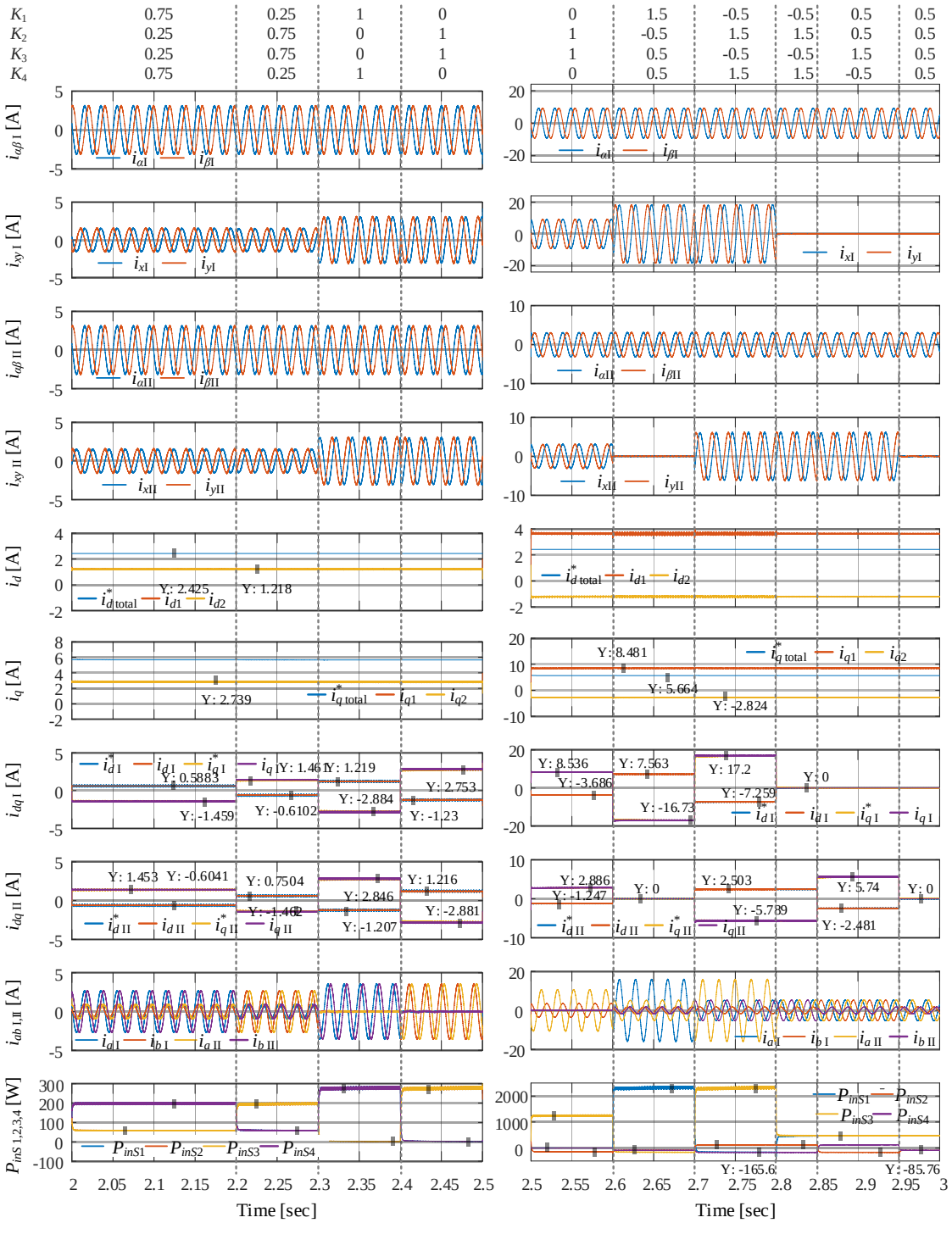

a) b)

Fig. 6.6: Zoomed section of Fig. 6.5 a) t = 2 sec – 2.5 sec, $G_{\mathrm{I}} = G_{\mathrm{II}}$ = 0.5; b) t = 2.5 sec – 3 sec, G_{I} = 1.5, G_{II} = –0.5.

second sub-motor has changed its power flow direction and operates in generation mode. This can be noticed from the last two subplots of the currents for the sub-motors $i_{abI,II}$ and from the input power of each winding set $P_{inS\ 1,2,3,4}$ shown in Fig. 6.6b. Hence, the first sub-motor works in motoring mode and the second works in generation mode. This can be utilised in directing the power to a specific storage unit depending on its state of charge (SOC). Also, note that the negative value of G_{II} does not mean all sub-windings of the second set must operate in generation mode. It also depends on values of K_i, as can be seen from the power subplot in Fig. 6.6b.

As mentioned earlier, during the power sharing operation the sharing should always be done with the torque producing currents only, rather than sharing both equally – flux and torque producing currents. In this way, the power sharing efficiency increases as established in Chapter 5. Fig. 6.7 and Fig. 6.8 illustrate the simulation results of the efficient power sharing scheme for a double-winding six-phase machine using the control algorithm from Fig. 6.4. The scheme is utilising torque producing currents

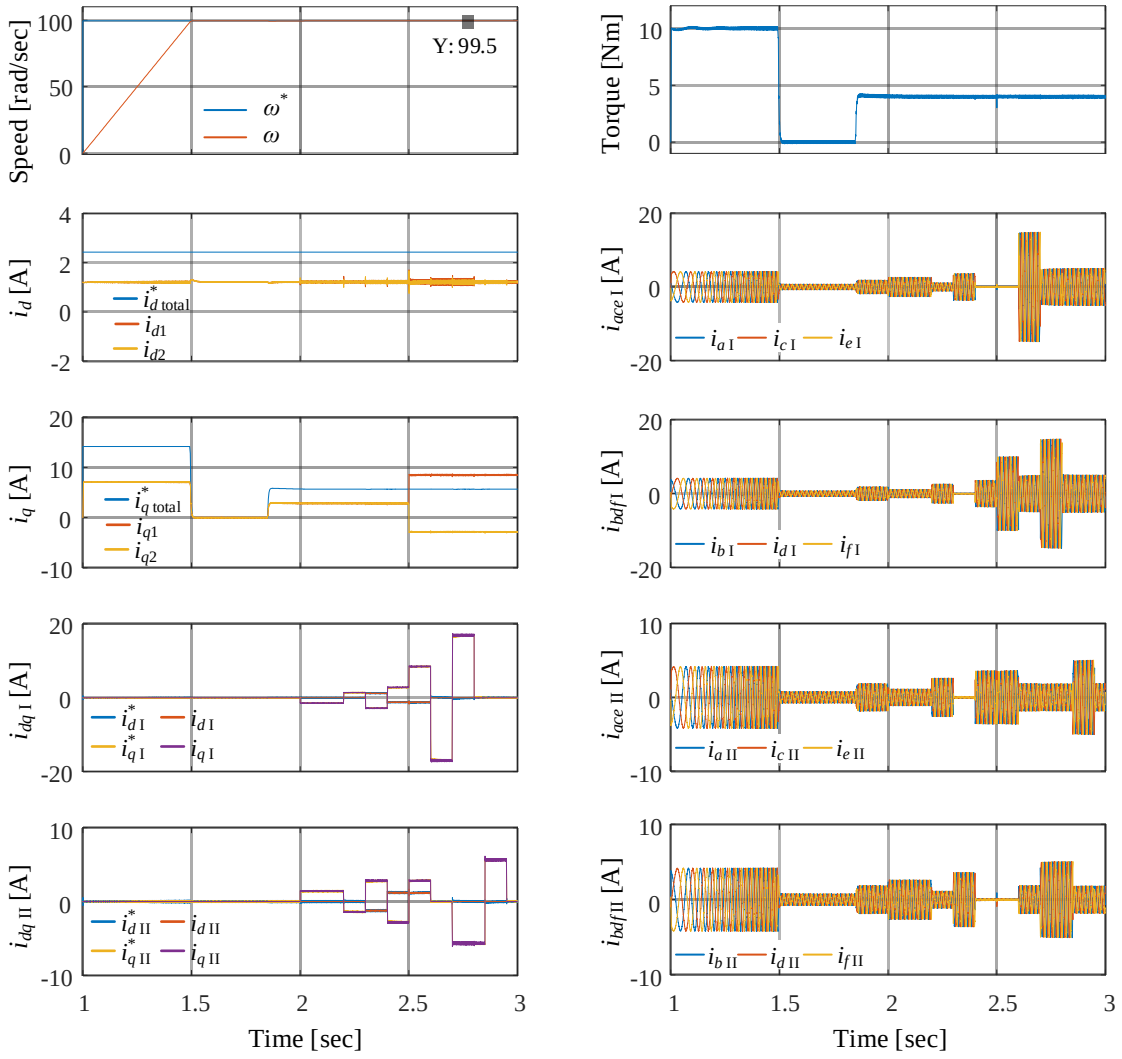

Fig. 6.7: Simulation results of efficient power sharing control for double-winding symmetrical six-phase induction machine.

only to control the power flow of the winding sets while maintaining the flux producing currents, as obvious from i_d and i_q subplots illustrated in Fig. 6.7. The *d*-axis current sharing coefficients are all constant and equal to each other ($K_{d1,2,3,4} = 1/2$). However, note that during the post-fault operation (shutting down of winding sets), the $i_{xI,II}$ currents of the sub-motors (which consist of pure K_{di} coefficients) are changed to maintain the K_d coefficients summation according to (6.21).

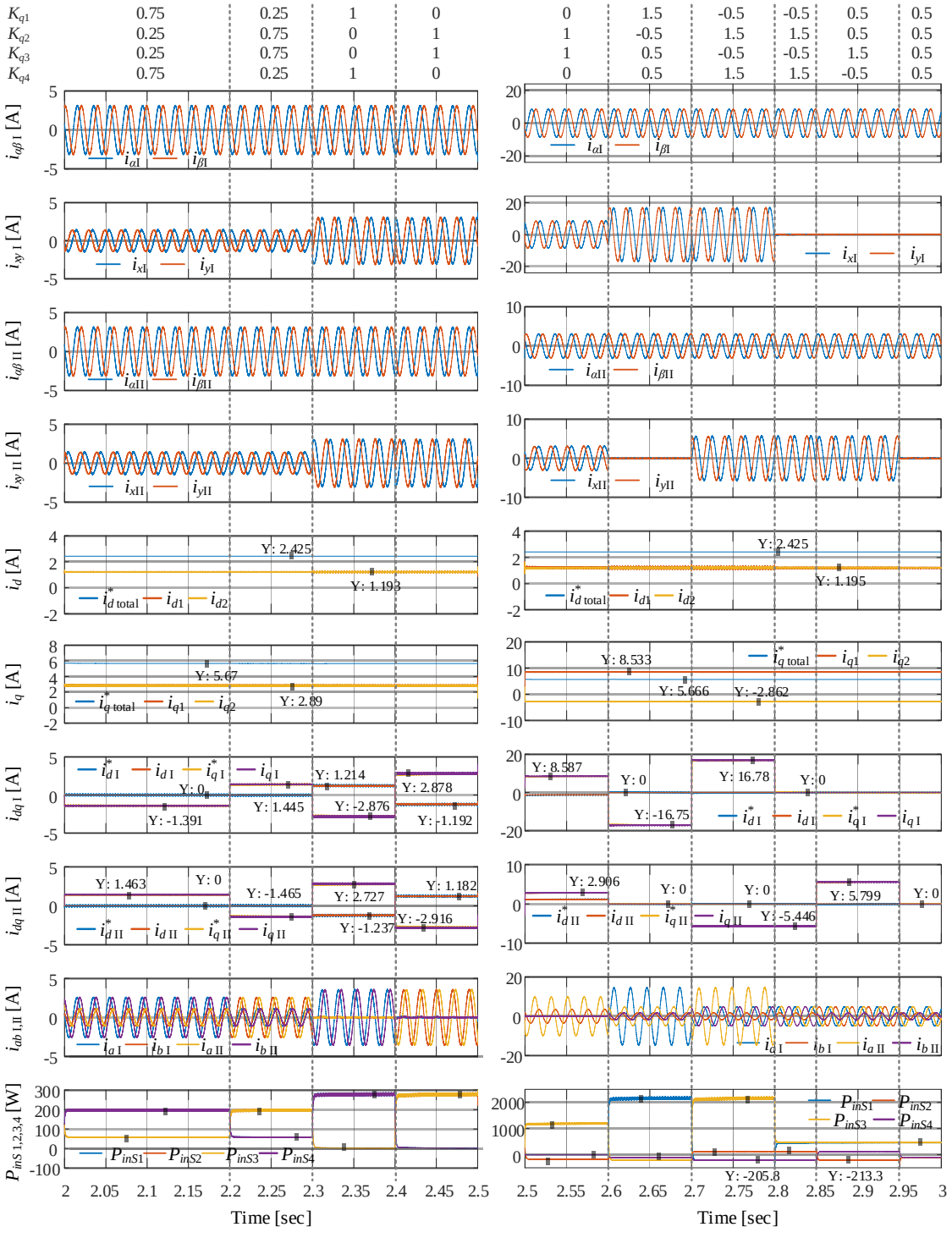

Fig. 6.8: Zoomed section of Fig. 6.7 a) t = 2 sec – 2.5 sec, $G_I = G_{II} = 0.5$; b) t = 2.5 sec – 3 sec, $G_I = 1.5$, $G_{II} = –0.5$.

Table 6.2: Average input power of each winding set for power sharing and efficient power sharing schemes.

Time Duration [sec.]	Power Sharing [W]					Efficient Power Sharing [W]				
	P_{inS1}	P_{inS2}	P_{inS3}	P_{inS4}	η	P_{inS1}	P_{inS2}	P_{inS3}	P_{inS4}	η
2.50 – 2.60	0	1250	-144	0	19.20%	0	1190	-169.5	0	24.56%
2.60 – 2.70	2330	-162	-90	-90	18.68%	2160	-208	-102	-102	24.82%
2.70 – 2.80	-165	2330	122	-165	16.90%	-210	2160	122	-210	23.57%
2.80 – 2.85	475	475	122	-165	28.84%	465	465	122	-210	38.04%
2.85 – 2.95	475	475	-165	122	28.84%	465	465	-210	122	38.04%

The same scenarios as in Fig. 6.5 and Fig. 6.6 are simulated in Fig. 6.7 and Fig. 6.8. Although a small difference appears in the input power consumed by each winding set (compare Fig. 6.6 and Fig. 6.8 bottom subplots), different current amplitudes are obtained during current sharing between the winding sets of each sub-motor. By comparing the results of power sharing illustrated in Fig. 6.6b and the efficient power sharing from Fig. 6.8b, it is evident from the last subplot of both figures that the efficient power sharing algorithm transfers the energy with better efficiency. For example, during the period between 2.50 sec – 2.60 sec one winding set of each motor is operating only. By observing this period in Fig. 6.8b, one can see that the input power of the motoring winding set is 1190 W, while the input power of the other winding set is operating in generation mode (and belonging to the second sub-motor) is –169.5 W. Comparing the same scenario with power sharing from Fig. 6.6b, one can see that the input power of the motoring winding set is 1250 W while the input power of the winding set in generation mode is –144 W. Note that in both scenarios the output power on the shaft is the same. Therefore, the efficiency of the power transfer is higher when using the efficient power sharing method.

The input power of each winding set is illustrated in Table 6.2. The efficiency of power transfer is calculated and shown in the table. Note that this is not the efficiency of the electro-mechanical conversion. The efficiency is calculated as the ratio of the total generated power ($\sum P_{inS\ Generation}$) over the additional input power that is needed compared to the regime when power sharing is not used, and for the same output speed and torque ($\sum P_{inS\ Motoring} - P_{inS\ Q}$). The input power when no power sharing is applied (e.g. during the period between 1.9 sec to 2 sec) is 125.44 W per set, hence $\sum P_{inS\ Q}$ = 501.6 W. The formula used is:

$$\eta = \frac{\left|\sum P_{inS\ Generation}\right|}{\sum P_{inS\ Motoring} - \sum P_{inS\ Q}} \cdot 100 \tag{6.23}$$

From the results obtained in Table 6.2 one can see that the efficiency of the power transfer itself is quite low. However, note that the cases shown are quite extreme (e.g. two sets completely off, or one set running in motoring mode, providing the mechanical power on the shaft and charging the other three-sets). Finally, it can be noticed from the results that the efficient power sharing is indeed more efficient in transferring the energy from one winding set to another.

Moreover, the proposed power sharing schemes are capable of controlling the two sub-motor (double-winding) machines during the post-fault operating condition. It can be noticed that the schemes maintain a constant speed and torque even when some of the winding sets were switched off (current set to 0). However, an upper limit of the winding sets' currents should be set, to ensure that the currents do not exceed the rated current of the machine or of the power electronics converter.

6.6 SUMMARY

In this chapter, two novel control schemes have been developed for the double-winding multiple three-phase induction machines. The ability to control the power flow direction of each winding set separately and the energy transfer from one sub-machine (winding layer) to another one is the main purpose of the developed control schemes. The schemes are utilising the *x-y* currents of the multiple three-phase machine to control the power flow direction and amount within each sub-motor, while it is utilising the multiple vector approach to control the power flow from one sub-machine to the other. The proposed schemes are validated through Matlab/Simulink with different operating scenarios. The simulation results illustrate the control scheme's capability to control the power flow direction and amount within each sub-motor or from one sub-motor to another while maintaining the same torque and speed. However, the efficiency of the machine can be improved by using the efficient power sharing scheme where the sharing of the power is done utilising the torque producing currents rather than flux and torque producing currents. Furthermore, the control schemes can be utilised to operate the double-winding machine during the post-fault operation.

CHAPTER 7

REGENERATIVE TEST FOR MULTIPLE THREE-PHASE MACHINES

7.1 INTRODUCTION

In this chapter, two novel regenerative test approaches for multiple three-phase machines have been introduced. The first one is utilising the current sharing strategy and it is applicable to all multiple three-phase machines. The second approach is utilising a unique *y*-current component to perform the regenerative test; however, this approach is only applicable to multiple three-phase machines with an even number of neutral points. The regenerative test can be utilised to find the efficiency and the temperature rise of the synchronous machines. Nevertheless, it can be used to separate constant and variable losses of the induction machine with an even number of neutral points. Although the scheme is applicable to synchronous and induction machines equally, simulation and experimental results are provided for induction machines only.

This chapter is organised as follows. In Section 7.2 a general background about the full-load test and the temperature rise test for three-phase machines has been introduced. This test is utilised to obtain the efficiency and the temperature rise of the machine under different operating points including nominal condition. Next, in section 7.3 the regenerative test utilising the multiple vector control (MS) approach is revisited for multiple three-phase machines. The approach is utilising different control variables for each winding set to operate the machine under nominal conditions. Then, the regenerative test utilising the current sharing strategy and power sharing strategy introduced in Chapter 3 and Chapter 5 is introduced in section 7.4. Afterwards, the regenerative test utilising a unique *y*-component current for multiple three-phase machines with an even number of neutral points is presented in section 7.5. In section 7.6, the regenerative test utilising multiple vector control and regenerative test based on current sharing and power sharing strategy plus the regenerative test utilising the unique *y*-current component for multiple three-phase machine with even number of neutral points is validated through simulation results. In order to validate the developed regenerative test schemes experimentally, six- and nine-phase induction machines are utilised and the experimental results are shown in section 7.7. Finally, the summary of the chapter is made in section 7.8.

Original contributions of this Chapter have been published in two conference [Abduallah et al. (2018a)] and [Abduallah et al. (2018b)] (presented at IEEE PEMC 2018, Budapest, Hungry and IEEE IECON 2018, Washington DC, USA, respectively) and one journal paper [Abduallah et al. (2019)] (published in the IEEE Transactions on Industrial Electronics journal).

7.2 FULL-LOAD AND TEMPERATURE RISE TEST

In order to develop high-power electric machines, lots of tests are required to validate their design and usability. The full-load test is one of the most important tests. During this test the machine's efficiency and performance are tested. Also, the temperature rise curve of the machine is obtained using this test. To perform the full-load test on the developed machine, another machine with the same (or higher) power ratings needs to be mechanically coupled to the developed machine. In this way a back-to-back configuration is formed. In the back-to-back configuration the dc-links of the machine's converters are connected to each other. This allows circulation of the power between the machines and hence reduces the power taken from the grid (dc-link) to perform the test. However, this test is costly and requires additional resources to couple the machines' shafts together [Trout (1935), Tada et al. (2017)]. Therefore, alternative approaches to conduct the full-load test have been suggested in the literature. These methods perform the full-load test without the need to couple the tested machine with another one. Some examples are: two-frequency method [Meyer and Lorenzen (1979)], phantom loading [Fong (1972)] and inverter driven method [Sheng and Grantham (1994), Soltani et al. (2002)]. The temperature rise curve of the developed machine obtained during these tests is equivalent to the one obtained using full-load test in the back-to-back configuration [Ho and Fu (2001)]. As mentioned earlier, the back-to-back configuration illustrated in Fig. 7.1 can recirculate the power while alternative methods cannot. Therefore, high power losses will occur using these methods.

In order to eliminate the need for mechanical coupling and to reduce the high power losses during the full-load test, a different regenerative test approach for the interior permanent magnet synchronous machines has been suggested in [Luise et al. (2012a), Luise et al. (2012b)]. In this method the power is circulated between the different sections of the machine. The analysed machine had four three-phase sections. The opposite sections were connected in parallel to the same three-phase converter. Hence, two converters were used. During this test the machine was actually loaded by itself. This was done by

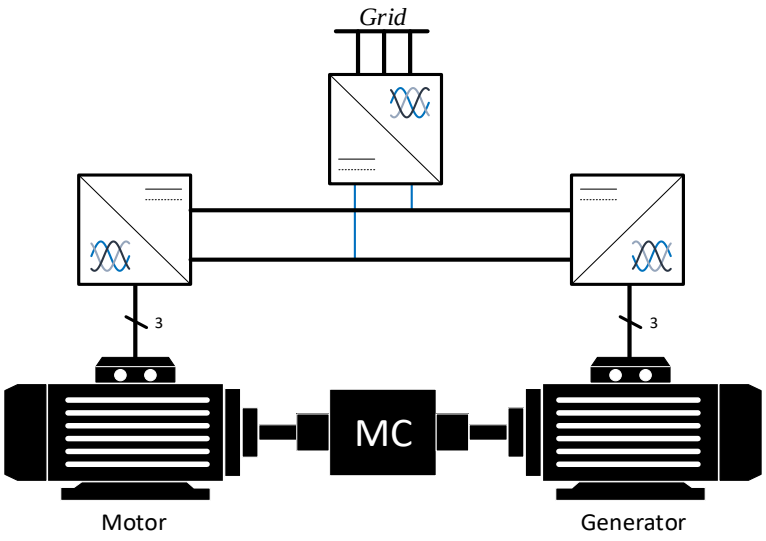

Fig. 7.1: Full-load back-to-back configuration.

setting one converter to operate in generation (the torque was set as the control variable) while the other converter was set to operate in motoring mode (the speed was set as the control variable). The applied control scheme can be considered as a multiple vector control.

In [Luise et al. (2012a), Luise et al. (2012b)] the considered machine's sections were completely decoupled due to the machine construction which significantly simplified the control algorithm. The same control approach has been used in [Zabaleta et al. (2018)] where a six-phase permanent magnet machine, with zero phase-shift between the dual three-phase winding sets, was considered. The control scheme in [Zabaleta et al. (2018)] is much more involved as the winding is distributed and the full coupling compensation is required. Therefore, the control algorithm implements additional cross-coupling decoupling among the double-winding three-phase winding sets.

In this chapter, three approaches to implement the regenerative test for multiple three-phase machines are presented. The approaches can be used for temperature rise and efficiency evaluation of synchronous machines and to segregate the losses of induction machines. The second and third approach are further greatly improved by using VSD instead of the MS approach, leading to a lower number of current controllers in the third approach compared to the MS and VSD utilising power sharing schemes (under ideal conditions). The third approach is based on IRFOC and is implemented by utilising a unique *y*-current component of the VSD matrix. However, this approach is only applicable to multiple three-phase machines with an even number of neutral points, such as six-, twelve- and eighteen-phase machines with symmetrical and asymmetrical configuration.

7.3 REGENERATIVE TEST USING MS APPROACH

The regenerative test can be used for testing the machine's full load capabilities. In this way the efficiency and the thermal design can be verified. One possible method for performing this test, without the need for coupling another machine to the tested machine, is presented in [Luise et al. (2012a), Luise et al. (2012b)]. The tested machine is a 780 kW, 14 rpm interior permanent-magnet (IPM), three-phase, 136-pole machine. The machine is split by its construction into four sections, where each section forms a three-phase machine. The specific construction of the machine makes those sections magnetically mutually decoupled. However, the method is also easily applicable to any other machine with multiple three-phase sections, but, if coupling is present, control becomes much more involved.

For testing this machine, two three-phase sections, which are opposite to each other (S_1–S_3 and S_2–S_4) are connected in parallel to one of the two converters (see Fig. 7.2). The first set-pair S_1–S_3 operates in motoring, while the second one S_2–S_4 is in generation mode. The set-pairs are controlled in speed and torque mode, respectively. Converter's motoring current i_m is halved between sections S_1 and S_3, while generated current i_g is equally contributed by S_2 and S_4. The control scheme used is sensorless four-quadrant FOC. The machine is accelerated using the first set-pair operating in the speed mode, and once it has accelerated and reached the steady state the rated (negative) torque is applied to the second

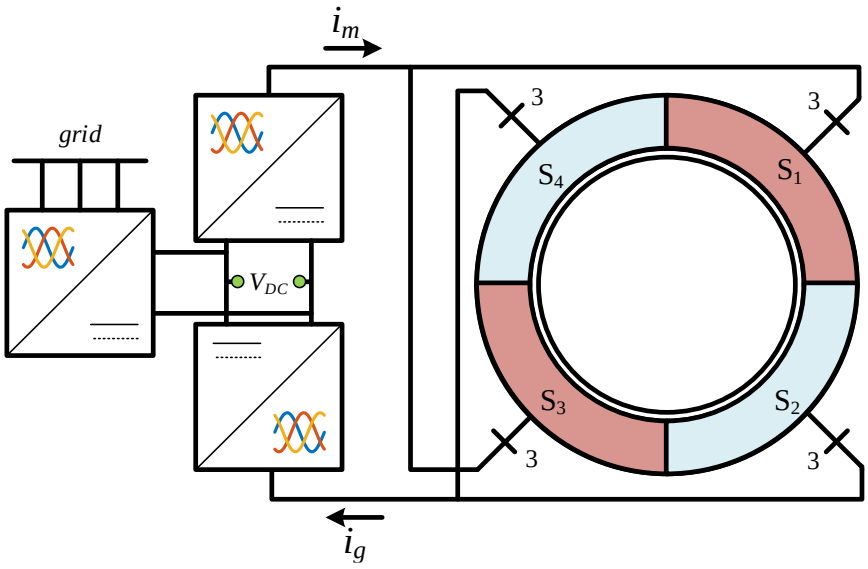

Fig. 7.2: Regenerative test layout of a machine with divided windings using MS approach.

set-pair. The generation torque and the motoring torque cancel each other within the machine itself. During the test, the phase flux-linkage is also controlled in order to obtain the same voltage fundamental for all four sections (two motoring and two generation sections).

Note that both converters share the same dc-link. Therefore, the power taken by S_1 and S_3 is re-circulated again by S_2 and S_4. The only losses present in the system during the test are the converters' and the machine losses (copper, core and friction losses). These power losses are compensated by the power taken from the grid in order to keep the machine running during the test, see Fig. 7.2.

The two main methods for multiple-three phase machine modelling are MS and VSD (multi-stator and vector space decomposition) approaches. Both methods are suitable for vector control operation. In the previous works [Luise et al. (2012b), Luise et al. (2012a), Zabaleta et al. (2018)], related to PM machines, the MS approach was used, while here VSD will be employed. In order to introduce and explain the newly developed regenerative test, these two modelling approaches and the correlations between them, derived in previous chapters, are needed. The correlation between the two approaches represents the starting point for formulation of the regenerative test.

One way to implement the regenerative test for these machines is by using the control based on the multiple *d-q* (i.e. MS) approach. This technique can be applied to any multiphase machine with multiple three-phase winding sets. The MS approach for machine modelling has been introduced in [Nelson and Krause (1974)] for an asymmetrical six-phase induction machine. By using this approach each three-phase winding set can be considered as a separate three-phase machine with different flux and torque current component current controllers (*d* and *q* currents); hence, it is also called the multi-stator (MS) approach. In [Hu et al. (2018)], the authors utilised the MS approach to control the power flow among different energy sources for a dual six-phase PMSM.

As the same number of sets should operate in the motoring and generation mode, the regenerative test can be easily implemented in the machines with an even number of winding sets, i.e. neutral points. Therefore, the machines considered in this chapter are six-, twelve-, eighteen-, etc., phase machines in symmetrical or asymmetrical configuration. However, another approach to apply the regenerative test for multiple three-phase machines with an odd number of neutral points will be discussed later. The regenerative test using the MS approach can be applied using the following steps:

1. For one half of the winding sets FOC scheme has the speed of the machine as the control variable, while the other sets are operated in the torque control mode.
2. During the start-up of the machine, all winding sets are controlled in the speed mode.
3. After reaching the desired speed and establishing a steady-state operating point, half of the winding sets are switched to the torque control mode.
4. The torque reference for these sets is set to a negative value. The total torque reference provided to the generation sets should be set to no more than one half of the rated torque of the machine.

By implementing the previous steps, half of the machine is set to the motoring mode and the other half is set to the generation mode. In other words, the machine is loaded using its own winding sets. For a six-phase machine, the equilibrium torque is expressed by the following equation:

$$T_{s1} - T_{s2} = T_{fw} \tag{7.1}$$

where T_{s1} and T_{s2} stand for the torque developed by the first and the second winding set, respectively, and T_{fw} stands for the friction and windage power losses. However, T_{fw} is usually very small and can be neglected. Thus, equation (7.1) can be rewritten as follows:

$$T_{s1} = -T_{s2} = T_{ag} \tag{7.2}$$

$$T_{s1} + T_{s3} = -\left(T_{s2} + T_{s4}\right) \tag{7.3}$$

where T_{ag} stands for the developed torque in the air-gap of the machine. For the twelve-phase machine, torque balancing equation can be written as follows:

$$T_{s1} = T_{s3} = -T_{s2} = -T_{s4} = T_{ag} \tag{7.4}$$

$$T_{s1} = -\left(T_{s2} + T_{s3}\right) \tag{7.5}$$

$$T_{s1} = -2T_{s2} = -2T_{s3} = T_{ag} \tag{7.6}$$

However, for nine-phase machine the torque equilibrium equation in the air-gap is not the same as for the six- and twelve-phase machines. The nine-phase machine torque equilibrium equation is as follows:

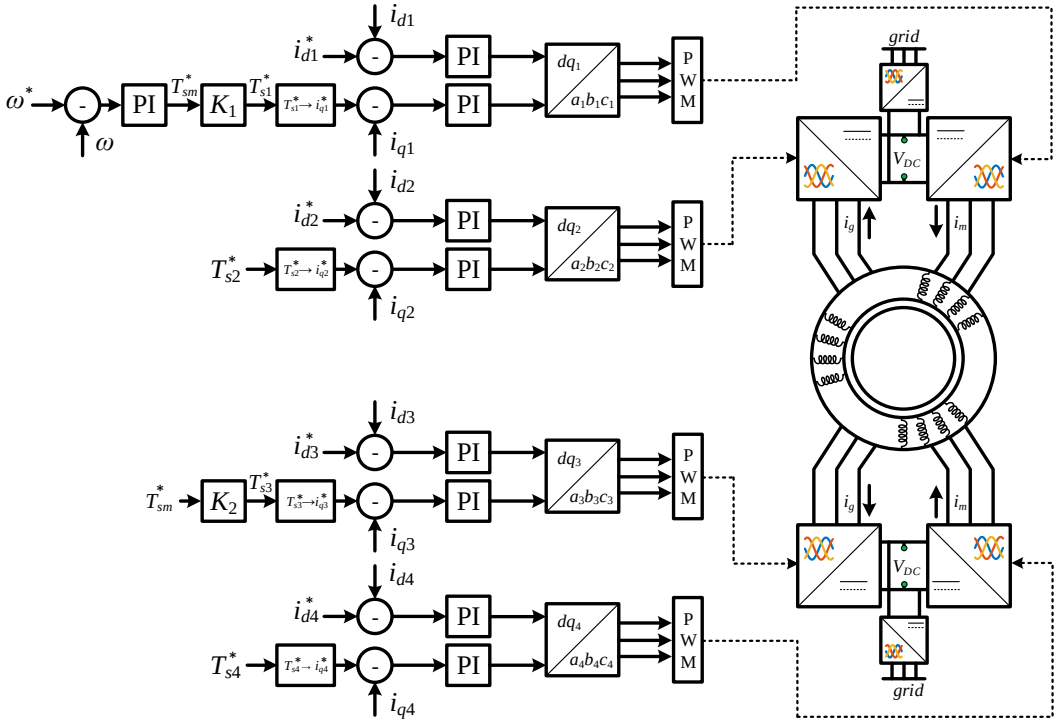

Fig. 7.3: Regenerative test scheme for twelve-phase machine using MS control scheme.

The schematic of the regenerative test for a twelve-phase machine using the MS control scheme is illustrated in Fig. 7.3. Torque balancing equation and MS control scheme are equally applicable to multiple three-phase machines with symmetrical and asymmetrical configuration. The only difference is in the Clarke's transformation that should be applied. Clarke's transformation for each winding set of a multiple three-phase machine is defined as in (3.85), where δ represents the spatial displacement of the winding set, with respect to the first winding set. If a symmetrical six-phase machine is taken as an example then, $\delta = 0$ for the first winding set and $\delta = 2\pi/6$ for the second winding set. However, for the asymmetrical six-phase machine, $\delta = \pi/6$ for the second winding set. Clarke's transformation presented in (3.85) can be utilised for a twelve-phase machine as well. For symmetrical configuration δ is equal to 0, $2\pi/12$, $4\pi/12$ and $6\pi/12$ for the first, second, third and fourth winding set, respectively. As far as the asymmetrical twelve-phase machine is concerned, δ is equal to 0, $\pi/12$, $2\pi/12$ and $3\pi/12$ for the first, second, third and fourth winding set, respectively.

7.4 Regenerative Test using Current Sharing Approach (VSD)

Controlling multiple three-phase machines using the MS approach is not trivial since there is a heavy coupling between the winding sets [Zabaleta et al. (2018)]. On the other hand, the VSD approach decouples a multiphase machine into $n/2$ subspaces. Moreover, there is only one flux/torque producing subspace (α-β subspace), instead of two (six-phase) or four (twelve-phase) when MS approach is used. Therefore, VSD is a preferable way for closed loop control of multiphase machines in general. The remaining subspaces (x-y subspaces) present in the VSD approach are the loss-producing subspaces. Theoretically, these subspaces do not need to be controlled, but in practice they are usually controlled

in order to eliminate any asymmetries of the machine or of the converter. Sometimes, the auxiliary *x-y* subspaces are also controlled to non-zero current values, to achieve post-fault operation of a multiphase machine.

Clarke's and VSD transformation matrices for symmetrical and asymmetrical machines with multiple isolated neutral points are obtainable from (3.87) and (4.36), respectively. The implementation of the regenerative test using VSD is possible utilising the auxiliary currents and the current sharing strategy shown in Chapter 3 and Chapter 4. The regenerative test schematic for a nine-phase induction machine is illustrated in Fig. 7.4. The configuration is equally applicable to symmetrical and asymmetrical nine-phase machines.

The aim of the test is to obtain the efficiency and the temperature rise curve of the machine. The temperature change is caused by the losses in the machine. Therefore, the machine should be run under the rated conditions in order to properly conduct the test. As discussed, the nine-phase machine has an odd number of winding sets. Therefore, the number of motoring winding sets cannot be equal to the number of generation winding sets. One has two options, either to divide the motoring power between two winding sets, or to use one winding set for motoring and another for generation while the third winding set is in no-load mode. The second option is chosen here. Therefore, the regenerative test can be applied using the following steps:

1. During the initial acceleration of the nine-phase machine, the auxiliary current control is off.
2. After the machine reached the reference speed, the synthetic loading test is started by applying T_l^* and the current sharing coefficients K_i.
3. The motoring, generation and no-load winding sets are exchanged periodically during the test by changing K_i.

The current sharing coefficients K_i are able to change the current's amplitude and direction. This happens when the coefficients are defined based on the electromechanical subspace's current α-β. However, in the implementation of the proposed regenerative test, the coefficients are defined based on $i_{\alpha\beta l}$ (see Fig. 7.4). Thus, the current sharing equations (3.106) and (3.107) can be rewritten as:

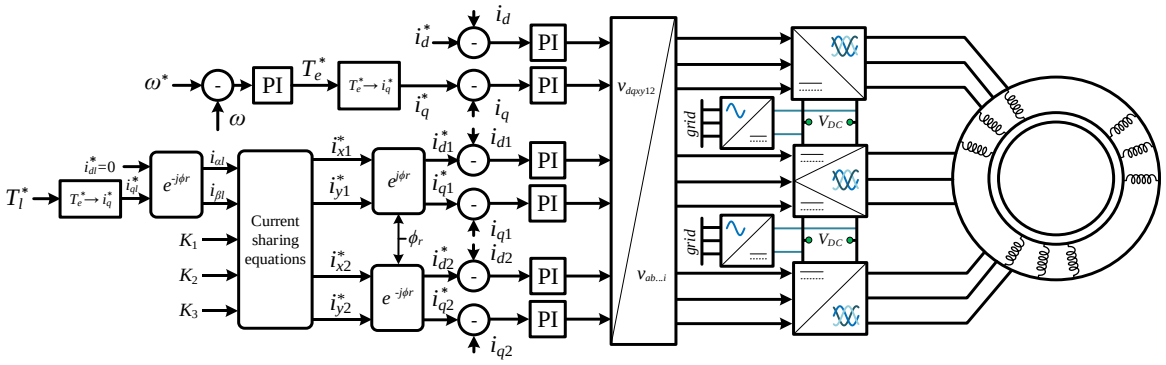

Fig. 7.4: Regenerative test schematic using IRFOC and VSD for (asymmetrical) nine-phase machine.

$$\bar{i}_{xy1} = \left(K_1 + K_2 e^{j\frac{2\pi}{3}} + K_3 e^{-j\frac{2\pi}{3}} \right) \hat{\bar{i}}^*_{\alpha\beta l} \tag{7.7}$$

$$\bar{i}_{xy2} = \left(K_1 + K_2 e^{j\frac{2\pi}{3}} + K_3 e^{-j\frac{2\pi}{3}} \right) \bar{i}_{\alpha\beta l} \tag{7.8}$$

By applying T_l^* and the appropriate sharing coefficients K_i, the temperature rise of the machine can be obtained.

7.5 REGENERATIVE TEST USING A UNIQUE Y-CURRENT COMPONENT

The links between the MS and VSD modelling approaches have been established first in [Tani et al. (2013)]. The *x*-*y* current components from VSD were used there to control the current amplitude of each winding set of a quadruple three-phase machine, i.e. for current sharing. In [Zoric et al. (2018)], the authors found the general correlations between the VSD and MS modelling approach for multiphase machines with multiple neutral points. These correlations express the *x*-*y* currents in terms of the winding set α_i-β_i currents. This provides the ability for the VSD approach to individually control the currents of each winding set through the control of *x*-*y* subspaces. For example, the correlation of the asymmetrical six-phase machine VSD and MS approach can be found by multiplying the inverse of (3.85) ($[C(\delta)]^{-1}$) for each winding set by the corresponding currents in the stationary reference frame (α_i-β_i-o_i). The result of the multiplication illustrates how the stationary reference frame currents (α_i-β_i-o_i) contribute to the phase currents. By multiplying the obtained correlations by [C_6], defined in (6.7) for the symmetrical six-phase machine, the product will define how the VSD currents are related to the individual winding set currents α_i-β_i-o_i. The final result for the highest (the *k*-th) *x*-*y* subspace is illustrated in the first row of Table 7.1. From Table 7.1, one can see that the *x*- and *y*-current components consist purely of either α_i or β_i components. It is interesting to note that repeating the same procedure for an asymmetrical six-phase machine will produce the same results as for the symmetrical six-phase machine in Table 7.1.

Table 7.1: MS and VSD equivalence for symmetrical and asymmetrical six-, twelve- and eighteen-phase machines (x_k-y_k subspace).

Six-phase	$i_x = \frac{1}{\sqrt{2}}\left(i_{\alpha 1} - i_{\alpha 2}\right)$
	$i_y = \frac{1}{\sqrt{2}}\left(-i_{\beta 1} + i_{\beta 2}\right)$
Twelve-phase	$i_{x3} = \frac{1}{2}\left(i_{\alpha 1} - i_{\alpha 2} + i_{\alpha 3} - i_{\alpha 4}\right)$
	$i_{y3} = \frac{1}{2}\left(-i_{\beta 1} + i_{\beta 2} - i_{\beta 3} + i_{\beta 4}\right)$
Eighteen-phase	$i_{x5} = \frac{1}{\sqrt{6}}\left(i_{\alpha 1} - i_{\alpha 2} + i_{\alpha 3} - i_{\alpha 4} + i_{\alpha 5} - i_{\alpha 6}\right)$
	$i_{y5} = \frac{1}{\sqrt{6}}\left(-i_{\beta 1} + i_{\beta 2} - i_{\beta 3} + i_{\beta 4} - i_{\beta 5} + i_{\beta 6}\right)$

The correlations between the MS and VSD approach for the twelve-phase machines can be found in the same way (second row in Table 7.1). The same can be repeated for the eighteen-phase machines with six neutral points and the results of the highest *x*-*y* subspace are included in the third row of Table 7.1. Once again, regardless of whether the twelve- or eighteen-phase machine is symmetrical or asymmetrical, the result is the same and is as given in Table 7.1.

One can notice from Table 7.1 that *y*-current component in the highest order subspace always consists of β_i currents only. Half of the β_i currents are subtracted from the sum of the other half. In case of six-phase machines this is clear from i_y component, for twelve- and eighteen-phase machines this can be seen from i_{y3} and i_{y5}, respectively. Looking back at the regenerative test and MS approach, the idea is to make half of the winding sets to have negative *q* current (generation) while the other sets should provide the same amount of positive *q* current (motoring). Note that, for IRFOC, rotating reference frame control is necessary, which requires use of *d*-*q* variables rather than *α*-*β*. In this way, half of the machine winding sets will load the other half.

The regenerative test can be applied to any multiple three-phase winding machine, with an even number of neutral points, by using IRFOC in *d*-*q* subspace and by controlling the last of the *y*-current components. The control schematic of a regenerative test for multiple three-phase winding machines with an even number of neutral points is illustrated in Fig. 7.5. The regenerative test can be implemented using the following steps:

1. During the initial acceleration, the machine is set to speed control mode, where *d* and *q* currents are regulated using PI controllers.
2. After the machine has reached the reference speed, the desired regenerative torque reference (T_{rg}^*) can be applied using the *y*-axes reference current, i_{yk}^* in the highest-order *x*-*y* subspace (see Fig. 7.5).
3. Half of the winding sets will be in generation mode (with negative $i_{\beta i}$), while the other half will be in motoring mode (with positive $i_{\beta i}$).

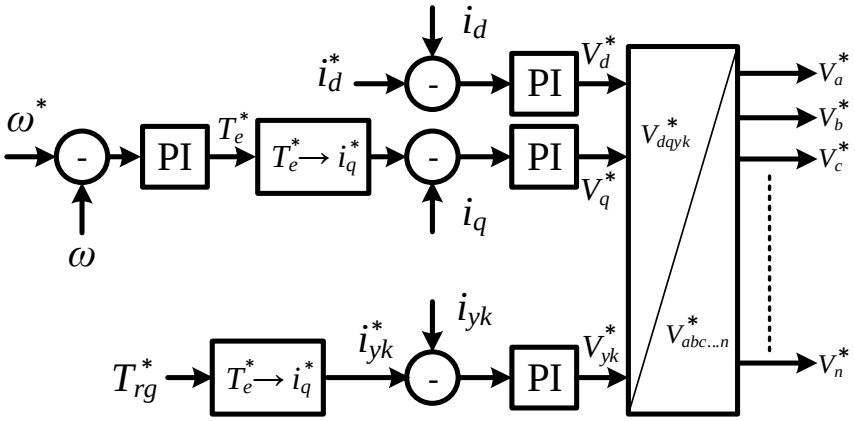

Fig. 7.5: Regenerative test control scheme for multiple three-phase winding machines with an even number of isolated neutral points.

The i_{yk}^{*} can be found from T_{rg}^{*} in the same way as the reference i_{q}^{*} is obtained from the torque reference T_{e}^{*} (output of the speed controller), as shown in Fig. 7.5. The other *x*-*y* subspace reference currents are set to zero. It should be noted that the Park's rotational transformation for *d*-*q* components is the standard one, leading to the synchronous reference frame; however, for the last x_k-y_k subspace the rotational transformation is implemented in such a way that the values are obtained in the anti-synchronous reference frame. Finally, one can see that the number of PI controllers is significantly reduced. For example, instead of using twelve PI current controllers to implement the regenerative test for eighteen-phase machines using the MS approach, only three PI current controllers are required to achieve the same result by utilising the proposed control scheme. Note that the reduction in the number of current controllers is valid in the ideal conditions only (no dead-time and no asymmetries in the machine), while in practice additional controllers are normally necessary.

7.6 SIMULATION RESULTS

No particular attention has been paid so far to the type of the multiphase machine under test. Indeed, the deliberations of sections 7.3 to section 7.5 are equally applicable to both synchronous and induction machines. The control schemes shown in section 7.3 and 7.4 are equally applicable to synchronous and induction machines with multiple neutral points. However, the control schematic illustrated in Fig. 7.5 is only applicable to multiple three-phase machines with even number of neutral points (i.e. six-, twelve- and eighteen-phase machines). The results in Table 7.1 are also universally valid, as is the control scheme of Fig. 7.5. However, the type of the machine leads to very important differences with regard to what can and what cannot be obtained from the regenerative test and this issue is addressed shortly.

Initially, the regenerative test is validated for a twelve-phase induction machine using the MS approach, as illustrated in Fig. 7.3, using Matlab/Simulink. The results are shown in Fig. 7.6. Afterward, the regenerative test using VSD and current sharing coefficients presented in section 7.4 is validated through simulation results using an asymmetrical nine-phase induction machine. Then, the regenerative test utilising the VSD and current sharing control is validated for the symmetrical nine-phase induction machine and the simulation results are illustrated in Fig. 7.7. Finally, the regenerative test utilising the approach based on VSD and IRFOC for multiple three-phase machines with an even number of neutral points is investigated for asymmetrical six- and twelve-phase induction machines through simulations in Matlab/Simulink and the results are illustrated in Fig. 7.8 and Fig. 7.9, respectively.

Simulation results of the regenerative test utilising the MS approach, illustrated in Fig. 7.3, for a symmetrical twelve-phase induction machine are illustrated in Fig. 7.6. The twelve-phase induction machine's parameters are illustrated in Table 7.2. Initially, the machine is magnetised for 0.2 sec. Then, the speed reference was set at 99.5 rad/sec (950 rpm) as shown by the first subplot of Fig. 7.6a. All winding sets were in motoring mode, which means the control variable was the output of the speed

Table 7.2: VSI's and six- and twelve-phase symmetrical/asymmetrical induction machine parameters.

f_{sw}	10 kHz	P	3 (pole-pairs)
L_{lr}	25.4 mH	R_r	11.55 Ω
L_{ls}	5.3 mH	R_s	13.75 Ω
L_m	593 mH	V_{dc}	320 V

controller (see Fig. 7.3) until the machine reaches steady state. Then, at t = 1.25 sec the regenerative test utilising the MS approach is implemented for different values of T_{rg} as shown above the zoomed simulation results of Fig. 7.6b. The reference regenerative torque was implemented as a sequence where the total torque is equal to 4 Nm, 8 Nm and 12 Nm. The regenerative torque implemented at each winding set of the generation winding sets is one quarter of the total torque of the machine for twelve-phase machines. However, the applied torque reference for the six-phase machine is half the total torque.

It can be noticed from the simulation results of the MS approach illustrated in Fig. 7.6 that controlling the multiple three-phase machine can be achieved easily and the regenerative test can be done easily by changing the control variables of the winding sets and the reference regenerative torque values of the winding sets. The validity of the approach can be comprehended from the last plot of the simulation results (P_{s1234}) illustrated in Fig. 7.6 where two of the winding sets input powers have positive values while the other two sets have a negative input power. The difference between the input powers of the winding sets in motoring and the ones in generation is equivalent to the stator copper losses of the machines. This is so due to the absence of the rotor currents and the neglecting of the core and friction losses in the simulation results. Therefore, the absence of the rotor currents leads to the absence of the rotor's copper losses which means the ability to use this approach to find the efficiency and verify the thermal design of the multiple three-phases is limited to synchronous machines where the rotor currents do not exist. However, the regenerative test can be utilised for multiple three-phase induction machines to separate the constant and varying losses as it will be discussed later on in this section.

The proposed regenerative test approach using IRFOC and VSD for nine-phase machines introduced in section 7.4 is validated through simulations in Matlab/Simulink. The control schematic illustrated in Fig. 7.4 is implemented for an asymmetrical nine-phase induction machine. The nine-phase machine parameters are shown in Table 3.1. Simulation results of the regenerative test for a nine-phase induction machine are illustrated in Fig. 7.7. Initially, the machine is magnetised for 1.5 sec. Afterwards, the machine speed reference is set to 157.1 (rad/sec). When the machine has reached steady state, the regenerative test is started (at t = 4 sec) by changing T_l^* from zero to 7 Nm. the regenerative test is applied by imposing the auxiliary currents according to (7.7) and (7.8). The sharing coefficients are defined as follows: K_i = 1 represents motoring winding set, K_i = –1 represents generation winding set and K_i = 0 represents no-load winding set. After applying T_l^*, the sharing coefficients K_i are altered between 1, 0 and –1. Each set is changing between motoring and no-load mode of operation (with trapezoidal change of K_i), staying in each mode for 0.1 sec. After repeating this ten times, i.e. after 2 sec

in total, the set goes to generation mode for another 1 sec. The sequence repeats in the way illustrated in the current waveforms in Fig. 7.7. Note that when the set is in no-load mode, $K_i = 0$, the current of the set is not zero but rather it is equal to the no-load current. This is because the coefficients K_i are sharing the regenerative torque and $\alpha\beta_l$ currents, rather than the real electromechanical torque and real $\alpha\beta$ currents.

When sets are operating with $K_i = 1$ and $K_i = -1$, the currents obtained correspond to the rated currents. From Fig. 7.7, one can note that the torque on the shaft, during the regenerative test process,

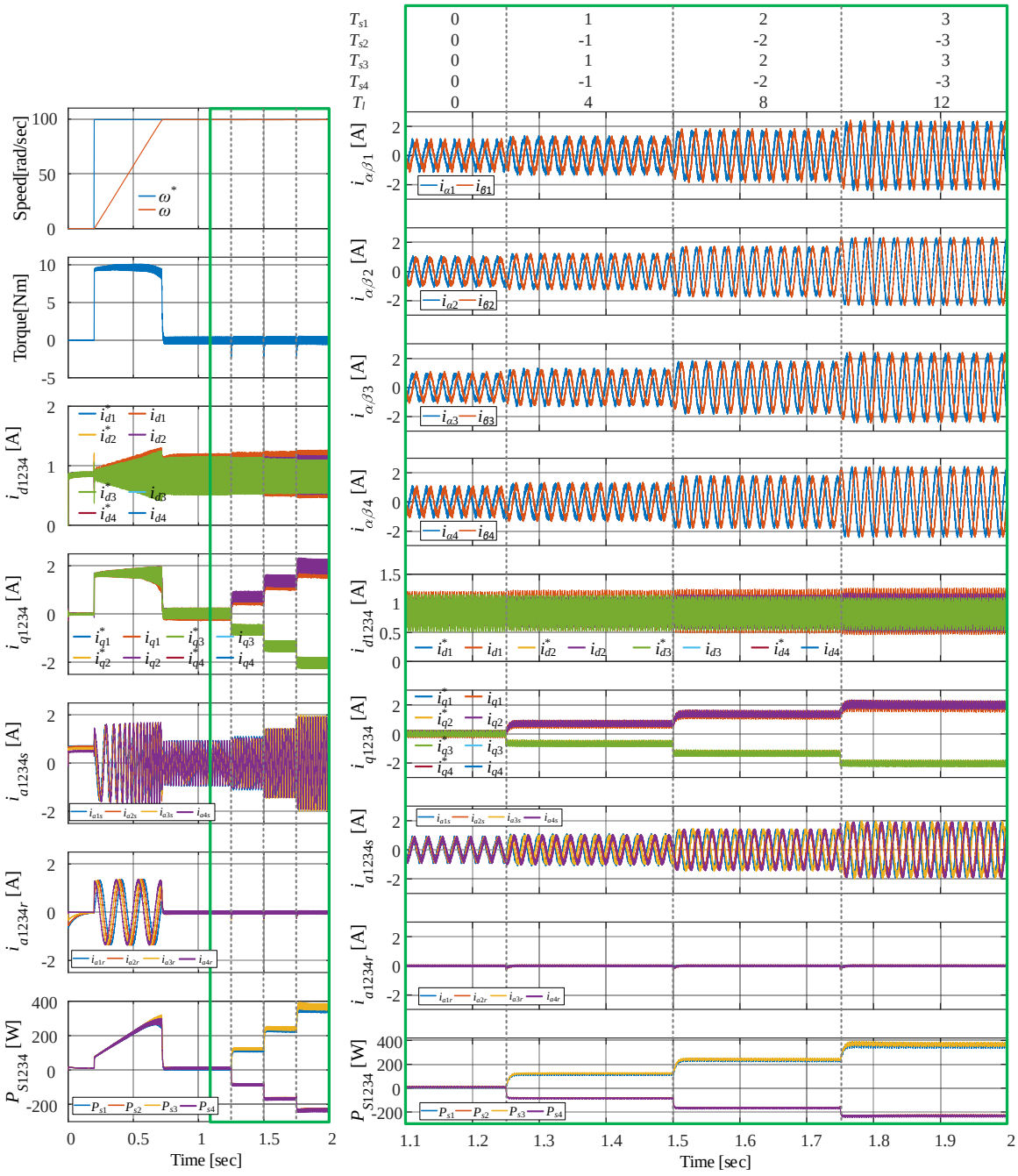

Fig. 7.6: Regenerative test simulation results for symmetrical twelve-phase induction machine using MS approach.
a) complete simulation, b) zoomed section between t = 1.1 sec – 2.0 sec.

remains stable at zero. The flux and the torque producing currents (i_d and i_q) are constant during the test. Note that, because there is no physical load on the shaft, $i_q = 0$.

The winding set input powers (P_{s123}) shown in Fig. 7.7 (bottom subplot) illustrate the ability of the test to re-circulate the power among the winding sets and to emulate the nominal conditions of the machine. The graph with the input power of the winding sets shows that the difference between the motoring and the generation winding set power is equivalent to the total copper losses of both winding sets. For example, looking at instant at $t = 4.175$ sec, the power consumed by the first set is $P_{s1} = 424$ W

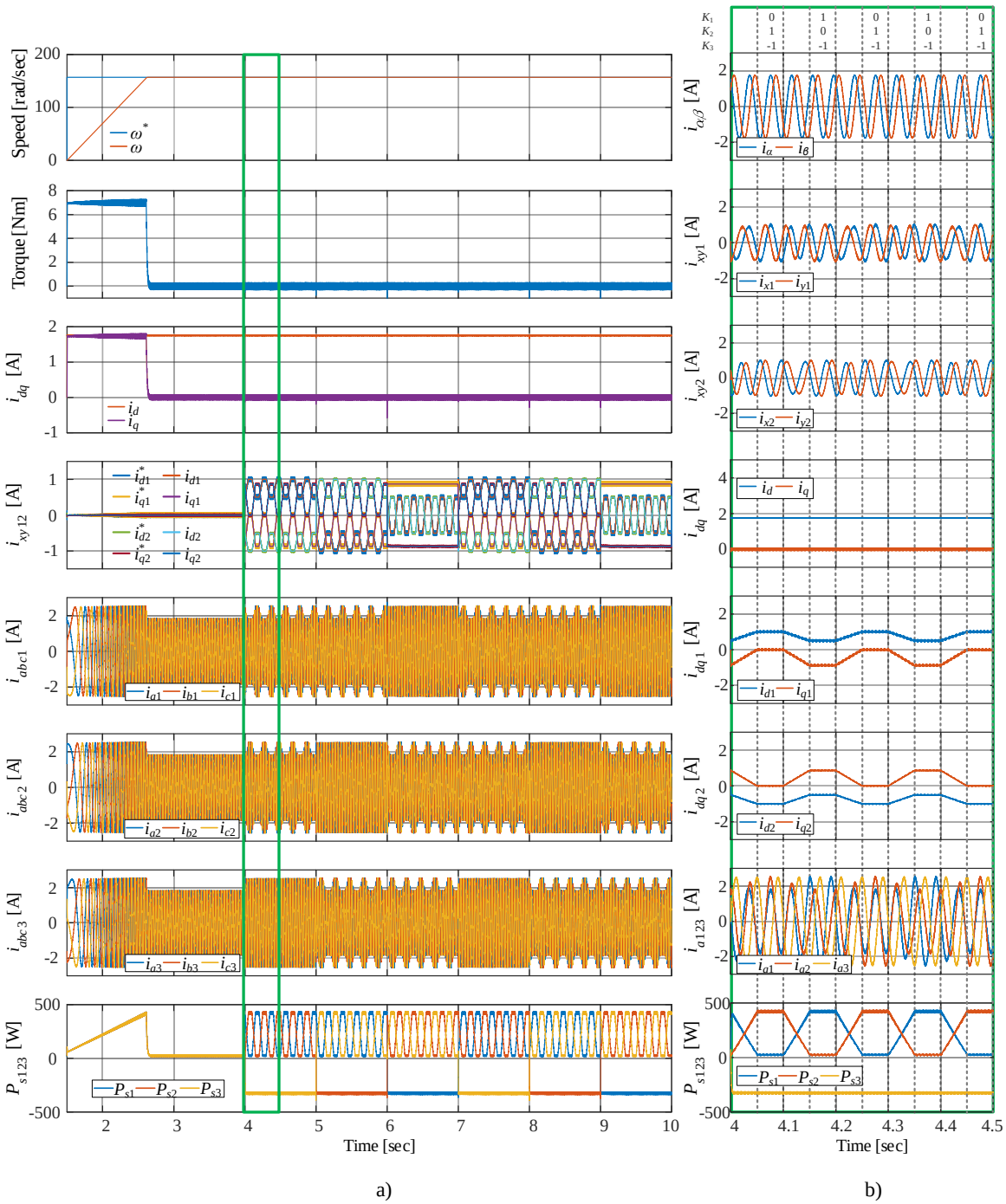

Fig. 7.7: Regenerative test simulation results for asymmetrical nine-phase induction machines using VSD and current sharing control. a) complete simulation, b) zoomed section between $t = 4.0$ sec – 4.5 sec.

(motoring mode) and by the second set P_{s2} = 25.45 W (no-load, hence consumed power equal the copper losses only). The third set is in generation mode with P_{s3} = –323 W. Therefore, the total power losses are 124.45 W. The total copper losses can be calculated from the winding sets in motoring and generation mode ($6 \cdot R_s \cdot 1.74^2$ = 98.6 W) plus the winding set in no-load mode ($3 \cdot R_s \cdot 1.241^2$ = 25.5 W) which is equal to 124.1 W. The windage and friction losses as well as power electronic converter losses are neglected in the simulation.

To demonstrate the validity of the regenerative test approach utilising the unique *y*-current for a higher number of phases, simulation results are provided for asymmetrical six-phase and twelve-phase induction machines. However, the experimental results, given in the next section, are collected using the asymmetrical six-phase induction machine, which is the one available in the laboratory.

The traditional speed IRFOC scheme is implemented for an asymmetrical six-phase machine with an extra current controller for i_y by using the general scheme of Fig. 7.5. Initially, the machine's reference speed is set to 950 rpm (99.5 rad/sec). After the machine has accelerated and reached the reference speed, the regenerative torque reference, T^*_{rg}, is changed from zero to the desired value at 1.7 sec. After that moment, the T^*_{rg} is increased every 0.1 sec by 2 Nm. The machine parameters are provided in Table 7.2. The obtained simulation results are illustrated in Fig. 7.8.

From the simulation results shown in Fig. 7.8, one can see that after applying the regenerative torque at 1.7 sec, the phase currents are changing in all winding sets (i_{a1}, i_{a2}) according to the change of T^*_{rg}. However, the i_{dq} currents are constant (i_q = 0, $i_d = 0.7\sqrt{3}$ A). The *x*, loss-producing, current is equal to zero. However, i_y, which leads to the T^*_{rg} application, changes as the torque demand T^*_{rg} changes. The phase current peak value corresponds to $\hat{\imath}_n = \sqrt{2} \cdot \sqrt{\left(i_d/\sqrt{3}\right)^2 + \left(i_y/\sqrt{3}\right)^2}$. The division by $\sqrt{3}$ appears because of the used power invariant version of the VSD transformation. Active powers (P_{s12}) consumed by each winding set are shown in the last subplot of Fig. 7.8. Note that the power converter losses, machine iron core losses and friction losses are neglected in the simulations. The power, and hence the torque (because of the same and constant speed), of the machine are distributed equally among the winding sets. Half of the winding sets are having positive power and torque while the other half have negative values. From Fig. 7.8, the total power losses (in this case, the total power consumed from the grid) can be easily obtained. The highest losses are in the last period of the regenerative testing between 1.9 sec and 2.0 sec. The total losses here are: (379.2 – 243.3) = 135.9 W. Table 7.3 illustrates the results of the complete analysis of the average input power and stator copper losses of the asymmetrical six-phase machine. The table shows the phase current rms values (I_{rms}) and average input power for each winding set (P_{Si}, where *i* is the winding set number), for different values of T^*_{rg}. The copper losses are calculated from the I_{rms} values of the phase currents presented in Fig. 7.8. The algebraic sum of the P_{S1} and P_{S2} is equal to the stator's winding losses (P_{cus}) of the machine since other losses are neglected.

The above given power-related considerations do not mention rotor winding losses. The reason for this is that the rotor currents during the test are zero, since no net torque production is achieved (mechanical losses are neglected). Rotor currents are illustrated in the penultimate plot in Fig. 7.8 to confirm this observation. This makes the applicability of the test to induction machines very different from the one related to permanent magnet (PM) synchronous machines in [Luise et al. (2012b), Luise et al. (2012a), Zabaleta et al. (2018)]. In particular, while the test is sufficient to determine the efficiency from no-load to full-load operation in the case of PM machines (and to also obtain related temperature rise when appropriate sensors exist), in the case of induction machines this cannot be done. The test only

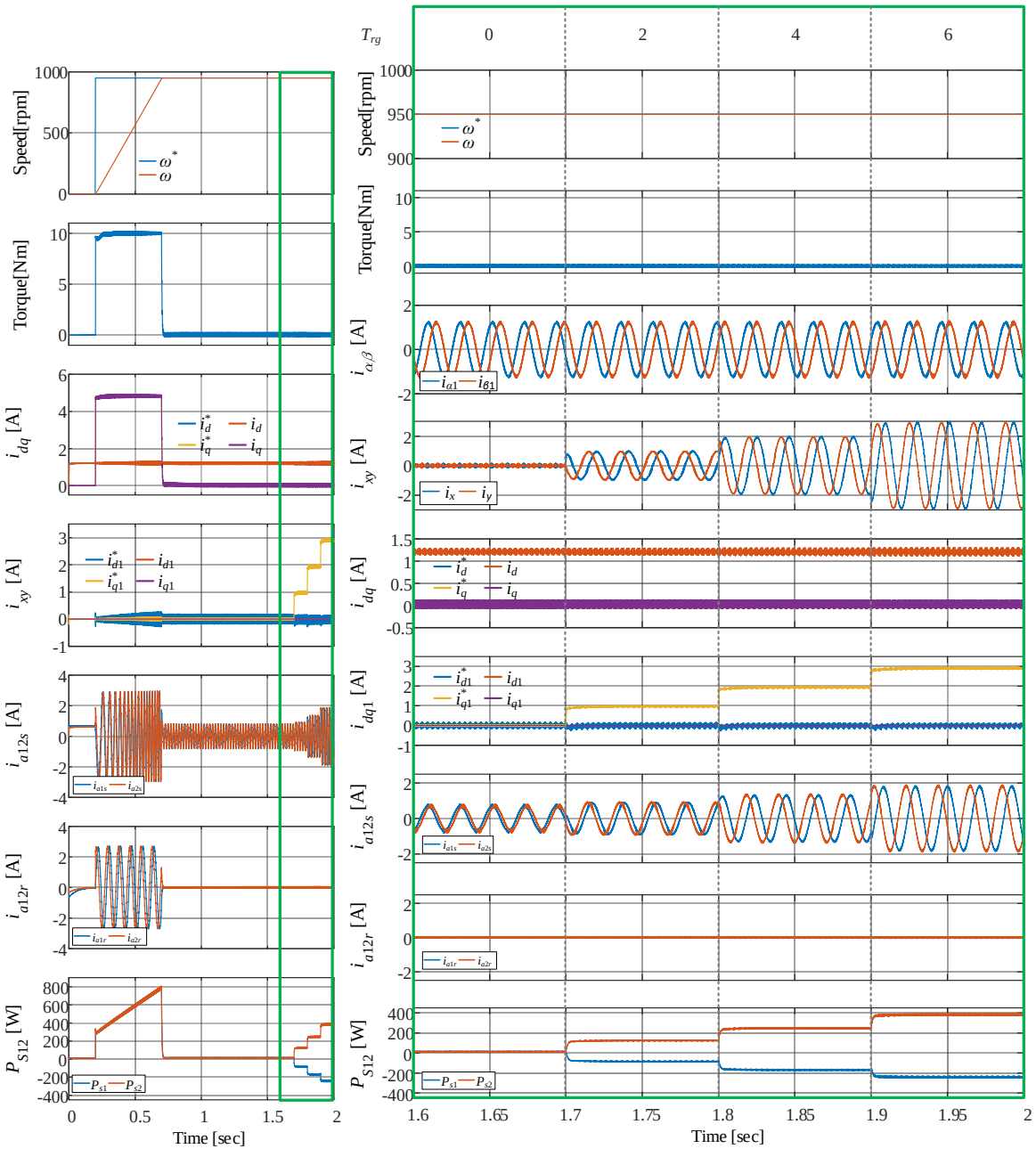

Fig. 7.8: Regenerative test simulation results for asymmetrical six-phase induction machine using unique *y*-current component. a) complete simulation, b) zoomed section between t = 1.6 sec – 2.0 sec.

enables obtaining the no-load to full-load sum of constant losses (iron plus mechanical; neglected in simulation) and corresponding stator winding losses. However, since the current is measured, it becomes easy to separate the constant and variable losses, as illustrated shortly.

The twelve-phase machine parameters are the same as for the six-phase machine and are hence as provided in Table 7.2. The simulation results of the asymmetrical twelve-phase machine are illustrated in Fig. 7.9. Initially, the machine's reference speed is set to 950 rpm. After the machine has accelerated and reached the reference speed, the regenerative torque reference, T_{rg}^*, is changed from zero to the desired value at 1.25 sec. The T_{rg}^* is applied using i_{y3} reference current. After that moment, the T_{rg}^*

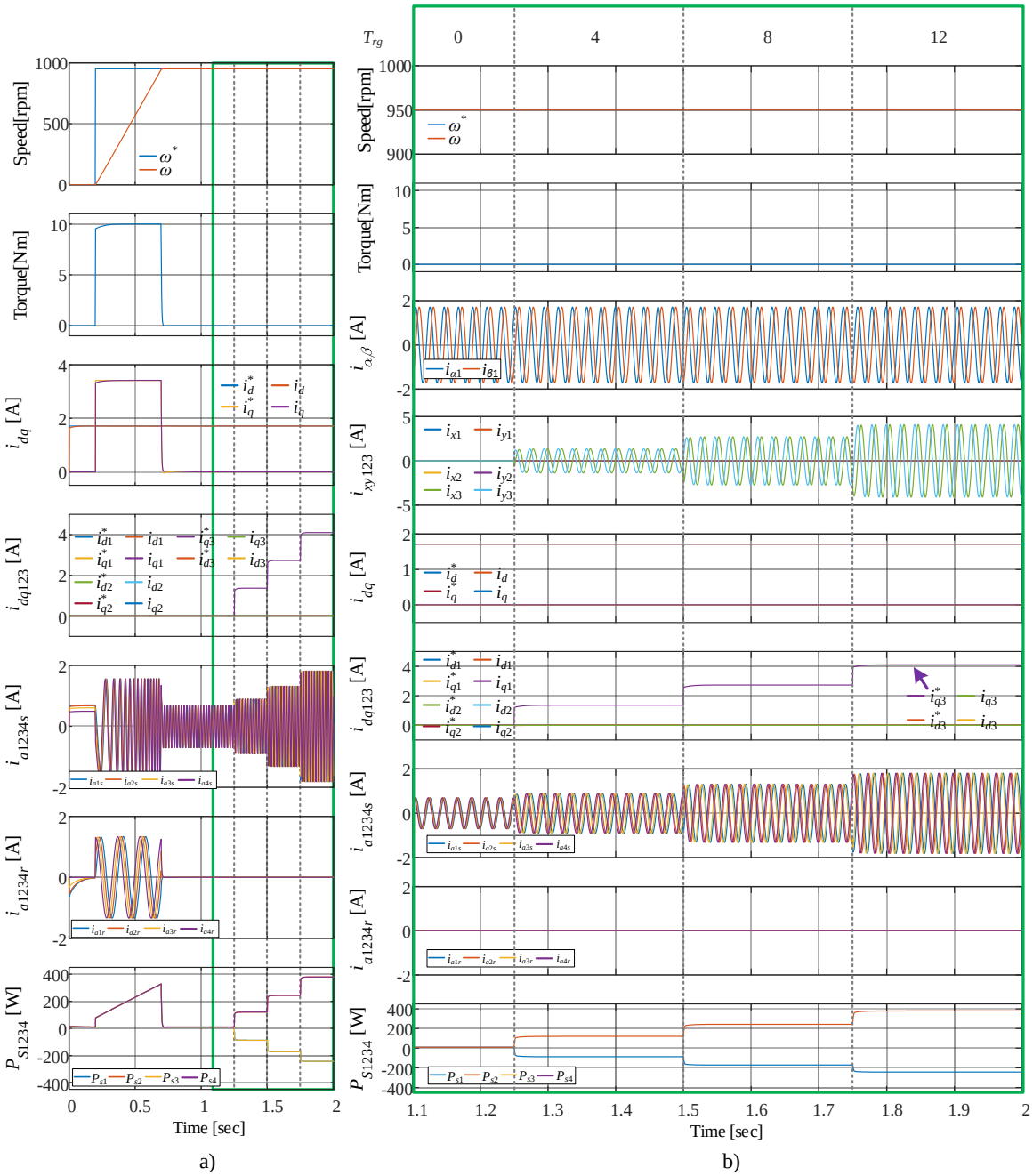

Fig. 7.9: Regenerative test simulation results for asymmetrical twelve-phase induction machine using a unique y-current component. a) complete simulation, b) zoomed section between t = 1.1 sec – 2.0 sec.

Table 7.3: Average power and stator copper losses of asymmetrical six-phase machine – Simulation results.

T_{rg} (Nm)	0	2	4	6
I_{rms} (A)	0.495	0.626	0.928	1.283
P_{S1} (W)	10.1	-87.2	-170.6	-243.3
P_{S2} (W)	10.1	120.3	243.3	379.2
P_{cus} (W)	20.2	32.3	71.1	135.9

Table 7.4: Average power and stator copper losses of asymmetrical twelve-phase machine – Simulation results.

T_{rg} (Nm)	0	4	8	12
I_{rms} (A)	0.495	0.626	0.928	1.283
$P_{S1,\,S3}$ (W)	10.1	-87.2	-170.6	-243.3
$P_{S2,\,S4}$ (W)	10.1	120.3	243.3	379.2
P_{cus} (W)	40.4	64.6	142.2	271.8

is increased every 0.25 sec by 4 Nm. The average power analysis for the twelve-phase machine using simulation results is shown in Table 7.4. The penultimate subplot in Fig. 7.9 again illustrates rotor currents and confirms once more that, since they are zero in steady state, rotor winding losses are zero.

The simulation results prove both the validity of the approach and its limitations in conjunction with induction machines. The efficiency and/or thermal design of a synchronous machine can be tested by using the suggested simple modification of the FOC, and without the need to mechanically couple another machine, with results expected to be the same as in [Luise et al. (2012b), Luise et al. (2012a), Zabaleta et al. (2018)]. However, in the case of an induction machine, the approach can only be used to segregate the machine losses (stator copper losses vs. constant – i.e. core (P_{Fe}) and friction and windage losses (P_{fw})).

7.7 EXPERIMENTAL RESULTS

In order to validate the proposed regenerative test schemes introduced in section 7.4 and 7.5, an experimental setup with asymmetrical six- and nine-phase induction machines has been utilised. Initially, the regenerative test utilising the current sharing strategy (VSD) is validated using an asymmetrical nine-phase induction machine and the experimental results are illustrated in Fig. 7.10. The utilised nine-phase induction machine's parameters are presented in Table 3.1. Afterwards, to examine the regenerative test for multiphase machines with an even number of neutral points (utilising a unique *y*-current component), an experimental setup with asymmetrical six-phase induction machine has been used. The machine parameters are the same as those used for the six- and twelve-phase machine, Table 7.2. However, the switching frequency f_{sw} is 5 kHz. The machine's rated power is 1.1 kW and it is configured with two isolated neutral points.

The asymmetrical nine-phase induction machine is utilised to illustrate the ability of the regenerative test for nine-phase machines (odd number of neutral points) using the current and power sharing strategy illustrated in Chapter 3 and Chapter 5. However, the difference appears between the

current sharing schematics illustrated in Fig. 3.10 and Fig. 7.4 is presented by the imposed regenerative torque reference. At first, the nine-phase machine is controlled using IRFOC and auxiliary current control. The speed reference is set to 1000 rpm (104.7 rad/sec). After the machine reaches steady state, the machine was loaded with regenerative loading torque $T_{rg}^{*} = 7$ Nm at $t = 1.0$ sec. Then, the sharing coefficients are changed to $K_3 = -1$ with K_1 and K_2 altered between 1 and zero between $t = 1.0$ sec – 2.0 sec as illustrated above Fig. 7.10b. It can be noticed from the penultimate plot of Fig. 7.10b that the third winding set current is equivalent in magnitude to the motoring winding set current when they reached the maximum sharing coefficient 1. It can be noticed from the last plot of Fig. 7.10a that the input power of the winding sets is changing according to the winding sets' sharing coefficients and while one winding set is in motoring the second motoring winding set is in no-load and the third set is in generation mode. The generation winding set is altered between the three winding sets each second while the motoring winding sets are changing each 0.1 sec, trapezoidally. The *d-q* subspace currents are constant during the regenerative testing operation ($t = 1.0$ sec – 7.0 sec). However, the x_i-y_i (d_i-q_i) are changing according to the sharing coefficients. Additional vector PI regulators have been added to the auxiliary current controllers in parallel to eliminate the low order harmonics (5^{th}, 7^{th}, 11^{th}, 13^{th}, 29^{th} and 31^{st}) existing in the machine due to the non-ideal design of the machine and due to the large dead-time of the VSI. However, during the regenerative test implementation, the additional vector PI regulators do not eliminate and compensate the targeted harmonics; this is noticeable from the penultimate plot of Fig. 7.10b.

The regenerative test control schematic illustrated in Fig. 7.5 is implemented using dSPACE. The flux/torque control is applied in the synchronous reference frame. The auxiliary current (*y*-current) control is implemented in the anti-synchronous reference frame. Due to the relatively large dead time of the VSI, the fifth and seventh harmonics are large in the phase currents. Thus, two additional resonant vector PI controllers have been added to the auxiliary (*x*-*y*) current PI controllers, since the fifth and seventh harmonics are mapped into this subspace.

Initially, the machine is accelerated using a speed reference of 950 rpm. After the machine has reached the set speed, the regenerative test with different values of the T_{rg}^{*} is applied. The T_{rg}^{*} is applied as a sequence with the values 0 Nm, 2 Nm, 4 Nm and 6 Nm. Each value is applied for a duration of 0.1 sec. The experimental results of the regenerative test are illustrated in Fig. 7.11. The current values in Fig. 7.11b are four times the actual currents of Fig. 7.11a, since four turns were used to measure the current. One can notice that during the period from 0 to 0.1 sec both windings of the tested six-phase machine are in motoring mode. This is obvious from the positive values of input powers of the winding sets (P_{Si}), illustrated in Fig. 7.11a. In addition, the i_y current is equal to zero in this period – hence, the regenerative test has not been initiated yet. The regenerative testing starts at 0.1 sec. The T_{rg}^{*} is set to 2 Nm during the interval from 0.1 sec – 0.2 sec. From Fig. 7.11a, one can see that at 0.1 sec a step change from 0 to 0.967 A happens in the i_y current. This change corresponds to the change of T_{rg}^{*}. During

this period, the behaviour of the input power of the winding sets is changed. The first winding set power has a negative value, while the second winding set has a positive input power (the last plot in Fig. 7.11a). Of course, the dc-link input power (black trace in the bottom plot of Fig. 7.11a) is still positive. This is the power that the drive is using to cover the converter and the machine losses. The losses of the system include power electronic converter losses, stator's winding and core losses of the machine, and the friction and windage losses (i.e. variable stator losses and constant losses). During the period between 0.2 sec – 0.3 sec the T_{rg}^{*} is set to 4 Nm. Finally, the rated stator current conditions of the machine are reached between 0.3 sec – 0.4 sec where the nominal torque and speed are applied.

The current and power values, for different regenerative torques, are summarised in Table 7.5. The machine losses are calculated by adding the input power (P_{Si}) of the two winding sets. The stator copper losses are calculated from the I_{rms} of the two winding sets and from the knowledge of stator

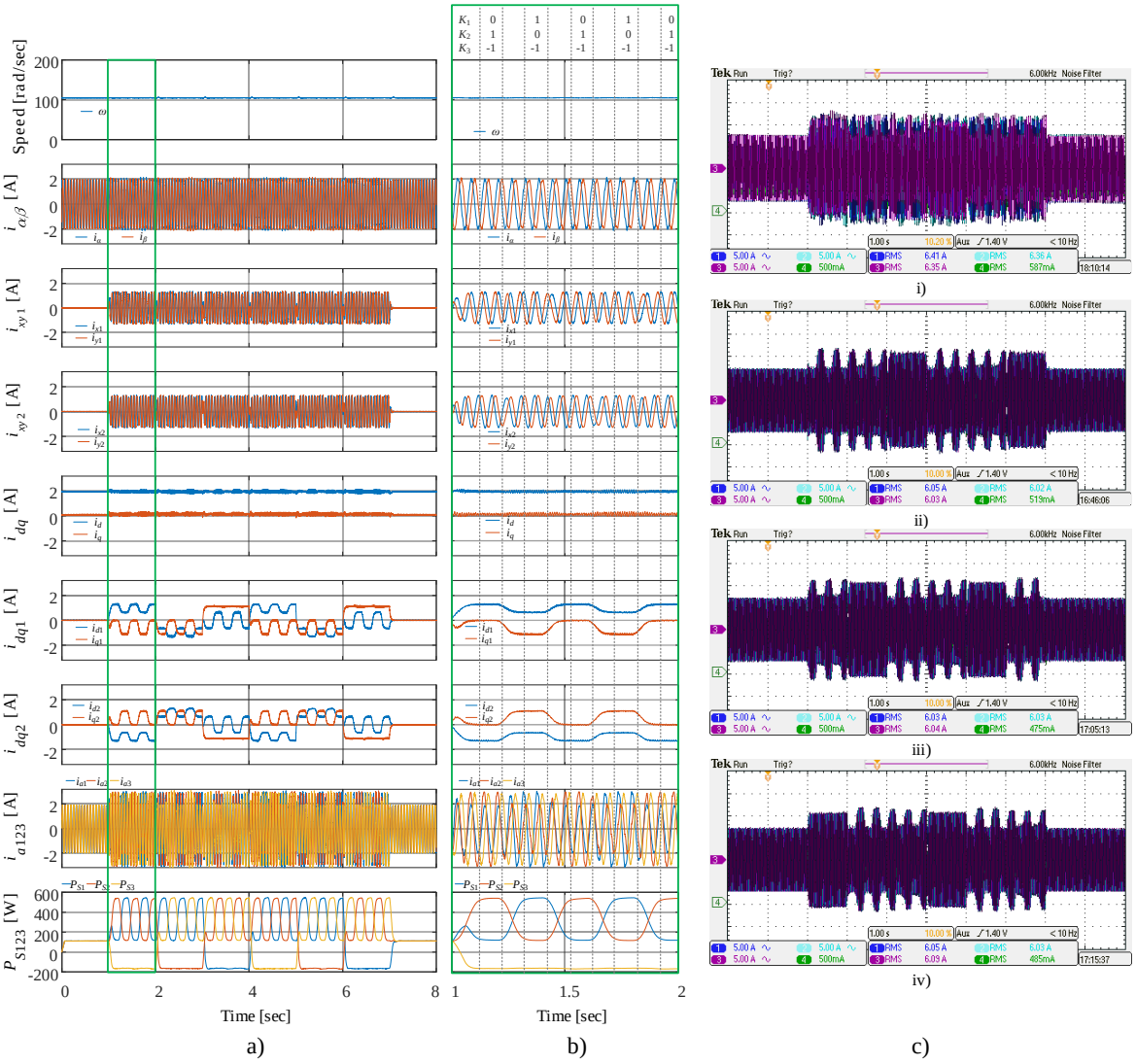

Fig. 7.10: Experimental results of regenerative test for asymmetrical nine-phase induction machine using VSD (current sharing strategy). Four turns of wire were used for the oscilloscope current measurement. a) dSPACE recorder results; b) Zoomed section between t = 1.0 sec to 2.0 sec; c) Oscilloscope screenshots i) Ch1-i_{a1}, Ch2-i_{a2} and Ch3-i_{a3} current, ii) first set currents Ch1-i_{a1}, Ch2-i_{b1}, Ch3-i_{c1} iii) second set currents Ch1-i_{a2}, Ch2- i_{b2} and Ch3-i_{c2}. iv) third set currents Ch1-i_{a3}, Ch2- i_{b3} and Ch3-i_{c3}.

resistance (Table 7.2). Next, the constant (mechanical and core) losses are calculated by subtracting the stator copper losses from the total machine losses. It is therefore simple to perform separation of constant losses and variable (load-dependent) losses using the test data. Finally, the converter losses are calculated by subtracting the total machine losses (P_{S1}+P_{S2}) out of the input power from the grid (P_{dc}).

Comparison of the experimental results in Fig. 7.11 and the simulation results, given in Fig. 7.8, shows that the difference appears in the winding set powers, since the core and mechanical losses have been neglected in simulation. Indeed, the total machine losses in Table 7.5 exceed the corresponding values in Table 7.3 by the amount of the constant losses, which were not included in the simulation.

The calculated stator winding losses, illustrated in Table 7.3, are approximately the same as in Table 7.5, while the stator current rms values I_{rms} are slightly higher in the experimental results (with

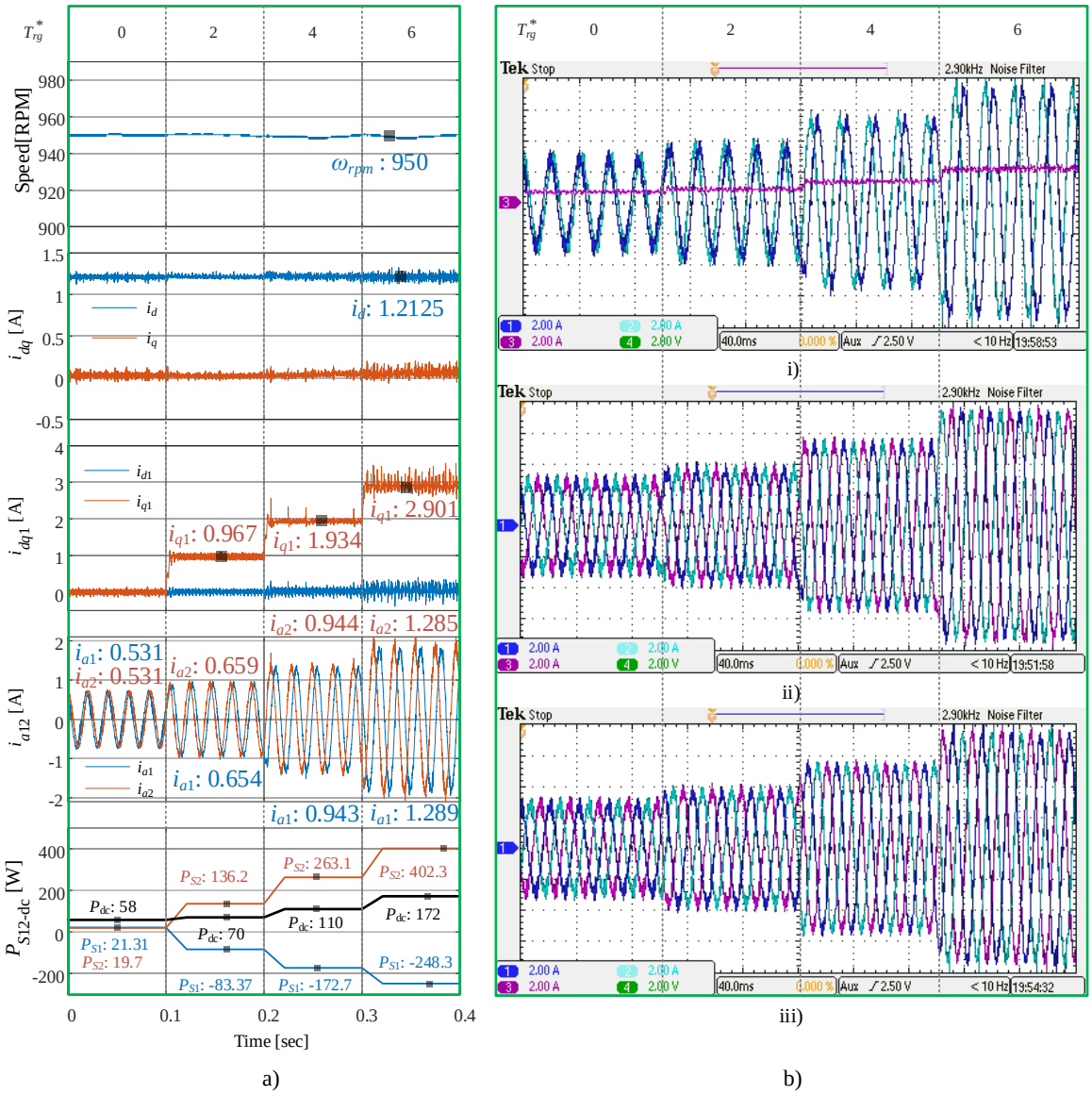

a) b)

Fig. 7.11: Experimental results of regenerative test for asymmetrical six-phase induction machine using unique *y*-current component. Four turns of wire were used for the oscilloscope current measurement. a) dSPACE recorder results; b) Oscilloscope screenshots i) Ch1-i_{a1}, Ch2-i_{a2} and Ch3-i_{dc} current, ii) first set currents Ch1-i_{a1}, Ch2-i_{b1}, Ch3-i_{c1} iii) second set currents Ch1-i_{a2}, Ch2- i_{b2} and Ch3-i_{c2}.

the difference reducing as the torque increases, due to the diminishing relative importance of the constant losses).

To verify the accuracy of the constant and load-dependent (stator winding) loss segregation, obtained using the regenerative test, the standard no-load test is performed as well, using the inverter supply and open-loop control. Stator voltage is varied by changing the modulation index of the inverter supply, while the frequency is set the same as for zero load torque in experimental regenerative test results of Table 7.5. The constant machine losses, determined from the no-load test, are shown in Fig. 7.12, plotted against the fundamental rms voltage squared. Using the fundamental rms voltage of 94.5 V (i.e., its squared value 8,930 V^2), it is possible to read the constant loss of the machine as approximately 19.5 W in Fig. 7.12. This voltage value corresponds to the phase rms fundamental voltage during the regenerative test with 0 Nm setting. The value of 19.5 W agrees well with approximately 18 W in Table 7.5, obtained from the regenerative test.

Table 7.5: Average power and stator copper losses of asymmetrical six-phase machine – Experimental results.

T^*_{rg} (Nm)	0	2	4	6
$I_{rms\ S1}$ (A)	0.531	0.654	0.943	1.289
$I_{rms\ S2}$ (A)	0.531	0.659	0.944	1.285
I_{dc} (A)	0.181	0.219	0.344	0.538
P_{S1} (W)	21.3	-83.4	-172.7	-248.3
P_{S2} (W)	19.7	136.2	263.1	402.3
P_{dc} (W)	58	70	110	172
Total Machine Losses (W)	41.0	52.8	90.4	154.0
P_{cus} (W)	23.3	35.6	73.4	136.7
$P_{fw} + P_{Fe}$ (W)	17.7	17.2	17.0	17.3
Converter Losses (W)	17.0	17.2	19.6	18.0

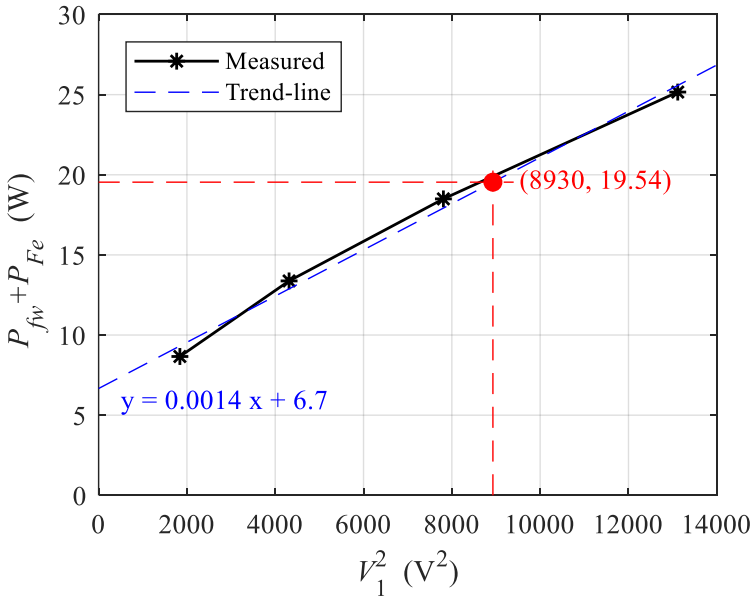

Fig. 7.12: Results of the standard no-load test of the asymmetrical six-phase induction machine – constant losses against fundamental rms voltage squared.

7.8 SUMMARY

In this chapter, two novel approaches for implementation of the regenerative test have been introduced for multiple three-phase machines. The first approach is meant for all multiple three-phase machines. The approach uses a modified current sharing strategy which is based on VSD rather than the MS approach to apply the rated current and circulate the power among the winding sets. Then, another novel approach to the regenerative test for multiple three-phase winding machines with an even number of neutral points has been introduced in this chapter. In contrast to the MS version of the regenerative test, it is based on the VSD modelling method. The regenerative test can be implemented by adding an extra current controller for the y_k-current component, where index k refers to the highest order x-y plane. It is elaborated in general terms for machine phase numbers up to eighteen. Compared to the existing version of the same test, based on the MS approach, control during testing is greatly simplified, since multiple decoupling terms are not required. The testing results are however independent of the control approach used.

The testing principles are the same for both synchronous and induction machines. However, the test outcomes are very different. In the case of a synchronous machine the rated power is circulated among the winding sets, the necessity for mechanical coupling at the shaft of the machine with another machine is eliminated, and the test enables efficiency evaluation and temperature rise measurement. As the test has been used in conjunction with a permanent magnet synchronous machine already, the emphasis in the chapter is placed on an induction machine. It is shown that, in contrast to synchronous machines, the test cannot be used to yield efficiency evaluation (and temperature rise results). This is so since, during the test, rotor currents are kept at zero, as there is no load attached to the shaft (neglecting mechanical losses). However, the test does enable a simple, straightforward and accurate way of determining the constant (sum of core and mechanical) losses.

The developed control schemes have been examined by simulation of six-, nine- and twelve-phase asymmetrical induction machines. Further, it has been validated experimentally using an asymmetrical nine- and six-phase induction machine. The results prove the theoretical considerations and show that the machine can operate at the nominal speed with rated stator currents and with zero total torque on the shaft, so that an accurate evaluation of the sum of the stator winding and constant machine losses can be obtained. Subject to the known stator resistance, further segregation of constant losses from the stator load-dependent losses is easily accomplished.

CHAPTER 8

CONCLUSION AND FUTURE WORK

8.1 SUMMARY AND CONCLUSIONS

In this thesis, an independent power flow control of the different winding sets within a single electrical machine is given. The considered machines are multiple three-phase induction machines with symmetrical or asymmetrical sinusoidal winding distribution. The analysis is equally applicable to synchronous machines with sinusoidal winding distribution. The independent power flow control is based on stator current control using IRFOC and auxiliary current control. In addition, the current and power sharing strategies are utilised to provide the efficiency and temperature rise for synchronous machines and segregation of the load dependent and constant losses of the induction machines. The proposed control schemes are validated through simulations and experimental results.

After the introduction and the literature review chapters, the current sharing strategy for symmetrical and asymmetrical multiple three-phase induction machines is introduced in Chapter 3 and 4, respectively. The current sharing strategy can be utilised to control the current of each three-phase winding set, and hence the amount of power taken/given to the energy source used to supply that winding set. By finding the correlations between the auxiliary *x-y* currents of VSD approach and the individual winding set currents α_i-β_i, controlling the individual winding set currents' amplitude is possible, as shown by the mathematical derivation for the nine-phase induction machine with three isolated neutral points. It has been shown that the correlations for symmetrical and asymmetrical multiple three-phase machines with the same number of phases and neutral points are the same. The theoretical derivations are validated by simulation in Matlab/Simulink and by experimental results utilising symmetrical and asymmetrical nine-phase induction machine. The results obtained from the experimental setup match those from simulation as presented at the end of each chapter. Utilisation of this approach provides current (power) sharing among the three-phase winding sets within a single induction machine by simply changing the sharing coefficient of the winding sets K_i. Furthermore, obtaining post fault operation of the multiple three-phase machines is possible utilising these coefficients as shown by the obtained simulation and experimental results. Although the derivation, simulation and experimental results are shown for induction machines, the current sharing method can be applied equally to synchronous machines with multiple neutral points.

Chapter 3 and 4 were considering a current sharing strategy when all the winding sets of the multiple three-phase machine are either in motoring or in generation mode. In Chapter 5 simultaneous operation in motoring and generation of the winding sets is studied in detail. Two power sharing

strategies have been proposed in this chapter. The first approach is based on sharing the flux and torque (*d*-*q*) producing currents equally. This is based on the current sharing strategy derived in Chapter 3 and 4, and is utilising the K_i coefficients. It is concluded that employing this approach produces unnecessary variation in the flux producing current (*d*-axis current) which increases the losses of the machine. Therefore, another approach for power sharing is introduced in this chapter. It is shown that this new power sharing approach, which is based on sharing the torque producing current (*q*-axis current) rather than both flux and torque producing currents of the individual winding sets, is more efficient. Therefore, the coefficients K_i are split into K_{di} and K_{qi} coefficients, which must be controlled in the synchronously rotating reference frame. Otherwise, having different sharing coefficients in the stationary reference frame would produce asymmetry within the three-phase winding set currents. An asymmetrical nine-phase induction machine is used to validate the power sharing approaches. The obtained simulation and experimental results confirm the theoretical analysis. The efficiency of both approaches has been compared and it is shown that sharing the torque producing currents only, using separate coefficients for flux and torque producing currents (K_{di} and K_{qi}), provides more efficient power transfer from one winding set to another.

In Chapter 6, power sharing for double-winding multiple three-phase machines is considered. Two approaches are proposed for sharing the power among the sub-machines and for transferring the energy from any winding set from one sub-machine to another or within the same sub-machine. A hybrid control scheme is proposed and validated using the double vector control and vector control based on VSD. The proposed schemes are validated for a twelve-phase (double-winding six-phase) machine. It is concluded that in order to obtain an efficient power transfer from one winding set to another, the sharing should be done between the torque producing currents only, as established in Chapter 5. It is also shown that the proposed control schemes can be utilised to control the double winding multiple three-phase machines in post-fault operation as presented by the simulation results.

Finally, Chapter 7 considered the regenerative test for multiple three-phase machines. Two approaches are suggested in this chapter. The first approach is a general approach for all multiple three-phase machines while the second one is only applicable to multiple three-phase machines with an even number of neutral points. Both proposed approaches are based on VSD. The first one is imposing the regenerative torque reference on the x_i-y_i currents of the VSD and utilising the K_i current sharing coefficients to achieve this objective. A different scheme should be used when there is an odd number of winding sets such that one of the winding sets should always be in no-load operation mode as explained in the chapter. However, when there is an even number of winding sets half of the winding sets should be in motoring mode while the other half is in generation mode. The second approach uses a unique *y*-current component of the VSD to circulate the power among the winding sets. The method is based on injecting the reference regenerative torque into the k^{th} y_k-current component of the VSD, where *k* represents the highest order of the x_i-y_i subspace. From observation of correlations between the

MS and VSD of this subspace it is concluded that it consists of pure β_i components of the individual winding sets and more interestingly that half of them is with positive sign while the other half is with negative sign. Therefore, by injecting the right reference current into this unique *y*-current component, motoring and generation can be achieved using a single component rather than the current sharing coefficients of the previous approach. The testing principle for both approaches is the same. It is shown that for an even number of neutral points, the same results can be obtained from the first and from the second regenerative test approach. The test can be applied to induction and synchronous machines equally. However, it is concluded that the obtained results are different. For synchronous machines, the test can be utilised to obtain the machine's efficiency and the temperature rise curve. On the other hand, the test can be utilised only to segregate the constant machine losses from the load dependent losses for induction machines. This is because the rotor currents are approximately zero during the regenerative test. The power is exchanged between the winding sets at the air-gap and as a result there is no any current in the rotor except to cover the friction and windage losses. The developed schemes have been tested and validated by simulation and experimentally. Three types of machines have been simulated, six-, nine- and twelve-phase induction machine. Both approaches have been examined by experiments using a nine-phase induction machine for the first approach and a six-phase induction machine for the second approach. The experimental approach was utilised for induction machines only due to the absence of six- or twelve phase synchronous machines in the laboratory. The obtained experimental results showed the validity of the method to segregate the constant losses (sum of core and mechanical) from the load dependent losses for the induction machine.

8.2 FUTURE WORK

The work presented in this thesis brings some considerable new knowledge in the area of current and power sharing of the multiple three-phase machines. In this thesis, several independent power flow control schemes have been presented. Although the control schemes are valid for both induction and synchronous machines, the simulation and experimental investigation were carried out only on induction machines with sinusoidal winding distribution. Similarly, in the previous chapter, the proposed regenerative test schemes can be utilised for two different purposes depending on the machine type. However, the simulation and experimental verification are carried out only for the induction machines. In addition, the power flow control and regenerative test have been carried out in the varying power region and it has not been investigated in the field weakening region. All of this gives a lot of scope for the new research that can be done. The following topics can be considered for the future work:

- Investigating the current and power sharing schemes for multiple five-phase machines, where each five-phase winding set has an *x*-*y* subspace in addition to the α-β subspace.
- Extension of the current and power sharing schemes in the field-weakening region for synchronous and induction machines.

- Investigation, using FEM analysis, of the influence of the current sharing and the power sharing algorithms on the flux distribution in the machine and the resulting impact on the current waveforms and limits.
- Experimental validation of the power sharing schemes for double winding machines.
- Implementation of the current and power sharing utilising different control approaches such as MPC and DTC.
- Investigating the regenerative test at the field-weakening region for induction and synchronous machines.

CHAPTER 9

REFERENCES

Abbas, M. A., Christen, R. and Jahns, T. M., (1984), Six-phase voltage source inverter driven induction motor, *IEEE Transactions on Industry Applications*, IA-20 (5), 1251-1259.

Abdel-Khalik, A. S. and Ahmed, S., (2012), Performance evaluation of a five-phase modular winding induction machine, *IEEE Transactions on Industrial Electronics*, 59 (6), 2654-2669.

Abdel-Khalik, A. S., Masoud, M. I. and Williams, B. W., (2012), Vector controlled multiphase induction machine: Harmonic injection using optimized constant gains, *Electric Power Systems Research*, 89, 116-128.

Abdelkhalik, A., Masoud, M. and Barry, W., (2010), Eleven-phase induction machine: steady-state analysis and performance evaluation with harmonic injection, *IET Electric Power Applications*, 4(8), 670-685.

Abduallah, A. A., Dordevic, O. and Jones, M., (2017), Multidirectional power flow control among double winding six-phase induction machine winding sets, in *IECON* 2017 - 43*rd Annual Conference of the IEEE Industrial Electronics Society*, 29 Oct.-1 Nov. 2017, 8001-8006.

Abduallah, A. A., Dordevic, O. and Jones, M., (2018a), Synthetic loading for symmetrical and asymmetrical six-phase machines, in *IEEE* 18*th International Power Electronics and Motion Control Conference (PEMC)*, 26-30 Aug. 2018, 617-622.

Abduallah, A. A., Dordevic, O., Jones, M. and Levi, E., (2018b), Synthetic loading for symmetrical and asymmetrical nine-phase induction machines, in *IECON* 2018 - 44*rd Annual Conference of the IEEE Industrial Electronics Society*, 21-23 Oct. 2018, 1-1.

Abduallah, A. A., Dordevic, O., Jones, M, and Levi, E., (2019), "Regenerative test for multiple three-phase machines with even number of neutral points," *IEEE Transactions on Industrial Electronics*, 2019 (Early Access, doi: 10.1109/TIE.2019.2903750).

Ahmed, S. M., Salam, Z. and Abu-Rub, H., (2015), An improved space vector modulation for a three-to-seven-phase matrix converter with reduced number of switching vectors, *IEEE Transactions on Industrial Electronics*, 62 (6), 3327-3337.

Alberti, L. and Bianchi, N., (2012), Experimental Tests of Dual Three-Phase Induction Motor Under Faulty Operating Condition, *IEEE Transactions on Industrial Electronics*, 59 (5), 2041-2048.

Apsley, J. and Williamson, S., (2006), Analysis of multiphase induction machines with winding faults, *IEEE Transactions on Industry Applications*, 42 (2), 465-472.

Apsley, J. M., (2010), Open-circuit fault mitigation for multiphase induction motors with a unified control structure, in 5*th IET International Conference on Power Electronics, Machines and Drives (PEMD* 2010*)*, 19-21 April 2010, 1-6.

Barrero, F. and Duran, M. J., (2016), Recent advances in the design, modeling, and control of multiphase machines part I, *IEEE Transactions on Industrial Electronics*, 63 (1), 449-458.

Boglietti, A., El-Refaie, A. M., Drubel, O., Omekanda, A. M., Bianchi, N., Agamloh, E. B., Popescu, M., Gerlando, A. D. and Bartolo, J. B., (2014), Electrical machine topologies: Hottest topics in the electrical machine research community, *IEEE Industrial Electronics Magazine*, 8 (2), 18-30.

Bojoi, R., Farina, F., Griva, G., Profumo, F. and Tenconi, A., (2005a), Direct torque control for dual three-phase induction motor drives, *IEEE Transactions on Industry Applications*, 41 (6), 1627-1636.

Bojoi, R., Profumo, F. and Tenconi, A., (2003), Digital synchronous frame current regulation for dual three-phase induction motor drives, in *IEEE* 34*th Annual Conference on Power Electronics Specialist*, 2003. *PESC* '03., 15-19 June 2003, 1475-1480.

Bojoi, R., Tenconi, A., Griva, G. and Profumo, F., (2005b), Vector control of dual-three phase induction motor drives using two current sensors, in *Fourtieth IAS Annual Meeting. Conference Record of the* 2005 *Industry Applications Conference*, 2-6 Oct. 2005, 1805-1812.

Bojoi, R., Tenconi, A., Griva, G. and Profumo, F., (2006), Vector control of dual-three-phase induction-motor drives using two current sensors, *IEEE Transactions on Industry Applications*, 42 (5), 1284-1292.

Camillis, L. D., Matuonto, M., Monti, A. and Vignati, A., (2001), Optimizing current control performance in double winding asynchronous motors in large power inverter drives, *IEEE Transactions on Power Electronics*, 16 (5), 676-685.

Capella, G. J., Pou, J., Ceballos, S., Konstantinou, G., Zaragoza, J. and Agelidis, V. G., (2015), Enhanced phase-shifted pwm carrier disposition for interleaved voltage-source inverters, *IEEE Transactions on Power Electronics*, 30 (3), 1121-1125.

Cavagnino, A., Li, Z., Tenconi, A. and Vaschetto, S., (2013), Integrated generator for more electric engine: Design and testing of a scaled-size prototype, *IEEE Transactions on Industry Applications*, 49 (5), 2034-2043.

Che, H. S., Duran, M. J., Levi, E., Jones, M., Hew, W. P. and Rahim, N. A., (2014a), Postfault operation of an asymmetrical six-phase induction machine with single and two isolated neutral points, *IEEE Transactions on Power Electronics*, 29 (10), 5406-5416.

Che, H. S., Hew, W. P., Rahim, N. A., Levi, E., Jones, M. and Duran, M. J., (2012a), Current control of a six-phase induction generator for wind energy plants, in 15*th International Power Electronics and Motion Control Conference (EPE/PEMC)*, 2012, 4-6 Sept. 2012, LS5b.2-1-LS5b.2-7.

Che, H. S., Hew, W. P., Rahim, N. A., Levi, E., Jones, M. and Duran, M. J., (2012b), A six-phase wind energy induction generator system with series-connected DC-links, in 2012 3*rd IEEE International Symposium on Power Electronics for Distributed Generation Systems (PEDG)*, 25-28 June 2012, 26-33.

Che, H. S., Levi, E., Jones, M., Duran, M. J., Hew, W. P. and Rahim, N. A., (2014b), Operation of a six-phase induction machine using series-connected machine-side converters, *IEEE Transactions on Industrial Electronics*, 61 (1), 164-176.

Che, H. S., Levi, E., Jones, M., Hew, W. P. and Rahim, N. A., (2014c), Current control methods for an asymmetrical six-phase induction motor drive, *IEEE Transactions on Power Electronics*, 29 (1), 407-417.

Cheng, C. and He, L., (2016), Flying-capacitor-clamped five-level inverter based on switched-capacitor topology, in 2016 *IEEE Energy Conversion Congress and Exposition (ECCE)*, 18-22 Sept. 2016, 1-5.

Choi, H., Ciobotaru, M. and Agelidis, V. G., (2014), Cascaded H-bridge converter with multiphase isolated DC/DC converter for large-scale PV system, in 2014 *IEEE International Conference on Industrial Technology (ICIT)*, 26 Feb.-1 March 2014, 455-461.

Chowdhury, S., Wheeler, P. W., Patel, C. and Gerada, C., (2016), A multilevel converter with a floating bridge for open-end winding motor drive applications, *IEEE Transactions on Industrial Electronics*, 63 (9), 5366-5375.

Deilamani, M., Kianinezhad, R., Seifossadat, S. G. H. and Keramatzade, M., (2011), A new insight into six phase induction machine modeling under open phase fault condition, in *International Aegean Conference on Electrical Machines and Power Electronics and Electromotion, Joint Conference*, 8-10 Sept. 2011, 201-204.

Ditmanson, C., Hein, P., Kolb, S., J, M. and Bernet, S., (2014), A new modular flux-switching permanent-magnet drive for large wind turbines, *IEEE Transactions on Industry Applications*, 50(6), 3787-3794.

Dordevic, O., (2013), PWM strategies for multilevel multiphase AC drives, *PhD Thesis*, Liverpool John Moores University, Liverpool, U.K.

Dordevic, O., Bodo, N. and Jones, M., (2010), Model of an induction machine with an arbitrary phase number in Matlab/Simulink for educational use, in 45*th International Universities Power Engineering Conference UPEC2010*, 31 Aug. - 3 Sept. 2010, 1-6.

Duran, M. J. and Barrero, F., (2016), Recent advances in the design, modeling, and control of multiphase machines part II, *IEEE Transactions on Industrial Electronics*, 63 (1), 459-468.

Duran, M. J., Gonzalez-Prieto, I., Guzman, H., Barrero, F. and Kim, H. M., (2015), Unbalanced operation of multiphase wind energy conversion systems connected to microgrids, in *IECON*

2015 - 41*st Annual Conference of the IEEE Industrial Electronics Society*, 9-12 Nov. 2015, 001891-001896.

Duran, M. J., Prieto, I. G., Bermudez, M., Barrero, F., Guzman, H. and Arahal, M. R., (2016), Optimal fault-tolerant control of six-phase induction motor drives with parallel converters, *IEEE Transactions on Industrial Electronics*, 63 (1), 629-640.

Ede, J. D., Atallah, K., Jewell, G. W., Wang, J. B. and Howe, D., (2007), Effect of axial segmentation of permanent magnets on rotor loss in modular permanent-magnet brushless machines', *IEEE Transactions on Industry Applications*, 43 (5), 1207-1213.

Fong, W., (1972), New temperature test for polyphase induction motors by phantom loading, in *Proceedings of the Institution of Electrical Engineers*, IET, 883-887.

Fortescue, C. L., (1918), Method of symmetrical co-ordinates applied to the solution of polyphase networks, *Transactions of the American Institute of Electrical Engineers*, XXXVII(2), 1027-1140.

Fu, J.-R. and Lipo, T. A., (1994), Disturbance-free operation of a multiphase current-regulated motor drive with an opened phase, *IEEE Transactions on Industry Applications*, 30 (5), 1267-1274.

Gao, L., Fletcher, J. E. and Zheng, L., (2011), Low-speed control improvements for a two-level five-phase inverter-fed induction machine using classic direct torque control, *IEEE Transactions on Industrial Electronics*, 58 (7), 2744-2754.

Gonzalez-Prieto, I., Duran, M. J., Che, H. S., Levi, E., Bermúdez, M. and Barrero, F., (2016), Fault-tolerant operation of six-phase energy conversion systems with parallel machine-side converters, *IEEE Transactions on Power Electronics*, 31 (4), 3068-3079.

Grandi, G., Tani, A., Sanjeevikumar, P. and Ostojic, D., (2010), Multi-phase multi-level AC motor drive based on four three-phase two-level inverters, in *SPEEDAM* 2010, 14-16 June 2010, 1768-1775.

Guzmán, H., Durán, M. J. and Barrero, F., (2012), A comprehensive fault analysis of a five-phase induction motor drive with an open phase, in 2012 15*th International Power Electronics and Motion Control Conference (EPE/PEMC)*, 4-6 Sept. 2012, LS5b.3-1-LS5b.3-6.

Guzman, H., Duran, M. J., Barrero, F., Bogado, B. and Toral, S., (2014), Speed control of five-phase induction motors with integrated open-phase fault operation using model-based predictive current control techniques, *IEEE Transactions on Industrial Electronics*, 61 (9), 4474-4484.

Hatua, K. and Ranganathan, V. T., (2005), Direct torque control schemes for split-phase induction machine, *IEEE Transactions on Industry Applications*, 41 (5), 1243-1254.

Ho, S. L. and Fu, W. N., (2001), Analysis of indirect temperature-rise tests of induction machines using time-stepping finite element method, *IEEE Power Engineering Review*, 21 (2), 53-53.

Hu, S., Liang, Z., Fan, D. and He, X., (2016a), Hybrid ultracapacitor-battery energy storage system based on quasi-Z-source topology and enhanced frequency dividing coordinated control for EV, *IEEE Transactions on Power Electronics*, 31 (11), 7598-7610.

Hu, S., Liang, Z. and He, X., (2016b), Ultracapacitor-battery hybrid energy storage system based on the asymmetric bidirectional Z-source topology for EV, *IEEE Transactions on Power Electronics*, 31 (11), 7489-7498.

Hu, S., Liang, Z., Zhang, W. and He, X., (2018), Research on the integration of hybrid energy storage system and dual three-phase PMSM drive in EV, *IEEE Transactions on Industrial Electronics*, 65 (8), 6602-6611.

Hu, Y., Zhu, Z. Q. and Liu, K., (2014), Current control for dual three-phase permanent magnet synchronous motors accounting for current unbalance and harmonics, *IEEE Journal of Emerging and Selected Topics in Power Electronics*, 2 (2), 272-284.

Hua, L., Yunping, Z. and Bi, H., (2006), The vector control strategies for multiphase synchronous motor drive systems, in 2006 *IEEE International Symposium on Industrial Electronics*, 9-13 July 2006, 2205-2210.

Iqbal, A. and Levi, E. (2005), Space vector modulation schemes for a five-phase voltage source inverter, in 2005 *European Conference on Power Electronics and Applications*, 11-14 Sept. 2005, P.1-P.12.

Jones, M., Vukosavic, S. N., Dujic, D. and Levi, E., (2009), A synchronous current control scheme for multiphase induction motor drives, *IEEE Transactions on Energy Conversion*, 24 (4), 860-868.

Jung, E., Yoo, H., Sul, S. K., Choi, H. S. and Choi, Y. Y., (2012), A nine-phase permanent-magnet motor drive system for an ultrahigh-speed elevator, *IEEE Transactions on Industry Applications*, 48 (3), 987-995.

Kallio, S., Andriollo, M., Tortella, A. and Karttunen, J., (2013), Decoupled d-q model of double-star interior-permanent-magnet synchronous machines, *IEEE Transactions on Industrial Electronics*, 60 (6), 2486-2494.

Karampuri, R., Prieto, J., Barrero, F. and Jain, S., (2014), Extension of the DTC technique to multiphase induction motor drives using any odd number of phases, in 2014 *IEEE Vehicle Power and Propulsion Conference (VPPC)*, 27-30 Oct. 2014, 1-6.

Karttunen, J., Kallio, S., Peltoniemi, P., Silventoinen, P. and Pyrhönen, O., (2014), Decoupled vector control scheme for dual three-phase permanent magnet synchronous machines, *IEEE Transactions on Industrial Electronics*, 61 (5), 2185-2196.

Kianinezhad, R., Nahid-Mobarakeh, B., Baghli, L., Betin, F. and Capolino, G., (2008), Modeling and control of six-phase symmetrical induction machine under fault condition due to open phases, *IEEE Transactions on Industrial Electronics*, 55 (5), 1966-1977.

Kim, S., Lee, J. and Lee, K., (2016), A modified level-shifted PWM strategy for fault-tolerant cascaded multilevel inverters with improved power distribution, *IEEE Transactions on Industrial Electronics*, 63 (11), 7264-7274.

Kollimalla, S. K., Mishra, M. K. and Narasamma, N. L., (2014), Design and analysis of novel control strategy for battery and supercapacitor storage system, *IEEE Transactions on Sustainable Energy*, 5 (4), 1137-1144.

Kuperman, A., Aharon, I., Malki, S. and Kara, A., (2013), Design of a semiactive battery-ultracapacitor hybrid energy source, *IEEE Transactions on Power Electronics*, 28 (2), 806-815.

Labak, A. and Kar, N. C., (2013), Designing and prototyping a novel five-phase pancake-shaped axial-flux SRM for electric vehicle application through dynamic FEA incorporating flux-tube modeling, *IEEE Transactions on Industry Applications*, 49 (3), 1276-1288.

Lega, A., Mengoni, M., Serra, G., Tani, A. and Zarri, L., (2009), Space vector modulation for multiphase inverters based on a space partitioning algorithm, *IEEE Transactions on Industrial Electronics*, 56 (10), 4119-4131.

Levi, E., (2008), Multiphase electric machines for variable-speed applications, *IEEE Transactions on Industrial Electronics*, 55 (5), 1893-1909.

Levi, E., (2016), Advances in converter control and innovative exploitation of additional degrees of freedom for multiphase machines, *IEEE Transactions on Industrial Electronics*, 63 (1), 433-448.

Levi, E., Bojoi, R., Profumo, F., Toliyat, H. A. and Williamson, S., (2007), Multiphase induction motor drives - a technology status review, *IET Electric Power Applications*, 1 (4), 489-516.

Levi, E., Dujic, D., Jones, M. and Grandi, G., (2008), Analytical determination of dc-bus utilization limits in multiphase VSI supplied ac drives, *IEEE Transactions on Energy Conversion*, 23 (2), 433-443.

Levi, E., Satiawan, I. N. W., Bodo, N. and Jones, M., (2012), A space-vector modulation scheme for multilevel open-end winding five-phase drives, *IEEE Transactions on Energy Conversion*, 27 (1), 1-10.

Lim, C. S., Levi, E., Jones, M., Rahim, N. A. and Hew, W. P., (2014), FCS-MPC-based current control of a five-phase induction motor and its comparison with PI-PWM control, *IEEE Transactions on Industrial Electronics*, 61 (1), 149-163.

Lim, C. S., Rahim, N. A., Hew, W. P., Jones, M. and Levi, E., (2011), Model predictive current control of a five-phase induction motor, in *IECON* 2011 - 37*th Annual Conference of the IEEE Industrial Electronics Society*, 7-10 Nov. 2011, 1934-1940.

Lipo, T. A., (1980), A d-q model for induction machines, in *Proc. Int. Conf. on Electrical Machines*, Athens, Greece, pp. 860-867.

Liu, Z., Zheng, Z., Xu, L., Wang, K. and Li, Y., (2016), Current balance control for symmetrical multiphase inverters, *IEEE Transactions on Power Electronics*, 31 (6), 4005-4012.

López, I., Ceballos, S., Pou, J., Zaragoza, J., Andreu, J., Kortabarria, I. and Agelidis, V. G., (2016), Modulation strategy for multiphase neutral-point-clamped converters, *IEEE Transactions on Power Electronics*, 31 (2), 928-941.

Lopez, O., Alvarez, J., Doval-Gandoy, J. and Freijedo, F. D., (2008), Multilevel multiphase space vector pwm algorithm, *IEEE Transactions on Industrial Electronics*, 55 (5), 1933-1942.

Lopez, O., Alvarez, J., Doval-Gandoy, J. and Freijedo, F. D., (2009), Multilevel multiphase space vector pwm algorithm with switching state redundancy, *IEEE Transactions on Industrial Electronics*, 56 (3), 792-804.

Luise, F., Pieri, S., Mezzarobba, M. and Tessarolo, A., (2012a), Regenerative testing of a concentrated-winding permanent-magnet synchronous machine for offshore wind generation --- part I: Test concept and analysis, *IEEE Transactions on Industry Applications*, 48 (6), 1779-1790.

Luise, F., Pieri, S., Mezzarobba, M. and Tessarolo, A., (2012b), Regenerative testing of a concentrated-winding permanent-magnet synchronous machine for offshore wind generation --- part II: Test implementation and results, *IEEE Transactions on Industry Applications*, 48 (6), 1791-1796.

McSharry, J. P., Hamer, P. S., Morrison, D., Nessa, J. and Rigsby, J. G., (1998), Design, fabrication, back-to-back test of 14200-hp two-pole cylindrical-rotor synchronous motor for ASD application, *IEEE Transactions on Industry Applications*, 34 (3), 526-533.

Mengoni, M., Sala, G., Zarri, L., Tani, A., Serra, G., Gritli, Y. and Duran, M., (2016), Control of a fault-tolerant quadruple three-phase induction machine for more electric aircrafts, in *IECON* 2016 42*nd Annual Conference of the IEEE Industrial Electronics Society*, Florence, Italy, 24-27 October 2016, 7.

Mese, E., Ayaz, M. and Tezcan, M. M., (2016), Design considerations of a multitasked electric machine for automotive applications, *Electric Power Systems Research*, 131, 147-158.

Meyer, A. and Lorenzen, H. W., (1979), Two-frequency heat run - a method of examination for three-phase induction motors, *IEEE Transactions on Power Apparatus and Systems*, PAS-98 (6), 2338-2347.

Nelson, R. and Krause, P., (1974), Induction machine analysis for arbitrary displacement between multiple winding sets, *IEEE Transactions on Power Apparatus and Systems*, PAS-93 (3), 841-848.

Offer, G. J., Howey, D., Contestabile, M., Clague, R. and Brandon, N. P., (2010), Comparative analysis of battery electric, hydrogen fuel cell and hybrid vehicles in a future sustainable road transport system, *Energy Policy*, 38 (1), 24-29.

Park, R. H., (1929), Two-reaction theory of synchronous machines generalized method of analysis-part I, *Transactions of the American Institute of Electrical Engineers*, 48 (3), 716-727.

Parsa, L., (2005), On advantages of multi-phase machines, in *IECON* 2005 31*st Annual Conference of IEEE Industrial Electronics Society*, 6-10 Nov. 2005, 6 pp.

Pereira, L. A., Scharlau, C. C., Pereira, L. F. A. and Haffner, S., (2012), Influence of saturation on the airgap induction waveform of five-phase induction machines, *IEEE Transactions on Energy Conversion*, 27 (1), 29-41.

Riveros, J. A., Barrero, F., Levi, E., Durán, M. J., Toral, S. and Jones, M., (2013), Variable-speed five-phase induction motor drive based on predictive torque control, *IEEE Transactions on Industrial Electronics*, 60 (8), 2957-2968.

Rockhill, A. A. and Lipo, T. A., (2010), A simplified model of a nine-phase synchronous machine using vector space decomposition, *Electric Power Components and Systems*, 38 (4), 477-489.

Rockhill, A. A. and Lipo, T. A., (2015), A generalized transformation methodology for polyphase electric machines and networks, in 2015 *IEEE International Electric Machines & Drives Conference (IEMDC)*, 10-13 May 2015, 27-34.

Rubino, S., Bojoi, R., Cavagnino, A. and Vaschetto, S., (2016), Asymmetrical twelve-phase induction starter/generator for more electric engine in aircraft, in 2016 *IEEE Energy Conversion Congress and Exposition (ECCE)*, 18-22 Sept. 2016, 1-8.

Rubino, S., Bojoi, R., Odhano, S. A. and Zanchetta, P., (2018a), Model predictive direct flux vector control of multi-three-phase induction motor drives, *IEEE Transactions on Industry Applications*, 54 (5), 4394-4404.

Rubino, S., Bojoi, R., Odhano, S. A. and Zanchetta, P., (2018b), Model predictive direct flux vector control of multi three-phase induction motor drives, *IEEE Transactions on Industry Applications*, 4394 - 4404.

Scarcella, G., Scelba, G., Cacciato, M., Spampinato, A. and Harbaugh, M. M., (2016), Vector Control Strategy for Multidirectional Power Flow in Integrated Multidrives Starter-Alternator Applications, *IEEE Transactions on Industry Applications*, 52 (6), 4816-4826.

Scuiller, F., Semail, E., Charpentier, J. and Letellier, P., (2009), Multi-criteria-based design approach of multi-phase permanent magnet low-speed synchronous machines, *IET Electric Power Applications*, 3 (2), 102-110.

Sheng, M. and Grantham, C., (1994), Synthetic loading of three-phase induction motors by magnetic field magnitude modulation, *IEE Proceedings: Electric Power Applications*, 141 (2), 95-100.

Singh, G., (2002), Multi-phase induction machine drive research—A survey, *Electric Power Systems Research*, 61 (2), 139-147.

Singh, G. K., Nam, K. and Lim, S. K., (2005), A simple indirect field-oriented control scheme for multiphase induction machine, *IEEE Transactions on Industrial Electronics*, 52 (4), 1177-1184.

Soltani, W., Szabados, B. and Hoolboom, G., (2002), A new synthetic loading for large induction machines with no feedback into the power system, *IEEE Transactions on Energy Conversion*, 17 (3), 319-324.

Subotic, I., Bodo, N. and Levi, E., (2016a), An EV drive-train with integrated fast charging capability, *IEEE Transactions on Power Electronics*, 31 (2), 1461-1471.

Subotic, I., Bodo, N. and Levi, E., (2016b), Single-phase on-board integrated battery chargers for EVs based on multiphase machines, *IEEE Transactions on Power Electronics*, 31 (9), 6511-6523.

Subotic, I., Bodo, N., Levi, E., Dumnic, B., Milicevic, D. and Katic, V., (2016c), Overview of fast on-board integrated battery chargers for electric vehicles based on multiphase machines and power electronics, *IET Electric Power Applications*, 10 (3), 217-229.

Subotic, I., Bodo, N., Levi, E. and Jones, M., (2015), Onboard integrated battery charger for EVs using an asymmetrical nine-phase machine, *IEEE Transactions on Industrial Electronics*, 62 (5), 3285-3295.

Subotic, I., Bodo, N., Levi, E., Jones, M. and Levi, V., (2016d), Isolated chargers for EVs incorporating six-phase machines, *IEEE Transactions on Industrial Electronics*, 63 (1), 653-664.

Subotic, I., Levi, E. and Bodo, N., (2014), A fast on-board integrated battery charger for EVs using an asymmetrical six-phase machine, in 2014 *IEEE Vehicle Power and Propulsion Conference (VPPC)*, 27-30 Oct. 2014, 1-6.

Sui, Y., Zheng, P., Wu, F., Yu, B., Wang, P. and Zhang, J., (2014), Research on a 20-slot/22-pole five-phase fault-tolerant pmsm used for four-wheel-drive electric vehicles, *Energies*, 7 (3).

Tada, K., Satake, A., Hashimura, K., Ogashi, Y., Masuda, H. and Oka, T., (2017), Study of full load test method for large VSDS driven by non-regenerative VSI, in 2017 *Petroleum and Chemical Industry Conference Europe (PCIC Europe)*, 16-18 May 2017, 1-9.

Taheri, A., Rahmati, A. and Kaboli, S., (2012), Efficiency improvement in DTC of six-phase induction machine by adaptive gradient descent of flux, *IEEE Transactions on Power Electronics*, 27 (3), 1552-1562.

Tani, A., Mengoni, M., Zarri, L., Serra, G. and Casadei, D., (2012), Control of multiphase induction motors with an odd number of phases under open-circuit phase faults, *IEEE Transactions on Power Electronics*, 27 (2), 565-577.

Tani, A., Serra, G., Mengoni, M., Zarri, L., Rini, G. and Casadei, D., (2013), Dynamic stator current sharing in quadruple three-phase induction motor drives, in *IECON* 2013 - 39*th Annual Conference of the IEEE Industrial Electronics Society*, 10-13 Nov. 2013, 5173-5178.

Tani, A., Zarri, L., Mengoni, M., Serra, G. and Casadei, D., (2014), Detection and localization of high resistance connections in quadruple three-phase induction motor drives, in 2014 *International Conference on Electrical Machines (ICEM)*, 2-5 Sept. 2014, 2094-2100.

Tenconi, A., Rubino, S. and Bojoi, R., (2018), Model predictive control for multiphase motor drives – a technology status review, in 2018 *International Power Electronics Conference (IPEC-Niigata 2018 -ECCE Asia)*, 20-24 May 2018, 732-739.

Tessarolo, A., (2009a), On the modeling of poly-phase electric machines through Vector-Space Decomposition: Numeric application cases, in 2009 *International Conference on Power Engineering, Energy and Electrical Drives*, 18-20 March 2009, 524-528.

Tessarolo, A., (2009b), On the modeling of poly-phase electric machines through Vector-Space Decomposition: Theoretical considerations, in 2009 *International Conference on Power Engineering, Energy and Electrical Drives*, 18-20 March 2009, 519-523.

Tessarolo, A., (2010), Experimental performance assessent of multiphase alternators supplying multiple AC/DC power converters, in 5*th IET International Conference on Power Electronics, Machines and Drives (PEMD* 2010*)*, 19-21 April 2010, 1-6.

Trout, N., (1935), A three-phase back-to-back alternator test, *Students' Quarterly Journal*, 5 (20), 194-197.

Wang, J., Qu, R. and Liu, Y., (2013), Comparison study of superconducting generators with multiphase armature windings for large-scale direct-drive wind turbines, *IEEE Transactions on Applied Superconductivity*, 23 (3), 5201005-5201005.

Wang, J., Qu, R., Liu, Y. and Li, J., (2014), Study of multiphase superconducting wind generators with fractional-slot concentrated windings, *IEEE Transactions on Applied Superconductivity*, 24 (3), 1-6.

Wang, K., Zhu, Z. Q. and Ombach, G., (2014), Torque improvement of five-phase surface-mounted permanent magnet machine using third-order harmonic, *IEEE Transactions on Energy Conversion*, 29 (3), 735-747.

Ward, E. E. and Härer, H., (1969), Preliminary investigation of an invertor-fed 5-phase induction motor, *Proceedings of the Institution of Electrical Engineers*, 116 (6), 980-984.

Xue, X., Zhao, W., Zhu, J., Liu, G., Zhu, X. and Cheng, M., (2013), Design of five-phase modular flux-switching permanent-magnet machines for high reliability applications, *IEEE Transactions on Magnetics*, 49 (7), 3941-3944.

Yepes, A. G., Malvar, J., Vidal, A., López, O. and Doval-Gandoy, J., (2015), Current harmonics compensation based on multiresonant control in synchronous frames for symmetrical-phase machines', *IEEE Transactions on Industrial Electronics*, 62 (5), 2708-2720.

Zabaleta, M., Jones, M. and Levi, E., (2017), A tuning procedure for the current regulator loops in multiple three-phase permanent magnet machines with low switching to fundamental frequency ratio, in 2017 19*th European Conference on Power Electronics and Applications (EPE'*17 *ECCE Europe)*, 11-14 Sept. 2017, P.1-P.10.

Zabaleta, M., Levi, E. and Jones, M., (2018), A novel synthetic loading method for multiple three-phase winding electric machines, *IEEE Transactions on Energy Conversion*, 34(1), 70-78.

Zarri, L., Mengoni, M., Gritli, Y., Tani, A., Filippetti, F., Serra, G. and Casadei, D., (2011), Behavior of multiphase induction machines with unbalanced stator windings, in 8*th IEEE Symposium on Diagnostics for Electrical Machines, Power Electronics & Drives*, 5-8 Sept. 2011, 84-91.

Zhao, Y. and Lipo, T. A., (1995), Space vector PWM control of dual three-phase induction machine using vector space decomposition, *IEEE Transactions on Industry Applications*, 31 (5), 1100-1109.

Zheng, L., Fletcher, J. E., Williams, B. W. and He, X., (2011), A novel direct torque control scheme for a sensorless five-phase induction motor drive, *IEEE Transactions on Industrial Electronics*, 58 (2), 503-513.

Zheng, P., Wu, F., Lei, Y., Sui, Y. and Yu, B., (2013), Investigation of a novel 24-slot/14-pole six-phase fault-tolerant modular permanent-magnet in-wheel motor for electric vehicles, *Energies*, 6 (10), 4980-5002.

Zhu, Z. Q., Thomas, A. S., Chen, J. T. and Jewell, G. W., (2009), Cogging torque in flux-switching permanent magnet machines, *IEEE Transactions on Magnetics*, 45 (10), 4708-4711.

Zoric, I., (2018), Multiple three-phase induction generators for wind energy conversion systems, *PhD Thesis*, Liverpool John Moores University, Liverpool, U.K.

Zoric, I., Jones, M. and Levi, E., (2018), Arbitrary power sharing among three-phase winding sets of multiphase machines, *IEEE Transactions on Industrial Electronics*, 65 (2), 1128-1139

APPENDIX A

DERIVATION AND MATLAB CODES

This appendix focuses on the derivation of current sharing strategy coefficients by finding the correlations between the MS and VSD currents. The appendix starts with the derivation for the asymmetrical fifteen-phase machines case (section A.1). Then the final correlation results between the MS and VSD for twelve-phase and eighteen-phase machines are provided in sections A.2 and A.3. Although the correlations are illustrated for asymmetrical configuration, exactly the same correlations can be obtained for the symmetrical configuration. Therefore, the correlations are valid for both configurations. Finally, in section A.4 Matlab/Simulink model of the multiphase machine in phase variables reference frame is provided.

A.1 ASYMMETRICAL FIFTEEN-PHASE MS AND VSD CORRELATIONS

The derivation of an asymmetrical fifteen-phase machine's power sharing strategy is illustrated next. To find the links between the MS and VSD modelling approach, the MS transformation matrices for each winding set should be defined first. The MS transformation matrices are defined with respect to the first winding sets. For the fifteen-phase machine with asymmetrical configuration and five three-phase winding sets, the transformation matrices are as follows:

$$\left[C_{3,i}\right]=\sqrt{\frac{2}{3}}\begin{bmatrix}\cos(\delta) & \cos(\delta+2\pi/3) & \cos(\delta+4\pi/3)\\ \sin(\delta) & \sin(\delta+2\pi/3) & \sin(\delta+4\pi/3)\\ 1/\sqrt{2} & 1/\sqrt{2} & 1/\sqrt{2}\end{bmatrix} \tag{A.1}$$

where δ represents the angular displacement between i-th winding set with respect to the first winding set. For asymmetrical fifteen-phase machine, δ can be expressed as follows:

$$\delta \in \{0 \quad \alpha \quad 2\alpha \quad 3\alpha \quad 4\alpha\} \tag{A.2}$$

where $\alpha = \pi/15$. By following the steps introduced in Chapter 4 for current sharing strategy for the asymmetrical nine-phase machine, the correlations between the winding set individual currents α_1, β_1, o_1, α_2, β_2, o_2, …, α_5, β_5, o_5 and the decoupled currents α, β, x_1, y_1, x_2, y_2, …, x_4, y_4, 0_1, 0_2, …, 0_5, can be found. The VSD transformation matrix for fifteen-phase machines with five winding sets is defined based on (4.36) and it can be expressed as in the following equation:

$$[VSD]=\sqrt{\frac{2}{15}}\left[\begin{array}{c|ccc|ccc|ccc|ccc|ccc} & a_1 & b_1 & c_1 & a_2 & b_2 & c_2 & a_3 & b_3 & c_3 & a_4 & b_4 & c_4 & a_5 & b_5 & c_5 \\ \hline \alpha & \multicolumn{15}{c}{\cos([\theta_s])} \\ \beta & \multicolumn{15}{c}{\sin([\theta_s])} \\ \hline x_1 & \multicolumn{15}{c}{\cos(5\cdot[\theta_s])} \\ y_1 & \multicolumn{15}{c}{\sin(5\cdot[\theta_s])} \\ x_2 & \multicolumn{15}{c}{\cos(7\cdot[\theta_s])} \\ y_2 & \multicolumn{15}{c}{\sin(7\cdot[\theta_s])} \\ x_3 & \multicolumn{15}{c}{\cos(11\cdot[\theta_s])} \\ y_3 & \multicolumn{15}{c}{\sin(11\cdot[\theta_s])} \\ x_4 & \multicolumn{15}{c}{\cos(13\cdot[\theta_s])} \\ y_4 & \multicolumn{15}{c}{\sin(13\cdot[\theta_s])} \\ \hline 0_1 & \sqrt{\frac{5}{2}} & \sqrt{\frac{5}{2}} & \sqrt{\frac{5}{2}} & 0 & 0 & 0 & 0 & 0 & 0 & 0 & 0 & 0 & 0 & 0 & 0 \\ 0_2 & 0 & 0 & 0 & \sqrt{\frac{5}{2}} & \sqrt{\frac{5}{2}} & \sqrt{\frac{5}{2}} & 0 & 0 & 0 & 0 & 0 & 0 & 0 & 0 & 0 \\ 0_3 & 0 & 0 & 0 & 0 & 0 & 0 & \sqrt{\frac{5}{2}} & \sqrt{\frac{5}{2}} & \sqrt{\frac{5}{2}} & 0 & 0 & 0 & 0 & 0 & 0 \\ 0_4 & 0 & 0 & 0 & 0 & 0 & 0 & 0 & 0 & 0 & \sqrt{\frac{5}{2}} & \sqrt{\frac{5}{2}} & \sqrt{\frac{5}{2}} & 0 & 0 & 0 \\ 0_5 & 0 & 0 & 0 & 0 & 0 & 0 & 0 & 0 & 0 & 0 & 0 & 0 & \sqrt{\frac{5}{2}} & \sqrt{\frac{5}{2}} & \sqrt{\frac{5}{2}} \end{array}\right] \tag{A.3}$$

where $[\theta_s]$ is the phase displacement angle between the stator windings and it can be expressed as:

$$[\theta_s]=\frac{\pi}{15}[0 \quad 10 \quad 20 \mid 1 \quad 11 \quad 21 \mid 2 \quad 12 \quad 22 \mid 3 \quad 13 \quad 23 \mid 4 \quad 14 \quad 24] \tag{A.4}$$

The contribution of the winding sets' individual currents to the total decoupled (VSD) current can be found by applying the Clarke's transformation for each winding set as in the following equation:

$$\begin{bmatrix} i_{a1} \\ i_{b1} \\ i_{c1} \end{bmatrix}=\left[C_{3,1}\right]^{-1}\begin{bmatrix} i_{\alpha 1} \\ i_{\beta 1} \\ i_{o1} \end{bmatrix} \qquad \begin{bmatrix} i_{a2} \\ i_{b2} \\ i_{c2} \end{bmatrix}=\left[C_{3,2}\right]^{-1}\begin{bmatrix} i_{\alpha 2} \\ i_{\beta 2} \\ i_{o2} \end{bmatrix} \quad \cdots \quad \begin{bmatrix} i_{a5} \\ i_{b5} \\ i_{c5} \end{bmatrix}=\left[C_{3,5}\right]^{-1}\begin{bmatrix} i_{\alpha 5} \\ i_{\beta 5} \\ i_{o5} \end{bmatrix} \tag{A.5}$$

The currents in the phase variables reference frame are expressed by the following matrix:

$$\left[i_{ph15}\right]=\left[i_{a1} \quad i_{b1} \quad i_{c1} \mid i_{a2} \quad i_{b2} \quad i_{c2} \mid i_{a3} \quad i_{b3} \quad i_{c3} \mid i_{a4} \quad i_{b4} \quad i_{c4} \mid i_{a5} \quad i_{b5} \quad i_{c5}\right]^T \tag{A.6}$$

To find the relationships between the currents in the two different reference frames, the stationary reference frame currents of the individual winding sets (A.5) are substituted into the phase variable currents (A.6), as in (A.7) (equation provided on top of the next page).

The mapping of the stationary reference frame currents of the individual winding sets into the phase variables currents is defined by the matrix in (A.7). This equation can be utilised also for the symmetrical fifteen-phase machines. The machine type, induction or synchronous machine, does not matter. The same method to find the correlations between the MS currents of the individual winding sets and the VSD or Clarke's currents provides the same correlations, as illustrated in Chapter 4. In other words, the decoupling transformations for the different machine types are the same, however the difference appears in the control part.

$$\left[i_{ph15}\right]=\begin{bmatrix} i_{a1}\\ i_{b1}\\ i_{c1}\\ i_{a2}\\ i_{b2}\\ i_{c2}\\ i_{a3}\\ i_{b3}\\ i_{c3}\\ i_{a4}\\ i_{b4}\\ i_{c4}\\ i_{a5}\\ i_{b5}\\ i_{c5} \end{bmatrix}=\begin{bmatrix} \left[\mathrm{C}_{3,1}\right]^{-1} & [0]_{3\times3} & [0]_{3\times3} & [0]_{3\times3} & [0]_{3\times3}\\ [0]_{3\times3} & \left[\mathrm{C}_{3,2}\right]^{-1} & [0]_{3\times3} & [0]_{3\times3} & [0]_{3\times3}\\ [0]_{3\times3} & [0]_{3\times3} & \left[\mathrm{C}_{3,3}\right]^{-1} & [0]_{3\times3} & [0]_{3\times3}\\ [0]_{3\times3} & [0]_{3\times3} & [0]_{3\times3} & \left[\mathrm{C}_{3,4}\right]^{-1} & [0]_{3\times3}\\ [0]_{3\times3} & [0]_{3\times3} & [0]_{3\times3} & [0]_{3\times3} & \left[\mathrm{C}_{3,5}\right]^{-1} \end{bmatrix}\cdot\begin{bmatrix} i_{\alpha1}\\ i_{\beta1}\\ i_{o1}\\ i_{\alpha2}\\ i_{\beta2}\\ i_{o2}\\ i_{\alpha3}\\ i_{\beta3}\\ i_{o3}\\ i_{\alpha4}\\ i_{\beta4}\\ i_{o4}\\ i_{\alpha5}\\ i_{\beta5}\\ i_{o5} \end{bmatrix} \tag{A.7}$$

In order to control the amplitude and direction of each winding set independently, the correlations between the MS currents of the winding sets (α_1, β_1, o_1, α_2, β_2, o_2, …, α_5, β_5, o_5) with the decoupled currents (α, β, x_1, y_1, x_2, y_2, …, x_4, y_4, 0_1, 0_2, …, 0_5), should be found. The correlations are found by multiplying (A.7) from the left by VSD transformation for the fifteen-phase machine (A.3). The final result is expressed by the following matrix:

$$\left[i_{VSD15}\right]=\left[\begin{array}{c|c} i_{\alpha} & \frac{1}{\sqrt{5}}\left(i_{\alpha1}+i_{\alpha2}+i_{\alpha3}+i_{\alpha4}+i_{\alpha5}\right)\\ i_{\beta} & \frac{1}{\sqrt{5}}\left(i_{\beta1}+i_{\beta2}+i_{\beta3}+i_{\beta4}+i_{\beta5}\right)\\ \hline i_{x1} & 0.44721i_{\alpha1}+0.13819\left(i_{\alpha2}+i_{\alpha5}\right)-0.36180(i_{\alpha3}+i_{\alpha4})+0.42532(i_{\beta2}-i_{\beta5})+0.26286(i_{\beta3}-i_{\beta4})\\ i_{y1} & 0.42532\left(i_{\alpha2}-i_{\alpha5}\right)+0.26286(i_{\alpha3}-i_{\alpha4})-0.44721i_{\beta1}-0.13819(i_{\beta2}+i_{\beta5})+0.36180(i_{\beta3}+i_{\beta4})\\ i_{x2} & 0.44721i_{\alpha1}+0.13819\left(i_{\alpha2}+i_{\alpha5}\right)-0.36180(i_{\alpha3}+i_{\alpha4})-0.42532(i_{\beta2}-i_{\beta5})-0.26286(i_{\beta3}-i_{\beta4})\\ i_{y2} & 0.42532\left(i_{\alpha2}-i_{\alpha5}\right)+0.26286(i_{\alpha3}-i_{\alpha4})+0.44721i_{\beta1}+0.13819(i_{\beta2}+i_{\beta5})-0.36180(i_{\beta3}+i_{\beta4})\\ i_{x3} & 0.44721i_{\alpha1}-0.36180\left(i_{\alpha2}+i_{\alpha5}\right)+0.13819(i_{\alpha3}+i_{\alpha4})+0.26286(i_{\beta2}-i_{\beta5})-0.42532(i_{\beta3}-i_{\beta4})\\ i_{y3} & 0.26286\left(i_{\alpha2}-i_{\alpha5}\right)-0.42532(i_{\alpha3}-i_{\alpha4})-0.44721i_{\beta1}+0.36180(i_{\beta2}+i_{\beta5})-0.13819(i_{\beta3}+i_{\beta4})\\ i_{x4} & 0.44721i_{\alpha1}-0.36180\left(i_{\alpha2}+i_{\alpha5}\right)+0.13819(i_{\alpha3}+i_{\alpha4})-0.26286(i_{\beta2}-i_{\beta5})+0.42532(i_{\beta3}-i_{\beta4})\\ i_{y4} & 0.26286\left(i_{\alpha2}-i_{\alpha5}\right)-0.42532(i_{\alpha3}-i_{\alpha4})+0.44721i_{\beta1}-0.36180(i_{\beta2}+i_{\beta5})+0.13819(i_{\beta3}+i_{\beta4})\\ \hline i_{01} & i_{o1}\\ i_{02} & i_{o2}\\ i_{03} & i_{o3}\\ i_{04} & i_{o4}\\ i_{05} & i_{o5} \end{array}\right] \tag{A.8}$$

From (A.8), the mapping of the individual winding sets α_i-β_i currents into the VSD currents is defined. The decoupled currents can be defined in space vectors (complex) form as:

$$\begin{aligned}
\bar{i}_{\alpha\beta} &= i_\alpha + ji_\beta \quad = I_{\alpha\beta}\angle\varphi_{\alpha\beta} \\
\bar{i}_{xy1} &= i_{x1} + ji_{y1} \;= I_{xy1}\angle\varphi_{xy1} \\
\bar{i}_{xy2} &= i_{x2} + ji_{y2} = I_{xy2}\angle\varphi_{xy2} \\
\bar{i}_{xy3} &= i_{x3} + ji_{y3} = I_{xy3}\angle\varphi_{xy3} \\
\bar{i}_{xy4} &= i_{x4} + ji_{y4} = I_{xy4}\angle\varphi_{xy4}
\end{aligned} \tag{A.9}$$

The current space vectors of the individual winding sets are represented by the following equations:

$$\begin{aligned}
\bar{i}_{\alpha\beta1} &= i_{\alpha1} + ji_{\beta1} = I_{\alpha\beta1}\angle\varphi_{\alpha\beta1} \\
\bar{i}_{\alpha\beta2} &= i_{\alpha2} + ji_{\beta2} = I_{\alpha\beta2}\angle\varphi_{\alpha\beta2} \\
\bar{i}_{\alpha\beta3} &= i_{\alpha3} + ji_{\beta3} = I_{\alpha\beta3}\angle\varphi_{\alpha\beta3} \\
\bar{i}_{\alpha\beta4} &= i_{\alpha4} + ji_{\beta4} = I_{\alpha\beta4}\angle\varphi_{\alpha\beta4} \\
\bar{i}_{\alpha\beta5} &= i_{\alpha5} + ji_{\beta5} = I_{\alpha\beta5}\angle\varphi_{\alpha\beta5}
\end{aligned} \tag{A.10}$$

The current sharing coefficients K_i are introduced as a percentage with which each winding set contributes to the total $i_{\alpha\beta}$ current. Hence, the following equation should always be satisfied:

$$K_1 + K_2 + K_3 + K_4 + K_5 = 1 \tag{A.11}$$

By using current sharing coefficients and the notation introduced in (A.9) and (A.10), and after some manipulation and simplification, (A.8) can be expressed as:

$$\bar{i}_{\alpha\beta} = (K_1 + K_2 + K_3 + K_4 + K_5)\bar{i}_{\alpha\beta} \tag{A.12}$$

$$\bar{i}_{xy1} = \left(K_1 + K_2 e^{j\frac{4\pi}{10}} + K_3 e^{j\frac{8\pi}{10}} + K_4 e^{j\frac{12\pi}{10}} + K_5 e^{j\frac{16\pi}{10}}\right)\bar{i}^*_{\alpha\beta} \tag{A.13}$$

$$\bar{i}_{xy2} = \left(K_1 + K_2 e^{j\frac{4\pi}{10}} + K_3 e^{j\frac{8\pi}{10}} + K_4 e^{j\frac{12\pi}{10}} + K_5 e^{j\frac{16\pi}{10}}\right)\bar{i}_{\alpha\beta} \tag{A.14}$$

$$\bar{i}_{xy3} = \left(K_1 + K_2 e^{j\frac{8\pi}{10}} + K_3 e^{j\frac{16\pi}{10}} + K_4 e^{j\frac{4\pi}{10}} + K_5 e^{j\frac{12\pi}{10}}\right)\bar{i}^*_{\alpha\beta} \tag{A.15}$$

$$\bar{i}_{xy4} = \left(K_1 + K_2 e^{j\frac{8\pi}{10}} + K_3 e^{j\frac{16\pi}{10}} + K_4 e^{j\frac{4\pi}{10}} + K_5 e^{j\frac{12\pi}{10}}\right)\bar{i}_{\alpha\beta} \tag{A.16}$$

The sharing equations (A.12) – (A.16) are valid in the stationary reference frame as mentioned earlier. The first and the third *x-y* space vectors are rotating in the anti-synchronous reference frame as shown in (A.13) and (A.15). The different reference frames involved in the power sharing strategy of the fifteen-phase machine are illustrated in Fig. A.1. The remaining subspaces are rotating in the same

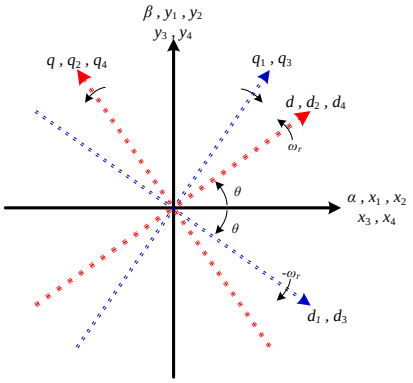

Fig. A.1: Illustration of the reference frames involved in the current sharing strategy of fifteen-phase machines.

direction as the *α-β* current space vector. Since the control of the machine is implemented in *d-q* reference frame and the sharing coefficients are a gain to the *α-β* space vector, the sharing coefficients can be multiplied by the *d-q* space vector of the machine.

Therefore, by using derived links and current sharing coefficients, by changing the current sharing coefficients K_i the amplitude of the individual winding sets' currents becomes controllable even with VSD approach. By changing the current sharing coefficients to any value, within the limit of the rated current, the power of each winding set is controlled. To change the winding set mode of operation between motoring and generation, a simple multiplication of the K_i with –1 will make the winding set operating in generation mode.

Finally, if fifteen-phase machine is aimed to be used for efficient power sharing, where K_{di} and K_{qi} currents are not shared in the same way (as introduced in Chapter 5), equation (A.8) becomes:

$$i_{d1} = \left(0.44721K_{d1} + 0.13819\left(K_{d2} + K_{d5}\right) - 0.36180(K_{d3} + K_{d4})\right)i_d + \left(0.42532(K_{q2} - K_{q5}) + 0.26286(K_{q3} - K_{q4})\right)i_q \quad \text{(A.17)}$$

$$i_{q1} = \left(0.42532\left(K_{d2} - K_{d5}\right) + 0.26286(K_{d3} - K_{d4})\right)i_d - \left(0.44721K_{q1} - 0.13819(K_{q2} + K_{q5}) + 0.36180(K_{q3} + K_{q4})\right)i_q \quad \text{(A.18)}$$

$$i_{d2} = \left(0.44721K_{d1} + 0.13819\left(K_{d2} + K_{d5}\right) - 0.36180(K_{d3} + K_{d4})\right)i_d - \left(0.42532(K_{q2} - K_{q5}) + 0.26286(K_{q3} - K_{q4})\right)i_q \quad \text{(A.19)}$$

$$i_{q2} = \left(0.42532\left(K_{d2} - K_{d5}\right) + 0.26286(K_{d3} - K_{d4})\right)i_d + \left(0.44721K_{q1} + 0.13819(K_{q2} + K_{q5}) - 0.36180(K_{q3} + K_{q4})\right)i_q \quad \text{(A.20)}$$

$$i_{d3} = \left(0.44721K_{d1} - 0.36180\left(K_{d2} + K_{d5}\right) + 0.13819(K_{d3} + K_{d4})\right)i_d + \left(0.26286(K_{q2} - K_{q5}) - 0.42532(K_{q3} - K_{q4})\right)i_q \quad \text{(A.21)}$$

$$i_{q3} = \left(0.26286\left(K_{d2} - K_{d5}\right) + 0.42532(K_{d3} - K_{d4})\right)i_d - \left(0.44721K_{q1} - 0.36180(K_{q2} + K_{q5}) + 0.13819(K_{q3} + K_{q4})\right)i_q \quad \text{(A.22)}$$

$$i_{d4} = \left(0.44721K_{d1} - 0.36180\left(K_{d2} + K_{d5}\right) + 0.13819(K_{d3} + K_{d4})\right)i_d - \left(0.26286(K_{q2} - K_{q5}) - 0.42532(K_{q3} - K_{q4})\right)i_q \quad \text{(A.23)}$$

$$i_{q4} = \left(0.26286\left(K_{d2} - K_{d5}\right) - 0.42532(K_{d3} - K_{d4})\right)i_d + \left(0.44721K_{q1} - 0.36180(K_{q2} + K_{q5}) + 0.13819(K_{q3} + K_{q4})\right)i_q \quad \text{(A.24)}$$

A.2 SYMMETRICAL AND ASYMMETRICAL TWELVE-PHASE MACHINE MS AND VSD CORRELATIONS

The same derivation approach can be repeated for twelve-phase machines. The final obtained results are illustrated in the following equation (note that $i_{0i} = i_{oi}$, hence omitted below):

$$\left[i_{\mathrm{VSD12}}\right]=\begin{bmatrix} i_{\alpha} \\ i_{\beta} \\ i_{x1} \\ i_{y1} \\ i_{x2} \\ i_{y2} \\ i_{x3} \\ i_{y3} \end{bmatrix}=\left[\mathrm{VSD}_{12}\right]\cdot\left[i_{ph12}\right]=\begin{bmatrix} \frac{1}{2}\left(i_{\alpha1}+i_{\alpha2}+i_{\alpha3}+i_{\alpha4}\right) \\ \frac{1}{2}\left(i_{\beta1}+i_{\beta2}+i_{\beta3}+i_{\beta4}\right) \\ \frac{1}{2}\left(i_{\alpha1}-i_{\alpha3}+i_{\beta2}-i_{\beta4}\right) \\ \frac{1}{2}\left(i_{\alpha2}-i_{\alpha4}-i_{\beta1}+i_{\beta3}\right) \\ \frac{1}{2}\left(i_{\alpha1}-i_{\alpha3}-i_{\beta2}+i_{\beta4}\right) \\ \frac{1}{2}\left(i_{\alpha2}-i_{\alpha4}+i_{\beta1}-i_{\beta3}\right) \\ \frac{1}{2}\left(i_{\alpha1}-i_{\alpha2}+i_{\alpha3}-i_{\alpha4}\right) \\ \frac{1}{2}\left(-i_{\beta1}+i_{\beta2}-i_{\beta3}+i_{\beta4}\right) \end{bmatrix} \tag{A.25}$$

A.3 SYMMETRICAL AND ASYMMETRICAL EIGHTEEN-PHASE MACHINE MS AND VSD CORRELATIONS

The final correlations between the MS and VSD of eighteen phase machines are presented in the following matrix (again, $i_{0i} = i_{oi}$, hence omitted below):

$$\left[i_{\mathrm{VSD18}}\right]=\begin{bmatrix} i_{\alpha} \\ i_{\beta} \\ i_{x1} \\ i_{y1} \\ i_{x2} \\ i_{y2} \\ i_{x3} \\ i_{y3} \\ i_{x4} \\ i_{y4} \\ i_{x5} \\ i_{y5} \end{bmatrix}=\begin{bmatrix} \frac{1}{\sqrt{6}}\left(i_{\alpha1}+i_{\alpha2}+i_{\alpha3}+i_{\alpha4}+i_{\alpha5}+i_{\alpha6}\right) \\ \frac{1}{\sqrt{6}}\left(i_{\beta1}+i_{\beta2}+i_{\beta3}+i_{\beta4}+i_{\beta5}+i_{\beta6}\right) \\ \frac{\sqrt{3}\left(2i_{\alpha1}+i_{\alpha2}-i_{\alpha3}-2i_{\alpha4}-i_{\alpha5}+i_{\alpha6}\right)+3\left(i_{\beta2}+i_{\beta3}-i_{\beta5}-i_{\beta6}\right)}{6\sqrt{2}} \\ \frac{-\sqrt{3}\left(2i_{\beta1}+i_{\beta2}-i_{\beta3}-2i_{\beta4}-i_{\beta5}+i_{\beta6}\right)+3\left(i_{\alpha2}+i_{\alpha3}-i_{\alpha5}-i_{\alpha6}\right)}{6\sqrt{2}} \\ \frac{\sqrt{3}\left(2i_{\alpha1}+i_{\alpha2}-i_{\alpha3}-2i_{\alpha4}-i_{\alpha5}+i_{\alpha6}\right)-3\left(i_{\beta2}+i_{\beta3}-i_{\beta5}-i_{\beta6}\right)}{6\sqrt{2}} \\ \frac{\sqrt{3}\left(2i_{\beta1}+i_{\beta2}-i_{\beta3}-2i_{\beta4}-i_{\beta5}+i_{\beta6}\right)+3\left(i_{\alpha2}+i_{\alpha3}-i_{\alpha5}-i_{\alpha6}\right)}{6\sqrt{2}} \\ \frac{i_{\alpha1}}{\sqrt{6}}-\frac{\sqrt{3}\left(i_{\alpha2}+i_{\alpha3}-2i_{\alpha4}+i_{\alpha5}+i_{\alpha6}\right)-3\left(i_{\beta2}-i_{\beta3}+i_{\beta5}-i_{\beta6}\right)}{6\sqrt{2}} \\ \frac{\sqrt{3}\left(-2i_{\beta1}+i_{\beta2}+i_{\beta3}-2i_{\beta4}+i_{\beta5}+i_{\beta6}\right)+3\left(i_{\alpha2}-i_{\alpha3}+i_{\alpha5}-i_{\alpha6}\right)}{6\sqrt{2}} \\ \frac{i_{\alpha1}}{\sqrt{6}}-\frac{\sqrt{3}\left(i_{\alpha2}+i_{\alpha3}-2i_{\alpha4}+i_{\alpha5}+i_{\alpha6}\right)+3\left(i_{\beta2}-i_{\beta3}+i_{\beta5}-i_{\beta6}\right)}{6\sqrt{2}} \\ \frac{\sqrt{3}\left(2i_{\beta1}-i_{\beta2}-i_{\beta3}+2i_{\beta4}-i_{\beta5}-i_{\beta6}\right)+3\left(i_{\alpha2}-i_{\alpha3}+i_{\alpha5}-i_{\alpha6}\right)}{6\sqrt{2}} \\ \frac{1}{\sqrt{6}}\left(i_{\alpha1}-i_{\alpha2}+i_{\alpha3}-i_{\alpha4}+i_{\alpha5}-i_{\alpha6}\right) \\ \frac{1}{\sqrt{6}}\left(-i_{\beta1}+i_{\beta2}-i_{\beta3}+i_{\beta4}-i_{\beta5}+i_{\beta6}\right) \end{bmatrix} \tag{A.26}$$

A.4 MATLAB AND SIMULINK CODE

The Simulink model of a multiphase machine using the phase variables (PV) reference frame is illustrated in Fig. A.2. The Matlab code of the PV block from Fig. A.2 is shown in the text box below. Note that this code is generic and applicable for any multiphase induction machine, only the phase angles should be readjusted. Another, less general, machine model implementation but showing full developed form of all matrices, is shown in the text box on the next page. Symmetrical nine-phase induction machine is used as an example. The full Simulink model of current sharing algorithm for nine-phase

```
function [Currents, Te]=PV(v, Po, S, i, Lls, Llr, Lm, Rs, Rr, P, ns, nr)

Lm=(2/ns)*Lm;

thetas = (pi/ns).*([0 17 16 12 11 10 6 5 4]); % for asymmetrical nine-phase induction machine
thetar = (2*pi/nr).*(0:1:nr-1);               % for asymmetrical nine-phase induction machine

% Lsr/Lrs
Lsr= Lm.*cos(repmat(Po.*ones(ns,1)+thetas', 1, nr) - repmat(thetar, ns, 1));
Lrs=Lsr';

% dLsr/dLrs
dLsr=-S*Lm.*sin(repmat(Po.*ones(ns,1)+thetas', 1, nr) - repmat(thetar, ns, 1));
dLrs=dLsr';

% Lss/Lsr
Lss=Lm.*cos(repmat(thetas', 1, ns) - repmat(thetas, ns, 1)) + Lls.*diag(ones(ns,1));
Lrr=Lm.*cos(repmat(thetar', 1, nr) - repmat(thetar, nr, 1)) + Llr.*diag(ones(nr,1));

% dLsrdtheta
dLsrdth=-Lm.*sin(repmat(Po.*ones(ns,1)+thetas', 1, nr) - repmat(thetar, ns, 1));

% Rss/Rrr
Rss=Rs.*diag(ones(ns,1));
Rrr=Rr.*diag(ones(nr,1));

L=inv([Lss, Lsr; Lrs, Lrr]);
RL=[Rss, dLsr; dLrs, Rrr];
Currents=-L*(-[v; zeros(nr,1)]+ RL*i);
SC=i(1:ns);
RC=i(ns+1:end);
Te=P.*(SC'*dLsrdth*RC);
```

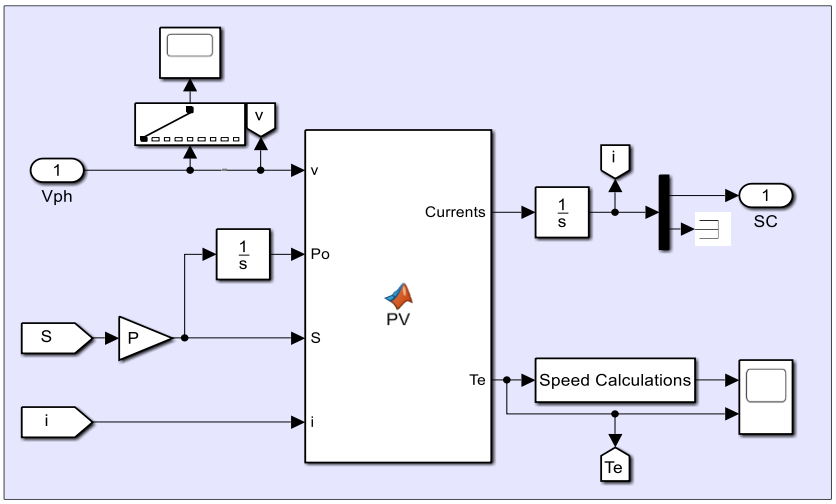

Fig. A.2: Simulink model for a generalised multiphase induction machine model using phase variables reference frame.

case is illustrated in Fig. A.3. The simulation schematic illustrated in Fig. A.3 illustrates the power and current sharing scheme for a nine-phase induction machine with multiple neutral points.

```
function [Currents, Te]=PV(v, Po, S, i, Lls, Llr, Lm, Rs, Rr, P)

M=(2/9)*Lm;
a=(2*pi/9);

%% Inducatance Matrices
Lsr=[M*cos(Po),       M*cos(Po-(8*a)), M*cos(Po-(7*a)), M*cos(Po-(6*a)), M*cos(Po-(5*a)), M*cos(Po-(4*a)), M*cos(Po-(3*a)), M*cos(Po-(2*a)), M*cos(Po-(a));
     M*cos(Po-(a)),   M*cos(Po),       M*cos(Po-(8*a)), M*cos(Po-(7*a)), M*cos(Po-(6*a)), M*cos(Po-(5*a)), M*cos(Po-(4*a)), M*cos(Po-(3*a)), M*cos(Po-(2*a));
     M*cos(Po-(2*a)), M*cos(Po-(a)),   M*cos(Po),       M*cos(Po-(8*a)), M*cos(Po-(7*a)), M*cos(Po-(6*a)), M*cos(Po-(5*a)), M*cos(Po-(4*a)), M*cos(Po-(3*a));
     M*cos(Po-(3*a)), M*cos(Po-(2*a)), M*cos(Po-(a)),   M*cos(Po),       M*cos(Po-(8*a)), M*cos(Po-(7*a)), M*cos(Po-(6*a)), M*cos(Po-(5*a)), M*cos(Po-(4*a));
     M*cos(Po-(4*a)), M*cos(Po-(3*a)), M*cos(Po-(2*a)), M*cos(Po-(a)),   M*cos(Po),       M*cos(Po-(8*a)), M*cos(Po-(7*a)), M*cos(Po-(6*a)), M*cos(Po-(5*a));
     M*cos(Po-(5*a)), M*cos(Po-(4*a)), M*cos(Po-(3*a)), M*cos(Po-(2*a)), M*cos(Po-(a)),   M*cos(Po),       M*cos(Po-(8*a)), M*cos(Po-(7*a)), M*cos(Po-(6*a));
     M*cos(Po-(6*a)), M*cos(Po-(5*a)), M*cos(Po-(4*a)), M*cos(Po-(3*a)), M*cos(Po-(2*a)), M*cos(Po-(a)),   M*cos(Po),       M*cos(Po-(8*a)), M*cos(Po-(7*a));
     M*cos(Po-(7*a)), M*cos(Po-(6*a)), M*cos(Po-(5*a)), M*cos(Po-(4*a)), M*cos(Po-(3*a)), M*cos(Po-(2*a)), M*cos(Po-(a)),   M*cos(Po),       M*cos(Po-(8*a));
     M*cos(Po-(8*a)), M*cos(Po-(7*a)), M*cos(Po-(6*a)), M*cos(Po-(5*a)), M*cos(Po-(4*a)), M*cos(Po-(3*a)), M*cos(Po-(2*a)), M*cos(Po-(a)),   M*cos(Po)];


Lrs=Lsr';

dLsr=-1.*[S*M*sin(Po),      S*M*sin(Po-(8*a)), S*M*sin(Po-(7*a)), S*M*sin(Po-(6*a)), S*M*sin(Po-(5*a)), S*M*sin(Po-(4*a)), S*M*sin(Po-(3*a)), S*M*sin(Po-(2*a)), S*M*sin(Po-(a));
        S*M*sin(Po-(a)),   S*M*sin(Po),      S*M*sin(Po-(8*a)), S*M*sin(Po-(7*a)), S*M*sin(Po-(6*a)), S*M*sin(Po-(5*a)), S*M*sin(Po-(4*a)), S*M*sin(Po-(3*a)), S*M*sin(Po-(2*a));
        S*M*sin(Po-(2*a)), S*M*sin(Po-(a)),   S*M*sin(Po),      S*M*sin(Po-(8*a)), S*M*sin(Po-(7*a)), S*M*sin(Po-(6*a)), S*M*sin(Po-(5*a)), S*M*sin(Po-(4*a)), S*M*sin(Po-(3*a));
        S*M*sin(Po-(3*a)), S*M*sin(Po-(2*a)), S*M*sin(Po-(a)),   S*M*sin(Po),      S*M*sin(Po-(8*a)), S*M*sin(Po-(7*a)), S*M*sin(Po-(6*a)), S*M*sin(Po-(5*a)), S*M*sin(Po-(4*a));
        S*M*sin(Po-(4*a)), S*M*sin(Po-(3*a)), S*M*sin(Po-(2*a)), S*M*sin(Po-(a)),   S*M*sin(Po),      S*M*sin(Po-(8*a)), S*M*sin(Po-(7*a)), S*M*sin(Po-(6*a)), S*M*sin(Po-(5*a));
        S*M*sin(Po-(5*a)), S*M*sin(Po-(4*a)), S*M*sin(Po-(3*a)), S*M*sin(Po-(2*a)), S*M*sin(Po-(a)),   S*M*sin(Po),      S*M*sin(Po-(8*a)), S*M*sin(Po-(7*a)), S*M*sin(Po-(6*a));
        S*M*sin(Po-(6*a)), S*M*sin(Po-(5*a)), S*M*sin(Po-(4*a)), S*M*sin(Po-(3*a)), S*M*sin(Po-(2*a)), S*M*sin(Po-(a)),   S*M*sin(Po),      S*M*sin(Po-(8*a)), S*M*sin(Po-(7*a));
        S*M*sin(Po-(7*a)), S*M*sin(Po-(6*a)), S*M*sin(Po-(5*a)), S*M*sin(Po-(4*a)), S*M*sin(Po-(3*a)), S*M*sin(Po-(2*a)), S*M*sin(Po-(a)),   S*M*sin(Po),      S*M*sin(Po-(8*a));
        S*M*sin(Po-(8*a)), S*M*sin(Po-(7*a)), S*M*sin(Po-(6*a)), S*M*sin(Po-(5*a)), S*M*sin(Po-(4*a)), S*M*sin(Po-(3*a)), S*M*sin(Po-(2*a)), S*M*sin(Po-(a)),   S*M*sin(Po)];

dLrs=dLsr';

Lss= [Lls+M,       M*cos((8*a)), M*cos((7*a)),      M*cos((6*a)), M*cos((5*a)), M*cos((4*a)), M*cos((3*a)), M*cos((2*a)),   M*cos((a));
     M*cos((a)),   Lls+M,        M*cos((8*a)),      M*cos((7*a)), M*cos((6*a)), M*cos((5*a)), M*cos((4*a)), M*cos((3*a)), M*cos((2*a));
     M*cos((2*a)), M*cos((a)),   Lls+M,             M*cos((8*a)), M*cos((7*a)), M*cos((6*a)), M*cos((5*a)), M*cos((4*a)), M*cos((3*a));
     M*cos((3*a)), M*cos((2*a)), M*cos((a)),        Lls+M,        M*cos((8*a)), M*cos((7*a)), M*cos((6*a)), M*cos((5*a)), M*cos((4*a));
     M*cos((4*a)), M*cos((3*a)), M*cos((2*a)),      M*cos((a)),   Lls+M,        M*cos((8*a)), M*cos((7*a)), M*cos((6*a)), M*cos((5*a));
     M*cos((5*a)), M*cos((4*a)), M*cos((3*a)),      M*cos((2*a)), M*cos((a)),   Lls+M,        M*cos((8*a)), M*cos((7*a)), M*cos((6*a));
     M*cos((6*a)), M*cos((5*a)), M*cos((4*a)),      M*cos((3*a)), M*cos((2*a)), M*cos((a)),   Lls+M,        M*cos((8*a)), M*cos((7*a));
     M*cos((7*a)), M*cos((6*a)), M*cos((5*a)),      M*cos((4*a)), M*cos((3*a)), M*cos((2*a)), M*cos((a)),   Lls+M,        M*cos((8*a));
     M*cos((8*a)), M*cos((7*a)), M*cos((6*a)),      M*cos((5*a)), M*cos((4*a)), M*cos((3*a)), M*cos((2*a)), M*cos((a)),   Lls+M];

Lrr= [Llr+M,       M*cos((8*a)), M*cos((7*a)),      M*cos((6*a)), M*cos((5*a)), M*cos((4*a)), M*cos((3*a)), M*cos((2*a)), M*cos((a));
     M*cos((a)),   Llr+M,        M*cos((8*a)),      M*cos((7*a)), M*cos((6*a)), M*cos((5*a)), M*cos((4*a)), M*cos((3*a)), M*cos((2*a));
     M*cos((2*a)), M*cos((a)),   Llr+M,             M*cos((8*a)), M*cos((7*a)), M*cos((6*a)), M*cos((5*a)), M*cos((4*a)), M*cos((3*a));
     M*cos((3*a)), M*cos((2*a)), M*cos((a)),        Llr+M,        M*cos((8*a)), M*cos((7*a)), M*cos((6*a)), M*cos((5*a)), M*cos((4*a));
     M*cos((4*a)), M*cos((3*a)), M*cos((2*a)),      M*cos((a)),   Llr+M,        M*cos((8*a)), M*cos((7*a)), M*cos((6*a)), M*cos((5*a));
     M*cos((5*a)), M*cos((4*a)), M*cos((3*a)),      M*cos((2*a)), M*cos((a)),   Llr+M,        M*cos((8*a)), M*cos((7*a)), M*cos((6*a));
     M*cos((6*a)), M*cos((5*a)), M*cos((4*a)),      M*cos((3*a)), M*cos((2*a)), M*cos((a)),   Llr+M,        M*cos((8*a)), M*cos((7*a));
     M*cos((7*a)), M*cos((6*a)), M*cos((5*a)),      M*cos((4*a)), M*cos((3*a)), M*cos((2*a)), M*cos((a)),   Llr+M,        M*cos((8*a));
     M*cos((8*a)), M*cos((7*a)), M*cos((6*a)),      M*cos((5*a)), M*cos((4*a)), M*cos((3*a)), M*cos((2*a)), M*cos((a)),   Llr+M];

dLsrdth=-1.*[M*sin(Po),      M*sin(Po-(8*a)), M*sin(Po-(7*a)), M*sin(Po-(6*a)), M*sin(Po-(5*a)), M*sin(Po-(4*a)), M*sin(Po-(3*a)), M*sin(Po-(2*a)), M*sin(Po-(a));
           M*sin(Po-(a)),   M*sin(Po),      M*sin(Po-(8*a)), M*sin(Po-(7*a)), M*sin(Po-(6*a)), M*sin(Po-(5*a)), M*sin(Po-(4*a)), M*sin(Po-(3*a)), M*sin(Po-(2*a));
           M*sin(Po-(2*a)), M*sin(Po-(a)),   M*sin(Po),      M*sin(Po-(8*a)), M*sin(Po-(7*a)), M*sin(Po-(6*a)), M*sin(Po-(5*a)), M*sin(Po-(4*a)), M*sin(Po-(3*a));
           M*sin(Po-(3*a)), M*sin(Po-(2*a)), M*sin(Po-(a)),   M*sin(Po),      M*sin(Po-(8*a)), M*sin(Po-(7*a)), M*sin(Po-(6*a)), M*sin(Po-(5*a)), M*sin(Po-(4*a));
           M*sin(Po-(4*a)), M*sin(Po-(3*a)), M*sin(Po-(2*a)), M*sin(Po-(a)),   M*sin(Po),      M*sin(Po-(8*a)), M*sin(Po-(7*a)), M*sin(Po-(6*a)), M*sin(Po-(5*a));
           M*sin(Po-(5*a)), M*sin(Po-(4*a)), M*sin(Po-(3*a)), M*sin(Po-(2*a)), M*sin(Po-(a)),   M*sin(Po),      M*sin(Po-(8*a)), M*sin(Po-(7*a)), M*sin(Po-(6*a));
           M*sin(Po-(6*a)), M*sin(Po-(5*a)), M*sin(Po-(4*a)), M*sin(Po-(3*a)), M*sin(Po-(2*a)), M*sin(Po-(a)),   M*sin(Po),      M*sin(Po-(8*a)), M*sin(Po-(7*a));
           M*sin(Po-(7*a)), M*sin(Po-(6*a)), M*sin(Po-(5*a)), M*sin(Po-(4*a)), M*sin(Po-(3*a)), M*sin(Po-(2*a)), M*sin(Po-(a)),   M*sin(Po),      M*sin(Po-(8*a));
           M*sin(Po-(8*a)), M*sin(Po-(7*a)), M*sin(Po-(6*a)), M*sin(Po-(5*a)), M*sin(Po-(4*a)), M*sin(Po-(3*a)), M*sin(Po-(2*a)), M*sin(Po-(a)),   M*sin(Po)];


Rrr=[Rr, 0, 0, 0, 0, 0, 0, 0, 0;
    0, Rr, 0, 0, 0, 0, 0, 0, 0;
    0, 0, Rr, 0, 0, 0, 0, 0, 0;
    0, 0, 0, Rr, 0, 0, 0, 0, 0;
    0, 0, 0, 0, Rr, 0, 0, 0, 0;
    0, 0, 0, 0, 0, Rr, 0, 0, 0;
    0, 0, 0, 0, 0, 0, Rr, 0, 0;
    0, 0, 0, 0, 0, 0, 0, Rr, 0;
    0, 0, 0, 0, 0, 0, 0, 0, Rr];

Rss=[Rs, 0, 0, 0, 0, 0, 0, 0, 0;
     0, Rs, 0, 0, 0, 0, 0, 0, 0;
     0, 0, Rs, 0, 0, 0, 0, 0, 0;
     0, 0, 0, Rs, 0, 0, 0, 0, 0;
     0, 0, 0, 0, Rs, 0, 0, 0, 0;
     0, 0, 0, 0, 0, Rs, 0, 0, 0;
     0, 0, 0, 0, 0, 0, Rs, 0, 0;
     0, 0, 0, 0, 0, 0, 0, Rs, 0;
     0, 0, 0, 0, 0, 0, 0, 0, Rs];
```

```
L=inv([Lss, Lsr; Lrs, Lrr]);

RL=[Rss, dLsr;
    dLrs, Rrr];

Currents=-L*(-[v; zeros(9,1)]+ RL*i);

StatorFlux=Lss*i(1:9)+Lsr*i(10:18);

RotorFlux=Lrr*i(10:18)+Lrs*i(1:9);

Te=P.*(i(1:9)'*dLsrdth*i(10:18));
```

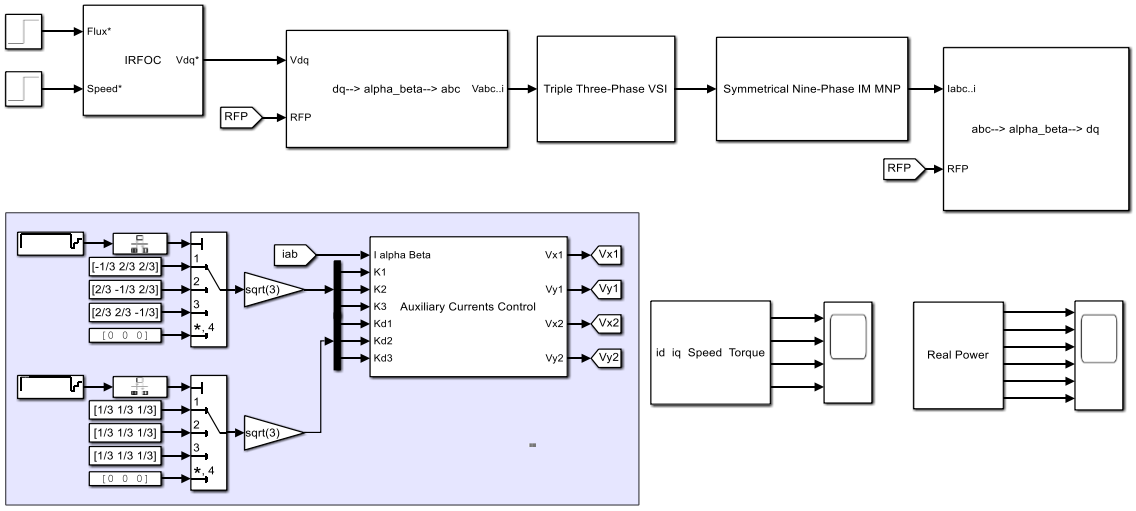

Fig. A.3: Simulink implementation of the current sharing IRFOC algorithm for nine-phase machine.

The voltage source inverter Matlab code is illustrated below for a six-phase machines with two neutral points.

```
function Voltages=ThreePhaseVSI(VDC, Vref)

A=[1, 0, 0;
   0, 1, 0;
   0, 0, 1];

B=[1, 1, 1;
   1, 1, 1;
   1, 1, 1];

Voltages=VDC.*(A*Vref-(1/3).*B*Vref);
```

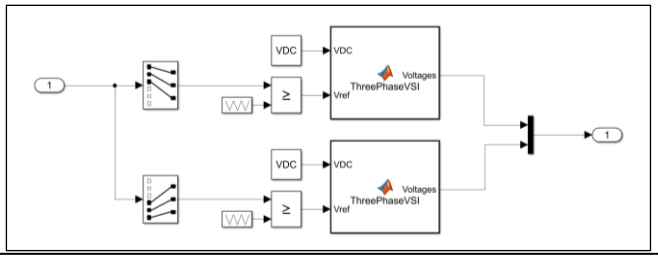

The Matlab model of the simulated twelve-phase double-winding induction machine is illustrated below. This code is considering the coupling among all twelve phases.

```
function [Currents, Te]=PV(v, Po, S, i, Lls, Llr, Lm, Rs, Rr, P)
n=12;
Lm=(2/12)*Lm;
Ls=Lls+Lm;
Lr=Llr+Lm;
a=(2*pi/6);


%% Inducatance Matrices
Lsr=[Lm*cos(Po),       Lm*cos(Po-(5*a)), Lm*cos(Po-(4*a)), Lm*cos(Po-(3*a)), Lm*cos(Po-(2*a)),   Lm*cos(Po-(a));
     Lm*cos(Po),       Lm*cos(Po-(5*a)), Lm*cos(Po-(4*a)), Lm*cos(Po-(3*a)), Lm*cos(Po-(2*a)),   Lm*cos(Po-(a));
     Lm*cos(Po-(a)),   Lm*cos(Po),       Lm*cos(Po-(5*a)), Lm*cos(Po-(4*a)), Lm*cos(Po-(3*a)),   Lm*cos(Po-(2*a));
     Lm*cos(Po-(a)),   Lm*cos(Po),       Lm*cos(Po-(5*a)), Lm*cos(Po-(4*a)), Lm*cos(Po-(3*a)),   Lm*cos(Po-(2*a));
     Lm*cos(Po-(2*a)), Lm*cos(Po-(a)),   Lm*cos(Po),       Lm*cos(Po-(5*a)), Lm*cos(Po-(4*a)),   Lm*cos(Po-(3*a));
     Lm*cos(Po-(2*a)), Lm*cos(Po-(a)),   Lm*cos(Po),       Lm*cos(Po-(5*a)), Lm*cos(Po-(4*a)),   Lm*cos(Po-(3*a));
     Lm*cos(Po-(3*a)), Lm*cos(Po-(2*a)), Lm*cos(Po-(a)),   Lm*cos(Po),       Lm*cos(Po-(5*a)),   Lm*cos(Po-(4*a));
     Lm*cos(Po-(3*a)), Lm*cos(Po-(2*a)), Lm*cos(Po-(a)),   Lm*cos(Po),       Lm*cos(Po-(5*a)),   Lm*cos(Po-(4*a));
     Lm*cos(Po-(4*a)), Lm*cos(Po-(3*a)), Lm*cos(Po-(2*a)), Lm*cos(Po-(a)),   Lm*cos(Po),         Lm*cos(Po-(5*a));
     Lm*cos(Po-(4*a)), Lm*cos(Po-(3*a)), Lm*cos(Po-(2*a)), Lm*cos(Po-(a)),   Lm*cos(Po),         Lm*cos(Po-(5*a));
     Lm*cos(Po-(5*a)), Lm*cos(Po-(4*a)), Lm*cos(Po-(3*a)), Lm*cos(Po-(2*a)), Lm*cos(Po-(a)),     Lm*cos(Po);
     Lm*cos(Po-(5*a)), Lm*cos(Po-(4*a)), Lm*cos(Po-(3*a)), Lm*cos(Po-(2*a)), Lm*cos(Po-(a)),     Lm*cos(Po)];


Lrs=Lsr';

dLsr=-1.*[S*Lm*cos(Po),       S*Lm*cos(Po-(5*a)), S*Lm*cos(Po-(4*a)), S*Lm*cos(Po-(3*a)), S*Lm*cos(Po-(2*a)),   S*Lm*cos(Po-(a));
          S*Lm*cos(Po),       S*Lm*cos(Po-(5*a)), S*Lm*cos(Po-(4*a)), S*Lm*cos(Po-(3*a)), S*Lm*cos(Po-(2*a)),   S*Lm*cos(Po-(a));
          S*Lm*cos(Po-(a)),   S*Lm*cos(Po),       S*Lm*cos(Po-(5*a)), S*Lm*cos(Po-(4*a)), S*Lm*cos(Po-(3*a)),   S*Lm*cos(Po-(2*a));
          S*Lm*cos(Po-(a)),   S*Lm*cos(Po),       S*Lm*cos(Po-(5*a)), S*Lm*cos(Po-(4*a)), S*Lm*cos(Po-(3*a)),   S*Lm*cos(Po-(2*a));
          S*Lm*cos(Po-(2*a)), S*Lm*cos(Po-(a)),   S*Lm*cos(Po),       S*Lm*cos(Po-(5*a)), S*Lm*cos(Po-(4*a)),   S*Lm*cos(Po-(3*a));
          S*Lm*cos(Po-(2*a)), S*Lm*cos(Po-(a)),   S*Lm*cos(Po),       S*Lm*cos(Po-(5*a)), S*Lm*cos(Po-(4*a)),   S*Lm*cos(Po-(3*a));
          S*Lm*cos(Po-(3*a)), S*Lm*cos(Po-(2*a)), S*Lm*cos(Po-(a)),   S*Lm*cos(Po),       S*Lm*cos(Po-(5*a)),   S*Lm*cos(Po-(4*a));
          S*Lm*cos(Po-(3*a)), S*Lm*cos(Po-(2*a)), S*Lm*cos(Po-(a)),   S*Lm*cos(Po),       S*Lm*cos(Po-(5*a)),   S*Lm*cos(Po-(4*a));
          S*Lm*cos(Po-(4*a)), S*Lm*cos(Po-(3*a)), S*Lm*cos(Po-(2*a)), S*Lm*cos(Po-(a)),   S*Lm*cos(Po),         S*Lm*cos(Po-(5*a));
          S*Lm*cos(Po-(4*a)), S*Lm*cos(Po-(3*a)), S*Lm*cos(Po-(2*a)), S*Lm*cos(Po-(a)),   S*Lm*cos(Po),         S*Lm*cos(Po-(5*a));
          S*Lm*cos(Po-(5*a)), S*Lm*cos(Po-(4*a)), S*Lm*cos(Po-(3*a)), S*Lm*cos(Po-(2*a)), S*Lm*cos(Po-(a)),     S*Lm*cos(Po);
          S*Lm*cos(Po-(5*a)), S*Lm*cos(Po-(4*a)), S*Lm*cos(Po-(3*a)), S*Lm*cos(Po-(2*a)), S*Lm*cos(Po-(a)),     S*Lm*cos(Po)];

dLrs=dLsr';

Lss=[Ls,       Lm,  Lm*cos((5*a)), Lm*cos((5*a)), Lm*cos((4*a)), Lm*cos((4*a)), Lm*cos((3*a)), Lm*cos((3*a)), Lm*cos((2*a)), Lm*cos((2*a)), Lm*cos((a)),   Lm*cos((a));
     Lm,       Ls,  Lm*cos((5*a)), Lm*cos((5*a)), Lm*cos((4*a)), Lm*cos((4*a)), Lm*cos((3*a)), Lm*cos((3*a)), Lm*cos((2*a)), Lm*cos((2*a)), Lm*cos((a  )),   Lm*cos((a));
     Lm*cos((a)),   Lm*cos((a)),   Ls,       Lm,  Lm*cos((5*a)), Lm*cos((5*a)), Lm*cos((4*a)), Lm*cos((4*a)), Lm*cos((3*a)), Lm*cos((3*a)), Lm*cos((2*a)), Lm*cos((2*a));
     Lm*cos((a)),   Lm*cos((a)),   Lm,       Ls,  Lm*cos((5*a)), Lm*cos((5*a)), Lm*cos((4*a)), Lm*cos((4*a)), Lm*cos((3*a)), Lm*cos((3*a)), Lm*cos((2*a)), Lm*cos((2*a));
     Lm*cos((2*a)), Lm*cos((2*a)), Lm*cos((a)),   Lm*cos((a)),   Ls,       Lm,  Lm*cos((5*a)), Lm*cos((5*a)), Lm*cos((4*a)), Lm*cos((4*a)), Lm*cos((3*a)), Lm*cos((3*a));
     Lm*cos((2*a)), Lm*cos((2*a)), Lm*cos((a)),   Lm*cos((a)),   Lm,       Ls,  Lm*cos((5*a)), Lm*cos((5*a)), Lm*cos((4*a)), Lm*cos((4*a)), Lm*cos((3*a)), Lm*cos((3*a));
     Lm*cos((3*a)), Lm*cos((3*a)), Lm*cos((2*a)), Lm*cos((2*a)), Lm*cos((a)),   Lm*cos((a)),   Ls,       Lm,  Lm*cos((5*a)), Lm*cos((5*a)), Lm*cos((4*a)), Lm*cos((4*a));
     Lm*cos((3*a)), Lm*cos((3*a)), Lm*cos((2*a)), Lm*cos((2*a)), Lm*cos((a)),   Lm*cos((a)),   Lm,       Ls,  Lm*cos((5*a)), Lm*cos((5*a)), Lm*cos((4*a)), Lm*cos((4*a));
     Lm*cos((4*a)), Lm*cos((4*a)), Lm*cos((3*a)), Lm*cos((3*a)), Lm*cos((2*a)), Lm*cos((2*a)), Lm*cos((a)),   Lm*cos((a)),   Ls,       Lm,  Lm*cos((5*a)), Lm*cos((5*a));
     Lm*cos((4*a)), Lm*cos((4*a)), Lm*cos((3*a)), Lm*cos((3*a)), Lm*cos((2*a)), Lm*cos((2*a)), Lm*cos((a)),   Lm*cos((a)),   Lm,       Ls,  Lm*cos((5*a)), Lm*cos((5*a));
     Lm*cos((5*a)), Lm*cos((5*a)), Lm*cos((4*a)), Lm*cos((4*a)), Lm*cos((3*a)), Lm*cos((3*a)), Lm*cos((2*a)), Lm*cos((2*a)), Lm*cos((a)),   Lm*cos((a)),   Ls,       Lm;
     Lm*cos((5*a)), Lm*cos((5*a)), Lm*cos((4*a)), Lm*cos((4*a)), Lm*cos((3*a)), Lm*cos((3*a)), Lm*cos((2*a)), Lm*cos((2*a)), Lm*cos((a)),   Lm*cos((a)),   Lm,       Ls];

Lrr=[Lr,            Lm*cos((5*a)), Lm*cos((4*a)), Lm*cos((3*a)), Lm*cos((2*a)),   Lm*cos((a));
     Lm*cos((a)),   Lr,            Lm*cos((5*a)), Lm*cos((4*a)), Lm*cos((3*a)),   Lm*cos((2*a));
     Lm*cos((2*a)), Lm*cos((a)),   Lr,            Lm*cos((5*a)), Lm*cos((4*a)),   Lm*cos((3*a));
     Lm*cos((3*a)), Lm*cos((2*a)), Lm*cos((a)),   Lr,            Lm*cos((5*a)),   Lm*cos((4*a));
     Lm*cos((4*a)), Lm*cos((3*a)), Lm*cos((2*a)), Lm*cos((a)),   Lr,              Lm*cos((5*a));
     Lm*cos((5*a)), Lm*cos((4*a)), Lm*cos((3*a)), Lm*cos((2*a)),   Lm*cos((a)),   Lr];


dLsrdth=-1.*[Lm*sin(Po),       Lm*sin(Po-(5*a)), Lm*sin(Po-(4*a)), Lm*sin(Po-(3*a)), Lm*sin(Po-(2*a)),   Lm*sin(Po-(a));
             Lm*sin(Po),       Lm*sin(Po-(5*a)), Lm*sin(Po-(4*a)), Lm*sin(Po-(3*a)), Lm*sin(Po-(2*a)),   Lm*sin(Po-(a));
             Lm*sin(Po-(a)),   Lm*sin(Po),       Lm*sin(Po-(5*a)), Lm*sin(Po-(4*a)), Lm*sin(Po-(3*a)),   Lm*sin(Po-(2*a));
             Lm*sin(Po-(a)),   Lm*sin(Po),       Lm*sin(Po-(5*a)), Lm*sin(Po-(4*a)), Lm*sin(Po-(3*a)),   Lm*sin(Po-(2*a));
             Lm*sin(Po-(2*a)), Lm*sin(Po-(a)),   Lm*sin(Po),       Lm*sin(Po-(5*a)), Lm*sin(Po-(4*a)),   Lm*sin(Po-(3*a));
             Lm*sin(Po-(2*a)), Lm*sin(Po-(a)),   Lm*sin(Po),       Lm*sin(Po-(5*a)), Lm*sin(Po-(4*a)),   Lm*sin(Po-(3*a));
             Lm*sin(Po-(3*a)), Lm*sin(Po-(2*a)), Lm*sin(Po-(a)),   Lm*sin(Po),       Lm*sin(Po-(5*a)),   Lm*sin(Po-(4*a));
             Lm*sin(Po-(3*a)), Lm*sin(Po-(2*a)), Lm*sin(Po-(a)),   Lm*sin(Po),       Lm*sin(Po-(5*a)),   Lm*sin(Po-(4*a));
             Lm*sin(Po-(4*a)), Lm*sin(Po-(3*a)), Lm*sin(Po-(2*a)), Lm*sin(Po-(a)),   Lm*sin(Po),         Lm*sin(Po-(5*a));
             Lm*sin(Po-(4*a)), Lm*sin(Po-(3*a)), Lm*sin(Po-(2*a)), Lm*sin(Po-(a)),   Lm*sin(Po),         Lm*sin(Po-(5*a));
             Lm*sin(Po-(5*a)), Lm*sin(Po-(4*a)), Lm*sin(Po-(3*a)), Lm*sin(Po-(2*a)), Lm*sin(Po-(a)),     Lm*sin(Po);
             Lm*sin(Po-(5*a)), Lm*sin(Po-(4*a)), Lm*sin(Po-(3*a)), Lm*sin(Po-(2*a)), Lm*sin(Po-(a)),     Lm*sin(Po)];

Rrr=[Rr, 0, 0, 0, 0, 0;
     0, Rr, 0, 0, 0, 0;
     0, 0, Rr, 0, 0, 0;
     0, 0, 0, Rr, 0, 0;
     0, 0, 0, 0, Rr, 0;
     0, 0, 0, 0, 0, Rr];

Rss=[Rs, 0, 0, 0, 0, 0, 0, 0, 0, 0, 0, 0;
     0, Rs, 0, 0, 0, 0, 0, 0, 0, 0, 0, 0;
     0, 0, Rs, 0, 0, 0, 0, 0, 0, 0, 0, 0;
     0, 0, 0, Rs, 0, 0, 0, 0, 0, 0, 0, 0;
     0, 0, 0, 0, Rs, 0, 0, 0, 0, 0, 0, 0;
     0, 0, 0, 0, 0, Rs, 0, 0, 0, 0, 0, 0;
     0, 0, 0, 0, 0, 0, Rs, 0, 0, 0, 0, 0;
     0, 0, 0, 0, 0, 0, 0, Rs, 0, 0, 0, 0;
     0, 0, 0, 0, 0, 0, 0, 0, Rs, 0, 0, 0;
     0, 0, 0, 0, 0, 0, 0, 0, 0, Rs, 0, 0;
     0, 0, 0, 0, 0, 0, 0, 0, 0, 0, Rs, 0;
     0, 0, 0, 0, 0, 0, 0, 0, 0, 0, 0, Rs];
```

```
L=inv([Lss, Lsr; Lrs, Lrr]);

RL=[Rss, dLsr;
    dLrs, Rrr];

Currents=-L*(-[v; zeros(6,1)]+ RL*i);

StatorFlux=Ls*i(1:9)+Lsr*i(10:18);

RotorFlux=Ls*i(10:18)+Lrs*i(1:9);

Te=P.*(i(1:12)'*dLsrdth*i(13:18));
```

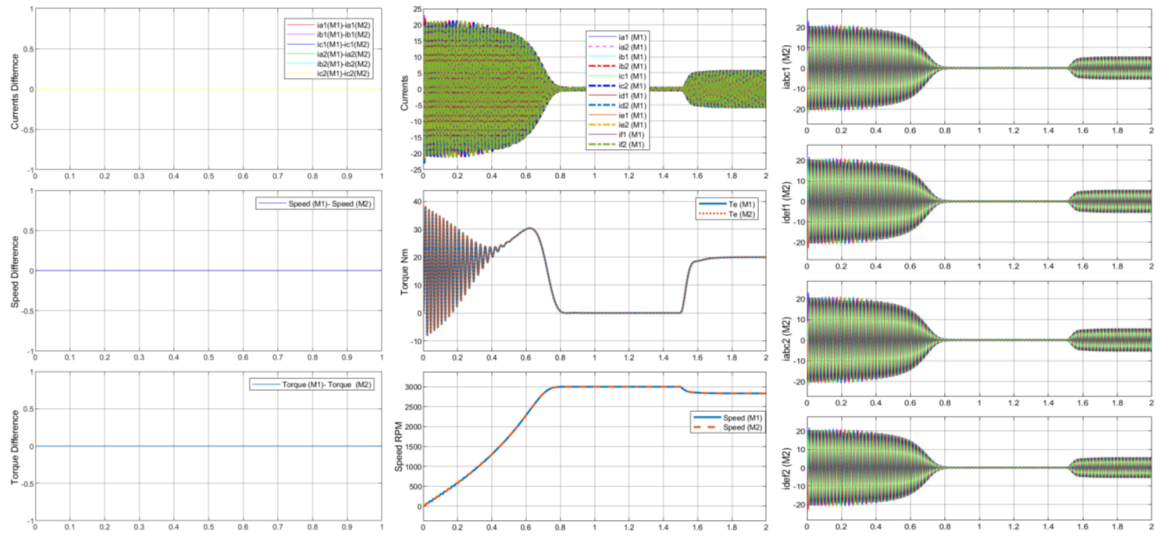

Fig. A.4: Comparison of double-winding twelve-phase induction machine models. Model 1 (M1) includes the coupling between all twelve phases, while Model 2 (M2) is a summation of the two independent six-phase sub-machines.

Fig. A.4 shows the simulation results comparison of the double-winding multiphase machine using two different modelling approaches. In the first modelling approach the coupling among all twelve phases is taken into account. The model of the machine using this modelling approach is shown on the previous page. Note that the model is used in Chapter 6 for the machine modelling (but not for control purposes). In the second approach the machine is modelled as a summation of two six-phase sub-machines without considering the cross coupling among sub-machines. The results of the open-loop acceleration test show that there is no difference between the two modelling approaches concerning the produced speed, electromagnetic torque and the currents. The second modelling approach is used in Chapter 6 for the control purposes.

APPENDIX B

DESCRIPTION OF EXPERIMENTAL SETUP

B.1 HARDWARE DESCRIPTION

In this thesis, two experimental setups have been utilised. The first experimental setup, presented in Chapters 3, 4, 5 and part of Chapter 7, is used to demonstrate and validate the proposed current and power sharing among the winding sets for a nine-phase induction machine with symmetrical and asymmetrical configuration. The same setup was utilised to illustrate the ability of applying a regenerative test for multiple three-phase machines with an odd number of neutral points. The same nine-phase machine is utilised for both configurations by changing the connection at the machine terminals. The second setup is utilising an asymmetrical six-phase induction machine to verify the regenerative test ability using a single *y*-current component for multiple three-phase machines with an even number of neutral points. The experimental setup is illustrated in Fig. B.1. The pieces of equipment used in the experimental verification are listed as follows:

- Two eight-phase two-level VSIs (custom made, based on Infineon FS50R12KE3 IGBT).
- dSPACE DS1006 rapid prototyping system and host PC.
- Asymmetrical six- and nine-phase induction machines (custom made).
- Four quadrant linear power amplifier (Spitzenberger & Spies PAS 2500).
- DC machine coupled to the nine-phase machine.
- Torque meter (Magtrol TM 210).
- Two Tektronix oscilloscopes (DPO 2014 and MSO 2014).

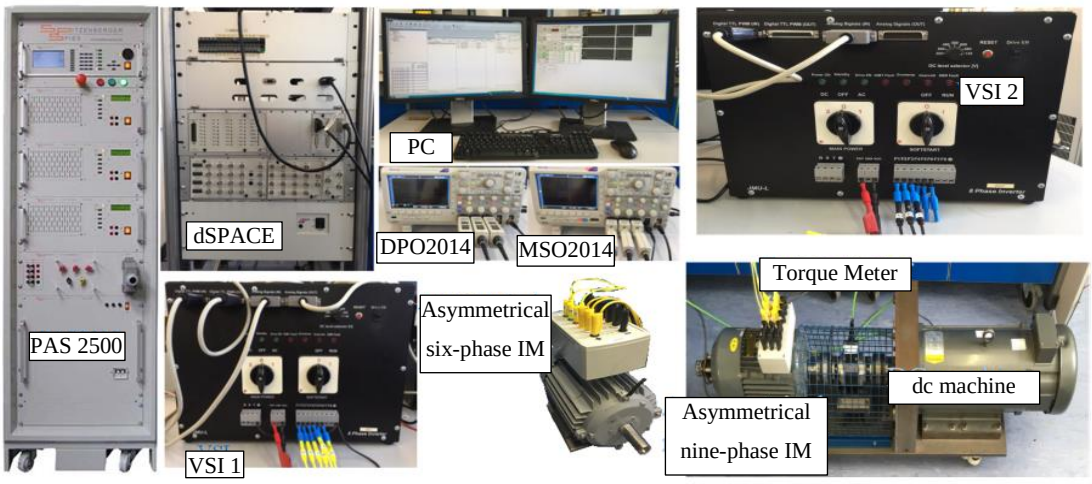

Fig. B.4: Experimental setup.

- Voltage and current probes (Tektronix P5205A, and Pico TA189)
- Resistive load box to load the DC machine.

The asymmetrical nine-phase and six-phase induction machines' parameters are illustrated in Table 3.1 and Table 6.2, respectively. The nine-phase machine was originally a three-phase machine with squirrel cage rotor. It had 36 slots and two pole pairs. The winding configuration was distributed winding. The machine has been rewound to nine-phase one pole-pair, such that each phase is occupying 4 slots. The original machine's rated power was 2.2 kW and the rated current was 4.5 A. After rewinding the machine to asymmetrical nine-phase machine, the rated power is kept the same while the rated current is decreased to 1.5 A. The phase winding is kept open at both ends to have the possibility of supplying it from both sides. The six-phase machine was also originally a three-phase machine which has been rewound to three pole-pairs asymmetrical six-phase machine with a power of 1.1 kW. However, some of the phases are sharing the same slot unlike the nine-phase machine where each phase is occupying 4 slots. This is due to the higher pole number of the six-phase machine. Both machines have an Omron incremental encoder (E6B2-CWZ1X) mounted on the shaft. The encoder produces a thousand pulses per revolution. The encoder output is connected to dSPACE DS3002 encoder board which provides the position and the position derivative (SPEED) to Matlab and dSAPCE ControlDesk.

The torque measurement is done using a Magtrol TM 210 torque meter. The data acquisition and the torque meter power supply are provided by a Magtrol 6400 signal amplifier. The signal amplifier provides a reading of the speed, mechanical torque and the output power on the shaft. The torque meter has a settable 2^{nd} order Butterworth low-pass filter. The cut-off frequency was set at 200 Hz during all experiments.

For the experiments with the nine-phase induction machine, two two-level VSIs with connected dc-links have been utilised. On the other hand, for the regenerative test experiments with a six-phase machine, a single two-level VSI has been used. Both VSIs are custom made and are consisting of three Infineon FS50R12KE3 EUPEC IGBT six-pack power modules. There are nine legs per VSI; however, eight are used as outputs while the remaining one is used to drive the braking resistor in case of power reversal. Control of two VSIs (supplying nine-phase machine), requires a single 16 channel DWO dSPACE board. Seven of the channels are available per VSI since the eight signal is used to enable the VSI. For the experiments of the nine-phase machine, the connections are made in such a way that the first VSI is supplying the first two winding sets while the second inverter is supplying the remaining winding set. The dc-link power is supplied by the Spitzenberger & Spies PAS 2500 where two power modules are utilised to provide the required power. Each power module can provide up to 2.5 kW. In the case of the six-phase machines, the first module is set to 160 V while the second one is set to –160 V. In the case of the experiments with the nine-phase machine, the first module is set to 300 V while the second power module is set to –300 V.

The power measurement of the experiments is done by using two oscilloscopes illustrated in Fig. B.1. dSPACE is not capable of measuring the power since the sampling frequency is twice the switching frequency and therefore PWM signals cannot be captured using dSAPCE. The Tektronix MSO2014 and DPO2014 are both four channel oscilloscopes with 100 MHz bandwidth, with 1 GS/s sample rate and with deep memory, of 1.25 million points, depth. The first scope (MSO2014) is a mixed signal oscilloscope. In order to measure the power, one scope is utilised to measure the three-phase winding set voltages while the other one is measuring the currents of the winding set. The power measurement is done set by set utilising the same sequence. Both oscilloscopes are precisely synchronously triggered from dSPACE.

B.2 SOFTWARE DESCRIPTION

The dSPACE control system is obtained using a modified Simulink model of the simulation file which is utilised to validate the proposed control schemes. The original Simulink files are changed to accommodate the requirements of the dSPACE and ControlDesk. These modifications include removing the machine and the VSI model and adding Real-time Interface blocks to connect the Simulink model control system with the dSPACE hardware and ControlDesk software. The gating signals are generated using DWO (DS5101) board by sending the dwell times. As mentioned earlier in this appendix, the sampling and control time of the dSPACE are set to be twice the switching frequency. Furthermore, the control is executed exactly at the beginning and in the middle of the switching period.

In order to control the machines using IRFOC, it is necessary to measure the phase currents and the position of the rotor. The position and speed are measured using a shaft-mounted encoder which is connected to the DS3002 encoder board. On the other hand, the current measurements are obtained using dSPACE DS2004 ADC board. Although the sampling frequency is twice the switching frequency, the current measurement is done using the burst mode where ten samples of the current are sampled within first 10 μsec (one sample each 1 μsec) and averaged to improve the current measurement accuracy. The speed and position measurements are sampled every ten periods and further filtered using a moving average filter with a window of 0.02 sec.

Finally, the experimental measurements illustrated in each chapter are measured synchronously between the dSPACE and the oscilloscopes. Currents and power measurements are measured using the oscilloscope while the stationary and rotating currents are measured using the dSPACE. The speed measurement is also measured using dSPACE. The synchronisation is obtained using the DAC board DS2101 such that a signal is sent from DAC channels to the trigger input of the oscilloscopes. The oscilloscopes were connected to PC and the data is captured from the oscilloscope using VISA protocol commands. The data is recorded from the dSPACE using the ControlDesk recorder built-in feature.

APPENDIX C

PUBLICATION RESULTING FROM THE THESIS

C.1 JOURNAL PUBLICATIONS

Abduallah, A. A., Dordevic, O., Jones, M. and Levi, E., (2019), "Regenerative test for multiple three-phase machines with even number of neutral points," *IEEE Transactions on Industrial Electronics*, 2019 (Early Access, doi: 10.1109/TIE.2019.2903750).

C.2 CONFERENCE PUBLICATIONS

Abduallah, A. A., Dordevic, O. and Jones, M. (2017), "Multidirectional power flow control among double winding six-phase induction machine winding sets," in *IECON 2017 - 43rd Annual Conference of the IEEE Industrial Electronics Society*, 29 Oct.-1 Nov. 2017, 8001-8006.

Abduallah, A. A., Dordevic, O. and Jones, M. (2018), "Synthetic loading for symmetrical and asymmetrical six-phase machines," in *IEEE 18th International Power Electronics and Motion Control Conference (PEMC)*, 26-30 Aug. 2018, 617-622.

Abduallah, A. A., Dordevic, O., Jones, M. and Levi, E. (2018), "Synthetic loading for symmetrical and asymmetrical nine-phase machines," in *IECON 2018 - 44rd Annual Conference of the IEEE Industrial Electronics Society*, 21-23 Oct. 2018, 5860-5865.